

SYNTHESIS, AQUEOUS SOLUTION BEHAVIOR AND LAYER-BY-LAYER
SELF-ASSEMBLY OF POLY(2-ALKYL-2-OXAZOLINE)S

A THESIS SUBMITTED TO
THE GRADUATE SCHOOL OF NATURAL AND APPLIED SCIENCES
OF
MIDDLE EAST TECHNICAL UNIVERSITY

BY

EDA AĐLI

IN PARTIAL FULFILLMENT OF THE REQUIREMENTS
FOR
THE DEGREE OF DOCTOR OF PHILOSOPHY
IN
CHEMISTRY

JANUARY 2019

Approval of the thesis:

SYNTHESIS, SOLUTION BEHAVIOUR AND LAYER-BY-LAYER SELF-ASSEMBLY OF POLY(2-ALKYL-2-OXAZOLINE)S

submitted by **EDA ÇAĞLI** in partial fulfillment of the requirements for the degree of **Doctor of Philosophy in Chemistry Department, Middle East Technical University** by,

Prof. Dr. Halil Kalıpçılar
Dean, Graduate School of **Natural and Applied Sciences**

Prof. Dr. Cihangir Tanyeli
Head of Department, **Chemistry**

Assoc. Prof. Dr. İrem Erel-Göktepe
Supervisor, **Chemistry, METU**

Examining Committee Members:

Prof. Dr. Halil İbrahim Ünal
Chemistry, Gazi University

Assoc. Prof. Dr. İrem Erel-Göktepe
Chemistry, METU

Assoc. Prof. Dr. Eda Ayşe Aksoy
Basic Pharmaceutical Sciences, Hacettepe University

Assoc. Prof. Dr. Erhan Bat
Chemical Engineering, METU

Assist. Prof. Dr. Salih Özçubukçu
Chemistry, METU

Date: 28.01.2019

I hereby declare that all information in this document has been obtained and presented in accordance with academic rules and ethical conduct. I also declare that, as required by these rules and conduct, I have fully cited and referenced all material and results that are not original to this work.

Name, Surname: Eda aęlı

Signature:

ABSTRACT

SYNTHESIS, AQUEOUS SOLUTION BEHAVIOR AND LAYER-BY-LAYER SELF-ASSEMBLY OF POLY(2-ALKYL-2-OXAZOLINE)S

Çağlı, Eda

Doctor of Philosophy, Chemistry

Supervisor: Assoc. Prof. Dr. İrem Erel-Göktepe

January 2019, 210 pages

Poly(2-alkyl-2-oxazoline)s (PAOXs), are of interest for biomedical applications due to their important biological properties such as nontoxicity and biocompatibility. PAOXs with short-alkyl chains exhibit temperature-responsive behaviour which is advantageous for various biomedical applications. This dissertation focused on synthesis, aqueous solution behaviour, post-functionalization and layer-by-layer (LbL) self-assembly of PAOXs. In addition, it aimed to examine the surface properties of PAOX LbL films and correlate them with biological properties of the multilayers.

First, the effect of pH on aqueous solution behaviour of poly(2-isopropyl-2-oxazoline) (PIPOX) was examined. In this respect, the effect of PIPOX end group, concentration of polymer and salt on pH-induced self-association of PIPOX was examined. Second, the effect of PIPOX end-group on loading capacity and release profile of a model antibiotic, Chloramphenicol (CAP) from PIPOX aggregates was investigated at neutral and acidic pH at a physiologically related temperature. Third, the effect of side chain variation on surface and biological properties of PAOX LbL films has been examined. In this context, PAOXs with varying side chains were co-assembled with Tannic Acid (TA) at the surface using LbL technique. The effect of chemical nature of PAOX side chains, phase behaviour of PAOX and the binding strength between the

layers on surface morphology, stability, wettability and stimuli-responsive drug release properties of the films were examined and correlated with anti-adhesive and antibacterial properties of the PAOX multilayers. Forth, PIPOX-*hyd*-Doxycycline conjugate was synthesized *via* hydrazone bond formation and characterized.

Overall, this dissertation generated fundamental knowledge about aqueous solution behaviour of PAOXs and structure-property relationship in PAOX multilayer films.

Keywords: Poly(2-alkyl-2-oxazoline)s, Stimuli-responsive polymer, Polymer self-aggregates, Polymer-drug conjugate, Antibacterial, bacterial anti-adhesive and protein repellent surfaces

ÖZ

POLİ(2-ALKİL-2-OKSAZOLİN) TÜREVLERİNİN SENTEZİ, ÇÖZELTİ DAVRANIŞLARI VE KATMAN-KATMAN KENDİLİĞİNDEN YAPILANDIRILMASI

Çağlı, Eda
Doktora, Kimya
Tez Danışmanı: Doç. Dr. İrem Erel-Göktepe

Ocak 2019, 210 sayfa

Poli(2-alkil-2-oksazolin)'ler (PAOX) toksik olmama ve biouyumluluk gibi önemli biyolojik özellikleri ile biyomedikal uygulamalarda ilgi çekmektedir. Ayrıca, kısa alkil zincirli PAOX türevlerinin sıcaklığa karşı duyarlılığı, onları ilaç salım uygulamaları için avantajlı kılmaktadır. Bu doktora tezinde, PAOX sentezi, sulu çözelti davranışı, uç grubunun fonksiyonelleştirilmesi ve katman-katman kendiliğinden yapılanması incelenmiştir. Ek olarak, PAOX çok katmanlı filmlerinin yüzey özellikleri ve bu özelliklerin birtakım biyolojik özellikler ile bağlantısının incelenmesi hedeflenmiştir.

İlk olarak, pH'ın PIPOX'un sulu çözelti içerisindeki davranışına etkisi incelenmiştir. Bu amaçla, pH indüklemesi ile PIPOX'un kendiliğinden yapılanma davranışı üzerine PIPOX uç grubunun, polimer konsantrasyonunun ve ortamdaki tuzun etkisi incelenmiştir. Ardından, PIPOX uç grubunun model antibiyotik Kloramfenikol (CAP)'un PIPOX agregatlarına yüklenme kapasitesi ve salım profili üzerine etkisi araştırılmıştır. PIPOX-OR ve PIPOX-CAP'in ilaç yükleme kapasiteleri ve salım davranışları nötr ve asidik koşullarda ve fizyolojik sıcaklıkta karşılaştırılmıştır. Sonrasında, yan zincir farklılaştırılmasının katman-katman kendiliğinden yapılanma metodu ile hazırlanmış PAOX filmlerinin yüzey ve biyolojik özellikleri üzerine etkisi

incelenmiştir. Bu amaçla, farklı yan zincirler barındıran PAOX lar ve tanik asit (TA), katman-katman kendiliğinden yapılanma tekniği kullanılarak yüzeyde yapılandırılmıştır. Bu filmlerin yüzey morfolojisi, kararlılığı, ıslanabilirliği ve belirli bir uyarana ile ilaç salım özellikleri, bakteri tutmama ve antibakteriyel özellikleri ile korelasyonu incelenmiştir. PAOX yan zincirinin kimyasal yapısının, PAOX'un faz özelliğine ve katmanlar arası bağlanma kuvvetinin film kalınlığı, pürüzlülüğü, ıslanabilirliği ve kararlılığına etkisi araştırılmıştır. Son olarak, PIPOX'un Doxycycline antibiyotiği ile konjugatı hidrozon bağı oluşturularak sentezlenmiş ve karakterize edilmiştir.

Genel olarak bakıldığında, bu tez çalışması PAOX'un sulu çözelti içerisindeki davranışına ve PAOX çok katmanlı filmlerindeki kimyasal yapı-özellik ilişkisine temel oluşturmuştur.

Anahtar Kelimeler: Poli(2-alkil-2-oksazolin)ler, Dış-uyarılara duyarlı polimer, Polimer self-agregatlar, Polimer-ilâç konjugatları, Antibakteriyel, bakteri ve protein tutmayan yüzeyler

To My Lovely Family and Fiancee...

ACKNOWLEDGMENTS

This thesis is the end of my PhD journey at METU. I have not travelled in a vacuum in this trip. I faced with and overcame numerous difficulties, fell down and stood up again, learned being patient, dedicated and strong. At the end, it is really hard to believe for me but I am here. This thesis has been kept on track and been seen through to completion with the support and encouragement of many people including my supervisor, faculty members, my friends, colleagues, my besties and family. At the end of my thesis I would like to thank all those people who made this thesis possible and a remarkable experience for me.

First, I pay homage to my advisor Assoc. Prof. Dr. İrem Erel Göktepe for the continuous support of my PhD study and related researches, for her patience, motivation, and immense knowledge. Her guidance helped me in all the time of research and writing of this thesis. Besides my advisor, I would like to thank the rest of my dissertation committee: Assoc. Prof. Dr. Erhan Bat and Assist. Prof. Dr. Salih Özçubukçu, for their insightful comments and questions which incanted me to widen my research from various perspectives.

My sincere thanks also goes to Prof. Dr. Sreeparna Banerjee for valuable advises about biological experiments and giving us opportunity to use their research facilities. I want to thank Dr. Erol Yıldırım and Sinem Ulusan to conduct computational studies and biological experiments which enhance the impact of my studies, respectively. I wish to thank Prof. Dr. Ali Çırpan, Prof. Dr. Mürvet Volkan, Assoc. Prof. Dr. Emren Esentürk and Assoc. Prof. Dr. Özgül Persil Çetinkol for let me to use their laboratory utilities whenever I need.

I thank my labmates for the long working days we were working together before deadlines and for all the fun we have had especially with Dilara Gündoğdu and Sinem Ulusan. Also, I thank my sweetie and hard-working undergraduate student Esmâ Uğur for her help and effort for especially 4th part of the study. I do not want to forget to write my thanks to our lovely undergraduate student Gökçe Tidim for her unbelievable

positive energy and attitude. Great thanks to Majid Akbar for serving me a green tea and many delicious cookies during the endless nights spent for experiments. We spent enjoyable discussion and chatting times with my ex-labmate Gökçe Çalış and new-labmate Nihan Saraçoğulları, thank you for all and friendship. I want to thank my lovely friends Ceren Uzun and Sinem Ulusan for their endless help and affords for SERS measurements and biological experiments, respectively. I would thank to Samet Aytekin, Halil İpek, Seza Göker for their friendship and psychological support.

I take this chance to sincerely acknowledge TUBITAK (Grant No.113Z586) to provide me financial support for the synthesis of polymers during my research.

Many special thanks are due to my besties; Aysun Gülseven, Seda Karahan, Ceren Uzun and Duygu Kuzyaka for their valuable friendship, help, love, motivation and suggestions. They were always with me when I really need. I know that we are the best friends forever and I am so happy to be with you in my whole life journey.

Nobody has been more significant to me in this life than the members of my family. I would like to thank to my dear dad Mehmet Çağlı and my dear mom Meliha Çağlı whose love, guidance and support are always with me in whenever and wherever I need. They are my ultimate role models and heroes. I hope they would forgive me since I could not spend much time together with them, even sometimes I went home for just sleeping. My little but huge-hearted engineer brother Okan Çağlı, my special thanks come to you. I am proud of you that you are so strong, compassionate, honest and kind-hearted person. However, you grew up fast but I could not be with you all the time you needed due to having things to do, sorry for that my lovely bro. The last but not the least, I wish to thank my lovely fiancée Muhammet İşci for his love, endless patience, support, inspiration and guidance. I could not find words to express my feelings to you, my darling. I feel your hand and heart in mine as we walk throughout life together.

TABLE OF CONTENTS

ABSTRACT	v
ÖZ	vii
ACKNOWLEDGMENTS.....	x
TABLE OF CONTENTS.....	xii
LIST OF TABLES.....	xvii
LIST OF FIGURES	xviii
LIST OF SCHEMES.....	xxv
LIST OF ABBREVIATIONS	xxvi
CHAPTERS	
1. INTRODUCTION	1
1.1. Goals and Objectives	1
1.2. Summary of thesis	1
1.3. Literature Review	6
1.3.1. Poly(2-alkyl-2-oxazoline)s	6
1.3.2. Synthesis of poly(2-alkyl-oxazoline)s.....	7
1.3.3. Biologically active PAOX derivatives	11
1.3.3.1. Therapeutic PAOXs.....	12
1.3.3.2. PAOX therapeutics	15
1.3.3.3. Therapeutic releasing PAOXs	18
1.3.4. Aqueous solution behavior of PAOXs	22
1.3.4.1. Temperature-dependent aqueous solution behavior of PAOXs	23
1.3.4.2. pH-dependent aqueous solution behavior of PAOXs	25

1.3.4.3. PAOX-based colloidal structures	27
1.3.5. Multilayers of PAOXs.....	30
1.3.5.1. H-bonded LbL self-assembly of PAOXs	33
2. AN EXPERIMENTAL AND COMPUTATIONAL APPROACH TO pH-DEPENDENT SELF-AGGREGATION OF POLY(2-ISOPROPYL-2-OXAZOLINE)*	39
2.1. Chapter Summary	39
2.2. Introduction	40
2.3. Experimental and Computational Methodology	42
2.3.1. Materials	42
2.3.2. Synthesis of 2-isopropyl-2-oxazoline and poly(2-isopropyl-2-oxazoline)s	42
2.3.3. Instrumentation	43
2.3.4. Computational Details.....	45
2.4. Results and Discussion.....	48
2.4.1. pH-dependent aqueous solution behavior of PIPOX	48
2.4.2. pH-dependent aqueous solution behavior of PIPOX	55
2.4.2.1. Affinity of H ₃ O ⁺ and OH ⁻ to PIPOX and H ₂ O	59
2.4.3. pH-dependent aqueous solution behavior of PIPOX	64
2.4.4. Effect of concentration on the size of PIPOX aggregates	69
2.4.5. Effect of salt concentration on the aqueous solution behaviour of PIPOX	73
2.4.6. Effect of pH on the cloud point temperature of PIPOX.....	75
2.5. Conclusion.....	77

3. EFFECT OF END-GROUP ON DRUG LOADING/RELEASE PROPERTIES OF PIPOX SELF-AGGREGATES	79
3.1. Chapter Summary	79
3.2. Introduction	79
3.3. Experimental	82
3.3.1. Materials	82
3.3.2. Synthesis and Characterization	83
3.3.3. Measurements	84
3.3.4. Preparation of self-aggregates and release from aggregates	85
3.4. Results and Discussion.....	86
3.4.1. Synthesis of PIPOX-OR and PIPOX-CAP.....	86
3.4.2. pH-induced self-aggregation of PIPOX-OR and PIPOX-CAP	92
3.4.3. CAP loading into PIPOX-OR and PIPOX-CAP aggregates	98
3.4.4. CAP release from PIPOX-OR and PIPOX-CAP aggregates.....	104
3.5. Conclusion.....	106
4. EFFECT OF SIDE CHAIN VARIATION ON SURFACE AND BIOLOGICAL PROPERTIES OF POLY(2-ALKYL-2-OXAZOLINE) MULTILAYERS*	109
4.1. Chapter Summary	109
4.2. Introduction	110
4.3. Experimental	111
4.3.1. Materials	111
4.3.2. NMR and GPC measurements.....	112
4.3.3. Synthesis of 2-IPOX, PEOX and PIPOX.....	112
4.3.4. Deposition of multilayers	113

4.3.5. CIP loading and release into/from multilayers	113
4.3.6. Stability of multilayers	114
4.3.7. Static contact angle measurements	115
4.3.8. Bacterial growth conditions	115
4.3.9. Minimum Inhibitory Concentration (MIC) analysis	115
4.3.10. Kirby-Bauer Test.....	116
4.3.11. Agar-Plating Method.....	116
4.3.12. Statistical analysis	117
4.4. Results and Discussion.....	117
4.4.1. Preparation of Multilayers	117
4.4.2. Stability and wettability testing after immersion into PBS	127
4.4.3. CIP release from multilayers	131
4.4.4. Antibacterial properties of multi-layer films of PIPOX/TA and PEOX/TA against E. coli and S. aureus.....	138
4.4.5. Bacterial anti-adhesive properties of multi-layers of PIPOX/TA and PEOX/TA against E.coli and S. aureus	140
4.4.6. Protein adhesion onto PIPOX/TA and PEOX/TA multilayers.....	143
4.5. Conclusion.....	144
5. SYNTHESIS AND CHARACTERIZATION OF PIPOX-DOXYCYCLINE CONJUGATE.....	147
5.1. Chapter Summary	147
5.2. Introduction	147
5.3. Experimental.....	151
5.3.1. Materials	151
5.3.2. Measurements	151

5.3.3. Synthesis and Characterization of Polymers	152
5.4. Results and Discussion.....	154
5.5. Conclusion.....	159
6. CONCLUSION AND OUTLOOK.....	161
APPENDICES	
A. NMR SPECTRA.....	201
B. GPC CHROMATOGRAMS	204
CURRICULUM VITAE	207

LIST OF TABLES

TABLES

Table 2.1. Interaction energies (eV) for pairwise and ternary interactions of PIPOX with H ₂ O, H ₃ O ⁺ and OH ⁻	59
Table 2.2. Ideal, vdW, electrostatic and total free energy of solvation.	63
Table 2.3. FH interaction parameters (χ) and mixing energies (E _{mix} , kcal/mol) calculated based on binding energies (E _{i-i} , E _{i-j} , E _{j-j}) and coordination numbers (Z _{i-i} , Z _{i-j} , Z _{j-i} , Z _{j-j}) where i is PIPOX and j is terminal group.	67

LIST OF FIGURES

FIGURES

Figure 1.1. Graphical representation of formation of poly(2-isopropyl-2-oxazoline) (PIPOX) self-aggregates.	2
Figure 1.2. Graphical representation of formation of CAP loaded PIPOX self-aggregates and CAP release from PIPOX self-aggregates under acidic pH conditions at 37 °C.....	3
Figure 1.3. Graphical representation of bacterial and protein anti-adhesive characteristics and anti-bacterial activity of PEOX/TA and PIPOX/TA multilayers..	5
Figure 1.4. Graphical representation of formation of PIPOX-doxycycline (PIPOX-hyd-DOXY) conjugate with hydrazone linker and hydrazone bond cleavage at acidic conditions	5
Figure 1.5. General chemical structure of poly(2-alkyl-2-oxazoline)s.....	6
Figure 1.6. Chemical structures of antimicrobial PAOXs with various distal and satellite groups.....	14
Figure 1.7. (A) Schematic representation of conformation of PAOXs below and above its LCST (adapted from Shakya and Nandakumar [137] with slight modification). (B) LCSTs of various PAOXs.	24
Figure 1.8. Reversible protonation of PAOX at pH below its pKa	26
Figure 1.9. (A): Schematic representation of the association of PAOX chains via hydrophobic interactions. (B): Schematic representation of water mediated hydrogen bonding interactions and associations among PAOX chains and water.	29
Figure 1.10. Schematic representation of H-bonded multilayers of PAOX have been constructed via H-bonding interactions between H-acceptor PAOX and any H-donor polymer	35
Figure 2.1. A) Evolution of hydrodynamic diameter of PIPOX as a function of pH. (B) The size distribution by number of PIPOX at pH 4.5 and pH 7.5. Right direction arrow denotes the shift in size distribution to higher values. Size distribution curves obtained from several individual measurements of the same sample are represented	

with different colors. (C) SEM images and the size distribution of PIPOX aggregates at pH 7.5 and 25 °C. The size distribution curve is prepared out of 40 different measurements.	50
Figure 2.2. Intensity average size distributions of PIPOX at pH 4.5 and pH 7.5.....	51
Figure 2.3. Hydrodynamic size distributions of PIPOX in 0.2 mg/mL solution at 25 °C via increasing and then decreasing pH. Size distribution curves obtained from several individual measurements of the same sample are represented with different colors.....	52
Figure 2.4. The change in number average hydrodynamic diameter of poly(2-ethyl-2-oxazoline) (PEOX) with increasing pH.	53
Figure 2.5. Emission spectra of pyrene in the absence of PIPOX and in the presence of PIPOX at pH 2.5 and pH 7.5. Inset shows the pH-dependent change in I ₁ /I ₃ ratio in the absence and presence of PIPOX with a final concentration of 0.2 mg/mL. I ₁ and I ₃ are fluorescence intensities at 372 nm and 383 nm, respectively.....	55
Figure 2.6. Potentiometric titration curve and its first derivative for PIPOX.	56
Figure 2.7. Evolution of zeta potential with increasing pH of the PIPOX solution. .	57
Figure 2.8. Lowest energy structures of A) PIPOX-H ₃ O ⁺ , B) PIPOX-OH ⁻ , C) PIPOX-H ₃ O ⁺ -H ₂ O and PIPOX-H ₂ O-H ₃ O ⁺ , D) PIPOX-OH ⁻ -H ₂ O and PIPOX-H ₂ O-OH ⁻ . Oxygen: red, carbon: grey, hydrogen: white, nitrogen: blue in color. PIPOX backbone atoms are shown by yellow in color	58
Figure 2.9. A) Initial and C) final structures of PIPOX-H ₂ O-H ₂ O-H ₃ O ⁺ system. B) Initial and D) final structures of PIPOX-OH ⁻ -H ₂ O-H ₂ O system. PIPOX-H ₂ O-H ₂ O-H ₃ O ⁺ is PIPOXH ⁺ -H ₂ O-H ₂ O-H ₂ O in its geometry optimized final structure, while PIPOX-OH ⁻ -H ₂ O-H ₂ O is in PIPOX-H ₂ O-OH ⁻ -H ₂ O form in final structure.....	62
Figure 2.10. Structure of PIPOXH ⁺ decamer with one protonated monomer and 600 water molecules under periodic boundary conditions, constructed for the free energy solvation calculations.....	63
Figure 2.11. The number average hydrodynamic size distributions of PIPOX terminated with 2-butanol (A) and N-boc-amino-piperidine (B) at pH 5.5. Size	

distribution curves obtained from several individual measurements of the same sample are represented with different colors.....	65
Figure 2.12. Evolution of hydrodynamic diameter of PIPOX and PIPOX-N-Boc-amino-piperidine with increasing pH in 0.2 mg/mL solution.	66
Figure 2.13. Structures of PIPOX dimers terminated with 2-butanol (A) and N-boc-amino-piperidine (B). Backbone is shown by yellow color.....	68
Figure 2.14. Free energy of interaction between PIPOX trimer and PIPOX dimer terminated with 2-butanol and N-boc-amino-piperidine end groups for different mole fractions.....	69
Figure 2.15. Number average hydrodynamic size distributions of PIPOX at pH 2.5 and pH 7.5 in 0.2 mg/mL, 0.6 mg/mL and 1 mg/mL solutions. Size distribution curves obtained from several individual measurements of the same sample are represented with different colors.	70
Figure 2.16. SEM images of PIPOX at pH 2.5 and pH 7.5 at 0.2 mg/mL, 0.6 mg/mL and 1.0 mg/mL concentration.....	71
Figure 2.17. A) Emission spectra of pyrene in the absence of PIPOX and in the presence of PIPOX with a final concentration of 0.2 mg/mL, 0.6 mg/mL or 1 mg/mL. (B) pH-dependent change in I_1/I_3 ratio of pyrene in the absence and presence of PIPOX with a final concentration of 0.2 mg/mL, 0.6 mg/mL and 1 mg/mL. I_1 and I_3 are fluorescence intensities at 372 nm and 383 nm, respectively.	72
Figure 2.18. Hydrodynamic size of PIPOX in 0.01 M (\square) or 0.1 M (\circ) phosphate buffer with increasing pH.....	73
Figure 2.19. The change in absorbance at 450 nm as a function of temperature for (A) 10 mg/mL PIPOX solution at pH 2.5 and (B) 10 mg/mL PIPOX solution whose pH was increased from 2.5 to 7.5.....	76
Figure 3.1. $^1\text{H-NMR}$ spectrum of PIPOX-CAP in CDCl_3	90
Figure 3.2. SERS spectra of (A) PIPOX-OR, (B) PIPOX-CAP and (C) CAP.	91
Figure 3.3. (A) Evolution of hydrodynamic diameter of PIPOX-OR and PIPOX-CAP in 10mM phosphate buffer with increasing pH at 25 °C. (B) Size distribution curves of PIPOX-OR and PIPOX-CAP by number at pH 7.5. Size distribution curves	

obtained from several individual measurements of the same sample are represented with different colors.....	94
Figure 3.4. Zeta potential changes for PIPOX-OR and PIPOX-CAP in 0.2 mg/mL via increasing pH.....	95
Figure 3.5. The evolution of hydrodynamic diameter of PIPOX-OR (A) and PIPOX-CAP (B) as a function of decreasing pH at 37 °C. Evolution of hydrodynamic diameter with increasing pH at 25 °C is plotted for comparison.	97
Figure 3.6. The hydrodynamic size distribution curves of PIPOX-OR (left) and PIPOX-CAP (right) with decreasing pH at 37 °C.	98
Figure 3.7. Comparison of the hydrodynamic size of PIPOX-CAP in 0.1 mg/mL CAP solution and in 10 mM phosphate buffer at pH 7.4 (A). Hydrodynamic size distributions of PIPOX-OR in 0.1 mg/mL CAP solution and in 10 mM phosphate buffer at pH 7.4 (B) are shown for comparison.....	101
Figure 3.8. SEM images of (A) PIPOX-OR aggregates in 10 mM phosphate buffer (left), in 0.1 mg/mL CAP solution (right), and (B) PIPOX-CAP aggregates in 10 mM phosphate buffer (left), in 0.1 mg/mL CAP solution (right) at pH 7.5.....	102
Figure 3.9. Normalized CAP-loading efficacies of PIPOX-OR and PIPOX-CAP self-aggregates. Normalized values were calculated by dividing the absorbance of CAP-loaded PIPOX-OR and CAP-loaded PIPOX-CAP to the absorbance of CAP at 220 nm.	103
Figure 3.10. A) CAP release profile from PIPOX-OR aggregates at pH 7.5/25 °C; pH 7.5/37 °C; pH 5.0/25 °C and pH 5.0/37 °C. (B) CAP release profile from PIPOX-CAP aggregates at pH 7.5/25 °C; pH 7.5/37 °C; pH 5.0/25 °C and pH 5.0/37 °C. (C) Comparison of the total CAP amount released from PIPOX-OR and PIPOX-CAP aggregates at pH 7.5/25 °C; pH 7.5/37 °C; pH 5.0/25 °C and pH 5.0/37 °C after 24 hours. (D) Comparison of relative % release from PIPOX-OR and PIPOX-CAP aggregates at pH 7.5/25 °C; pH 7.5/37 °C; pH 5.0/25 °C and pH 5.0/37 °C. Relative % release were calculated.....	105
Figure 3.11. The hydrodynamic size distribution curves of PIPOX-OR (A) and PIPOX-CAP (B) with decreasing pH at 25 °C.	106

Figure 4.1. (A) Chemical structures of PAOXs, TA and CIP. (B) LbL growth of PIPOX/TA (square) and PEOX/TA(circle) films at pH 2.5 and 25 °C. Multilayers were deposited onto BPEI/TA precursor layers with a thickness of 4.7 nm. Thickness values do not include the precursor thickness. 119

Figure 4.2. A) AFM topography images of 13 layers of PEOX/TA and PIPOX/TA. Roughness values were recorded from images with 2x2 μm^2 scan size. (B) Evolution of static contact angle of PEOX/TA (\circ) and PIPOX/TA (\square) films as a function of layer number. Multilayers were deposited onto BPEI/TA precursor layers. Odd layer numbers correspond to PEOX or PIPOX topmost layer. 121

Figure 4.3. AFM topography images of (A) 7-layer PEOX/TA and PIPOX/TA films with 2x2 μm^2 scan size. Roughness values were recorded from images with 2x2 μm^2 scan size. (B) AFM topography images of 1-layer of TA with 5x5 μm^2 scan size. 122

Figure 4.4. UV-Visible spectra of (A) TA in 10 mM phosphate buffer at pH 2.5 and (B) CIP in 10 mM phosphate buffer at pH 7.4. Concentrations of TA and CIP were both 0.001 mg/mL..... 124

Figure 4.5. UV-Visible spectra of 49-layer PEOX/TA (Panel A) and PIPOX/TA (Panel B) films coated on both sides of quartz substrates before (solid-line) and after CIP loading (dash-line). 125

Figure 4.6. AFM topography (1 μm x 1 μm) images of 13-layer PEOX/TA and PIPOX/TA films before and after CIP loading. Roughness values were recorded from images with 2x2 μm^2 scan size. 127

Figure 4.7. Fraction retained at the surface of 13-layer unloaded (A) and CIP loaded (B) PEOX/TA (circles) and PIPOX/TA (squares) films as a function of time after immersed into PBS at pH 7.4/25 °C or pH 7.4/37 °C. Fractions were calculated by normalizing the thickness values to the initial thickness of the films. 129

Figure 4.8. Normalized absorbance values at 215 nm for unloaded (A) and CIP-loaded (B) 49-layer PEOX/TA and PIPOX/TA films (coated on both sides of quartz substrates) as a function of time after immersed into PBS at pH 7.4/25 °C or pH 7.4/37 °C. Normalized absorbance values were calculated by normalizing the absorbance of the films at 215 nm to the initial absorbance at 215 nm. 130

Figure 4.9. Static contact angle measurements of 3- and 7- layer PEOX/TA and PIPOX/TA films before and after immersion into PBS at pH 7.4/37 °C.....	131
Figure 4.10. Fraction retained at the surface of CIP loaded 13-layer PEOX/TA and PIPOX/TA films as a function of time after immersed into PBS at pH 6.0/25 °C (A) and pH 6.0/37 °C (B). Fractions were calculated by normalizing the thickness values to the initial thickness of the films.....	132
Figure 4.11. (A) Amount of CIP released from 49-layer PIPOX/TA and PEOX/TA films (deposited onto 1 cm x 1 cm glass substrates) at pH 7.4/25 °C, pH 7.4/37 °C, pH 6.0/25 °C and pH 6.0/37 °C after 24 hours. (B) % release of CIP from 49-layer PIPOX/TA and PEOX/TA films at pH 7.4/25 °C, pH 7.4/37 °C, pH 6.0/25 °C and pH 6.0/37 °C after 24 hours.	135
Figure 4.12. Concentration of CIP released from 49-layer (A) PEOX/TA and (B) PIPOX/TA films (deposited onto 1 cm x 1 cm glass substrates) at pH 7.4/37 °C; pH 6.0/37 °C; pH 7.4/25 °C and pH 6.0/25 °C as a function of time.....	136
Figure 4.13. AFM height (1µm x 1µm) images of 13-layer PIPOX/TA and PEOX/TA films before and after CIP release at pH 6.0 and 37 °C. Roughness values were recorded from images with 2x2 µm ² scan size.....	138
Figure 4.14. Kirby-Bauer test from CIP-loaded PIPOX/TA and PEOX/TA multilayers (coated onto glass substrates) against E.coli and S.aureus at pH 6.0/25 °C; pH 7.4/25 °C; pH 6.0/37 °C and pH 7.4/37 °C. Uncoated sterile glass substrates were used as control substrates.	139
Figure 4.15. Number of colonies on 3- and 7-layer PIPOX/TA and PEOX/TA films (coated onto glass substrates) after 1 hour incubation at pH 7.4 with E.coli and S. aureus. Uncoated sterile glass substrates were used as control substrates. (*P<0.05, **P<0.005, ***P<0.0005, ****P<0.0001 and ns= not significant).....	142
Figure 4.16. AFM height (1µm x 1µm) images and surface roughness of 3- and 13-layer PEOX/TA films. Roughness values were recorded from images with 2x2 µm ² scan size.	143
Figure 4.17. Evolution of film thickness upon BSA deposition at pH 7.4 and 37 °C. Dark and light grey parts correspond to the initial thickness and increment in film	

thickness upon BSA adsorption, respectively. Uncoated silicon wafer was used as control.	144
Figure 5.1. ¹ H-NMR spectra of (A) N-Boc-L cysteine methyl ester functionalized PIPOX, (B) PIPOX-hyd-DOXY. (C) Thin layer chromatograms of (1) PIPOX-NHNH ₂ , (2) PIPOX-hyd-DOXY, (3) DOXY and (4) NH ₂ NH ₂ ; DOXY and PIPOX-hyd-DOXY, demonstrating fluorescence under 366 nm. (D) GPC chromatogram of N-Boc-L cysteine methyl ester functionalized PIPOX. ¹ H-NMR samples were dissolved in deuterated DMSO159	159
Figure A 1. ¹ H-NMR of 2-isopropyl-2-oxazoline.	201
Figure A 2. ¹ H-NMR of α -bromo- ω -2-butoxy-PIPOX.....	202
Figure A 3. ¹ H-NMR of α -bromo- ω -N-boc-aminopiperidine-PIPOX.....	202
Figure A 4. ¹ H-NMR spectra of Chloramphenicol (CAP)	203
Figure B 1. GPC traces of α -bromo- ω -2-butoxy-PIPOX.....	204
Figure B 2. GPC traces of α -bromo- ω -N-boc-aminopiperidine-PIPOX.	204
Figure B 3. GPC chromatogram of poly (2-isopropyl-2-oxazoline)-chloramphenicol (PIPOX-CAP) conjugate.....	205
Figure B 4. GPC traces of poly(2-ethyl-2-oxazoline) (PEOX).	205

LIST OF SCHEMES

SCHEMES

Scheme 1.1 Schematic representation of synthesis of 2-alkyl-2-oxazolines via Witte-Seeliger reaction (Adapted from Witte et al. with slight modification[27]).	7
Scheme 1.2 General scheme of cationic ring-opening polymerization of 2-alkyl-2-oxazolines including initiation, propagation and termination steps (Adapted from Becer et al. with slight modification[46]).	9
Scheme 1.3 Representative end-group PEG-bioactive agent conjugate via PEG modification (Adapted from Abuchowski et al. with slight modification[92]).	16
Scheme 1.4 Schematic representation of LbL self-assembly technique (A) and common driving molecular associations to be used for LbL multilayer film construction (B).	32
Scheme 2.1 Chemical structure of PIPOX.	49
Scheme 3.1 Synthesis of PIPOX-OR and PIPOX-CAP by direct termination methodology and the reaction mechanism for the CROP of 2-alkyl-2-oxazoline.	88
Scheme 3.2 Schematic illustration of the molecular interactions of PIPOX and CAP.	99
Scheme 4.1. Schematic representation of CIP release from PEOX/TA and PIPOX/TA multilayers at pH 6.0 and 37 °C.	137
Scheme 5.1 Synthesis routes of ester functionalized PIPOX precursor via termination of CROP of 2-IPOX.	155

LIST OF ABBREVIATIONS

AFM	Atomic force microscopy
Ag NPs	Silver nanoparticles
AmB	Amphotericin B
ATRP	Atom transfer radical polymerization
Boc	<i>tert</i> -Butyloxycarbonyl
BPEI	Branched poly(ethylene imine)
BSA	Bovine serum albumin
CAP	Chloramphenicol
CIP	Ciprofloxacin
COMPASS	Condensed phase optimized molecular potentials for atomistic simulation studies
CP	Cloud point
CROP	Cationic Ring Opening Polymerization
DDA	N,N-dimethyl dodecylamine
DDA-X	N,N-dodecyl trimethyl ammonium
DFT	Density functional theory
DI water	Deionized water
DLS	Dynamic light scattering
DMF	Dimethyl formamide
DOX	Doxorubicine
DOXY	Doxycycline
DSPE	Distearoylphosphatioly ethanolamine

E.coli	Escherichio coli
EDA	Ethylene diamine
FDA	Food and Drug Administration
GPC	Gel permeation chromatography
GS	Ground state
H-acceptor	Hydrogen-acceptor
H-bonded	Hydrogen-bonded
H-bonding	Hydrogen-bonding
H-donor	Hydrogen-donor
IPOX	2-isopropyl-2-oxazoline
LB broth	Luria Bertoni broth
LbL	Layer-by-layer
LCST	Lower critical solution temperature
MH broth	Mueller-Hinton broth
NMR	Nuclear magnetic resonance
PAA	Poly (acrylic acid)
PAOX	Poly(2-alkyl-2-oxazoline)
PBS	Phosphate buffer saline
PcPOX	Poly(2-cyclo-propyl-2-oxazoline)
PEG	Poly(ethylene glycol)
PEG-PLA	Poly(ethylene glycol)-co-poly(lactic acid)
Pen G	Penicilline G

Pen V	Penicilline V
PEO	Poly(ethylene oxide)
PEO-PAGE	Poly(ethylene oxide)-b-poly(allyl glycidyl ether)
PEOX	Poly(2-ethyl-2-oxazoline)
PEOX- <i>hyd</i> -DOX	Poly(2-ethyl-2-oxazoline) Doxorubicin conjugate with hydrazone bond
PIPOX	Poly(2-isopropyl-2-oxazoline)
PIPOX-CAP	Chloramphenicol end-capped Poly(2-isopropyl-2-oxazoline)
PIPOX- <i>hyd</i> -DOXY	Poly(2-isopropyl-2-oxazoline) Doxycycline conjugate with hydrazone bond
PIPOX-OR	2-Butoxy end-capped Poly(2-isopropyl-2-oxazoline)
PLGA-DOX	Poly(DL-lactic-co-glycolic acid)-doxorubicin conjugate
PMEOX	Poly(2-methyl-2-oxazoline)
PNIPAM	Poly(N-isopropyl acrylamide)
PnPOX	Poly(2-n-propyl-2-oxazoline)
RAFT	Reversible addition fragmentation chain transfer
R_f	Retardation factor
RI	Refractive index

S.aureus	Staphylococcus aureus
SEM	Scanning electron microscopy
SERS	Surface enhanced raman spectroscopy
TA	Tannic acid
TLC	Thin layer chromatography
vdW	Van der Waals
α -BIBB	α -bromo isobutyrylbromide

CHAPTER 1

INTRODUCTION

1.1. Goals and Objectives

Poly(2-alkyl-2-oxazoline)s (PAOXs) are hydrophilic polymers demonstrating non-toxicity, biocompatibility, high chemical stability and stealth behavior [1–5]. Short-alkyl pendant chain containing derivatives have been widely pronounced by their response toward temperature, so called "temperature-responsive behavior" [2,6–17]. Temperature trigger can be induced either internally or externally that lead to a change in conformation of the temperature responsive polymer. PAOXs with short-alkyl pendant chain are known to exhibit lower critical solution temperature (LCST)-type phase behavior in aqueous media [2].

This dissertation aimed:

- i) investigation of the effect of pH in aqueous solution behavior of PAOXs;
- ii) investigation of the effect of PAOX end group on loading/release behaviour of pH-responsive PIPOX aggregates;
- iii) investigation of the effect of side chain variation on layer-by-layer self-assembly of PAOXs and surface and biological properties of PAOX multilayers;
- iv) investigation of synthesis of PIPOX-antibiotic conjugate with labile hydrazone linkage.

1.2. Summary of thesis

The study presented in Chapter 2 aimed understanding the effect of pH on aqueous solution behaviour of PIPOX. For the first time, pH-induced formation of well-

distributed spherical PIPOX self-aggregates in aqueous environment was explored (Figure 1.1). PIPOX solution was prepared at acidic pH and titrated with NaOH solution. It was found that, above pH 5, self-association of PIPOX enhanced resulting in formation of PIPOX aggregates. The mechanism of self-association is explained by unprotonation of amide units as the pH was increased resulting in a decrease in electrostatic repulsion among PIPOX chains and enhanced hydrophobic association among PIPOX chains. The mechanism of pH-induced self-aggregation was further explored using density functional (DFT) methods in collaboration with Dr. Erol Yildırım (Institute of High Performance Computing, Agency for Science, Technology and Research (A*STAR)). Moreover, the effect of PIPOX and salt concentration as well as end-group moiety on self-association of PIPOX and size of PIPOX aggregates have been examined. It was found that increasing salt concentration at acidic pH also induced formation of PIPOX aggregates through acting like a bridge between the protonated amide units of PIPOX. Finally, the effect of formation of pH-induced PIPOX aggregates on cloud point temperature of PIPOX was explored. The cloud point of PIPOX was detected at 42 °C at acidic pH, whereas it was found as 37 °C in the presence of PIPOX aggregates.

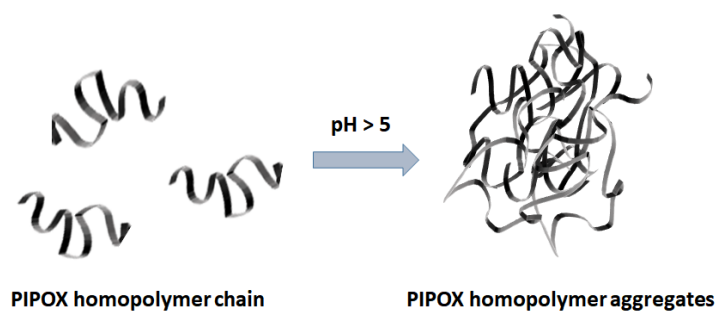


Figure 1.1. Graphical representation of formation of poly(2-isopropyl-2-oxazoline) (PIPOX) self-aggregates.

The study presented in Chapter 3 aimed to understand the effect of PIPOX end-group on loading capacity and release profile of a model antibiotic, Chloramphenicol (CAP) into/from pH-responsive PIPOX aggregates. In this context, PIPOX was permanently

conjugated with CAP to obtain PIPOX-CAP conjugate. For comparison, PIPOX terminated using 2-Butanol (PIPOX-OR) was also prepared. Self-aggregation of PIPOX-OR and PIPOX-CAP was triggered via increasing pH in 10 mM phosphate buffer (prepared using $\text{NaH}_2\text{PO}_4 \cdot 2\text{H}_2\text{O}$) and CAP solution. The size of both PIPOX-OR and PIPOX-CAP aggregates were found to be similar in phosphate buffer. On the other hand, PIPOX-CAP formed larger self-aggregates in CAP solution compared to PIPOX-OR. The reason for the formation of larger aggregates can be explained by enhanced association among PIPOX chains owing to CAP end-groups. Free CAP molecules possibly provided greater association among higher number of chains through interaction with CAP end-groups leading to formation of larger aggregates. Furthermore, the effect of polymer end group on CAP loading and release profiles of PIPOX self-aggregates was examined under acidic pH conditions at a physiologically related temperature (Figure 1.2). Maximum amount of CAP released from both types of aggregates at slightly acidic pH and 37 °C due to disintegration of self-aggregates at mild acidic environment and temperature-induced conformational transition of PIPOX from extended to globular form. The amount of CAP released from PIPOX-CAP self-aggregates was higher than that from PIPOX-OR at all conditions due to higher CAP loading capacity of PIPOX-CAP aggregates.

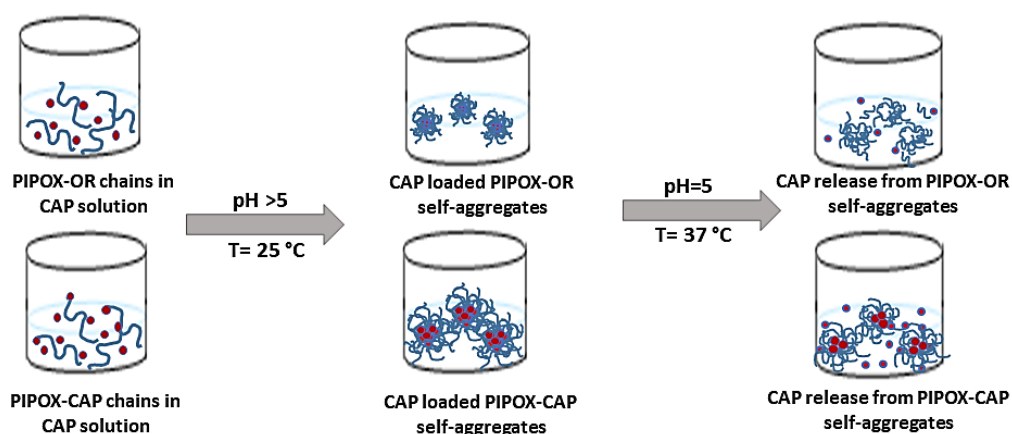
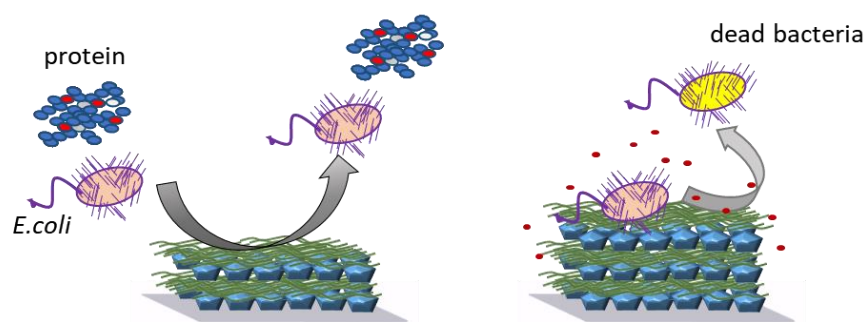


Figure 1.2. Graphical representation of formation of CAP loaded PIPOX self-aggregates and CAP release from PIPOX self-aggregates under acidic pH conditions at 37 °C.

The study presented in Chapter 4 aimed to explore the effect of side chain variation on surface and biological properties of PAOX multilayers. In this context, multilayer films of PIPOX and poly (2-ethyl-2-oxazoline) (PEOX) were prepared at acidic conditions (pH 2.5) using LbL self-assembly technique. The driving force for multilayer growth was hydrogen bonding interactions between the phenolic hydroxyl groups of TA and carbonyl groups of PEOX or PIPOX. PAOX multilayers were contrasted with respect to their surface properties. It was found that surface properties such as thickness, roughness, wettability and stability of multilayers were affected by the chemical nature of PAOX side chain, phase behaviour of PAOX and the binding strength between the layers. Ciprofloxacin (CIP) which is a wide-spectrum antibiotic, was loaded into multilayers at neutral conditions (pH 7.4) via post-loading approach through mainly electrostatic interactions between free ionized phenolic hydroxyl groups of TA and protonated piperiziny amino group of CIP together. CIP release from multilayers were examined at pH 6.0, pH 7.4 and 25 °C, 37 °C. At 25 °C, all PAOX multilayers showed pH-responsive release of CIP at varying amounts at neutral and moderately acidic pH. At 37 °C, PAOX multilayers released remarkably different amounts of CIP at moderately acidic pH. The difference in the amount of CIP released from multilayers was correlated with the difference in the phase behaviour of PAOXs at 37 °C. Finally, surface morphology, stability, wettability and stimuli-responsive drug release properties of the films were correlated with anti-adhesive and antibacterial properties of the surfaces (Figure 1.3). PEOX/TA multilayers were found to be highly anti-adhesive against *Escherichia coli* (*E.coli*) and bovine serum albumin (BSA) due to higher wettability of PEOX/TA films compared to PIPOX/TA multilayers. Antibacterial activity of multilayers were examined using Kirby-bauer method against Gram (-) *E.coli* and Gram (+) *Staphylococcus aureus* (*S. aureus*). Results obtained from release experiments were in good agreement with the antibacterial activity of the surfaces against *S.aureus*. Although the amount of CIP released from different PAOX multilayers were different, all films showed antibacterial activity against *E.coli*.



Poly(2-ethyl-2-oxazoline)/Tannic acid vs Poly(2-isopropyl-2-oxazoline)/Tannic acid multilayers

Figure 1.3. Graphical representation of bacterial and protein anti-adhesive characteristics and antibacterial activity of PEOX/TA and PIPOX/TA multilayers.

The study presented in Chapter 5 aimed synthesizing PIPOX-doxycycline (PIPOX-*hyd*-DOXY) conjugate with acid labile hydrazone linker which can release DOXY at acidic conditions (Figure 1.4). In this respect, methyl thioglycolate, methyl 2-aminobenzoate and N-(*tert*-butoxycarbonyl)-L-cysteine methyl ester functionalized PIPOX precursors were synthesized by directly terminating PIPOX using these three different esters. Then, starting from N-(*tert*-butoxycarbonyl)-L-cysteine methyl ester functionalized PIPOX, hydrazide derivative of PIPOX precursor was synthesized which was then converted into PIPOX-*hyd*-DOXY conjugate through formation of hydrazone linker between PIPOX and DOXY. Precursors and the final conjugate were characterized using $^1\text{H-NMR}$, TLC and GPC.

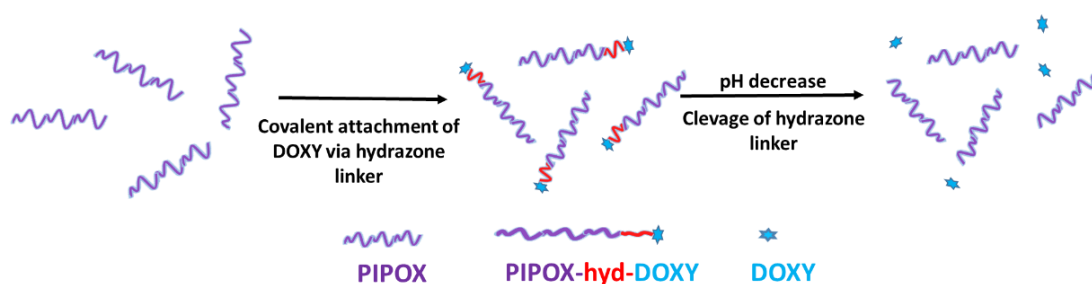


Figure 1.4. Graphical representation of formation of PIPOX-doxycycline (PIPOX-*hyd*-DOXY) conjugate with hydrazone linker and hydrazone bond cleavage at acidic conditions .

1.3. Literature Review

1.3.1. Poly(2-alkyl-2-oxazoline)s

Poly(2-alkyl-2-oxazoline)s (PAOX), also called pseudo-peptides due to structural similarity to peptides (Figure 1.5), are promising materials for biomedical and life-science applications due to their readily availability, low toxicity, precisely controlled chemical structures and physical characteristics, high variety of solubility and tremendous biocompatibility [18–22]. Their popularity has been risen in the last years due to their ability to be indistinguishable by the immune system in living organisms, so called “stealth behavior” [13,23]. Importantly, PAOXs are considered as an alternative to poly(ethylene glycol) (PEG) which is a commonly used polymer in biomedical applications [24]. This is due to higher oxidative stability and interfacial properties of PAOXs than that of PEG. To date, poly(2-ethyl-2-oxazoline) (PEOX) is the only derivative to be approved by Food and Drug Administration (FDA) as food contact mediator. In addition, Phase 1 clinical trials have begun for side-chain drug attached PAOX to be used as therapeutic for Parkinson’s disease treatment. Moreover, various PAOX derivatives are being figured out as flocculants, additives, compatibilizers etc. in many different applications. The striking characteristics of short-alkyl chain PAOXs is thermal responsivity that make them potential candidate to be used in biomedical applications [20,23,25].

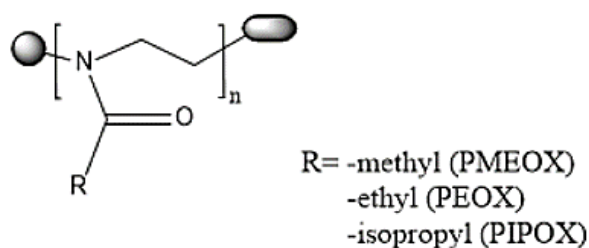
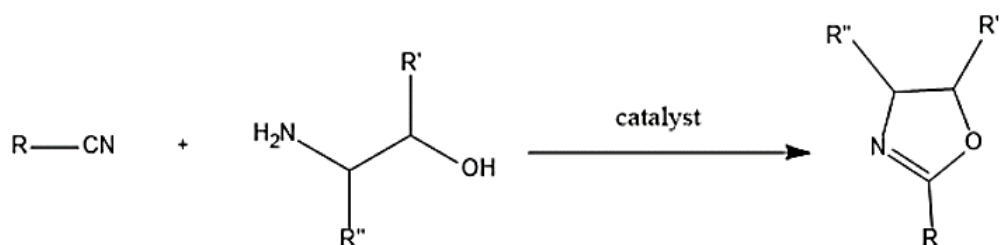


Figure 1.5. General chemical structure of poly(2-alkyl-2-oxazoline)s.

1.3.2. Synthesis of poly(2-alkyl-oxazoline)s

2-alkyl-2-oxazolines are well-known class of 5-membered heterocyclic imino-ethers since 1889 [26]. They become popular after mid 1960's due to their existence in various biologically active intermediates [27–29] or final compounds [30–32], potential to be used as catalysts and ligands [33–35] and as monomers in cationic ring opening polymerization (CROP) [13,35–39]. Various derivatives of 2-alkyl-2-oxazolines were obtained by following various chemical routes such as catalytic isomerization reaction of N-acylethylenimines precursor prepared from acyl chlorides and ethyleneimine by Achotten-Baumann reaction [40], sulfuric acid catalyzed cyclodehydration of N-hydroxyethylamides [41], base catalyzed cyclodehalogenation of N-chloroethylamides [41] and nucleophilic attachment of existing 2-oxazoline to organohalogen compound [42]. Furthermore, one-pot basic synthesis of 2-alkyl-2-oxazolines has been achieved with higher conversions *via* Witte-Seeliger reaction starting from nitriles and aminoalcohols in presence of Lewis acid catalyst [43–45] (Scheme 1.1). Wide commercial availability of various nitriles and aminoalcohols makes this method preferable for preparation of different 2-alkyl-2-oxazoline derivatives.

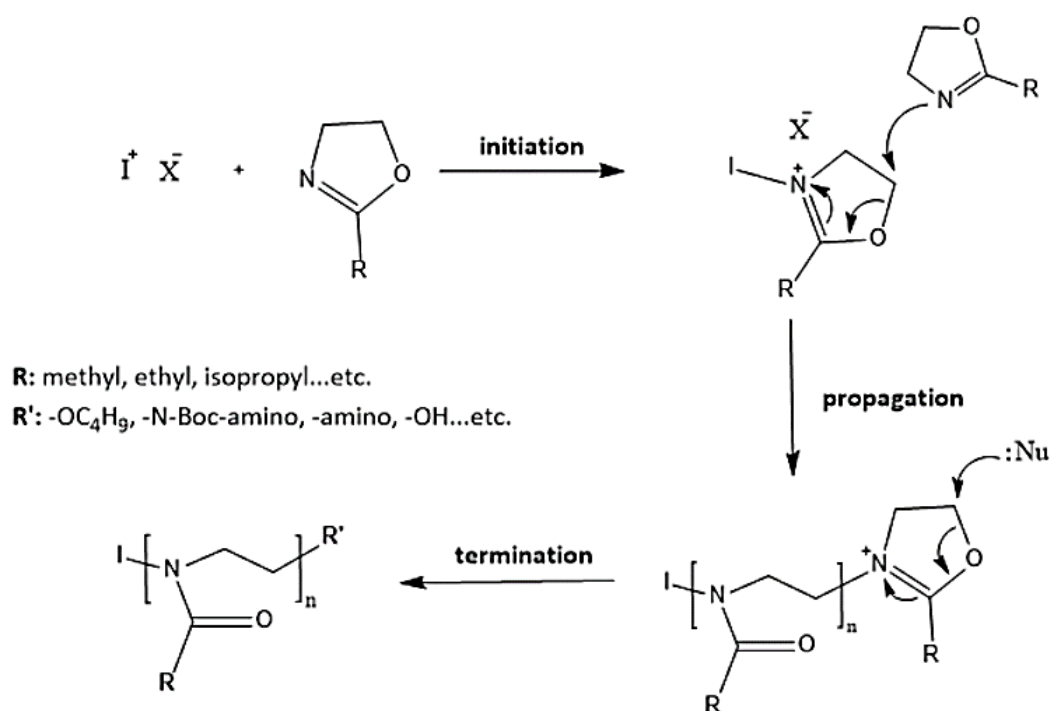


Scheme 1.1 Schematic representation of synthesis of 2-alkyl-2-oxazolines via Witte-Seeliger reaction (Adapted from Witte et al. with slight modification[27]).

2-alkyl-2-oxazolines was converted into polymers including N-acylethylenimine repeating units in presence of cationic initiators that are strong acids or their esters or anhydrides or even Friedel-Crafts type complexation agents (i.e. sulfuric acid, alkyl

iodides, iodine, p-toluenesulfonicbenzoic anhydride and p-toluene sulfonate or perchlorate derivatives) [41,46–48]. Nowadays, CROP of 2-alkyl-2-oxazolines have been carried out mostly using alkyl tosylates, triflates, alkyl, benzyl or acetyl halides as initiator [25,49–53]. Moreover, functional initiators that do not possess nucleophilic character could also be used in CROP [54].

Polymerization mechanism contains three steps; initiation, propagation and termination. The attack of unpaired electrons of nitrogen of 2-alkyl-2-oxazoline monomer onto the electrophilic part of initiator initiates the polymerization and results in formation of oxazolinium cation. Afterwards, polymerization propagates by the attack of inactive monomer molecule to the cationic oxazolinium intermediate proceeding with the formation of PAOX backbone with amide functionality *via* ring-opening. During propagation, living oxazolinium chain-end is still intact that allows the achievement of polymer with desired molecular weight up to termination. In an ideal polymerization, chain coupling and chain transfer reactions are not pronounced so living character of the CROP is preserved. Unlike the ideal case, chain transfer or coupling reactions are the main termination reactions occurring under reaction conditions and they are undesired when high molecular weight polymers are needed (Scheme 1.2). Living nature of the cationic ring opening polymerization could be explicitly terminated to attach various functional units to ω -chain end [55–57]. Water and sodium hydroxide are the mainly used terminating agents to leave hydroxide at the chain terminus [7,58–60]. In termination step, nucleophilic addition of the terminating agent to the living chain end takes part in. By use of strong nucleophiles like methanolic sodium hydroxide, amines, carboxylates, termination occurs on the 5-position of the activated oxazolinium intermediate while in case of using weak nucleophiles such as water, termination arises on the 2-position of the activated intermediate. ω -chain end functionalization has been achieved *via* attachment of oxygen, nitrogen, carbon and sulphur centered nucleophiles.



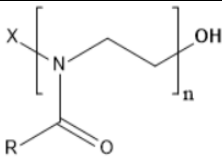
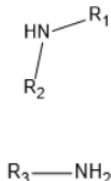
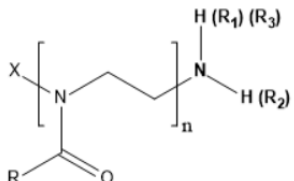
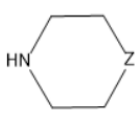
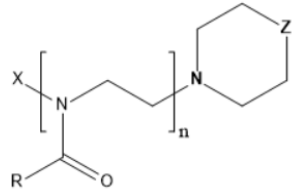
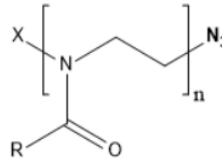
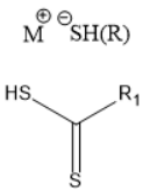
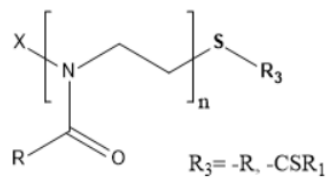
Scheme 1.2 General scheme of cationic ring-opening polymerization of 2-alkyl-2-oxazolines including initiation, propagation and termination steps (Adapted from Becer et al. with slight modification[46]).

Moreover, the use of well-purified initiator, monomer and solvent are needed to achieve PAOX with narrow molecular weight distribution because any impurity or traces of moisture prompt the chain transfer and termination reactions [25,41,61,62]. Recently, Hoogenboom and Monnery published a patent reporting the synthesis of PAOX with well-defined molar mass using special vacuum techniques and low temperatures which eliminates the probable side reactions [63].

The termini being converted to different functional moieties could be desirable to reach PAOX telecheletics be used in various applications. By this point of view, aliphatic [50,64,65] or cyclic [49,66–70] amines, azides [71,72] and thiols [73,74] are convenient alternatives to be used for end group modification (Table 1.1). In last ten years, bioactive molecules have been coupled with PAOXs *via* either permanent conjugation of therapeutics with nucleophilic sides in termination step of CROP (non-

released strategy) [75,76] or *via* labile attachment of therapeutics to PAOXs by modification of termini (labile attachment strategy) [77].

Table 1. 1. Terminating agents to be mostly used in CROP of 2-alkyl-2-oxazolines and the resultant structures of poly(2-alkyl-2-oxazoline)s.

Terminating agent	Resulting PAOX	Ref #
H ₂ O and NaOH		42-45
		34,49,50
 Z = -CH ₂ , -NH, -NR		33,51-55
NaN ₃		56,57
	 R ₃ = -R, -CSR ₁	58,59

1.3.3. Biologically active PAOX derivatives

In general, biologically active polymers are described as polymers with antimicrobial functionalities in their structures providing them superior intrinsic characteristics compared to their small-molecule counterparts. They show (i) long-lasting physical/chemical stability and enhanced activity against bacteria/fungi possessing high number of bioactive groups [78–81], (ii) nontoxicity or lower toxicity to healthy tissue [78–80,82,83], (iii) longer shelf-life [79,81], (iv) possible contact killing ability against bacteria [79,82], (v) lower cost compared to advanced bioactives such as antibiotic peptides [78], (vi) easy purification [81], (vii) non-volatility [80–83] and (viii) lower possibility of development of multi-drug resist bacterial species [78–80]. In addition, polymeric systems can be equipped with various biofunctional groups to be gained synergistic effects and promising combinations [79,83,84].

Bioactive polymeric systems are classified as, therapeutic polymers, polymeric therapeutics, therapeutic releasing polymers. Therapeutic polymers intrinsically display therapeutic characteristics. Lacking of release of harmful biocides to the environment make those polymers advantageous [78,85]. On the other hand, polymeric therapeutics include therapeutic attached to their structure with uncleavable bond (permanant conjugation of therapeutics). In this type, the shielding of the activity of biocides by polymeric backbone due to steric effects and deactivation of biocidal function in presence of any contamination predominate [86]. Different from those, therapeutic releasing polymers are loaded or temporarily linked (labile conjugation) with biocides and upon external or internal trigger, the bioactive is released from the system *via* cleavage of the linkage. Toxicity and development of resistant microorganisms are significant problems for this type as high amounts of biocides released at once [85,86].

1.3.3.1. Therapeutic PAOXs

Therapeutic polymers, that are mainly antimicrobials, display common functionalities in their structure which determine their antibacterial activity. They are amphiphilic in nature with various hydrophilic and hydrophobic segments, amine functionality and intrinsically antimicrobial groups on side chains [78,87,88]. Polycations, mostly possessing quarternary ammonium, phosphonium, or tertiary sulfonium groups and primary/tertiary amino groups, are reported as one of the most effective macrobiocides due to their tendency to cooperate with the negatively charged phospholipid membrane of the bacterial cell which enhance the interaction and contact-killing ability [89,90]. In addition to this biocidal functionalities, the satellite groups-groups with no intrinsic biocidal activity but enhance the antimicrobial activity of polymer *via* interacting with antibacterial end have been examined. It has been shown that, nonactive group distal to the antibacterial end of the polymer has major effect on the antibacterial activity of the whole polymer [79,82,91].

In the last fifteen years, many studies published on antimicrobial PAOXs. Waschinski et. al. reported the synthesis of poly(2-alkyl-1,3-oxazoline)s end capped with N,N-dimethyldodecylamine(DDA) with different alkyl, aminoalkyl, and polyphenyloxazoline satellite groups. They obtained 2-3 times higher antimicrobial activity with polymers possessing 4–10 carbon alkyl chain satellites against *Staphylococcus aureus* (*S. aureus*) and *Escherichia coli* (*E.coli*) compared to low molecular weight biocide counterparts [92]. Same group also synthesized poly(2-alkyl-1,3-oxazoline)s with quarternary ammonium groups at the chain end. They compared the antibacterial activity of polymer with various α -end functionality (the functionality coming from the initiator) together with the DDA terminal moiety and they concluded that α -end group has significant impact on the antibacterial characteristics of ω -end capping [91]. Three years later, same researchers compared three different poly(2-methyl-2-oxazoline) (PMEOX) derivatives with DDA end group and methyl, decyl and hexadecyl satellite groups with respect to antimicrobial activity. They found that variety of interactions between polymers and phospholipid

membranes indicated the different antimicrobial function of polymers [93]. Recently, Fik et. al. presented a work on the synthesis and examination of antimicrobial activity of PMEOX with various satellite groups such as hydroxy, amino and double bond-including moieties. The best result was obtained with PMEOX including DDA distal and ethylenediamine (EDA) satellite groups due to distinct functions on penetration throughout membrane and attractions with surface [94]. Figure 1.6. shows the chemical structures of antimicrobial PAOXs with various distal and satellite groups.

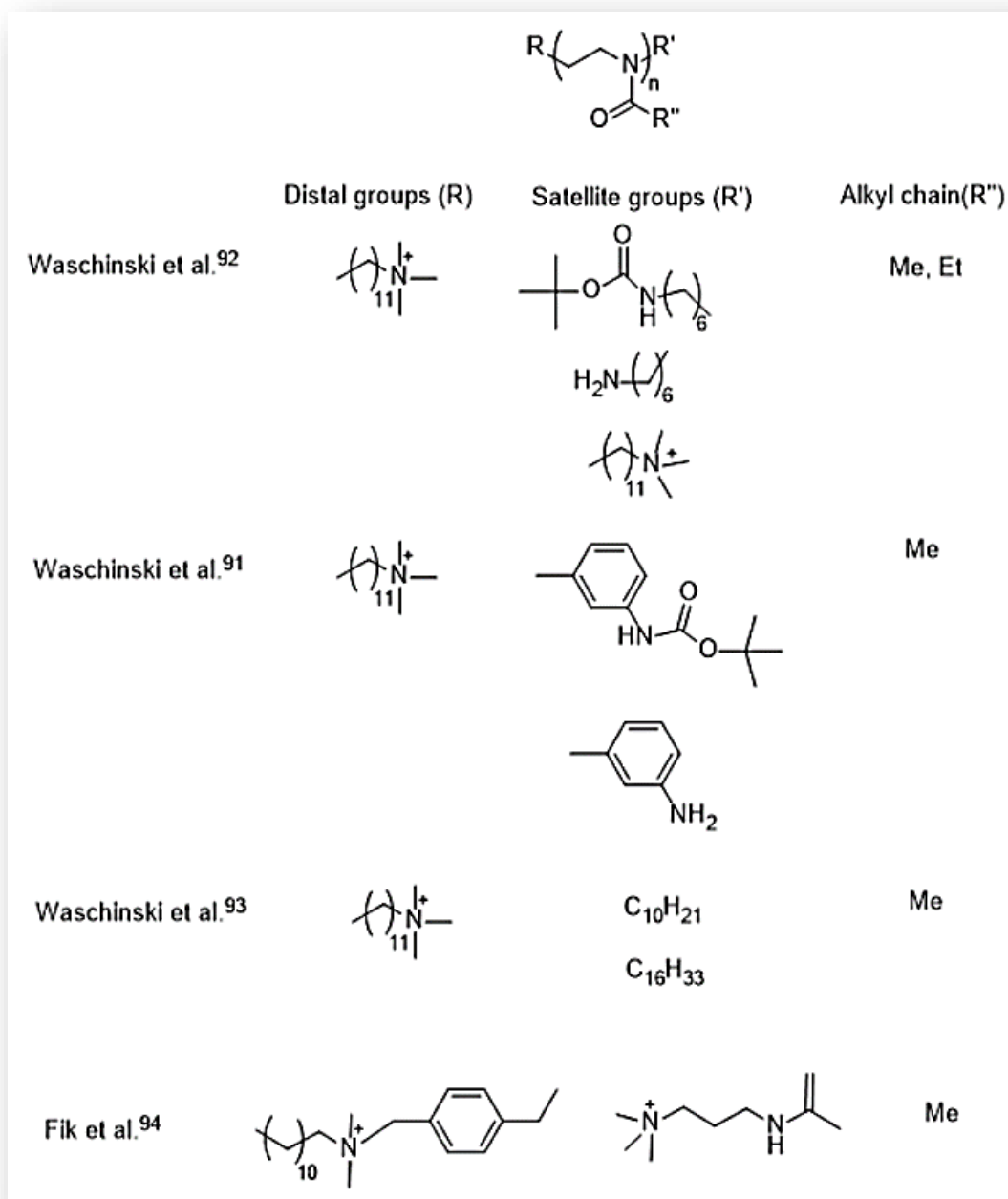
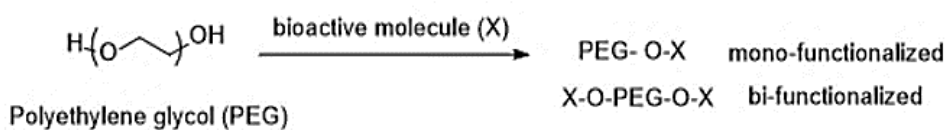


Figure 1.6. Chemical structures of antimicrobial PAOXs with various distal and satellite groups.

1.3.3.2. PAOX therapeutics

Although conjugation of polymers with bioactive agents without aiming release of active molecule is one of the successful concepts in prodrug design, it has been rarely preferred. The common features of polymers used in this type of conjugation are non-toxicity, non-immunogenicity, high solubility, high purity, biocompatibility and controlled average molecular weight to avoid immediate renal excretion but for easy clearance due to prevention of accumulation in body. Polymer-drug conjugates are mostly preferred to diminish the toxicity, increasing stability as well as blood circulation time and enhancing pharmacokinetic characteristics of anticancer drugs such as doxorubicin and paclitaxel. By this way, most of the problems occurring as a result of the application of cytotoxic drugs which are directly coupled with targeting antibodies could be prevented *via* using polymeric carriers as a linkage within the drug and targeting moiety [95–97]. There are also couple of examples of permanently bonded conjugates of PEG, Dextrin and PAOX with antibiotics focusing on the treatment of infections caused by bacteria [75,76,98–101].

Despite the great diversity of polymers with various compositions, PEG is one of the most commonly used synthetic polymer for bioactive molecule conjugation due to being non-toxic and cheap, easy elimination from the living organisms by kidneys, easy activation for conjugation, hydrophilic characteristics confirming the solubilization of hydrophobic drugs and having regulated permeation from biological barriers [102–105]. The significant application era for PEG conjugates, so-called pegylation, is mainly focus on the conjugation of PEG to bioactive agents to protect them from the immune-recognition as well as extending its circulation time in living body systems [106]. All of the type of conjugates have been established *via* the replacement of end-group functionalities (mostly hydroxyl moiety) with bioactive molecules such as proteins [107], peptides [108], drugs [109,110], oligonucleotides [111], antibodies and fragments [112].



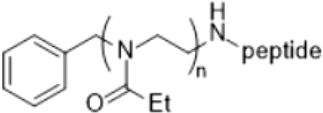
Scheme 1.3 Representative end-group PEG-bioactive agent conjugate via PEG modification (Adapted from Abuchowski et al. with slight modification[92]).

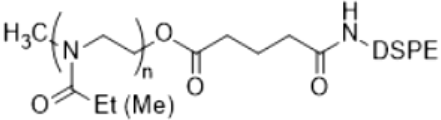
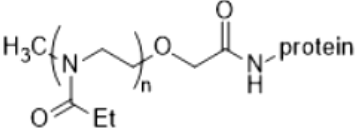
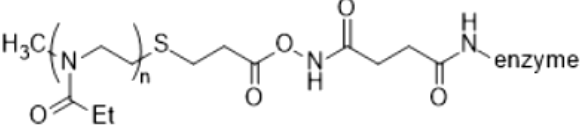
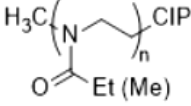
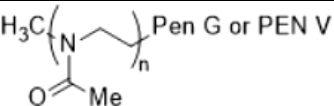
As a good alternative to PEG, a review of literature revealed that poly(2-alkyl-2-oxazoline)s that are more stable against enzymatic cleavage in living systems compared to PEG, have been conjugated with various bioactives [113]. One of the pioneer study on conjugation of drug with PEOX and PMEOX was conducted by Valender et al. That study was the first study of PAOX-adduct chemistry in which the “living” polymer was directly conjugated to lysyl-amino moiety of a peptide. It was shown that the polymer-peptide conjugate was still active through antibody binding as a result of ELISA assay. On the other hand, purification, isolation and characterization of PAOX were not achieved prior to conjugation [114]. Woodle et al. revealed the synthesis of PEOX and PMEOX conjugated with distearoylphosphatidylethanolamine (DSPE). Conjugates displayed prolonged circulation times *via* intravenous injection with low hepato-splenic uptake in rats. This study was the first illustration of the prevention of rapid recognition and clearance by using a polymer which can be an alternative to PEG [115]. Mero et. al. reported the synthesis of stable PEOX-trypsin and PEOX-Cytosine arabinose conjugates. They obtained comparable results for enzymatic activity of the trypsin conjugate and cytotoxicity activity of Cytosine arabinose conjugates against HeLa cell [116]. Viegas et. al. prepared functionalized PEOX in various molecular weights and then conjugated them with model bioactives such as bovine serum albumin, catalase, ribonuclease, uricase and insulin by non-labile bonds. Their results revealed that PEOX-insulin conjugate displayed higher activity to lower the blood glucose levels for a given time period when compared to pristine insulin. Similar to PEG, PEOX could also reduce the immunogenic characteristics of bovine serum albumin (BSA).

PEOXs in 10-20 kDa molecular weights were safely administered when intravenous injected to rats [4].

Recently, Schmidt et. al. published an article on synthesis and well-defined characterization of PEOX-Ciprofloxacin (CIP) conjugate. They realized that direct conjugation of CIP to polymer diminishes the antimicrobial activity of CIP due to blockage of functionality corresponding to antimicrobial activity *via* covalent bond formation. Other chain end functionality was also altered but this also resulted in poor antimicrobial activity of conjugates revealing that direct termination of PEOX with CIP was not a good strategy for preserving antimicrobial activity of antibiotic. Alternatively, they also synthesized PEOX-CIP conjugate with ethylene diamine spacer and displayed higher antibacterial activity that is also highly depending on molecular weight of the polymer [76]. Two years later, same group coupled Penicillines (Pen G and Pen V) to PMEOX from their carboxylic acid functionality. They showed up to 350 times higher antimicrobial activity against *S.aureus* in comparison to free antibiotics. When conjugates were functionalized with second antimicrobial group dodecyltrimethylammonium group (DDA-X) from free chain end, they became more active in presence of penicillinase [75]. Table 1.2 reveals the chemical structures of permanently bonded PAOX-biomolecule conjugates.

Table 1. 2. Chemical representation of permanently bonded PAOX conjugates.

Chemical structure of PAOX-bioactive agent conjugate	Reference #
Valender et. al.	

Woodle et. al.		115
Mero et. al.		116
Viegas et. al.		4
Schmidt et. al.		76
		75

1.3.3.3. Therapeutic releasing PAOXs

Alternating to permanent attachment of bioactive compounds to polymers, conjugation of bioactive compound with polymers through labile linkages has been a commonly used strategy especially for controlled release applications. By this way, the drawback of losing activity of bioactive molecule after conjugation with the moiety that is directly related with biological function could be eliminated. In this type of systems, bioactive agent could be released *via* stimuli responsive [117–120], enzymatic [102,121–124], hydrolytic [125–130] cleavage of labile bonds from polymer-therapeutic conjugates. In case of the use of biodegradable polymers in

conjugate systems, release of bioactive occurred upon degradation of polymer under physiological conditions [128–132]. Many studies have been conducted on the synthesis of different polymer-conjugates with great variety of bioactive compounds to be used for controlled release of therapeutics under ambient conditions in presence of stimuli being focused on. For this purposes, various methods and procedures are followed to adjust the release rate of the bioactives (especially drugs) by covalently linking them with hydrolytically labile bonds such as disulfide [120,133,134], imine [135], acetal [136] or oxime [137]. In addition to those, hydrazone bonds are most commonly preferred linkage between drugs and polymers due to easy cleavage at slightly acidic circumstances (pH 5.0–6.0). This is important when minimal drug release at physiological conditions (pH 7.4) but fast drug release at slightly acidic conditions such as infectious side of body or cancer tissues are desired [138,139].

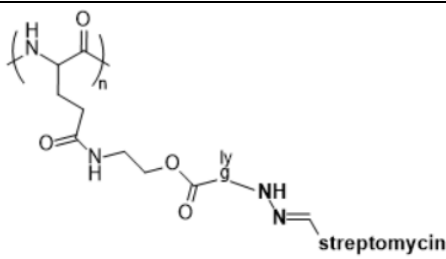
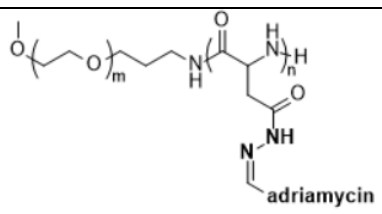
Prior to studies on PAOX-drug conjugates, various studies reported on polymer-drug conjugate systems designed *via* using hydrazone bonds to attach drug to hydrophilic polymer. Coessens et. al. reported the conjugation of streptomycin with polyglutamin and dextran *via* hydrazone spacer. They attached 6-aminohexyl- α -D-mannopyranoside side groups for targeting the conjugate to macrophages. The results revealed that polymer-stretomycin conjugate was non-hemolytic and hydrolytically stable at physiological pH while showing faster drug release at lysosomal pH conditions due to cleavage of hydrazone bond [140]. Bae et. al. studied pH-sensitive release of anticancer drug, adriamycin from the micelles of PEG-poly-(aspartate hydrazone adriamycin), in which the adriamycin was linked to the hydrophobic core *via* acid-sensitive hydrazone spacers. In this system, adriamycin was selectively released *via* sensing the decrease of intracellular pH in endosomes and lysosomes (pH 5.0-6.0) while drug is preserved stably under physiological circumstances (pH 7.4). In vivo and in vitro experiments revealed that micelles have ability to intracellular pH-triggered drug release, tumor-infiltrating penetrability and effective antitumor activity with enormously low toxicity [141]. Same year, Hruby et. al. published a work on preparation of micelles from amphiphilic diblock copolymers of poly(ethylene oxide)

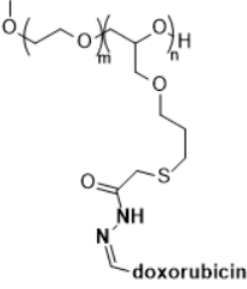
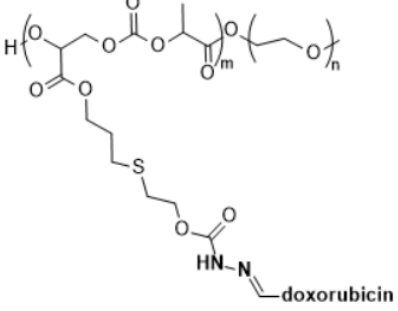
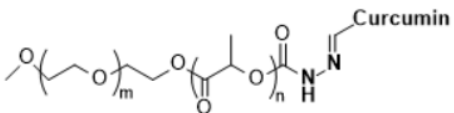
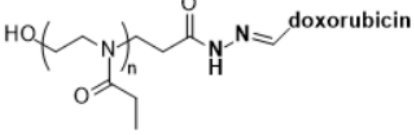
(PEO) and poly(allyl glycidyl ether) covalently linked with anthracycline antibiotic doxorubicin (DOX). Hydrazone bond between poly(allyl glycidyl ether) and DOX was created with alteration of methyl sulfanylacetate functionality with hydrazide and hydrazone bonds subsequently. Higher DOX-release rates were recorded at pH 5.0 compare to pH 7.4 [142]. Hue et. al. stated the preparation of DOX-coupled mPEG-b-P(LA-co-ME/DOX) to examine antitumor action. They formed hydrozone linkage *via* changing 4-nitrophenyl chloroformate (NPC)-activated copolymer to hydrazide group and then reacting this copolymer with DOX. Their in vitro release studies displayed that the polymer–DOX conjugate micelles showed a pH-dependent release characteristics [138]. Wang et. al. reported two PEG-co-poly(lactic acid) (PEG-PLA) copolymers conjugated with levulinic acid modified curcumin *via* hydrazone spacer resulting in linear (PEG-PLA-Cur) and phospholipid-like (Bi(PEG-PLA)-Cur) conjugates, respectively. Hydrazone spacer created *via* reaction of hydrazide moiety formed from ester group at the chain end and hydrazine hydrate with an antibiotic, curcumin. In case of linear conjugate micelles, loading dose, release rate and cellular uptake were higher but cytotoxicity was enhanced due to higher critical micelle concentration compared to phospholipid-like conjugate micelles [143]. In same year, same group published another study *via* working on same conjugate but in that study, they showed that after cleavage of hydrazone bond between PEG-PLA copolymer and levulinic acid modified curcumin, the residual hydrazide functionalized PEG-PLA-NH-NH₂ induced extensive cytotoxicity in a Hela cell-line. Therefore, they emphasized the significance of spacer selection for design of polymer-drug conjugate [144]. This studies of Wang et. al. are the examples of end-group conjugation of drug with polymer *via* hydrazone linkage.

The studies reported up to now all use block copolymers or random copolymers for conjugation of drugs due to (i) attach drug into functionalizable moiety of one of the block to provide multi attachment of drug (ii) to achieve 3D structures, micelles for controlled release applications except the oldest study mentioned. Different from those, Li et. al. published a work showing the synthesis and characterization of DOX

conjugated PEOX homopolymer *via* hydrazone bonds from chain end. They realized that, without need of any other group in different hydrophilicity forming copolymer, the micelles could also be constructed from PEOX-DOX conjugate itself. They confirmed the pH-induced cleavage of hydrazone bond and faster release of drug at acidic conditions. However, in order to increase the content of drug released, they also physically entrapped DOX into PEOX-DOX conjugate micelles. They revealed that the antitumor efficacy was noticeably enhanced by application of dual endosomal pH-sensitive micelles and side-effects of free DOX was reduced [77]. The chemical structures of polymer-drug conjugates *via* hydrazone linkage were shown in Table 1.3.

Table 1. 3. Chemical representations of polymer-drug conjugates obtained via hydrazone linkage.

Chemical structures of polymer-drug conjugates <i>via</i> hydrazone bond		Reference #
Coessens et. al.		140
Bae et. al.		141

Hruby et. al.		142
Hue et. al.		138
Wang et. al.		143, 144
Li et. al.		77

1.3.4. Aqueous solution behavior of PAOXs

PAOXs are in class of tertiary polyamides having usually achiral structure based on main chain so they cannot reorganize into secondary structures by secondary forces. Nevertheless, there are also chiral alternatives of PAOX in which the chirality is introduced by chiral groups onto the alkyl-moiety on the side chains or chain ends [13,39,145]. That enables them to form biomimetic self-assemblies possessing complex or hierarchical arrangements. In addition to chirality, the alkyl groups on the side chain also have great importance on some fundamental characteristics such as

water solubility [146] and crystallinity [147]. PAOXs with short alkyl side chains (PMEOX, PEOX, poly(2-n-propyl-2-oxazoline) (PnPOX) and PIPOX) are highly soluble in water at room temperature while the ones with longer and brached alkyl-side chains are insoluble in aqueous media. Among those, PEOX, PnPOX and PIPOX display temperature-dependent phase change that make them highly popular especially in biomedical era. Contrary to the popularity of temperature-sensitive behavior, only few studies conducted on their pH-dependent conformation change since they are generally known as neutral polymers [77,148,149].

1.3.4.1. Temperature-dependent aqueous solution behavior of PAOXs

Derivatives of PAOX possessing short alkyl chains, i.e. PEOX, poly(2-cyclopropyl-2-oxazoline) (PcPOX), PnPOX and PIPOX attracted great attention due to their lower critical solution temperature (LCST) type phase behavior. LCST is the temperature below which polymer chains are in extended conformation and highly solubilized while above which they adopted more contracted conformation and become more hydrophobic (Figure 1.7, Panel A) . LCST of PEOX, PIPOX, PcPOX and PnPOX were recorded as 60 °C, 35 °C, 30 °C and 25 °C, respectively (Figure 1.7, Panel B) [5].

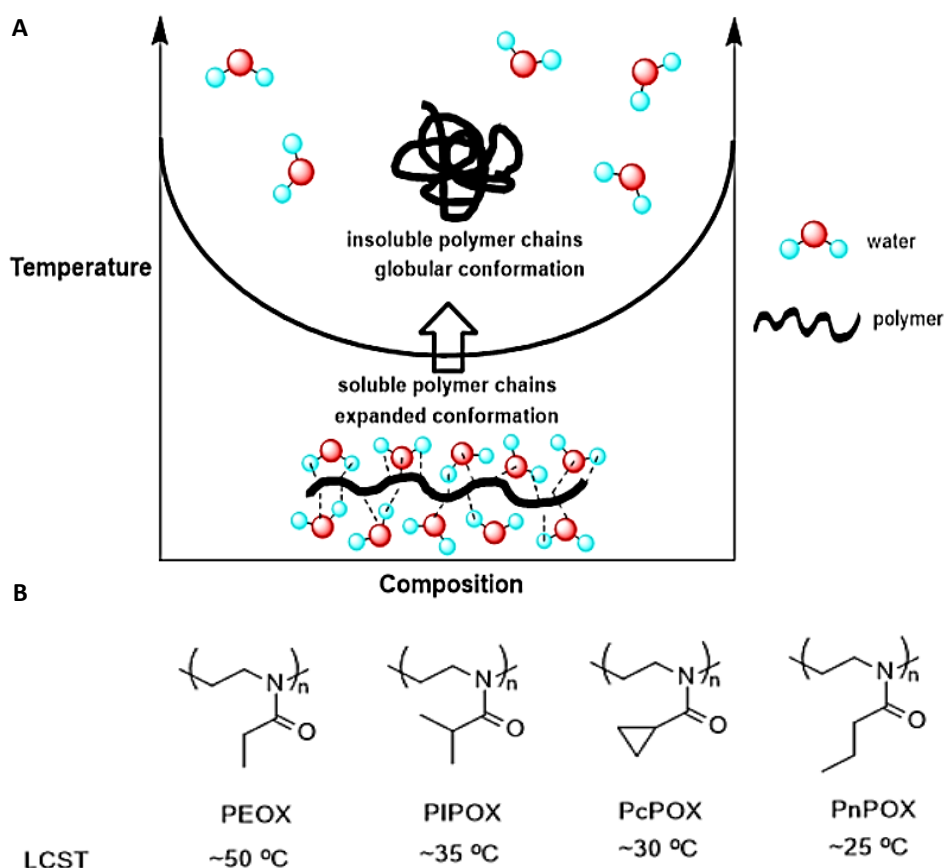


Figure 1.7. (A) Schematic representation of conformation of PAOXs below and above its LCST (adapted from Shakya and Nandakumar [137] with slight modification). (B) LCSTs of various PAOXs.

Among PAOXs, PIPOX attracted greater attention due to its LCST which is close to the body temperature. For the first time, temperature-responsive behavior of PIPOX was investigated by Uyama and Kobayashi. They reported cloud point (CP) of PIPOX as 36 °C in aqueous media which can be altered in presence of additives and concentration of polymer solution. They examined gel forming tendency of PIPOX upon rising temperature. They found that the swelling transition temperature of PIPOX hydrogels was near to the CP of PIPOX revealing the high potential of PIPOX being used in biomedical field soon [16]. Meyer and Schlaad were the pioneers of the research on temperature-induced self-coagulation of PIPOX in aqueous environment above its LCST. They correlate this irreversible phase transition with self-organization

or crystallization of homopolymer at elevated temperatures [150]. Then, Katsumoto et al. displayed that the phenomena under crystallization of PIPOX at high temperatures is so similar to two-step nucleation of protein crystals in aqueous media. The difference in LCST values of poly(N-isopropylacrylamide) (PNIPAM) and PIPOX was directly correlated with the hydration/dehydration of amide structural motifs on the side chain for former and on the backbone for the latter [151]. Haladjova et. al also published a study on formation of PAOX mesoglobules in aqueous environment at elevated temperature and suggested a similar mechanism to the one reported by Katsumoto et. al. Besides, some researchers demonstrated loading/release of bioactive into/from mesoglobules in response to temperature [11]. Later, Oleszko et. al. showed the crystallization tendency of PIPOX in organic solutions such as acetonitrile, dimethyl sulfoxide, or propylene carbonate by formation of micron-sized fibril structures and compared the results with the ones in bulk and in aqueous solution [152]. In addition to the studies concerning experimental evidences for conformational changes of PIPOX chains in aqueous media, Ozaltin et. al. recently inspected the morphological characteristics of PIPOX at temperatures below and above its LCST through computational methods such as MD simulations, DPD simulations and reverse-mapping procedures. They demonstrated that PIPOX chains turned into helical conformation prior to crystallization in water above its LCST [153].

1.3.4.2. pH-dependent aqueous solution behavior of PAOXs

Temperature-responsive behavior of PAOX derivatives possessing short alkyl chains have been extensively examined as mentioned in Section 1.4.1. However, the number of studies concerning pH-responsive aqueous solution behavior of PAOXs is limited. pH-sensitivity of PAOX has been explained *via* reversible protonation of amide nitrogen below its pK_a (Figure 1.8). For the first time, Wang and Hsiue revealed the shrinkage of PEOX/PLA hydrogels at $pH < 5.3$ at constant ionic strength and temperature conditions. They correlated this result with ionization of amide units at

pH values lower than 5.3. This triggers the formation of H-bonded complexes between PEOX chains and resulted in restriction of swelling of hydrogels as a consequence of increase of cohesion [154]. Later, same group synthesized PLLA-*b*-PEOX-*b*-PLLA triblock copolymers and examined their biodegradation, pH- and temperature-responsive properties. They determined the pK_a of triblock copolymer ~ 8.1 which was slightly higher than that previously reported for PEOX ($pK_a \sim 6.44$ [149]). They related pH-sensitive behavior of PEOX with the reduction of hydrogen exchange rate between the chains and water as a consequence of intermolecular hydrogen bonding between the carbonyl functionality of PEOX and protonated amide nitrogen [148]. Zhao et al. designed pH-responsive PEOX-PLA diblock copolymer micelles with folate targeting moiety for simultaneous release of DOX and TPGS1000, a potent P-gp inhibitor. They correlated pH sensitivity of micelles with PEOX blocks for which pK_a was determined as ~ 6.95 , slightly higher than that of unmodified PEOX homopolymer ($pK_a \sim 6.44$). They reported that the release at pH 6.4 (pH at tumor tissue) was mainly due to repulsion between protonated amide units of PEOX and expansion of PEOX-corona. On the other hand, the release at endosomal/lysosomal pH (pH 5.0) was as a result of disintegration of micellar structure due to degradation of PLA block [149]. Recently, Cagli and Erel-Goktepe reported a study on pH-dependent self-aggregation of PIPOX through both experimental and computational approaches in collaboration with Yildirim and Yang [155].

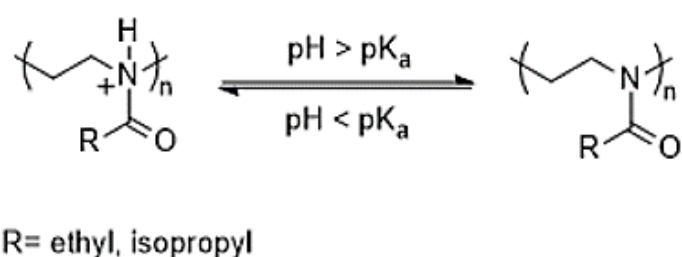


Figure 1.8. Reversible protonation of PAOX at pH below its pK_a

1.3.4.3. PAOX-based colloidal structures

Living matter is constituted from controlled and organized self-assembled structures such as self-association of phospholipids into cell-membranes and protein folding. Self-assembled conformation provide them to enhance specific characteristics like mechanical strength [156]. The striking point of development of the self-assembly of synthetic molecules was the motivation of chemists to mimic the nature [157]. Recently, the self-association of synthetic polymers with well-defined structures is a significant era of research based on the conformational change *via* phase separation either in bulk phase or in solution phase [158,159]. The latter is specifically significant era of research for poly(2-oxazoline)s.

1.3.4.3.1. PAOX homopolymer self-aggregates

Self-assembly of PAOXs have been induced either *via* hydrophobic association of chain ends or alkyl chain attached to the side chain [160,161] or attachment of bulky dendritic functionalities to the side chain [14,162–165]. Hydrophobic interactions lead to dehydration of chains that loosens the polymer-water interactions but enhance polymer-polymer associations. Hydrophobic polymer-polymer associations could be between either alkyl groups at chain ends, main chain ethylene groups and alkyl groups at side chain or alkyl group at repeating unit and end groups of PAOXs (Figure 1.9A). The shapes of reorganized aggregates which might be spherical, cylindrical and bilayers etc. depend on the configuration of polymer chains and geometric packing parameter. Spherical shaped aggregates could be obtained by polymers with long hydrophilic chain and short hydrophobic segments. Altering the length of hydrophobic and hydrophilic segments of homopolymer, the conversion from spherical to cylindrical shapes might be possible. Besides to hydrophobic interactions, hydrogen bonding interactions between water-polymer or polymer-polymer (Figure 1.9B), π - π stacking, van der waals and dipole-dipole associations are the mostly pronounced secondary forces affecting aggregate formation of polymers [165].

Jin synthesized a basic star shaped PMEOX and examined its hierarchical self-association into crystalline spherical colloids. They suggested that rigid core of the spherical PMEOX self-aggregates is formed from benzene moiety attached to one end of the polymer at the initiation step and this core is surrounded by the flexible PMEOX coronae [161]. Volet et al. prepared monoalkyl-end functionalized PMEOX and examined its self-assembly to form micelle restructured *via* hydrophobic-hydrophobic interactions between alkyl end capping. Disintegration of micelles were achieved *via* addition of β -cyclodextrin that captures the alkyl chains and makes end cappings hydrophilic [166]. Demirel et al. published work on self-association of PAOX homopolymer triggered *via* temperature resulted in crystallization from the solution and construction of nanoribbons and fibers of PIPOX [160]. Obeid et al. studied on the temperature effect on self-association of telechelic and semi-telechelic octadecyl attached to the α - end of PIPOX and PEOX. Self-assembly of both polymers was achieved below LCSTs due to hydrophobic interactions of the moieties at the chain ends [167].

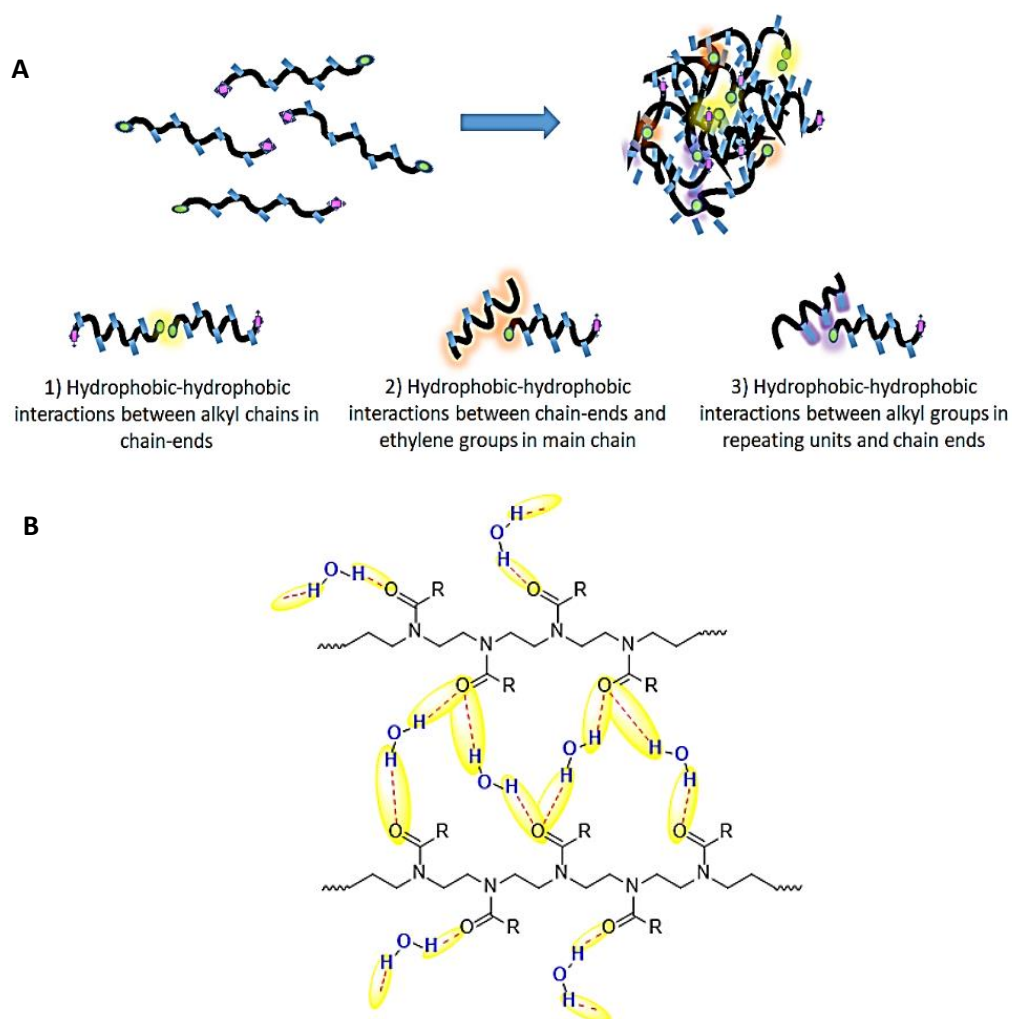


Figure 1.9. (A): Schematic representation of the association of PAOX chains via hydrophobic interactions. (B): Schematic representation of water mediated hydrogen bonding interactions and associations among PAOX chains and water.

In addition to these monoalkyl and dialkyl-end capped PAOXs, lipopAOXs have been investigated. Previously, it was shown that lipopolymer monolayers at the air-water interface are mostly worked on as a model systems to mimic the association in biological membranes [168]. Baekmark et al. showed the crystallization of long hydrophobic alkyl chains of lipopolymer throughout van der Waals (vdW) associations leading to locally ordering of lipopolymer [169]. Ahrens et al. reported

formation of weakly ordered lipid lined nanostructures in monolayers of lipopolymer onto mica surface once the polymer rests on the water-air boundary [170]. Different from the tendency of association of long alkyl chains throughout van der waals interactions, Naumann et al. displayed formation of physical complexes of dioctadecylglycerol/PMEOX *via* microcondensation of alkyl groups as a consequence of hydrogen bonding interactions among adjacent polymer chains [171]. Later, it was shown that alkyl chain association occurred as a result of hydrophobic interactions rather than hydrogen bonding within the polymer strains and led to formation of physical complexes is more significant mechanism (Figure 1.9) [172,173].

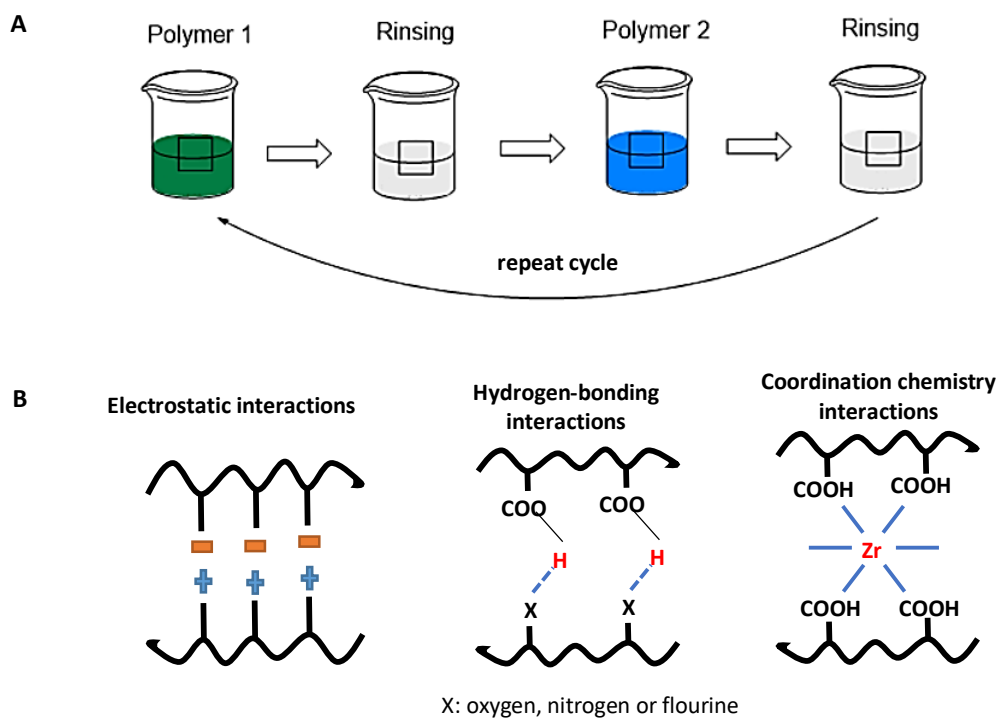
1.3.5. Multilayers of PAOXs

Layer-by-layer (LbL) self-assembly technique is a simple and powerful technique to prepare functional surfaces through deposition of macromolecules on substrates with a wide variety of interactions (i.e hydrogen bonding, electrostatic, hydrophobic, donor/acceptor attractions) [174,175]. LbL self-assembly was first investigated by Iler in 1966 through alternating construction of oppositely charged colloidal particles onto glass [176]. In early 1990's, Decher et al. applied this technique to oppositely charged polyelectrolytes, resulting in construction of multilayer thin films [177]. Since then, LbL self-assembly technique have attracted great attention to fabricate ultra-thin films for both fundamental and applied studies. In principle, various compounds having controlled architectures and roles such as polymers [178,179], colloidal structures [180–185] (i.e micelles, nanoparticles), dyes [186], proteins [187], enzymes [188,189], DNA [190,191] and viruses [192]...etc. can be integrated into multilayers. Conventional LbL self-assembly is described when those components are incorporated into multilayers basically *via* alternating adsorption to the solid-liquid interface. On the other hand, for incorporation of singly charged or water insoluble constituents which cannot be assembled into multilayers *via* conventional strategies, unconventional LbL methods are taken into account. In case of unconventional LbL

strategy, multi-step assembly route has to be followed for deposition onto surface such that first, supramolecular complex can be structured in solution and then this complex is used as a building block for LbL assembly process [193].

LbL technique is applied simply *via* immersion of substrate into first polymer solution followed by rinsing step to remove loosely bonded polymer chains from the surface. Afterwards, same substrate is immersed into second polymer solution and followed by the rinsing of substrate. This cycle can be repeated up to reaching the desired layer number and thickness of films (Scheme 1.4A). This technique provides many advantages such as easy application, being cost-effective and ease of controlling film thickness. In case of LbL films of polymers, molecular weight, chemical structure, temperature, pH and ionic strength are significant parameters influencing the assembly and deposition progression [174,175,194–196]. LbL self-assembly process is a kinetically controlled adsorption process. In- and out-diffusion of components of LbL films lead to interpenetration of layers and continued up to reaching to thermodynamic equilibrium. When thermodynamic equilibrium has established, in- and out-diffusion of components become slower. As a result, morphology, pH stability and durability of multilayers against high ionic strength could be altered [197–200].

Multilayers are mostly prepared using polyelectrolytes through electrostatic interactions. Besides the electrostatic interactions, secondary interactions such as hydrogen bonding, transition metal coordination complexes and hydrophobic interactions are generally and effectively used (Scheme 1.4B) [181,183,184,197]. Although hydrophobic interactions are not the main driving force for LbL self-assembly, they significantly affect the surface morphology, architecture and stability of the films [201].



Scheme 1.4 Schematic representation of LbL self-assembly technique (A) and common driving molecular associations to be used for LbL multilayer film construction (B).

Construction of hydrogen-bonded (H-bonded) multilayers are of interest due to pH-response of multilayers at mild pH conditions. Wang [202] and Stockton [203] et al. are known as pioneers of construction of LbL self-assembled multilayers with H-bonding interactions with published studies concurrently in 1997. Polymers with hydrogen-donating and hydrogen-accepting moieties in their structures are considered as building blocks of H-bonded LbL self-assembled multilayers (Figure 1.6). The polymers used in H-bonded films are generally chemically neutral polymers (polyamides, polyesters..etc.) that makes them considerably significant due to being used as nontoxic alternatives of cytotoxic polycations in multilayer construction. For the first time, Granick and Sukhishvili represented the construction of erasable hydrogen-bonded multilayers using water-soluble neutral polymers and polyacids [204,205]. Of note, erasable films are obtained at the pH above the “critical dissolution

pH”, that is closely depend on the pK_a of the polyacid, due to disruption of binding points within the multilayers [179].

In H-bonded multilayer construction, multilayers are generally prepared at acidic conditions at which polyacids are in protonated state. Hydrogen bonding interactions occur between the protonated acid group and electronegative atoms (i.e oxygen and nitrogen) of the hydrogen bond accepting polymer. At pH above pK_a of polyelectrolytes, hydrogen bonding attractions collapse due to ionization of polyacids resulting in disintegration of multilayers [179,204,205]. The pH-dependent stability of multilayers constructed could be adjusted *via* choosing the different hydrogen-donor polyacids with various pK_a values and changing the hydrophobicity and chemical identity of neutral polymer counterpart [193]. Hydrogen-bonded multilayer films have been used for controlled therapeutic, nucleic acid or nanoparticle release applications at mild acidic circumstances upon exposure to internal or external stimuli [206,207]. Formation of coordination bonds between coordination metals and polymers can also drive LbL self-assembly at the surface.

1.3.5.1. H-bonded LbL self-assembly of PAOXs

H-bonded multilayers of PAOX have been constructed *via* H-bonding interactions between H-acceptor PAOX and any H-donor polymer as shown in Figure 1.10. For the first time, Erel et al. prepared PAOX multilayers and compared the pH-stability of PIPOX and PNIPAM multilayers co-assembled with tannic acid (TA). In addition, they examined the effect of polymer end group on pH-stability of PIPOX multilayers. Their findings showed that the association among PIPOX/TA films was greater than that among PNIPAM/TA film resulting in thinner but more stable films. This study also demonstrated the improvement of pH-stability of H-bonded multilayers simply by functionalization of the PIPOX end-group [208]. Two years later, Antunes et al. published a study on hydrogen-bonded multilayers of PnPOX and TA. They showed that the film growing mechanism differed when multilayers were deposited at two

different temperatures, i.e. below and above the CP of PnPOX (25 °C). They found that PnPOX turned to dehydrated, collapsed state above its cloud point resulting in enhanced hydrophobic-hydrophobic interactions among PnPOX chains. This results in adsorption of higher mass of polymer onto the surface compared to the amount deposited below its cloud point when PnPOX was in coiled state [209]. Soon after, Sundaramurthy et al. investigated the multilayer deposition of PMEOX, PEOX and PnPOX with TA mainly through hydrogen-bonding interactions and examined the effect of hydrophilicity of the side chain onto film growth profile. Linearly grown, smooth thin films were obtained for all three types of PAOXs. Yet, while PMEOX exhibited mostly enthalpy driven LbL growth, PEOX and PnPOX displayed mostly entropy driven LbL growth as a result of release of bound water that enhance the hydrophobic-hydrophobic interactions. The reason for this was explained by the conformational difference. PMEOX adopted to highly expanded and hydrated conformation in aqueous media while PEOX and PnPOX were in more contracted and less hydrated state in water at room temperature due to hydrophilicity difference [210].

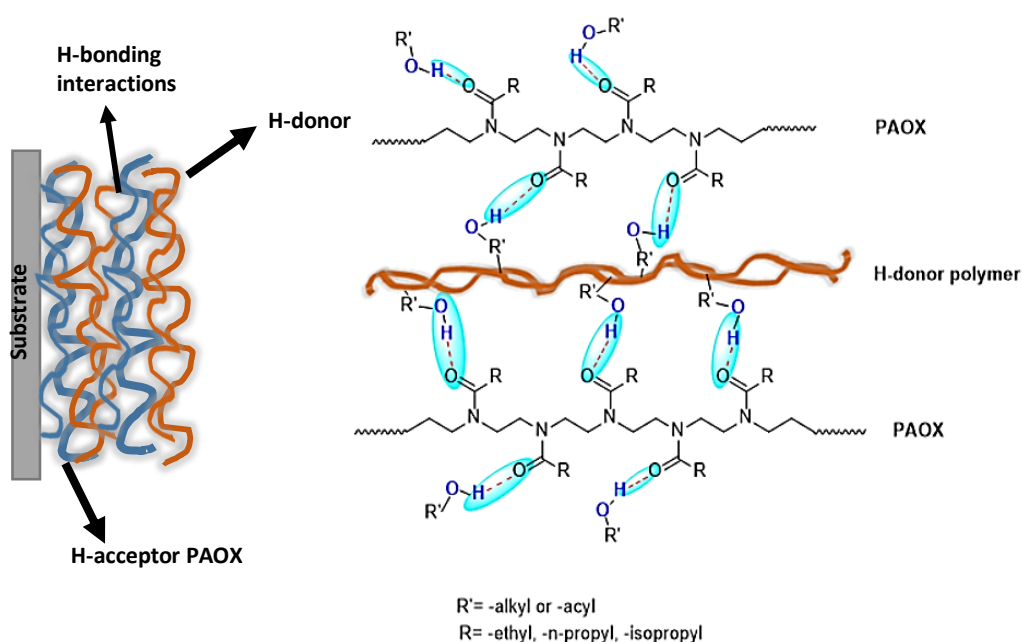


Figure 1.10. Schematic representation of H-bonded multilayers of PAOX have been constructed via H-bonding interactions between H-acceptor PAOX and any H-donor polymer

More recently, Hendessi et. al. constructed H-bonded LbL films of PEOX stabilized silver nanoparticles (Ag-NPs) and TA at pH 4.5 that revealed sensitivity upon pH variation. Multilayers were reported to release Ag^+ ions below critical disintegration pH of the films, while released Ag-NPs at the critical pH through disintegration of the layers [211]. Erel-Goktepe and co-workers recently demonstrated hydrogen-bonded multilayers of PIPOX and water soluble complexes of TA and DOX at pH 6.5. They showed that PIPOX/TA-DOX multilayers released small quantity of DOX under physiological conditions while released greater amount of DOX at acidic environment. This finding can be explained by greater association of TA and DOX at neutral pH due to increment of ionization degree of TA *via* increasing pH. On the other hand, under acidic conditions, TA became more protonated leading to disruption of electrostatic interactions between DOX and TA, resulting in higher amount of DOX release. The effect of temperature on the amount of DOX release was also studied in the same study. It was reported that the increasing temperature enhanced DOX release

due to the conformational transition of temperature responsive PIPOX close to its cloud point [178]. In another study, the construction of healable antifouling hydrogen-bonded LbL films of partially hydrolyzed PEOX and poly(acrylic acid) (PAA) was demonstrated by Li et al. PEOX/PAA multilayers were thermally crosslinked to enhance the stability. Such multilayers displayed resistance to adhesion of both *Escherichia coli* (*E.coli*) and *Bacillus subtilis* bacteria. Repeated healing characteristics of multilayers for cuts up to several tens of micrometers were correlated with the dynamic nature of hydrogen-bonding attractions and high mobility of polymers in aqueous media [212]. Hollow capsules produced by Paramasivam et al. through LbL self-assembly of PnPOX and TA through hydrogen bonding interactions provided multilayers which could release therapeutics at physiological temperature. Such capsules were found to form porous structure beyond LCST of PnPOX. Moreover, various probes with different hydrodynamic sizes could be loaded into capsules and the change of incubation time and radius of probe led to efficient manipulation of open and closed state of the capsules [213].

Nowadays, similar to the study conducted by Li et al., He et al. constructed LbL self-assembled films of PEOX and PAA at nano- to micron thicknesses. By heat-triggered crosslinking, stability of pre-constructed multilayers was improved and pH-induced swelling of films in aqueous media at pH 5.0 and above was achieved. Protein repelling characteristics of multilayers against BSA were directly correlated with the thickness of the cross-linked multilayers. Minimum BSA adhesion was recorded for films having ~220 nm thickness. Furthermore, multilayers with 220 nm and thicker prevented fibroblast, *E-coli* and *S. aureus* attachments [214]. Apart from these, Adatoz et al. prepared free-standing hydrogen-bonded and pH-responsive PEOX/TA multilayers through LbL self-assembly which can be reorganized to pH-sensitive fibers at pH 3.0 phosphate buffer solution. Restructuring of PEOX/TA multilayers into fibers at acidic conditions were affirmed by scanning electron microscopy (SEM). They were monitored as if combined hollow tubes on solid template which can be formed as a consequence of bending of planar multilayer fragments. This fibrous

structures are significant for biomedical application since they show pH-response and can be disintegrated at pH 8.5 which may be promising for drug release applications [206].

CHAPTER 2

AN EXPERIMENTAL AND COMPUTATIONAL APPROACH TO PH-DEPENDENT SELF-AGGREGATION OF POLY(2-ISOPROPYL-2- OXAZOLINE)*

2.1. Chapter Summary

Besides temperature, self-aggregation of PIPOX can also be triggered *via* pH in aqueous solution (25 °C, pH>5.0). Lowest energy structures and interaction energies of PIPOX with H₃O⁺, OH⁻ and H₂O were calculated by DFT methods showed that, in addition to their ability to protonate PIPOX, H₃O⁺ ions had strong interaction with both water and PIPOX in acidic conditions. H₃O⁺ ions acted as compatibilizer between PIPOX and water and increased the solubility of PIPOX. OH⁻ ions were found to have stronger interaction with water compared to PIPOX resulting in desorption of water molecules from PIPOX phase and decreased solubility, leading to enhanced hydrophobic interactions among isopropyl groups of PIPOX and formation of aggregates at high pH. Results concerning the effect of end-groups on aggregate size were in good agreement with statistical mechanics calculations. Aggregate size was found to be affected by polymer concentration and amount of salt in the solution. Moreover, cloud point temperature of PIPOX was found to be pH-dependent.

* The content of this chapter (see reference [155]) was previously published by Wiley Ltd. (Cagli, E.; Yildirim, E.; Yang, S. W.; Erel-Goktepe, I. *Journal of Polymer Science Part B: Polymer Physics*, 57 (4), 210. DOI: 10.1002/polb.24773).

2.2. Introduction

PAOXs are an important class of bioinspired polymers that has attracted increasing attention in the recent years for biomedical applications. The structural similarity to polypeptides has imparted significant biological properties to PAOXs, such as biocompatibility, nontoxicity, anti-fouling [1–3] and stealth behaviour [4,5], providing them potential use in biomedical applications.

Phase behaviour and temperature-responsive properties of PAOXs have been extensively investigated [2,6–17]. Among PAOXs, PIPOX is of specific interest due to the LCST-type phase behaviour in aqueous solution with a critical temperature (35–39°C for PIPOX with varying M_n and concentrations) [2] within the physiological range. Temperature-induced self-assembly and crystallization of PIPOX in aqueous and organic solutions has been reported [9,10,152,160]. Besides, temperature-induced formation of PIPOX mesoglobules above the critical temperature and release of biomolecules from mesoglobule templates has been demonstrated [215].

In contrast to extensive research conducted on temperature-responsive behaviour, the number of studies concerning pH-sensitivity of PAOXs is limited. Wang and Hsiue reported on pH-response of PEOX based hydrogels which showed swelling behaviour below the pK_a of PEOX due to protonation of the amide groups of PEOX leading to strong hydration as well as electrostatic repulsion among the PEOX chains [154]. In another study, Li et al. reported disintegration of micelles with PEOX corona at pH lower than the pK_a of PEOX due to protonation of amide units and electrostatic repulsion among the PEOX chains, loosening the micelle structure [77]. It has been reported that pH-sensitivity could also be introduced to PEOX by chemical modification, e.g. partial hydrolysis of PEOX and formation of ethylene imine units or formation of tertiary amino groups as a result of crosslinking partially hydrolyzed PEOX [216].

Different from these studies, herein, we show that in addition to temperature, pH can also be used as a trigger to induce self-association of PIPOX chains in aqueous

solution at 25 °C which was significantly lower than its LCST. DFT methods were used to calculate the lowest energy structures and interaction energies of pairwise, ternary and quaternary structures of PIPOX with H_3O^+ , OH^- and H_2O molecules to understand the mechanism of pH-induced self-assembly. The chemical nature of the end-groups was found to be critical on the self-association of PIPOX, thus the aggregate size. Calculations based on binary binding energies and coordination numbers were utilized to examine the effect of end-groups on self-association of PIPOX and were found to be in agreement with the experimental data.

Polymeric assemblies are formed through either formation of chemical bonds (e.g. microgels, latexes) or physical interactions (e.g. some kind of micelles, nanoparticles) [217]. The self-assemblies prepared through physical interactions is based on various mechanisms, e.g. solvent selective copolymer self-assembly [218,219], electrostatic association of polyelectrolytes with opposite charges [220,221], interactions of two or more types of homopolymers *via* intermolecular H-bonding interactions [205,222], surfactant triggered association of copolymers [223,224] and self-association of homopolymers through chain end functionality [225]. Among them, homopolymer self-assemblies have attracted growing attention due to their relatively easy synthesis compared to the diblock copolymers [226–228]. Among neutral polymers, self-assembly of PEO in aqueous environment has been reported. It was found to form nanoclusters as a result of hydrogen bonding between ether oxygen of PEO and water as well as hydrophobic interactions among $-\text{CH}_2\text{CH}_2-$ units [229–232].

As far as we are aware, pH-dependent self-aggregation of PAOXs has not been reported before. In this perspective, this study is the first demonstrating that not only temperature but also pH can be used as a trigger to self-assemble PAOXs in aqueous medium. Moreover, this study scrutinizes the mechanism of pH-induced self-assembly using DFT methods. Results obtained in this study contribute to fundamental understanding of chemical structure-property relationship in PAOXs. Considering the interesting biological properties of PIPOX together with its dual responsive behavior,

this study may form a basis for the development of PAOX based materials for biomedical applications.

2.3. Experimental and Computational Methodology

2.3.1. Materials

All chemicals were used as received unless otherwise specified. Ethanolamine (>99%), cadmium acetate dihydrate (98%), α -bromoisobutyl bromide (98%), acetonitrile (>99.9%), 2-butanol (>99%), 4-(N-Boc-amino)-piperidine (96%), calcium hydride (96%), NaOH pellet (>98%), HCl (37%), (2-ethyl-2-oxazoline (>99%)) were purchased from Sigma-Aldrich. Isobutyronitrile (>98%) and sodium dihydrogen phosphate dehydrate ($\text{NaH}_2\text{PO}_4 \cdot 2\text{H}_2\text{O}$) were purchased from Merck chemicals. Buffering range for monobasic phosphate buffer is 5.8-8.0 which fit our conditions well. The deionized water (DI) was purified by passage through a Milli-Q system (Millipore). SpectroPor7 regenerated cellulose dialysis membrane (molecular weight cutoff: 3.5 kDa) was used for purification of polymers.

2.3.2. Synthesis of 2-isopropyl-2-oxazoline and poly(2-isopropyl-2-oxazoline)s

Synthesis of 2-isopropyl-2-oxazoline

2-isopropyl-2-oxazoline (2-IPOX) was synthesized as described previously [233] with slight modifications. Briefly, ethanolamine (0.052 mol, 3.5 mL) and isobutyronitrile (0.043 mol, 3.9 mL) were added into a schlenk reactor containing cadmium acetate dihydrate (1.08 mmol, 0.29 g) under argon atmosphere. The reaction was stirred under reflux at 130°C for 48 hours. The crude product was distilled at 45°C under reduced pressure and dried over CaH_2 prior to use. ^1H - NMR (CDCl_3 , 400 MHz): δ (ppm) = 4.21 (t, J= 9.02 Hz, 2 H), 3.82 (t, J= 9.26 Hz, 2 H), 2.57 (m, J= 7.27 Hz, 1 H), 1.2 (d, J= 6.90 Hz, 3 H) (Appendix A: Figure A.1).

Synthesis of ω -2-butoxy-poly(2-isopropyl-2-oxazoline) (PIPOX)

In an argon purged schlenk flask capped with a condenser, acetonitrile (10.0 mL) and 2-IPOX (41.0 mmol, 4.9 mL) were added and magnetically stirred for homogenization. After addition of α -bromoisobutyl bromide (0.4 mmol, 0.01 equivalent), the reaction flask was placed in a preheated oil bath at 80°C. After 24 hours of stirring, reaction mixture was cooled to room temperature and quenched with 2-Butanol (1.2 mmol, 0.03 equivalent). The mixture was then stirred for 2 additional days at 80°C. The dark orange solution turned to a yellow foamy solid upon evaporation of the solvent under reduced pressure. The product was dissolved in DI water and dialyzed against DI water for 2 days. Finally, the aqueous solution was freeze-dried. ¹H-NMR (400 MHz) δ 3.50 (br, 4H), 2.9- 2.75 (br, 1H), 2.18 (m, 1H), 1.15 (s, 6H), 1.10 (br, 6H) (Appendix A: Figure A.2). GPC traces of PIPOX: Mn = 6210 g/mol, PDI 1.25 (Appendix B: Figure B.1).

Synthesis of ω -N-boc-aminopiperidine-PIPOX

ω -N-boc-aminopiperidine-PIPOX was synthesized and purified using the same procedure described above except the polymerization was terminated with 4-(N-Boc-amino)-piperidine (1.2 mmol, 0.03 equivalent) instead of 2-Butanol. ¹H-NMR (400 MHz) δ 3.45 (br, 4H), 2.83- 2.70 (br, 1H), 2.15 (m, 1H), 1.42 (s, 9H), 1.2 (s, 6H), 1.0 (br, 6H) (Appendix A: Figure A.3). GPC traces of PIPOX: Mn = 7854 g/mol, PDI 1.39 (Appendix B: Figure B.2).

2.3.3. Instrumentation

Nuclear magnetic resonance spectroscopy (NMR) and gel permeation chromatography (GPC) measurements

¹H-NMR measurements were obtained using a Bruker spectropin Avance DPX-400 Ultra shield instrument at 400 MHz. ¹H-NMR data were reported as chemical shifts (δ , ppm) relative to tetramethylsilane (δ 0.00) with multiplicity (s=singlet, br=broad

singlet, d=doublet, t=triplet, m=multiplet), coupling constant (Hz) and integration. Gel permeating chromatography (GPC) measurements were carried out Agilent instrument (Model 1100) consisting of refractive index (RI) detectors and three Macherey-Nagel columns which are packed with a highly cross-linked macroporous, spherical polystyrene-divinyl-benzene polymer matrix (Columns 300×7.7 mm, particles $5 \mu\text{m}$). 0.01 M LiBr/DMF was used as an eluent at a flow rate of 0.7 mL/min at 50°C. The calibration was performed using poly(methyl methacrylate) standards (Polymer Laboratories).

Dynamic light scattering measurements

PIPOX was dissolved in 0.01 M phosphate buffer at pH 2.5 with a concentration of 0.2 mg/mL, 0.6 mg/mL or 1.0 mg/mL. pH of PIPOX solutions was adjusted using 0.1 M NaOH or 0.1 M HCl solutions. Hydrodynamic size measurements were performed using Zetasizer Nano-ZS equipment (Malvern Instruments Ltd., U.K.). Size values were obtained by cumulants analysis of the autocorrelation data. The detection angle was 173° Backscatter.

SEM imaging

SEM imaging of PIPOX in 0.001 M phosphate buffer at pH 2.5 and pH 7.5 was performed using high resolution QUANTA 400F Field Emission SEM after Au-Pd coating.

Fluorescence spectroscopy studies

PIPOX was dissolved in 7×10^{-7} M pyrene solution prepared using 0.01 M phosphate buffer at pH 2.5 with a final PIPOX concentration of 0.2 mg/mL, 0.6 mg/mL, and 1.0 mg/mL. pH adjustments were performed using either 0.1 M NaOH or 0.1 M HCl solution. Pyrene was excited at 335 nm and the fluorescence spectra was collected within 350-500 nm using a fluorescence spectrophotometer (Hitachi, F-2500).

Turbidimetric Analysis

A single, collimated beam Agilent Cary 8454 UV-Visible spectrophotometer with Agilent 89090A Peltier Temperature Controller was used for the turbidity measurements. The PIPOX solution in concentration of 10 mg/ mL was placed in a 10 mm path length quartz cuvette with PTFE capping. The temperature was increased between 25 °C and 60 °C by 2.5 °C or 5 °C steps via waiting 30 minutes at each temperature. The cloud point was determined within the range of the abrupt change of the optical density.

2.3.4. Computational Details[^]

This part of the study was conducted by Dr. Erol Yildirim from Institute of High Performance Computing, Agency for Science, Technology and Research (A*STAR), Singapore.

DFT calculations to determine binary and ternary interactions

Density Functional Theory (DFT) is the most widely applied first principle approach to predict the ground-state (GS) properties of organic molecules and oligomers in water [234]. DFT calculations for the model systems constructed by methyl terminated PIPOX repeat unit, water molecules, H_3O^+ and OH^- ions were carried out at M06-2X/6-311+g(d,p) [235] level by using Gaussian09 software [236] to determine lowest energy structures as well as pairwise, ternary and quarternary interaction energies with each other and with PIPOX.

[^]Calculations by density functional theory methods and statistical mechanics calculations were performed by Dr. Erol Yildirim and Dr. Shuo-Wang Yang.

The interaction energies were validated by comparing calculations with B3LYP exchange–correlation functional [237,238] at DNP basis set implemented in DMOL3 software [239,240] and mPW91PW91 functional at 6-311+g(2d,2p) basis set also implemented in Gaussian09 software. Noncovalent forces, such as hydrogen bonding and van der Waals (vdW) interactions, are crucial for the formation and stability of molecular aggregates. Grimme’s parameters [241] were applied for van der Waals dispersion corrections. All calculations were conducted under implicit water effect by using COSMO and IEFPCM solvent models [242];[243].

Calculation of free energy of solvation

Free energy of solvation in water was calculated for protonated and neutral PIPOX oligomer with 10 repeat unit and 600 water molecules under periodic boundary conditions based on the coupling parameter method and thermodynamic integration [244–247]. The free energy of solvation was determined in three steps: the protonated or neutral PIPOX oligomer in the vacuum is discharged as a first step, and the free energy change associated with this discharge was calculated, called ideal contribution to the free energy of solvation. Then the neutralized PIPOX was brought into contact with the water molecules. The free energy change for this discharged interaction was calculated which is called van der Waals contribution to free energy of solvation. Finally, the solvated, but discharged, protonated and neutral PIPOX molecule is charged again in water environment to calculate the electrostatic contribution to free energy of solvation. Total free energy of solvation was calculated as the sum of the free energy contributions from ideal, vdW and electrostatic solvation free energies [247]. COMPASS (Condensed-Phase Optimized Molecular Potentials for Atomistic Simulation Studies) force field and its water model for the free energy calculations that have been validated extensively for solubility and phase properties of polymers in water [248,249].

Calculation of end group interactions

The compatibility of PIPOX terminated with 2-butanol and N-boc-amino-piperidine end group were studied based on off-lattice calculations of binary interaction energies based on statistical mechanics method [250,251]. The miscibility behavior of the interacting end groups with PIPOX can then be predicted based on modified Flory-Huggins Theory. For this aim, interacting PIPOX end blocks, i and j were represented by the interaction parameter, χ which was calculated by the combination of Flory-Huggins model and force field based molecular mechanics techniques. Monte Carlo type minimizations of a high number of cluster interactions were performed to obtain the number of neighboring components, known as coordination numbers, Z_{ij} and the binding energies, $\langle E_{ij} \rangle$ for each pairs of PIPOX and terminal groups. Head and tail atoms of PIPOX backbone were chosen to be not in interaction to represent the real polymer behaviour. Coordination numbers were calculated by generating 10^6 clusters. The average binding energy was calculated by generating 10^8 configurations of blocks at room temperature by using the average of the weighted distribution function, $P_{ij}(E)$ (Eq. 1).

$$\langle E_{ij} \rangle_T = \frac{\int dE E P_{ij}(E) e^{-E/RT}}{\int dE P_{ij}(E) e^{-E/RT}} \quad \text{Eq. 1}$$

E_{mix} is defined as the difference in free energy due to interaction between the mixed PIPOX and terminal groups with their pristine state Eq. (2).

$$E_{\text{mix}} = \frac{1}{2} \left(Z_{ij} \langle E_{ij} \rangle_T + Z_{ji} \langle E_{ji} \rangle_T - Z_{ii} \langle E_{ii} \rangle_T - Z_{jj} \langle E_{jj} \rangle_T \right) \quad \text{Eq. 2}$$

Finally, χ parameter for PIPOX and terminal groups were calculated from the temperature dependent mixing free energy, E_{mix} at 298 K as given in Eq. (3).

$$\chi = \frac{E_{\text{mix}}}{RT} \quad \text{Eq. 3}$$

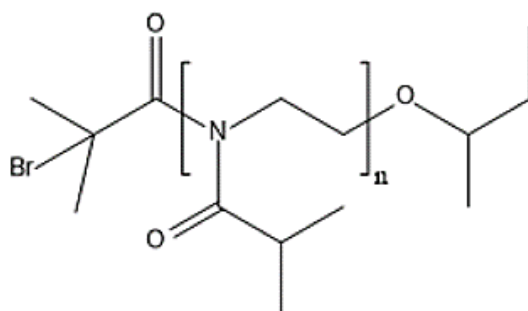
Free energies (ΔG) for PIPOX backbone and terminal group interactions are calculated by using Flory-Huggins equation (Eqn. 4) where Φ represent the volume fractions and n represents the degree of polymerization of components. The calculations for free energies are performed for 100 times higher degree of polymerization for PIPOX backbones compared to terminal groups.

$$\frac{\Delta G}{RT} = \frac{\Phi_i}{n_i} \ln \Phi_i + \frac{\Phi_j}{n_j} \ln \Phi_j + \chi \Phi_i \Phi_j \quad \text{Eqn. 4}$$

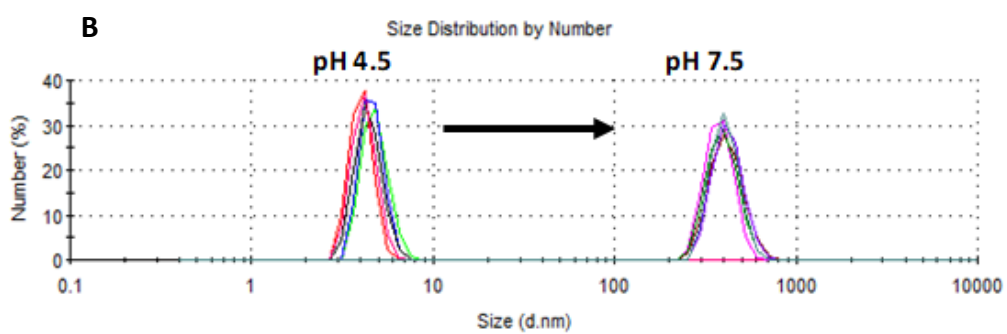
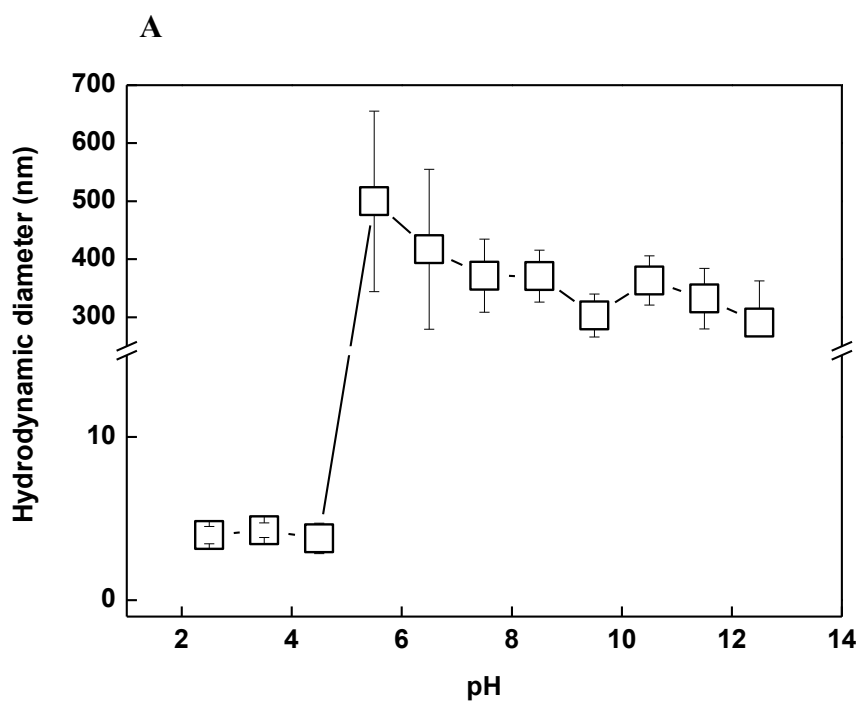
2.4. Results and Discussion

2.4.1. pH-dependent aqueous solution behavior of PIPOX

pH-dependent aqueous solution behavior of PIPOX was examined by monitoring the hydrodynamic diameter as a function of pH using dynamic light scattering (DLS) technique. Scheme 2.1 shows the chemical structure of PIPOX. 0.2 mg/mL PIPOX solution (prepared using 0.01 M phosphate buffer) was titrated with 0.2 M NaOH solution and the number average hydrodynamic diameter of PIPOX was followed as a function of solution pH (Figure 2.1a). The size values were obtained after 10 minutes of waiting at each pH value. At strongly acidic conditions (between pH 2.5-pH 4.5), hydrodynamic size of PIPOX was recorded as ~ 4 nm. At pH 5.0, a sharp increase in size was detected and further increasing pH resulted in a slight decrease in hydrodynamic size. PIPOX aggregates with 300-370 nm of average size were detected between neutral and basic conditions. Figure 2.1b contrasts the size distributions of PIPOX by number at pH 4.5 and pH 7.5 and clearly demonstrates the shift of the size distribution curve to higher values with increasing pH. Of note, we also followed size distributions of PIPOX by intensity at pH 4.5 and pH 7.5 (Figure 2.2). Two peaks were observed at pH 4.5 corresponding to size values below 10 nm and above 100 nm, respectively. The peak corresponding to size values below 10 nm disappeared at pH 7.5. The intensity (%) of the peak corresponding to larger sizes increased and the distribution curve shifted to higher values at pH 7.5.



Scheme 2.1 Chemical structure of PIPOX.



C

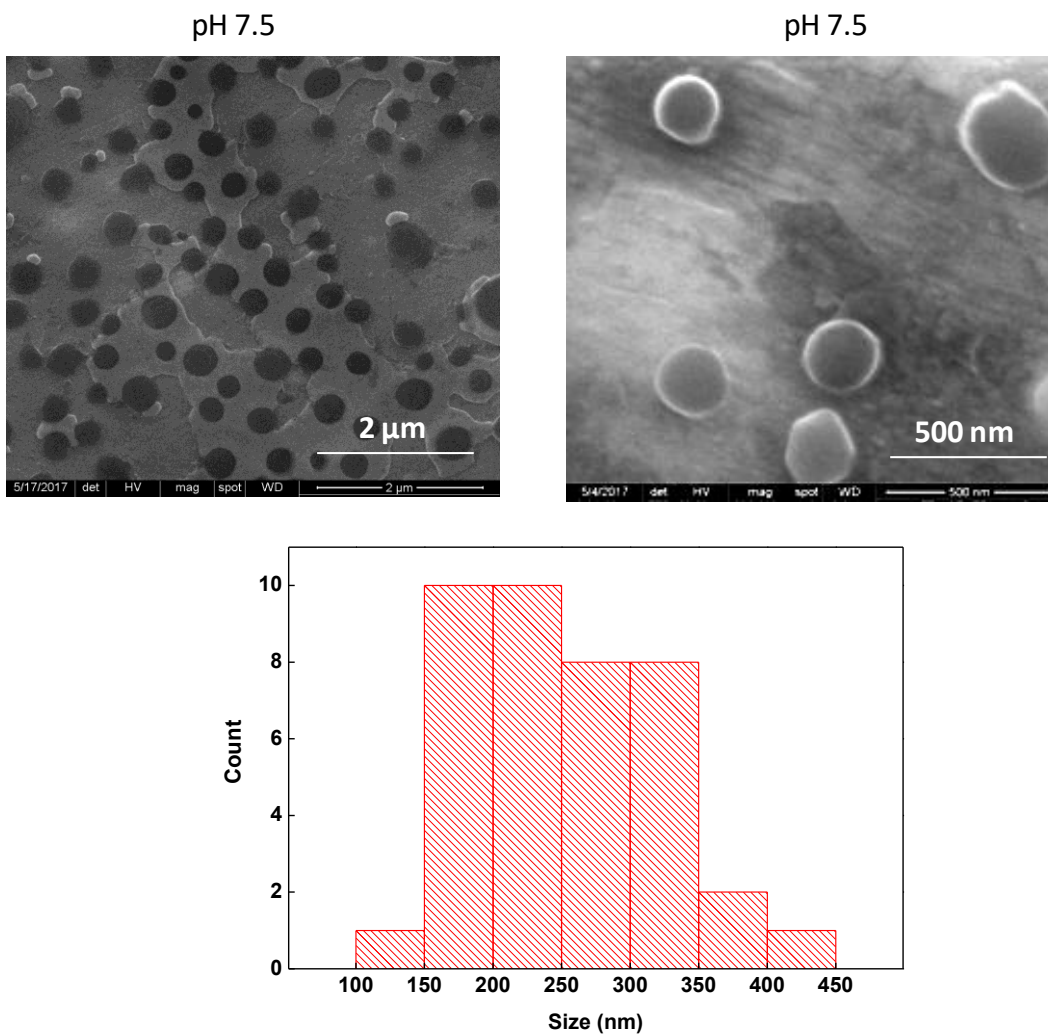


Figure 2.1. A) Evolution of hydrodynamic diameter of PIPOX as a function of pH. (B) The size distribution by number of PIPOX at pH 4.5 and pH 7.5. Right direction arrow denotes the shift in size distribution to higher values. Size distribution curves obtained from several individual measurements of the same sample are represented with different colors. (C) SEM images and the size distribution of PIPOX aggregates at pH 7.5 and 25 °C. The size distribution curve is prepared out of 40 different measurements.

Self-assembly of PIPOX *via* pH-trigger was also confirmed *via* SEM imaging. Figure 2.1c shows SEM image of PIPOX aggregates at pH 7.5 and 25 °C and the corresponding size distribution curves obtained out of 40 different size measurements.

The lower particle size values obtained by SEM imaging than that by DLS technique can be correlated with the fact that DLS measured the hydrodynamic diameter, the diameter of the particles together with the water layer attached to them, whereas SEM provided information about the projected area diameter of PIPOX aggregates.

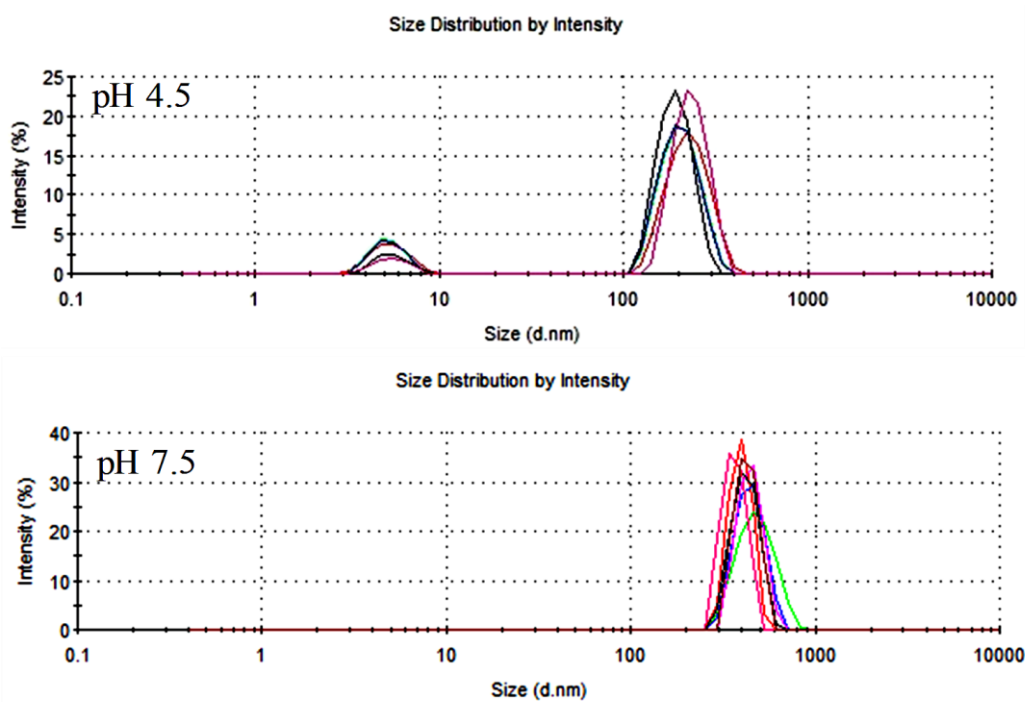


Figure 2.2. Intensity average size distributions of PIPOX at pH 4.5 and pH 7.5.

Importantly, we observed that pH-induced self-aggregation of PIPOX was reversible with some hysteresis. The hysteresis was possibly due to intra- and inter-molecular hydrophobic association between the PIPOX chains, suppressing the protonation of the amide nitrogens and partial removal of PIPOX chains from the aggregates (Figure 2.3). Of note, we have also conducted similar experiments with PEOX. Similar to PIPOX, PEOX also formed aggregates with ~250 nm in size above pH 5.0 (Figure 2.4).

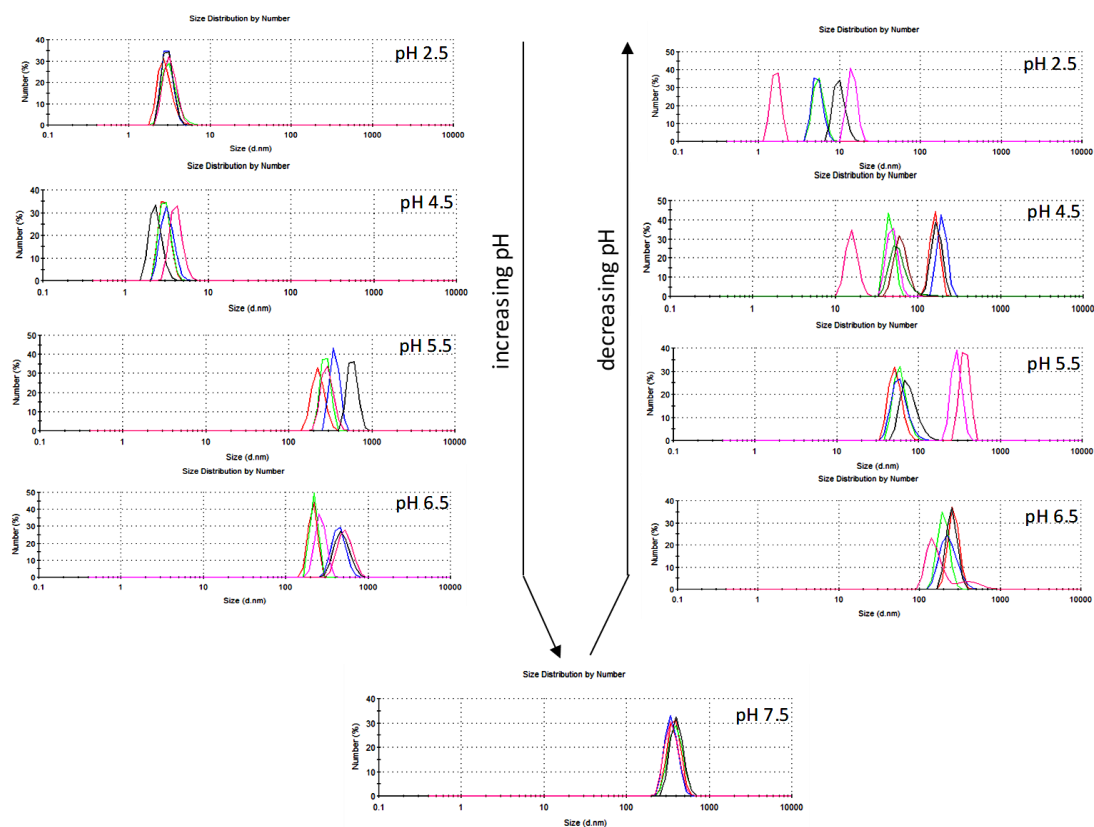


Figure 2.3. Hydrodynamic size distributions of PIPOX in 0.2 mg/mL solution at 25 °C via increasing and then decreasing pH. Size distribution curves obtained from several individual measurements of the same sample are represented with different colors.

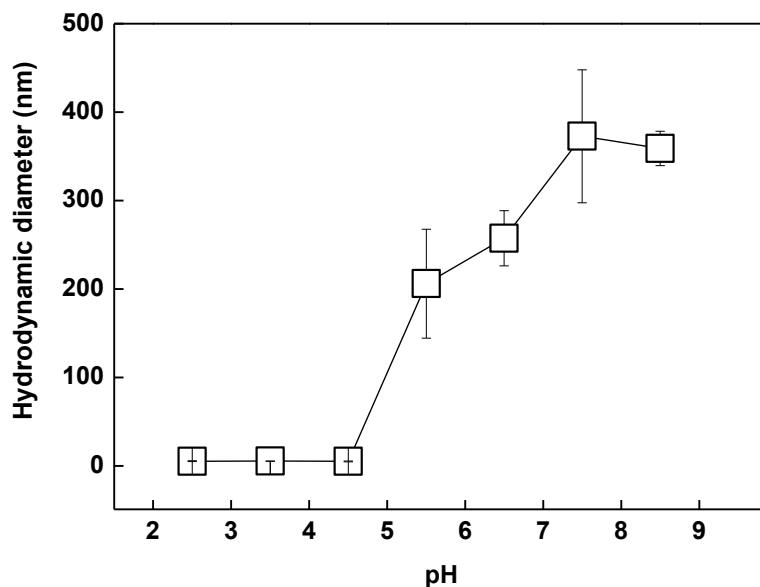


Figure 2.4. The change in number average hydrodynamic diameter of poly(2-ethyl-2-oxazoline) (PEOX) with increasing pH.

Fluorescence Studies

pH-induced self-association of PIPOX was also confirmed using fluorescence spectroscopy technique. Pyrene was used as a probe to examine the pH-induced change in the polarity of the environment in PIPOX solutions. First, PIPOX was dissolved in 7×10^{-7} M pyrene solution (prepared in 0.01 M phosphate buffer) at pH 2.5 and 25 °C with a final PIPOX concentration of 0.2 mg/mL. The solution was splitted into 2 portions. The pH of one of the two solutions was gradually increased to pH 7.5 at 25 °C. Both solutions were stirred at dark for 24 hours at 25 °C. Besides, as a control experiment, two different pyrene solutions (7×10^{-7} M, prepared in 0.01 M phosphate buffer) at pH 2.5 and pH 7.5 which did not contain PIPOX were also stirred at dark for 24 hours at 25 °C. Figure 2.5 represents the normalized emission spectra of pyrene and pyrene in the presence of PIPOX at pH 2.5 and pH 7.5 at 25 °C. The difference in the emission spectra of pyrene in the presence of PIPOX at pH 2.5 and pH 7.5 was remarkable. Of note, this difference was significantly higher than that

between the emission spectra of pyrene (no PIPOX) at pH 2.5 and pH 7.5 at 25 °C. The relatively large fluorescence quenching at pH 7.5 in the presence of PIPOX is a result of preferential solubilization of pyrene within the hydrophobic domains and thus isolation of the hydrophobic pyrene molecules from the aqueous phase by the PIPOX aggregates. In addition, the shape of the spectrum changed at pH 7.5 in the presence of PIPOX which is indicative of a change in the polarity of the environment. The intensity of the peak centered at 375 nm (the first vibrational band) decreased distinctly because the energy was quenched by the enhanced association of the pyrene molecules with the PIPOX chains within the aggregates. Note that, the intensity of the first vibrational band of pyrene (I_1) is affected by the polarity of the environment and decreases as the polarity of the medium decreases whereas the third vibrational band (I_3) remains almost unchanged [252,253]. I_1/I_3 ratio for pyrene in the presence of PIPOX with a final concentration of 0.2 mg/mL at pH 7.5 was lower than that at pH 2.5, indicating solubilization of pyrene within PIPOX aggregates. The pH-dependent change of this ratio in the absence of PIPOX was not remarkable (Figure 2.5, inset).

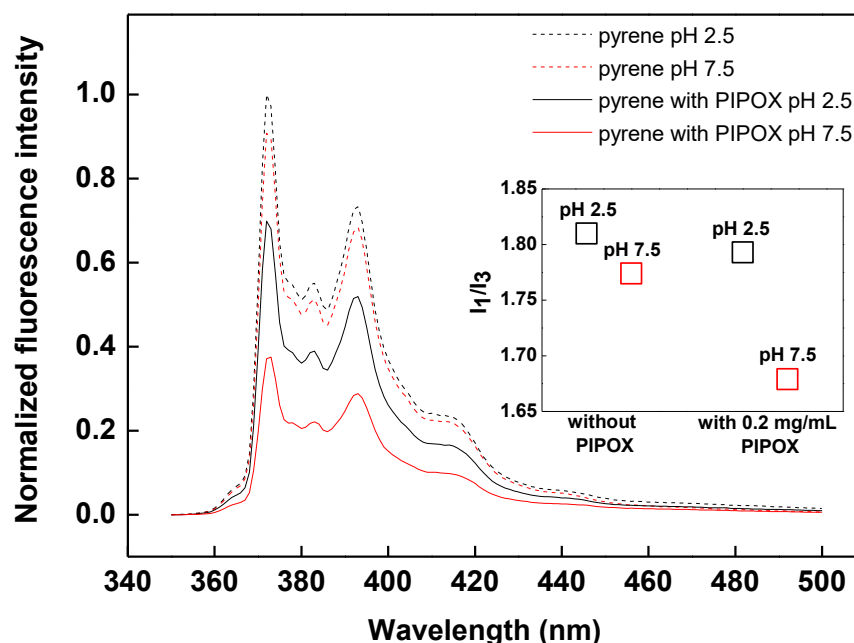


Figure 2.5. Emission spectra of pyrene in the absence of PIPOX and in the presence of PIPOX at pH 2.5 and pH 7.5. Inset shows the pH-dependent change in I_1/I_3 ratio in the absence and presence of PIPOX with a final concentration of 0.2 mg/mL. I_1 and I_3 are fluorescence intensities at 372 nm and 383 nm, respectively.

2.4.2. pH-dependent aqueous solution behavior of PIPOX

pK_a of PIPOX was approximated as ~ 5.2 via potentiometric titration (Figure 2.6). The zeta-potential values gradually became less positive as the pH of PIPOX solution was increased from pH 2.5 to pH 4.5 (Figure 2.7). The negative zeta potential between pH 5.5 and pH 11.0 was possibly due to salt anions adsorbed on the PIPOX aggregates. In the light of these findings, the hydrodynamic size of ~ 4 nm between pH 2.5-4.5 suggested that PIPOX existed as isolated chains or clusters of only few chains in strongly acidic conditions due to protonation of amide units and electrostatic repulsion among PIPOX chains. However, as the pH was increased above the pK_a of PIPOX, electrostatic repulsion among the chains diminished due to unprotonation of the amide units, leading to self-association of PIPOX and formation of the aggregates. To further

understand the pH-induced aggregation of PIPOX, lowest energy optimized structures and interaction energies for PIPOX- H_3O^+ , PIPOX- H_3O^+ - H_2O , PIPOX- H_2O - H_3O^+ , PIPOX- OH^- , PIPOX- OH^- - H_2O and PIPOX- H_2O - OH^- were calculated by DFT methods (Figure 2.8).

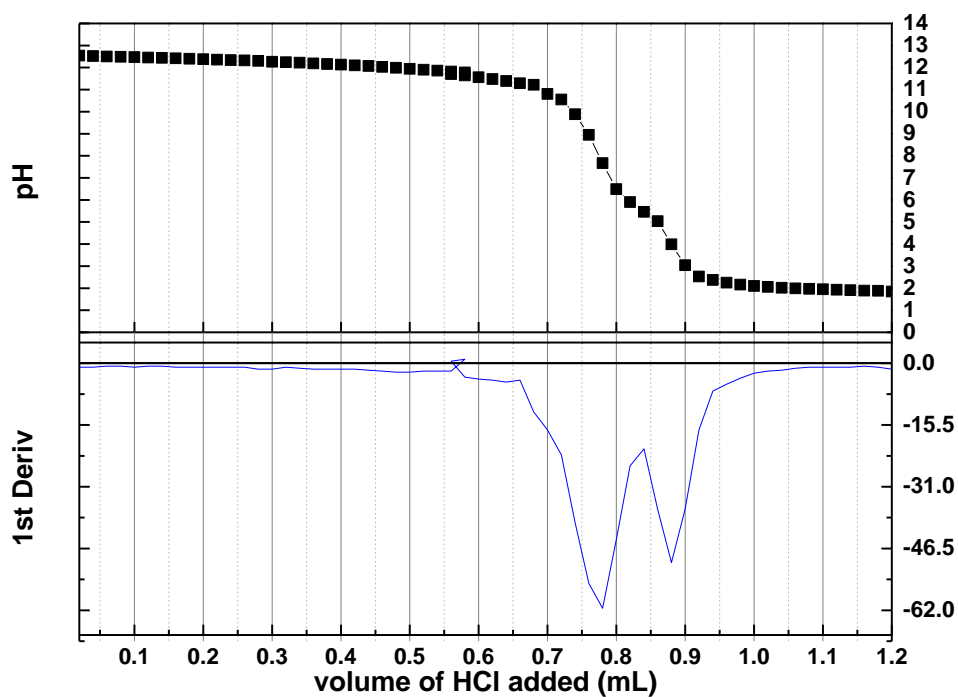


Figure 2.6. Potentiometric titration curve and its first derivative for PIPOX.

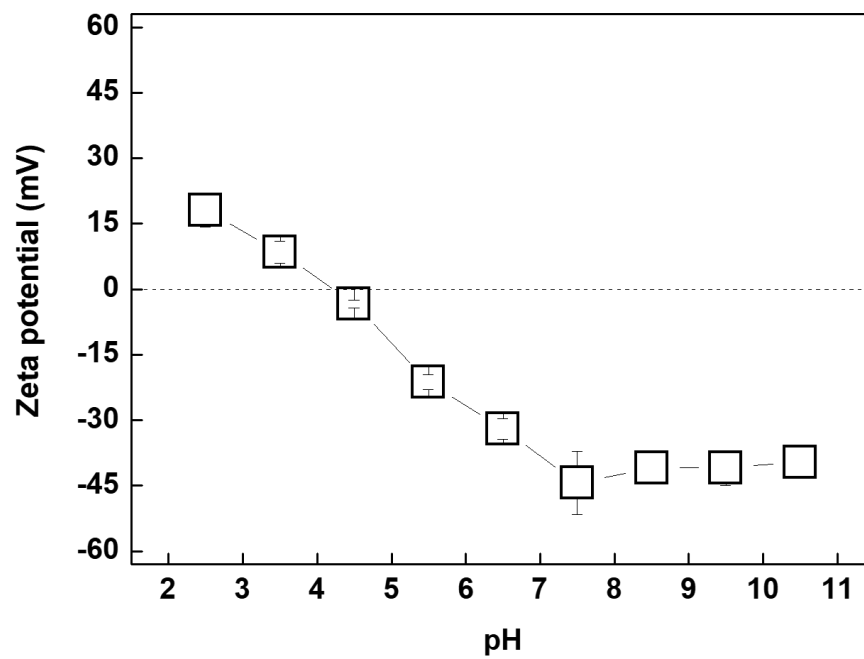


Figure 2.7. Evolution of zeta potential with increasing pH of the PIPOX solution.

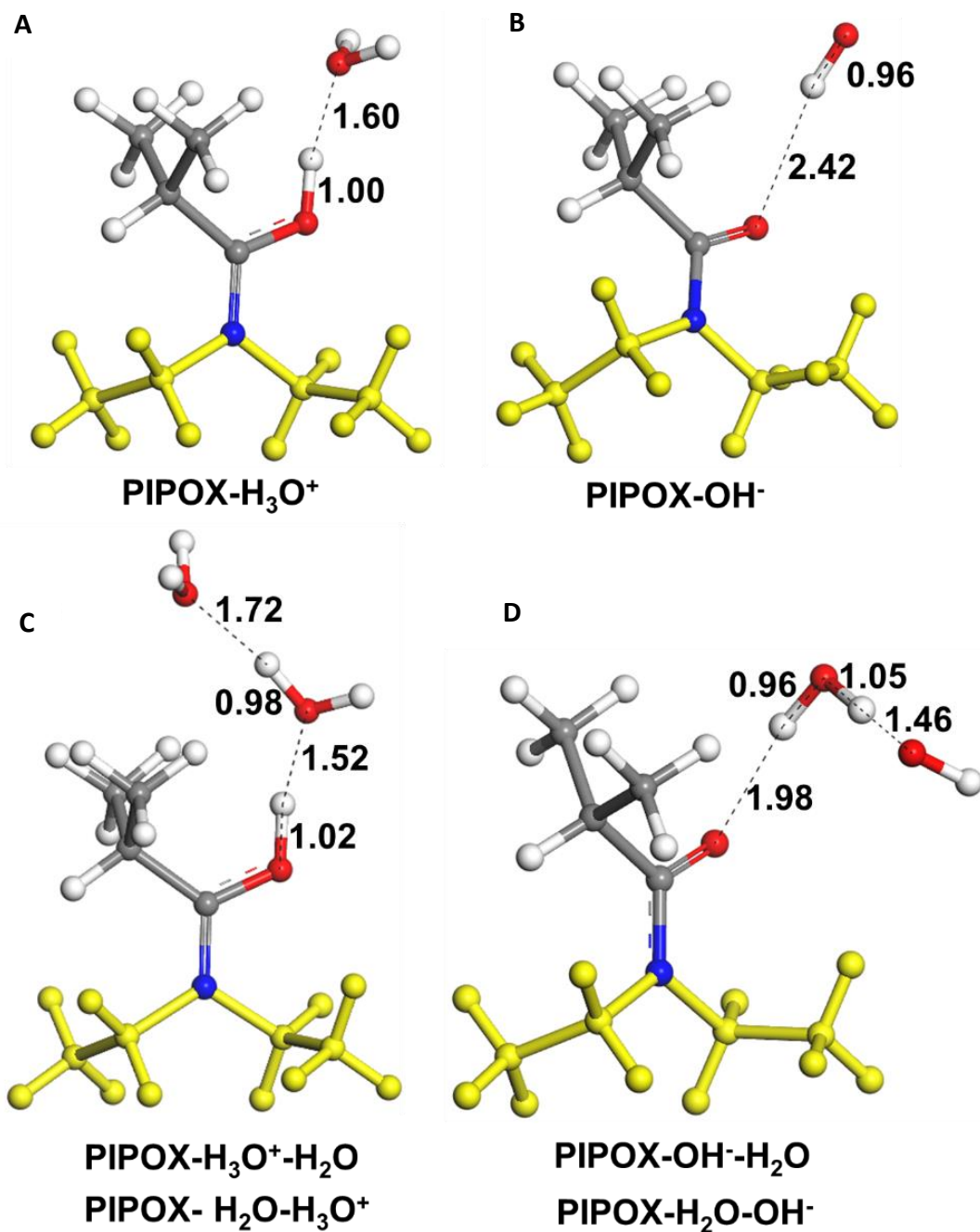


Figure 2.8. Lowest energy structures of A) PIPOX-H₃O⁺, B) PIPOX-OH⁻, C) PIPOX-H₃O⁺-H₂O and PIPOX-H₂O-H₃O⁺, D) PIPOX-OH⁻-H₂O and PIPOX-H₂O-OH⁻. Oxygen: red, carbon: grey, hydrogen: white, nitrogen: blue in color. PIPOX backbone atoms are shown by yellow in color

2.4.2.1. Affinity of H₃O⁺ and OH⁻ to PIPOX and H₂O

Lowest Energy Structures and Interaction Energies

Lowest energy structures determined by geometry optimizations of pairwise and ternary interactions for PIPOX repeat unit with H₃O⁺ and OH⁻ based on by M06-2X/6-311+g(d,p) calculations were given in Figure 2.8. Interaction energies for these structures calculated by different DFT methods were given in Table 2.1. Protonation of amide group oxygen was observed in PIPOX for all the final structures of PIPOX-H₃O⁺, PIPOX-H₃O⁺-H₂O and PIPOX-H₂O-H₃O⁺ structures at low pH (Figure 2.8a, 2.8c). This result indicated that low pH solutions increased the solubility of PIPOX by protonation of the amide groups that enhance the polarity and hydrophilicity of the chains.

Table 2.1. Interaction energies (eV) for pairwise and ternary interactions of PIPOX with H₂O, H₃O⁺ and OH⁻

	M06-2X 6-311+(d,p)	B3LYP DNP	mPW1PW91 6-311+g (2d,2p)
PIPOX-H₂O	-0.29	-0.20	-0.22
PIPOX-H₃O⁺	-4.81*, -0.53**	-4.14*, -0.52**	-4.73*, -0.43**
PIPOX-H₃O⁺-H₂O PIPOX- H₂O-H₃O⁺	-4.23*, -0.70**	-3.86*, -0.69**	-4.02*, -0.60**
PIPOX-OH⁻	-0.06	-0.21	-0.02
PIPOX-OH⁻-H₂O PIPOX-H₂O-OH⁻	-0.22	-0.34	-0.09

(*) PIPOX interaction with the rest of the system at low pH, for PIPOX---H₃O⁺ and PIPOX---H₃O⁺-H₂O. (**) PIPOXH⁺ interaction with the rest of the system at low pH, for PIPOXH⁺---H₂O, and PIPOXH⁺---H₂O-H₂O.

It should be noted that the interaction energies given in Table 2.1 are calculated for both the protonated PIPOX repeat unit and water interaction, denoted by $\text{PIPOXH}^+-\text{H}_2\text{O}$ and also for neutral PIPOX and hydronium interactions, denoted by $\text{PIPOX}-\text{H}_3\text{O}^+$. Different initial structures did not change the interaction energies significantly. Interaction energy between PIPOX and H_3O^+ components was over -4 eV at equilibrium which was another strong evidence for bond formation by proton transfer to PIPOX at low pH. Interaction energy between PIPOXH^+ and H_2O is -0.53 eV with M06-2X functional. Interaction energies for $\text{PIPOX}-\text{H}_2\text{O}$ are higher than (M06-2X and mPW1PW91 methods) or comparable (B3LYP method) with $\text{PIPOX}-\text{OH}^-$ where both interactions are significantly lower than $\text{PIPOX}-\text{H}_3\text{O}^+$ and $\text{PIPOXH}^+-\text{H}_2\text{O}$ interactions. mPW1PW91 method was determined to lower estimate $\text{PIPOX}-\text{OH}^-$ interactions.

While $\text{PIPOX}-\text{H}_2\text{O}-\text{OH}^-$ keeps its initial structure intact, another proton transfer was observed for $\text{PIPOX}-\text{OH}^- - \text{H}_2\text{O}$ where the structure transformed into $\text{PIPOX}-\text{H}_2\text{O}-\text{OH}^-$. That means hydroxide anions are excluded from PIPOX chains through proton transfer and PIPOX chains preferred to be in contact with water molecules instead of hydroxide anions (Figure 2.9d). Optimized structures for $\text{PIPOX}-\text{H}_2\text{O}-\text{OH}^-$ and $\text{PIPOX}-\text{H}_2\text{O}-\text{H}_3\text{O}^+$ given in Figure 2.8 also demonstrated that, while $\text{PIPOX}-\text{H}_2\text{O}-\text{OH}^-$ is stable, $\text{PIPOX}-\text{H}_2\text{O}-\text{H}_3\text{O}^+$ prefer to be in $\text{PIPOXH}^+-\text{H}_2\text{O}-\text{H}_2\text{O}$ structure through proton transfer to PIPOX chains. At low pH values, hydronium ions tended to donate its proton to PIPOX which increased polarity and interaction with water and hence the solubility of aggregates. Protonation of PIPOX at low pH and affinity of PIPOX to avoid from direct interaction with hydroxyl anions at high pH are important evidences to explain observed aggregation behavior of chains at various pH.

In all binary and different configurations of ternary interactions $\text{PIPOX}---\text{H}_3\text{O}^+$ and $\text{PIPOXH}^+---\text{H}_2\text{O}$ interactions are stronger than $\text{PIPOX}---\text{OH}^-$ interaction. We also calculated $\text{H}_3\text{O}^+-\text{H}_2\text{O}$, $\text{OH}^- - \text{H}_2\text{O}$, $\text{H}_2\text{O}-\text{H}_2\text{O}$ interactions as -1.63 eV, -0.94 eV, -0.21 eV, respectively. The order of interaction energies was $\text{PIPOX}---\text{H}_3\text{O}^+ > \text{H}_3\text{O}^+---\text{H}_2\text{O} > \text{OH}^----\text{H}_2\text{O} > \text{PIPOX}---\text{OH}^-$ which can explain all the observed structures and

experimental results. While H_3O^+ ions had strong affinity to PIPOX compared to their affinity for water molecules, OH^- ions had affinity to interact with water molecules compared to their affinity towards PIPOX. Since H_3O^+ ions had strong interaction with both water and PIPOX in addition to their ability to protonate chains, these ions acted as compatibilizer between PIPOX and water and improve chain solubility and decrease aggregate size by increasing hydrophilicity at low pH. However, OH^- ions having stronger interaction with water and having weak interaction with PIPOX among all constituents indicate that these ions not only excluded from polymer phase but also could desorb water molecules around PIPOX. Hydrophobic interactions between isopropyl groups became more dominant with the decreasing solubility and water desorption leads to formations of larger PIPOX aggregates at high pH.

These results were confirmed by quaternary interactions of PIPOX with water, H_3O^+ , OH^- given in Figure 2.9. DFT calculations showed that $\text{PIPOX-H}_2\text{O-H}_2\text{O-H}_3\text{O}^+$ is converted to $\text{PIPOXH}^+-\text{H}_2\text{O-H}_2\text{O-H}_2\text{O}$ in the optimized structure after step by step proton transfer towards PIPOX. However, $\text{PIPOX-OH-H}_2\text{O-H}_2\text{O}$ is in $\text{PIPOX-H}_2\text{O-OH-H}_2\text{O}$ form in final structure due to the affinity of OH^- ions for water molecules compared to OH^- affinity to PIPOX. PIPOX interactions with the rest of the system for $\text{PIPOX}---\text{H}_3\text{O}^+-\text{H}_2\text{O-H}_2\text{O}$, $\text{PIPOXH}^+---\text{H}_2\text{O-H}_2\text{O-H}_2\text{O}$ at low pH and $\text{PIPOX}---\text{H}_2\text{O-OH}^--\text{H}_2\text{O}$ at high pH were calculated as -4.1 eV, -0.78 eV and -0.22 eV, respectively that are in agreement with the results given in Table 2.1.

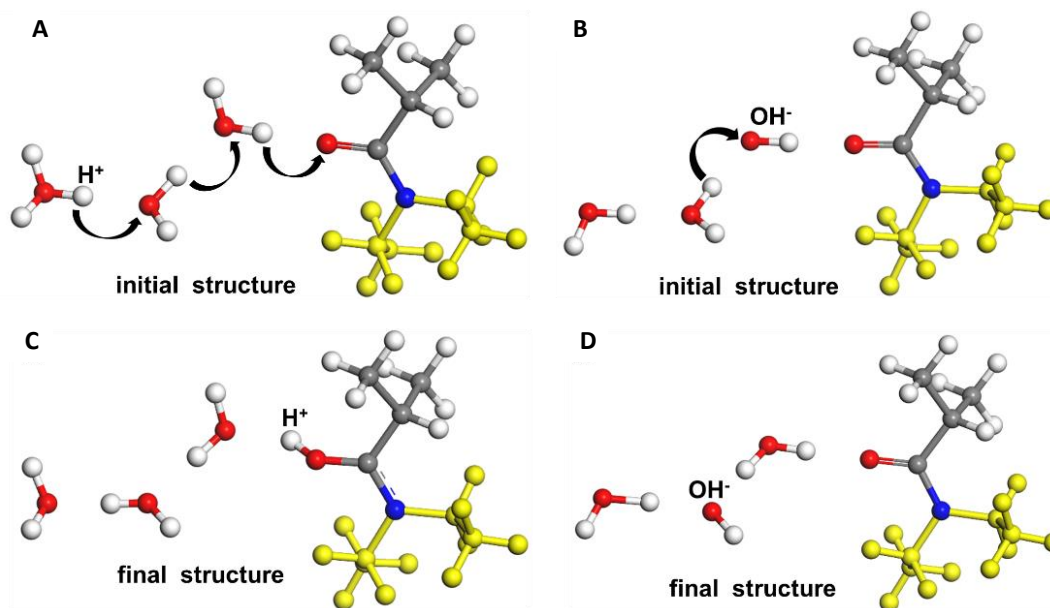


Figure 2.9. A) Initial and C) final structures of PIPOX-H₂O-H₂O-H₃O⁺ system. B) Initial and D) final structures of PIPOX-OH-H₂O-H₂O system. PIPOX-H₂O-H₂O-H₃O⁺ is PIPOXH⁺-H₂O-H₂O-H₂O in its geometry optimized final structure, while PIPOX-OH-H₂O-H₂O is in PIPOX-H₂O-OH-H₂O form in final structure

Free Energy of Solvation Calculations

Total free energy of solvation and its contributions from ideal, vdW and electrostatic components were calculated for a neutral PIPOX decamer and a PIPOX decamer protonated at one amide group at low pH, denoted as PIPOXH⁺ given in Table 2.2. The cell constructed for free energy of solvation calculations of PIPOXH⁺ model in water is given in Figure 2.10. All three step of thermodynamic cycle to calculate solvation free energy that are removal of charges from oligomer (ideal), coupling of PIPOX to the solvent using solely vdW interactions (vdW), and finally switching back the charges onto PIPOX in the water environment (electrostatic), demonstrated that protonation increases the solvation free energy of PIPOX chain by water molecules significantly. vdW contribution to solvation energy did not change significantly and ideal contribution to solvation free energy decreases. The main reason for this solubility enhancement is the increase in electrostatic contribution to solvation energy

by hydronium cations in acidic environment. We can conclude that electrostatic interactions such as ionic interactions and hydrogen bonds increased significantly by protonation of chains at low pH which led to the reduced aggregation of PIPOX chains.

Table 2.2. Ideal, vdW, electrostatic and total free energy of solvation.

	Ideal free energy (kcal/mol)	vdW free energy (kcal/mol)	Electrostatic free energy (kcal/mol)	Total solvation free energy (kcal/mol)
PIPOX	-117.18	18.26	91.84	-7.08
PIPOXH⁺	-96.72	17.59	64.28	-14.83

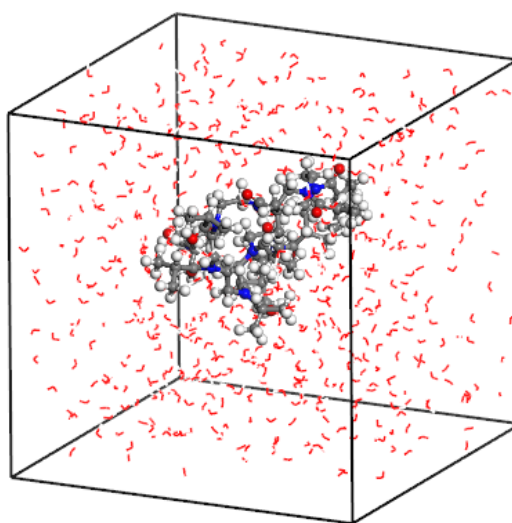


Figure 2.10. Structure of PIPOXH⁺ decamer with one protonated monomer and 600 water molecules under periodic boundary conditions, constructed for the free energy solvation calculations.

2.4.3. pH-dependent aqueous solution behavior of PIPOX

To explore the effect of end-groups on the self-association of PIPOX, 2-butoxy was replaced with a more hydrophobic end-group, i.e. N-boc-amino-piperidiny and the hydrodynamic sizes of both polymers were measured at pH 5.5. Of note, both PIPOX-2-butoxy and PIPOX-N-boc-amino-piperidiny had similar hydrodynamic sizes at acidic conditions. However, higher size values were recorded for PIPOX with N-boc-amino-piperidiny than that for PIPOX with 2-butoxy under the same pH conditions, indicating the effect of end-groups on self-aggregation of PIPOX (Figure 2.11). Although the aggregate sizes were different for PIPOX and PIPOX-N-Boc-amino-piperidine, the pH at which the aggregates were formed was found to be similar for both polymers. Figure 2.12 contrasts the evolution of hydrodynamic diameter of PIPOX and PIPOX-N-Boc-amino-piperidine as the pH was gradually increased from acidic to neutral conditions. The effect of chain end units on the self-assembly of hydrophilic polymers has been reported before. A study by Hammouda and co-workers demonstrated that PEO with $-OCH_3$ groups at both terminals formed strong clusters, whereas PEO with $-OH$ groups at both ends formed the weakest clusters in aqueous environment [230]. Homopolymers synthesized *via* reversible addition fragmentation chain transfer (RAFT) or atom transfer radical polymerization (ATRP) and have hydrophobic terminal groups at both ends have been reported to form well-defined nanostructures [225]. Self-assembly of PEOX and PIPOX with hydrophobic end-groups have also been reported by Winnik and co-workers [254].

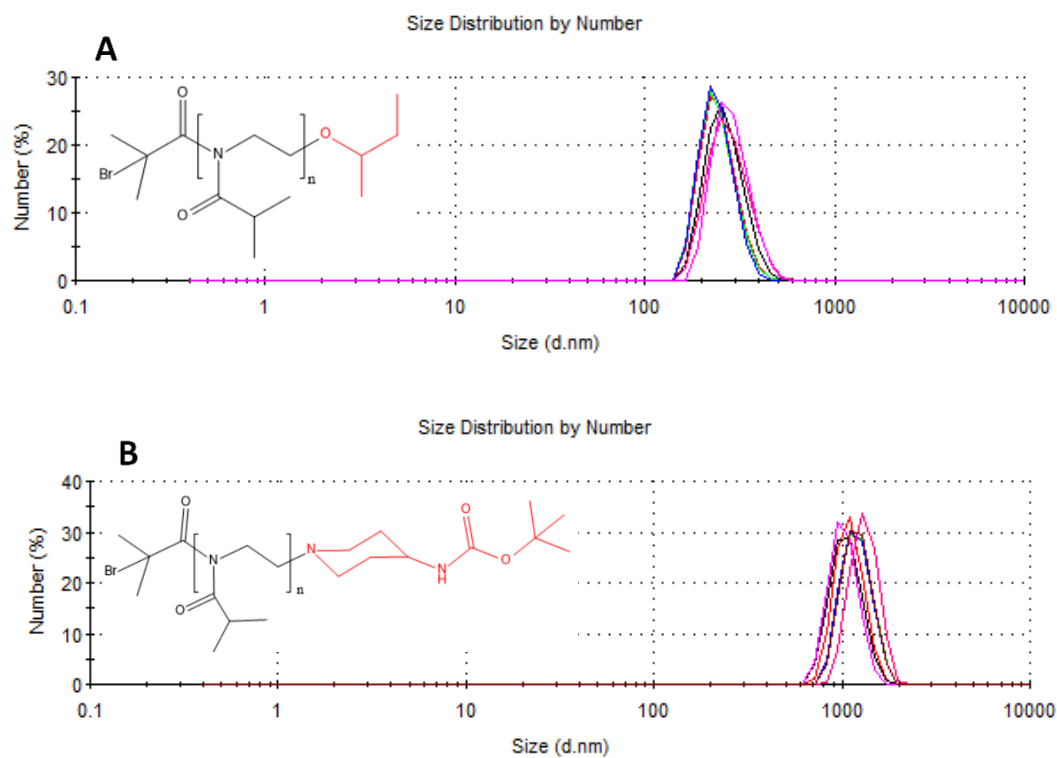


Figure 2.11. The number average hydrodynamic size distributions of PIPOX terminated with 2-butanol (A) and N-boc-amino-piperidine (B) at pH 5.5. Size distribution curves obtained from several individual measurements of the same sample are represented with different colors.

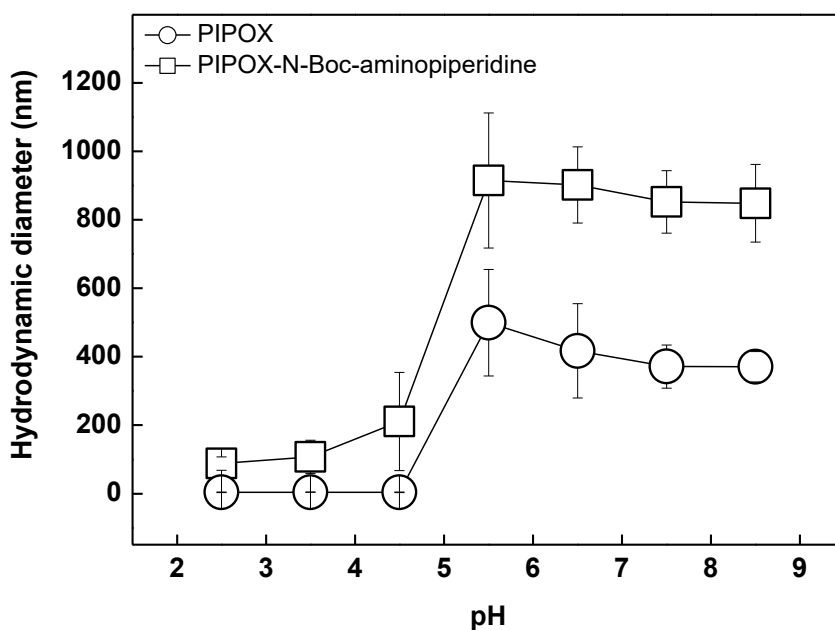


Figure 2.12. Evolution of hydrodynamic diameter of PIPOX and PIPOX-N-Boc-amino-piperidine with increasing pH in 0.2 mg/mL solution.

Statistical mechanics calculations for end group effect on self-association of PIPOX

Off-lattice statistical mechanics calculations based on binary binding energies and coordination numbers given in Eqn 1-4 were performed to explain the effect of terminal groups on PIPOX aggregate sizes. Of note, molecular dynamics simulations in periodic cells are not sensitive enough to calculate effect of terminal groups due to their small size in long chains and limited number of cells that can be analyzed. Coordination numbers (Z) and binding energies (E) between are used to calculate FH interaction parameters (χ) and mixing energies (E_{mix}) given in Table 2.3, for two components which are PIPOX trimer and PIPOX dimer with different terminal groups (Figure 2.13). We demonstrated that pairwise binding energy E_{i-j} and E_{j-j} are significantly lower for 2-butoxy terminal groups. These binding energies are corresponding to terminal group self-interaction and terminal group-PIPOX backbone

interaction. N-boc-amino-piperidine which involve –NH groups having ability to form self-hydrogen bond as well as hydrogen bond with PIPOX, can lead to larger aggregates compared to 2-butoxy terminal groups that lack the ability to form self-hydrogen bond or hydrogen bond with PIPOX backbone.

χ interaction parameters and mixing energies (E_{mix}) calculated based on these binding energies showed that PIPOX backbones have 5-6 times higher mixing energies with N-boc-amino-piperidine terminal groups that explain the observed difference in the aggregate sizes. Free energy (ΔG) of interactions between backbones and terminal groups calculated by the addition of entropic contribution (Figure 2.14) was also found as 3-4 times higher for N-boc-amino-piperidine terminal groups.

Table 2.3. FH interaction parameters (χ) and mixing energies (E_{mix} , kcal/mol) calculated based on binding energies (E_{i-i} , E_{i-j} , E_{j-j}) and coordination numbers (Z_{i-i} , Z_{i-j} , Z_{j-i} , Z_{j-j}) where i is PIPOX and j is terminal group.

I	j	X	E_{mix}	E_{i-i}	E_{i-j}	E_{j-j}	Z_{i-i}	Z_{i-j}	Z_{j-i}	Z_{j-j}
PIPOX	2-butanol	-3.6	-2.2	-7.8	-6.3	-4.1	5.6	5.5	5.6	5.6
PIPOX	N-boc-amino-piperidine	-20.5	-12.1	-7.8	-10.0	-8.1	5.6	4.8	6.3	5.6

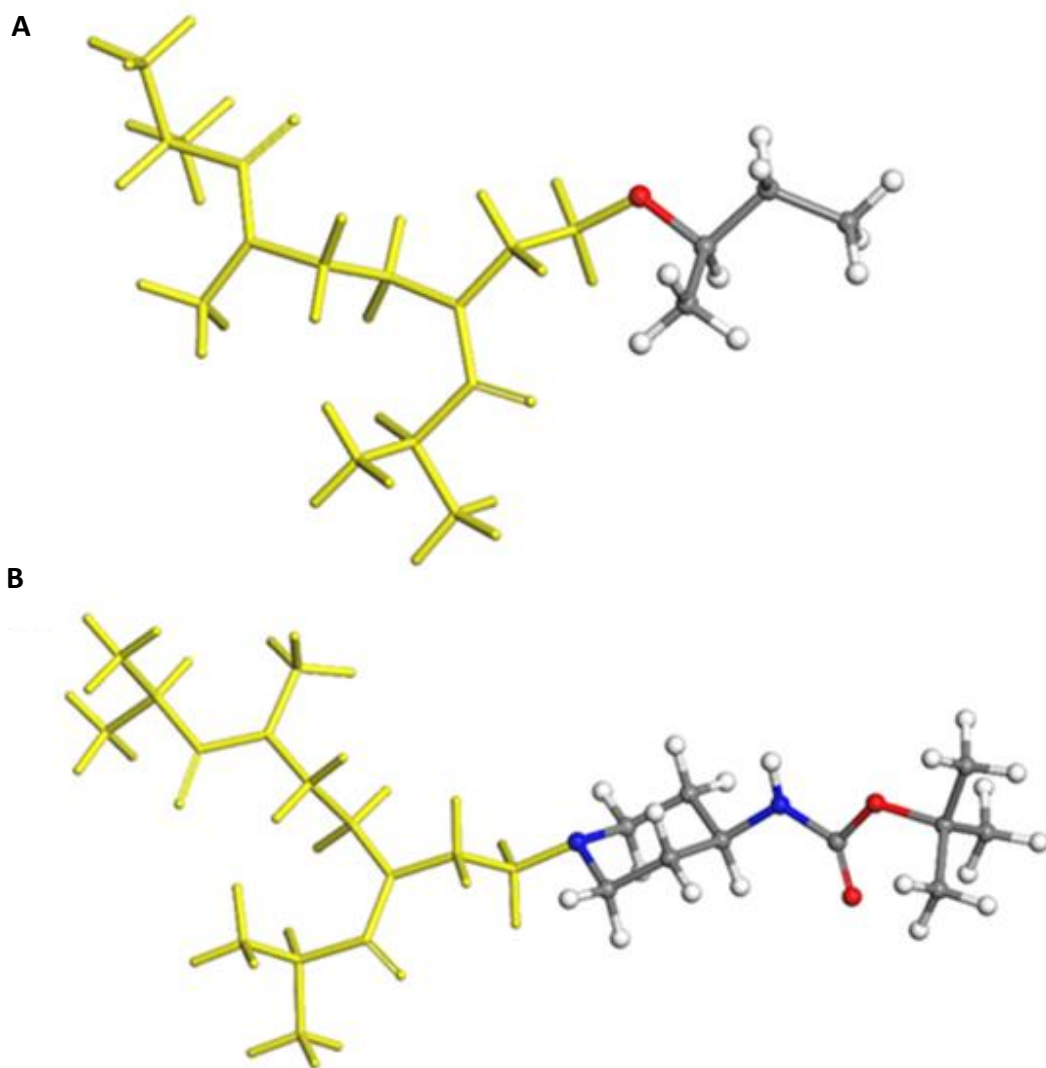


Figure 2.13. Structures of PIPOX dimers terminated with 2-butanol (A) and N-boc-amino-piperidine (B). Backbone is shown by yellow color.

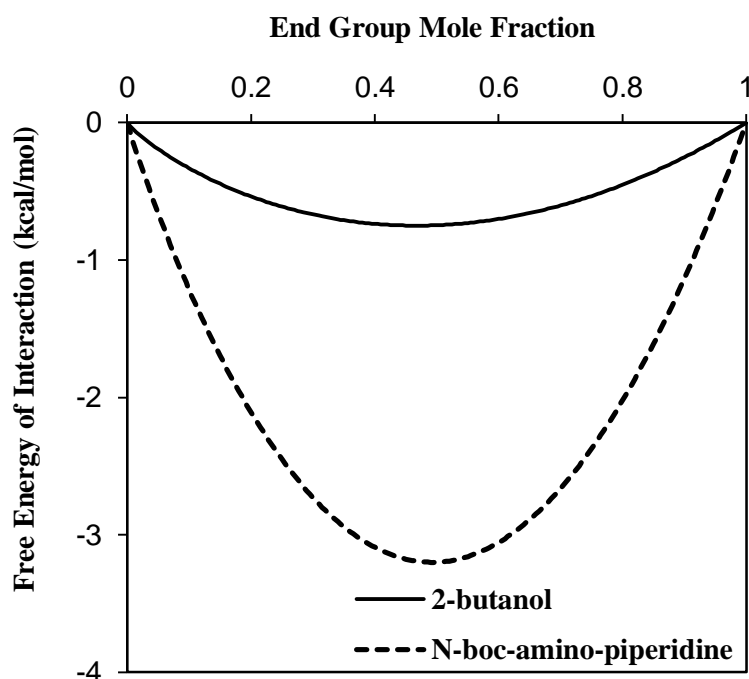


Figure 2.14. Free energy of interaction between PIPOX trimer and PIPOX dimer terminated with 2-butanol and N-boc-amino-piperidine end groups for different mole fractions.

2.4.4. Effect of concentration on the size of PIPOX aggregates

Hydrodynamic diameter of PIPOX in 0.2 mg/mL, 0.6 mg/mL or 1 mg/mL solution was monitored at pH 2.5 and pH 7.5. The number average hydrodynamic diameter distributions of PIPOX under each condition are presented in Figure 2.15. We observed a pH-dependent concentration effect on the aggregate size. The size of PIPOX aggregates was not affected by increasing concentration at pH 2.5 when the electrostatic repulsion was strong enough to inhibit the aggregation. In contrast, the size distribution curve shifted to higher values at pH 7.5 when the concentration was increased, indicating formation of larger aggregates. The formation of PIPOX aggregates was expected to start by the formation of many nuclei which were self-associating PIPOX chains. The aggregates then grew by the continuous addition of PIPOX chains onto the nuclei. At high concentrations of PIPOX, greater number of PIPOX chains could have been added onto each nucleus within the same time period

resulting in formation of larger aggregates. We also confirmed the increase in size of the aggregates with increasing PIPOX concentration *via* SEM imaging. Figure 2.16 contrasts SEM images of PIPOX at pH 2.5 and pH 7.5 at 0.2 mg/mL, 0.6 mg/mL, and 1 mg/mL concentrations. The effect of concentration on the aggregate size has been reported for polymers [225,255,256] and biological molecules such as proteins and oligopeptides [257,258]. The concentration was found to be more critical on the aggregate size above the critical association (aggregation) concentration.

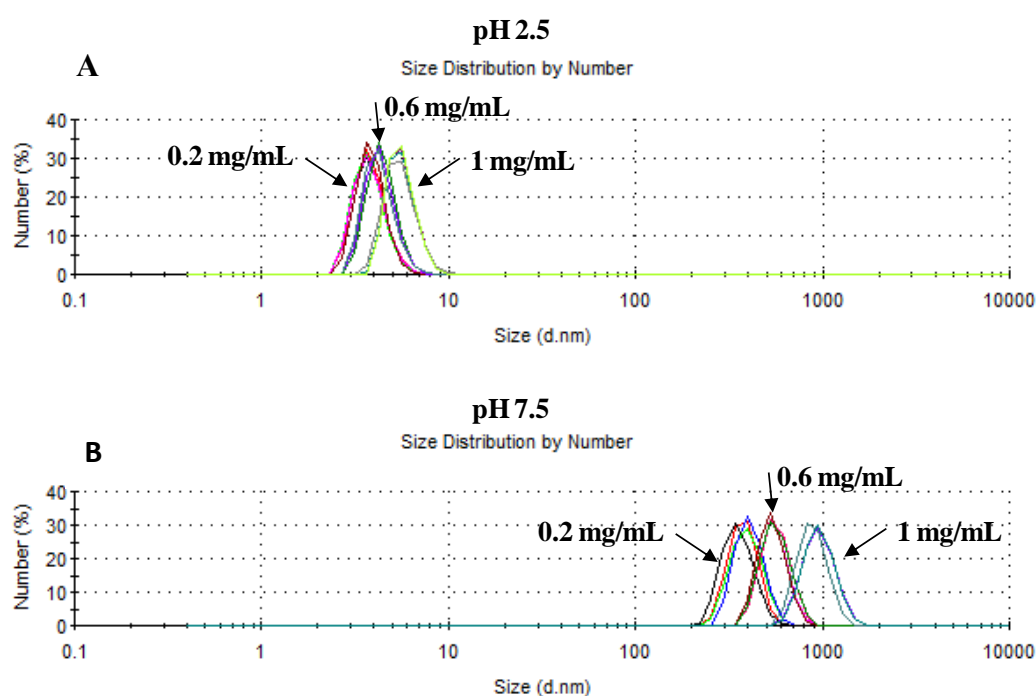


Figure 2.15. Number average hydrodynamic size distributions of PIPOX at pH 2.5 and pH 7.5 in 0.2 mg/mL, 0.6 mg/mL and 1 mg/mL solutions. Size distribution curves obtained from several individual measurements of the same sample are represented with different colors.

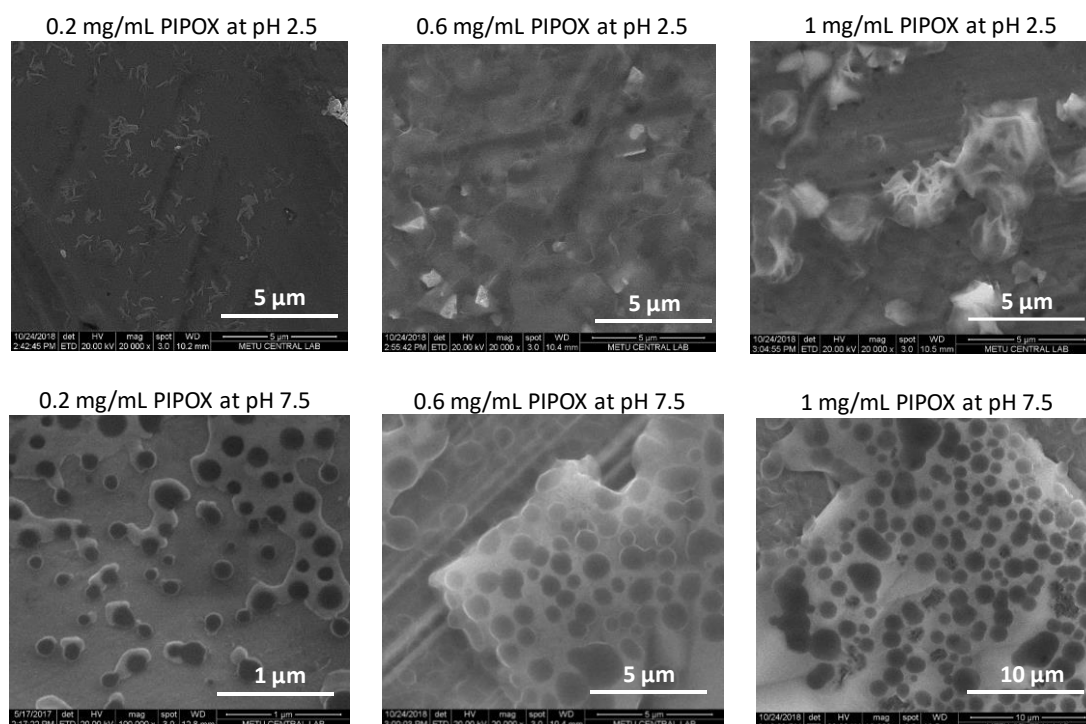


Figure 2.16. SEM images of PIPOX at pH 2.5 and pH 7.5 at 0.2 mg/mL, 0.6 mg/mL and 1.0 mg/mL concentration.

Finally, we examined pH-dependent encapsulation of pyrene in the presence of PIPOX with a final concentration of 0.2 mg/mL, 0.6 mg/mL or 1 mg/mL. As seen in Figure 2.17a, increasing PIPOX concentration in pyrene solution resulted in relatively large quenching at both pH 2.5 and pH 7.5. I_1/I_3 ratios of pyrene were found to be lower at pH 7.5 than that at pH 2.5 and were similar in magnitude at all PIPOX concentrations (Figure 2.17b). As also mentioned in Section 2.3.1, such a remarkable pH-dependent change in I_1/I_3 ratio was not observed for the control samples (pyrene in the absence of PIPOX).

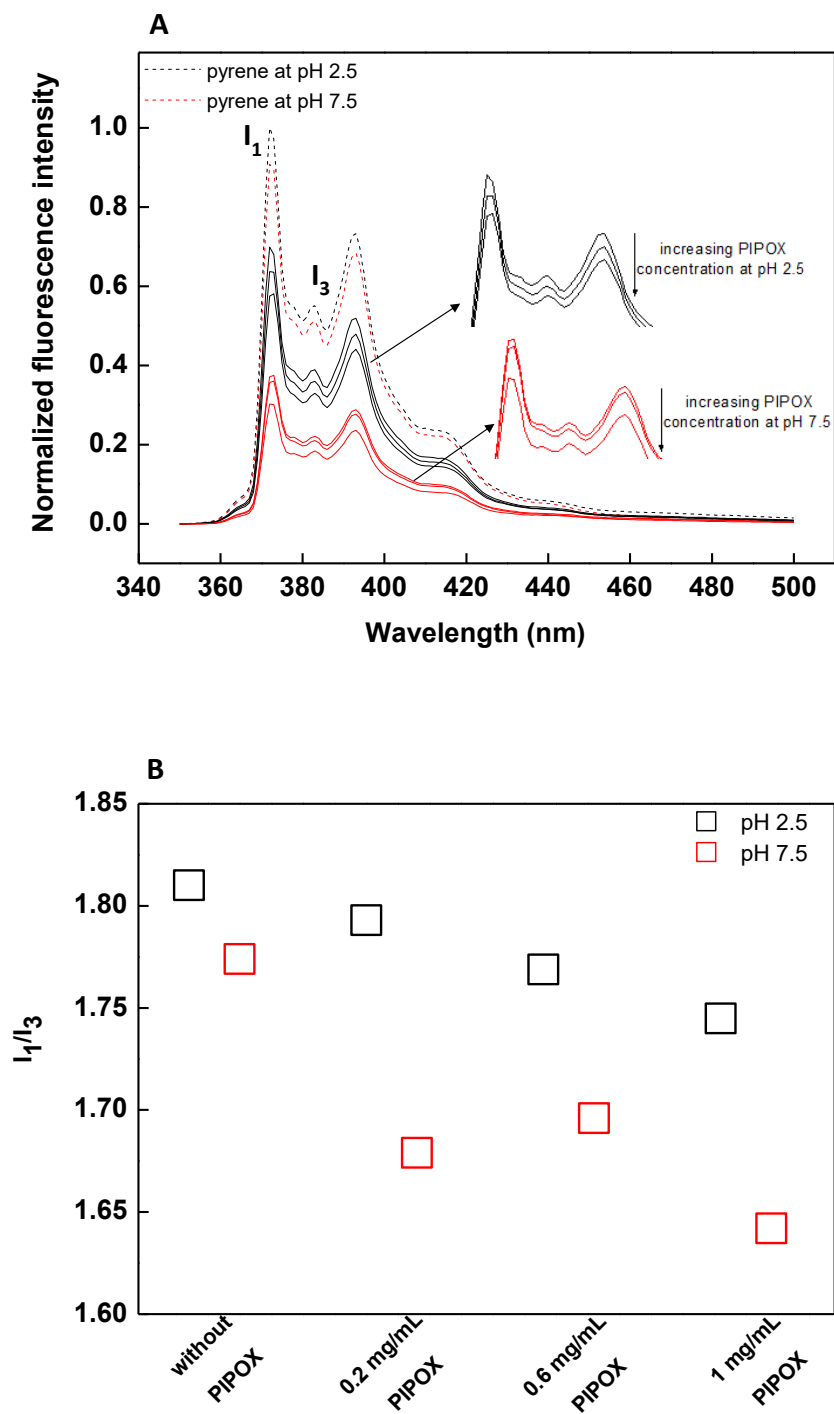


Figure 2.17. A) Emission spectra of pyrene in the absence of PIPOX and in the presence of PIPOX with a final concentration of 0.2 mg/mL, 0.6 mg/mL or 1 mg/mL. (B) pH-dependent change in I_1/I_3 ratio of pyrene in the absence and presence of PIPOX with a final concentration of 0.2 mg/mL, 0.6 mg/mL and 1 mg/mL. I_1 and I_3 are fluorescence intensities at 372 nm and 383 nm, respectively.

2.4.5. Effect of salt concentration on the aqueous solution behaviour of PIPOX

The hydrodynamic size of PIPOX was followed as a function of pH in 0.1 M phosphate buffer (Figure 2.18) and the data is contrasted with the hydrodynamic size values obtained in 0.01 M phosphate buffer, reported in Section 2.4.1 (Figure 2.1). In contrast to results obtained in 0.01 M phosphate buffer, aggregates with size varying between 300-450 nm were obtained between pH 2.5-4.5 in 0.1 M phosphate buffer solution. Further decreasing the acidity resulted in a significant decrease in size exactly at the same pH where a jump in hydrodynamic size was observed for PIPOX in 0.01 M phosphate buffer solution. The size reached almost a constant value between pH 6.5 – 8.5 in both solutions.

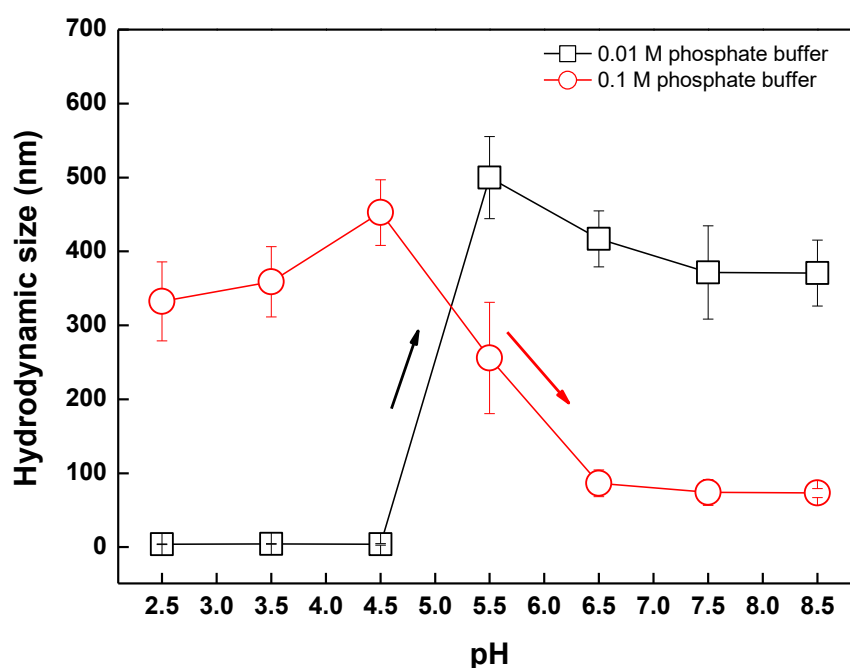


Figure 2.18. Hydrodynamic size of PIPOX in 0.01 M (\square) or 0.1 M (\circ) phosphate buffer with increasing pH.

The effect of salt concentration on the phase separation of non-ionic homopolymers has been investigated before. However, the mechanism is still under debate. Three main mechanisms have been proposed for the change in the conformation and LCST of PNIPAM at high salt concentration; i) nonpolar group stabilization [259–261], ii) alteration in the structure of water [259,262] and iii) amide-salt interactions [263]. It has been suggested that the cations of the salts take the major role in the first two mechanisms while anions are believed to have greater role than the cations in the third mechanism [259].

In the light of these findings, we attribute the formation of aggregates in 0.1 M phosphate buffer at acidic conditions to greater amide-salt interactions at high salt concentrations when the amide nitrogens were protonated. The salt anions acted as bridges between the positively charged amide units, inducing the aggregation of PIPOX chains. In addition, salt anions were expected to screen the positive charge arising from the amide units, thus decrease the electrostatic repulsion and enhance the hydrophobic-hydrophobic interactions among PIPOX chains. As the pH was increased above the pK_a of PIPOX, salt-induced aggregates did not exist in solution any longer due to unprotonation of the amide nitrogens. Importantly, the size of PIPOX aggregates above pH 5 in 0.1 M phosphate buffer was significantly lower than that obtained in 0.01 M phosphate buffer solution. This difference can be explained by the salting out effect of hydrogen phosphate ions. Hydrogen phosphate ions tend to have stronger attraction with water molecules compared to interactions among water molecules. Thus, increasing concentration of the phosphate buffer was expected to destroy the hydrogen bonding among water molecules as well as the hydrogen-bonding network constructed by water molecules and PIPOX. This led to formation of smaller PIPOX aggregates in 0.1 M phosphate buffer solution above pH 5 than that formed in 0.01 M phosphate buffer solution. Remember that hydrogen bonding interactions among the PIPOX chains mediated by water molecules was suggested as one of the driving forces for the formation of PIPOX aggregates.

2.4.6. Effect of pH on the cloud point temperature of PIPOX

LCST-type phase behaviour of PIPOX has earlier been reported [2,5,7–9]. In this part of the study, we examined the effect of pH on the cloud point temperature of PIPOX. PIPOX solutions at pH 2.5 and pH 7.5 were examined separately. Cloud point temperatures of these solutions were determined *via* turbidimetric analysis. The change in absorbance of 10 mg/mL PIPOX solution at 450 nm was followed as a function of temperature using UV-Visible Spectroscopy (Figure 2.19). Turbidity of the solution increases above the critical temperature due to a transition in conformation from extended to globular coil and enhanced hydrophobic interactions among the PIPOX aggregates. At pH 2.5, the remarkable increase in absorbance was detected at 42.5 °C when the solution was heated by 2.5 °C steps from 25 °C to at 60 °C. The critical temperature was detected within 42-47 °C range during the cooling cycle. At pH 7.5, CP was detected at 37 °C for heating and within 40-60 °C during cooling cycles, respectively. The higher cloud point temperature at pH 2.5 than that at pH 7.5 was because of the protonation of amide units and greater hydrophilicity of PIPOX chains. The effect of pH on the LCST of polyelectrolytes has been examined earlier and an increase in LCST was observed with increasing charge density on the polyelectrolyte [264–268].

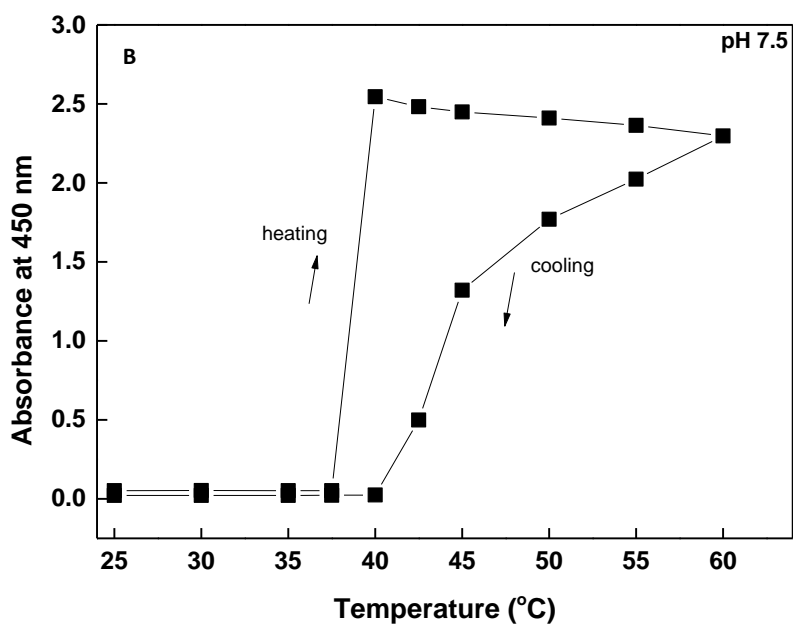
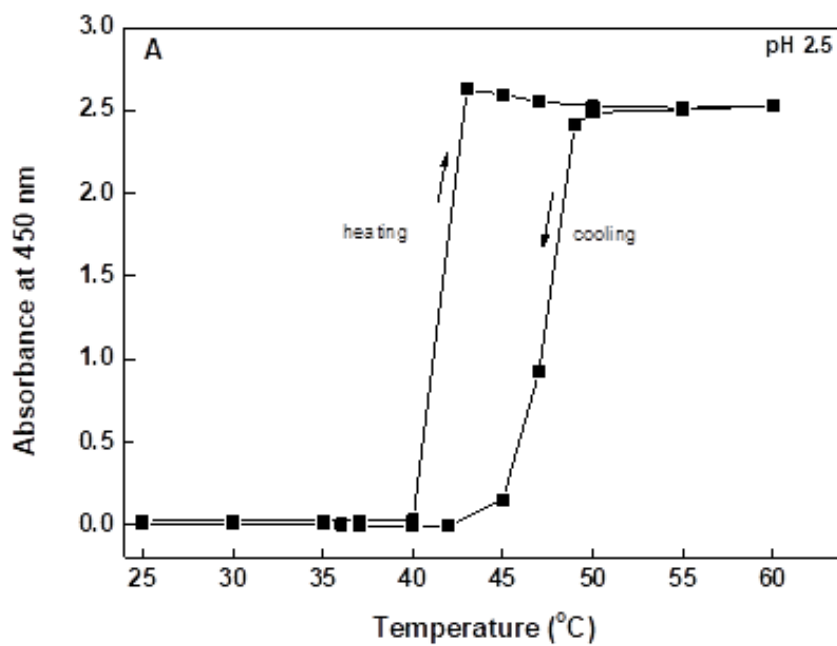


Figure 2.19. The change in absorbance at 450 nm as a function of temperature for (A) 10 mg/mL PIPOX solution at pH 2.5 and (B) 10 mg/mL PIPOX solution whose pH was increased from 2.5 to 7.5.

2.5. Conclusion

PIPOX aggregates were formed *via* pH trigger above pH 5.0 at 25 °C. Lowest energy structures and interaction energies of PIPOX - H₃O⁺, H₃O⁺ - H₂O, OH⁻ - H₂O, PIPOX - OH⁻ calculated by DFT methods showed that, in addition to their ability to protonate PIPOX that increase free energy of solvation in water, H₃O⁺ ions had strong interaction with both water and PIPOX at acidic conditions. Therefore, H₃O⁺ ions acted as compatibilizer between PIPOX and water and increased the solubility of PIPOX at low pH. However, OH⁻ ions were found to have stronger interaction with water compared to PIPOX resulting in desorption of water molecules around PIPOX and a decrease in solubility. This has led to more dominant hydrophobic interactions among isopropyl groups of PIPOX and formation of PIPOX aggregates at high pH. The chemical nature of the end-groups was found to affect the self-association of PIPOX, thus the aggregate size. Experimental results were in good agreement with statistical mechanics calculations based on binary binding energies and coordination numbers. Moreover, we found that increasing salt concentration of PIPOX solution led to formation of larger aggregates at acidic conditions but smaller aggregates at higher pH values when compared to the size of PIPOX aggregates in solutions with low salt concentration. The large aggregates at high salt concentrations under acidic conditions were formed *via* salt-trigger where the salt anions acted as bridges between the positively charged amide units, inducing the aggregation of PIPOX chains. In contrast, above pH 5.0, where PIPOX got unprotonated and formation of aggregates was induced *via* pH-trigger, increasing salt concentration destroyed the hydrogen bonding among water molecules as well as the hydrogen bonding network constructed by water molecules and PIPOX, resulting in formation of smaller aggregates. We have also found that cloud point temperature of PIPOX solutions was affected by the formation of PIPOX aggregates in solution. The cloud point temperature for PIPOX at acidic pH was slightly lower than that observed for PIPOX solution at pH 7.5 due to greater hydrophilicity of the PIPOX chains at acidic pH. This study presents a new triggering mechanism to prepare PIPOX aggregates and examines pH-dependent

aqueous solution behaviour of PIPOX through both experimental and computational approaches.

CHAPTER 3

EFFECT OF END-GROUP ON DRUG LOADING/RELEASE PROPERTIES OF PIPOX SELF-AGGREGATES

3.1. Chapter Summary

Homopolymer self-aggregates has driven great attention due to easier synthetic procedures, higher capacity for therapeutic storage and controlled release of cargo at desired conditions. In this part of the thesis, loading and release of a model antibiotic, Chloramphenicol (CAP) into/from PAOX aggregates have been examined at neutral and acidic pH at a physiologically related temperature. PAOX end-group was found to be critical on loading and release properties of CAP from PAOX aggregates. CAP conjugated PAOX chains were found to form larger aggregates and had higher loading capacity than that of 2-Butoxy terminated PIPOX (PIPOX-OR). Moreover, PIPOX-CAP and PIPOX-OR showed remarkably different CAP release profiles especially at moderately acidic pH and 37 °C. CAP loading/release properties of aggregates were correlated with pH and temperature responsive behaviour of PAOX.

3.2. Introduction

Polymer self-assemblies provide significant advantages over other carriers for biomedical applications such as higher storage capacity and stability, controlled release of encapsulated drug, prolonged blood circulation time and enhanced ocular availability [269,270]. Polymer self-assemblies can be formed through either covalent bond formation, e.g. microgels, latexes) or self-association of polymer chains *via* physical interactions [271]. Polymer self-assemblies formed through physical interactions can be further classified based on the mechanism of formation, e.g. solvent selective self-association of copolymers [182,272–275] self-association of

zwitterionic polymers *via* electrostatic interactions [181,276–278], association of different homopolymers *via* H-bonding [205,222,279], surfactant induced copolymer assembly [280,281], self-association of neutral homopolymers *via* end-groups (including polymer-drug conjugates) [75–77,79,91]. Homopolymer self-aggregation has driven attention of the researchers due to relatively easy synthetic procedures compared to diblock counterparts [227,228]. Specifically, self-assembly of PEO- a neutral polymer commonly used in biomedical applications- in aqueous solution has earlier been reported. It was shown that hydrogen bonding interactions between the ether oxygen of PEO and water together with hydrophobic interactions among ethylene units induced formation of PEO nanoclusters [230,231,282].

PAOXs which are also defined as “pseudo-peptides” due to the similarity between the chemical structures of PAOXs and peptides are biocompatible polymers and attract growing attention of the researchers for use in biomedical applications. They are considered as an alternative to PEG due to their enhanced stability against oxidative degradation [283]. PEOX and PIPOX are of specific interest due to their temperature responsive behaviors in aqueous media. For example, Meyer et. al. reported the unexpected self-coagulation of PIPOX above its cloud point and formation of micron-sized assemblies [9]. Winnik and coworkers investigated the temperature-induced self-association of PIPOX-*b*-PEOX providing formation of star-like micelles at 50°C [284]. Haladjova et al. revealed the construction of nano- and microcapsules using thermosensitive PNIPAM and PIPOX templates. Those smart templates were formed basically in three steps; (i) formation of mesoglobules *via* increasing temperature above the LCST of polymer, (ii) coating by seeded radical copolymerization and (iii) dissolution of core through cooling [11]. In another study, Ozaltin et al. examined the morphological characteristics of PIPOX at i) well-below, ii) above and iii) well-above its LCST and supported their experimental findings with computational approaches. They realized that at temperatures well-below the LCST of PIPOX, PIPOX chains had been miscible in aqueous media due to hydrophilic nature of PIPOX. At temperatures above LCST, PIPOX formed spherical shaped aggregates due to enhanced

hydrophobic association among PIPOX chains. At temperatures well-above LCST, they found that helical shaped polymer pitches had come together to form PIPOX fibers [153]. Recently, the first report on pH-induced self-aggregation of PIPOX was reported by our research group. It was found that titrating PIPOX solution with 0.1 M NaOH solution triggered formation of PIPOX aggregates above pH 5.0 at 25 °C [285].

Encapsulation of therapeutics into colloidal polymeric self-assemblies enhance the drug efficacy, diminishes the side effects and toxicity of drugs, overcomes solubility limitation of drug, makes targetability probable *via* attachment of targeting moieties onto the coronae and provides controlled release of drug from them compared to free counterparts. Among polymer drug carriers, polymer-drug conjugate self-assemblies are attracting increasing attention due to high drug loading capacities, unique disintegration properties, and improved plasma half-life with enhanced accumulation in tumors in the body [286]. Yoo et al. discovered that DOX-loading efficacy of poly(DL-lactic-co-glycolic acid)–DOX (PLGA-DOX) conjugate micelles was far greater than the amount loaded into PLGA particles with 95% loading into the former [287]. Same group also synthesized DOX-conjugated poly(DL-lactic-co-glycolic acid) (PLGA) and PEG (DOX–PLGA–PEG) and reported the enhanced loading efficacy of DOX into conjugate micelles reaching to 99% compared to loading into PLGA-PEG micelles which only reached 23% [288]. In another study, Sedlak and coworkers reported PEG conjugated Amphotericin B (AmB) and found that its liposomal form increased the therapeutic index of AmB and decreased nephrotoxicity [102]. Additionally, Li et al. reported that enhanced antitumor efficacy and reduced side effects could be achieved with DOX loaded pH-sensitive PEOX-*hyd*-DOX conjugate micelles compared to unloaded PEOX-*hyd*-DOX conjugate micellar counterpart due to higher amount of DOX release from the former [77].

In this study, pH- and temperature triggered release of CAP, a model antibiotic from PIPOX self-aggregates which formed *via* pH-trigger in aqueous solution at 25 °C has been examined at neutral and moderately acidic conditions at a physiologically related temperature. CAP is a topically applied ocular antibiotic in a form of eye-drops that

has been used for the prevalent infection called “acute bacterial conjunctivitis”. It has high activity against *S.aureus* in cornea and conjunctiva as well as against methicillin-resistant *S.aureus* (*MRSA*) causing ocular surface infections [289]. Two different PIPOX samples with varying end-groups were used: i) PIPOX-OR with 2-butoxy as the end-group and ii) PIPOX-CAP in which CAP was used as the terminating agent. PIPOX-OR and PIPOX-CAP were contrasted with respect to CAP loading capacities and release behaviours at both neutral and acidic conditions. This is the first study demonstrating direct conjugation of CAP onto PIPOX and dual-responsive release of CAP from PIPOX self-assemblies. Such 3D polymeric self-assemblies may be promising for controlled and sustained release of CAP for antibacterial applications.

3.3. Experimental

3.3.1. Materials

All reactions and polymerizations were carried out under inert atmosphere. All chemicals were used as received unless otherwise specified. Ethanolamine (>99%), cadmium acetate dihydrate (98%), α -bromo isobutyrylbromide (98%), acetonitrile (>99.9%), 2-butanol (>99%), 2-ethyl-2-oxazoline (>99%), chloramphenicol (CAP) ($\geq 98\%$) were purchased from Sigma-Aldrich. Isobutyronitrile (>98%) were purchased from Merck chemicals. The deionized water (DI) was purified by passage through a Milli-Q system (Millipore). SpectroPor7 regenerated cellulose dialysis membrane (molecular weight cutoff: 3.5 kDa) was used for purification of polymers and release experiments.

Hydrodynamic size measurements were performed using Zetasizer Nano-ZS equipment (Malvern Instruments Ltd., U.K.). Size values were collected by cumulants analysis of the autocorrelation data. Prior to measurement, PIPOX or PIPOX-CAP was dissolved in either 0.01 M phosphate buffer at pH 2.5 with a concentration of 0.2 mg/mL and pH of PIPOX or PIPOX-CAP solutions was adjusted using 0.2 M NaOH or 0.2 M HCl solutions. SEM images of PIPOX and PIPOX-CAP (in 0.001 M phosphate buffer at pH 7.5) were taken using high resolution QUANTA 400F Field Emission SEM after Au-Pd coating. A double beam Varian Cary 100 UV–Visible Spectrophotometer was used for the detection of CAP release from PIPOX and PIPOX-CAP conjugate self-aggregates. The release solution was placed in a 10 mm path length quartz cuvette with PTFE capping.

3.3.2. Synthesis and Characterization

2-IPOX and PIPOX-OR were synthesized as described Chapter 2, Section 2.3.2. GPC chromatogram for PIPOX-OR was given in Appendix B: Figure B1.

Characterization of CAP

¹H-NMR (Appendix A: Figure A4) and SERS (Appendix B: Figure B3) spectra of CAP were taken for comparison. Characteristic SERS peaks of CAP; 1609 cm⁻¹ (aromatic ring stretching), 1361 cm⁻¹ (–NO₂ symmetric stretching) and 1114 cm⁻¹ (–NH in plane bending).

Synthesis and characterization of PIPOX-chloramphenicol (PIPOX-CAP) conjugate

The same procedure was followed as described in Section 2.3.2 except that CAP (2.4 mmol, 0.78 g) was used as terminating agent. Then, the reaction mixture was stirred for 2 days at 25 °C. Reaction mixture was concentrated under vacuum at room temperature. The resultant product was dissolved in DI water and dialyzed against DI water for 2 days. Finally, the solution was freeze-dried. ¹H-NMR (DMSO-d₆, 400 MHz) δ 8.34 (d, *J*=8.8 Hz, 1H), 8.16 (d, *J*=8.8 Hz, 2H), 7.59 (d, *J*=8.7 Hz, 2H),

6.47 (s, 1H), 6.07 (br, 1H), 5.06 (br, 1H), 5.02 (t, $J = 5.5$ Hz, 4.4 Hz, 1H), 3.94 (dd, $J = 5.1$ Hz, 6.3 Hz, 1H), 3.40 (br, 4H), 2.8- 2.64 (br, 2H), 2.30 (m, 1H), 1.04 (s, 6H), 0.97 (br, 6H). GPC traces of PIPOX-CAP: $M_n = 9715$ g/mol, PDI 1.13 (Appendix B: Figure B4).

3.3.3. Measurements

$^1\text{H-NMR}$ measurements were recorded in deuterated solvents (CDCl_3 , DMSO-d_6) using a Bruker spectropin Avance DPX-400 Ultra shield instrument at 400 MHz. The residual protons of the not fully deuterated solvents used as an internal standard. $^1\text{H-NMR}$ data were reported as chemical shifts (δ , ppm) relative to tetramethylsilane (δ 0.00) with multiplicity (s=singlet, br=broad singlet, d=doublet, t=triplet, m=multiplet), coupling constant (Hz) and integration. $^1\text{H-NMR}$ samples were prepared via dissolving 5 mg sample into 0.5 mL solvent. Sample was scanned for 50 seconds during measurement. Gel permeating chromatography (GPC) measurements were performed by Agilent instrument (Model 1100) consisting of refractive index (RI) detectors and three Macherey-Nagel columns packed with a highly cross-linked macroporous, spherical polystyrene-divinyl-benzene polymer matrix (Columns 300×7.7 mm, particles $5 \mu\text{m}$). 0.01 M LiBr/DMF was used as an eluent at a flow rate of 0.7 mL/min at 50°C . The calibration was carried out using poly(methyl methacrylate) standards (Polymer Laboratories). Raman measurements were performed with a Horiba-Jobin-Yvon, model Lab Ram Raman micro spectrometer operating with 632.8 nm He-Ne laser. The spectra were collected with Olympus model LMPlanFL, 10x and 50x microscope objective lens *via* focusing the laser to a spot size $\sim 1 \text{ mm}^2$. The laser power was approximately 20.0 mW and the integration time was 10 s. The signal was detected with a Peltier-cooled CCD camera.

Hydrodynamic size measurements were performed using Zetasizer Nano-ZS equipment (Malvern Instruments Ltd., U.K.). Size values were collected by cumulants analysis of the autocorrelation data. Prior to measurement, PIPOX or PIPOX-CAP

was dissolved in either 0.01 M phosphate buffer at pH 2.5 with a concentration of 0.2 mg/mL and pH of PIPOX or PIPOX-CAP solutions was adjusted using 0.2 M NaOH or 0.2 M HCl solutions. SEM images of PIPOX and PIPOX-CAP (in 0.001 M phosphate buffer at pH 7.5) were taken using high resolution QUANTA 400F Field Emission SEM after Au-Pd coating. A double beam Varian Cary 100 UV–Visible Spectrophotometer was used for the detection of CAP release from PIPOX and PIPOX-CAP conjugate self-aggregates. The release solution (2.0 mL) was placed in a 10 mm path length quartz cuvette with PTFE capping. Cumulative amount of CAP released from aggregates were monitored without changing the release media in constant time intervals up to 24 hours.

3.3.4. Preparation of self-aggregates and release from aggregates

Self-aggregation of PIPOX-OR and PIPOX-CAP conjugate

PIPOX-OR or PIPOX-CAP was dissolved in 0.01 M NaH₂PO₄ buffer at pH 2.5 in 0.2 mg/mL concentration. Self-aggregation was triggered by gradually increasing the solution pH to 7.5. The pH was adjusted using 0.2 M and 0.1 M NaOH or 0.2 M and 0.1 M HCl solutions.

CAP-loading into self-aggregates of PIPOX-OR and PIPOX-CAP conjugate

CAP was used as a model antibacterial agent. CAP solution in pure ethanol was prepared in 0.02 mg/mL concentration. 0.2 mL of this solution was added drop-wise into vigorously stirred 20 mL of 0.01 M 0.01 M NaH₂PO₄ buffer at pH 2.5. Then, PIPOX-OR or PIPOX-CAP was dissolved in CAP solution prepared at pH 2.5 in a concentration of 0.2 mg/mL. Self-aggregation was induced *via* gradual increase the solution pH to 7.5. The solution was gently stirred overnight for efficient loading of CAP into self-aggregates. In order to remove free CAP molecules, the solution was filtered *via* centrifugation at 6000 rpm for 10 minutes using 10 kDa cut-off centrifuge filters.

Release from self-aggregates of PIPOX and PIPOX-CAP

Release experiments were conducted *via* using SpectroPor7 regenerated cellulose dialysis membrane (molecular weight cutoff: 3.5 kDa) against phosphate buffer saline solution (50 mL) at pH 7.4, pH 5 and 25 °C and 37 °C with gentle magnetic stirring. The aliquots are taken from the PBS solution and UV absorption of CAP was followed in reported time intervals.

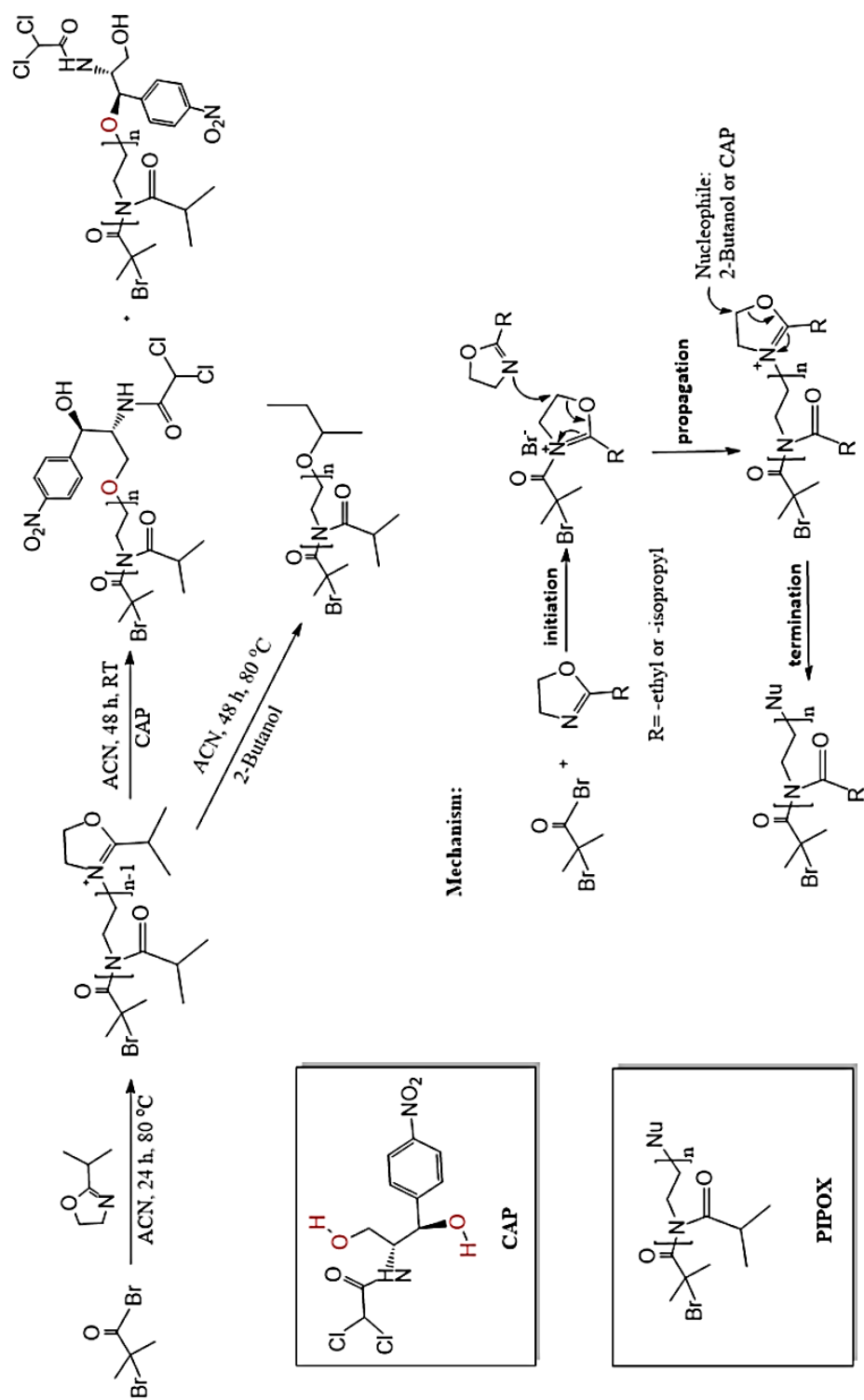
3.4. Results and Discussion

3.4.1. Synthesis of PIPOX-OR and PIPOX-CAP

PIPOX-OR was synthesized using the procedure described by Meyer and Schlaad [285] except the initiator. α -bromoisobutyl bromide (α -BIBB) was used rather than methyl *p*-toluenesulfonate as the initiator. Simply, initiation starts with the nucleophilic attack of amine group in oxazoline ring to the α -BIBB electrophile resulting in formation of the bromine ion and the cationic oxazoline ring. Propagation proceeds by addition of another 2-alkyl-2-oxazoline to the cationic oxazoline ring. To terminate the polymerization, either 2-butanol or CAP was used as the nucleophile to obtain different ω -terminated homopolymers.

In case of termination with 2-Butanol, nucleophilic oxygen of 2-Butanol attacked to -CH₂ carbon neighbouring to oxygen in five-membered oxazoline ring to terminate the polymerization. In case of termination with CAP, both primary and secondary alcohol groups of CAP possibly acted as the nucleophile and attacked to -CH₂ carbon neighbouring to oxygen in five-membered oxazoline ring followed by the ring opening and termination of polymerization. Scheme 3.1 shows the synthesis of PIPOX-OR and PIPOX-CAP and the reaction mechanism for the CROP of 2-alkyl-2-oxazolines. Conjugation of drugs to poly(2-alkyl-2-oxazoline)s at termination step [91–94,290–292] or through post-modification of the end groups [75,76] has been

reported before to achieve powerful agents to be used against microbial infections, to minimize adverse side effects and to overcome solubility problem of antibiotics.



Scheme 3.1 Synthesis of PIPOX-OR and PIPOX-CAP by direct termination methodology and the reaction mechanism for the CROP of 2-alkyl-2-oxazoline.

PIPOX-OR and PIPOX-CAP conjugate were characterized by $^1\text{H-NMR}$ and Raman spectroscopy techniques. In case of $^1\text{H-NMR}$ spectrum of PIPOX-OR, the typical PIPOX backbone signals appeared at 3.50 ppm together with side chain $-\text{CH}-$ proton arose within 2.9-2.75 ppm and $-\text{CH}_3$ protons arose at 1.10 ppm. The small peak appeared at 1.15 ppm corresponded to the two methyl groups of initiator attached from α -position of PIPOX. On the other hand, $^1\text{H-NMR}$ spectrum of PIPOX-CAP (Figure 3.1) conjugate displays the typical PIPOX backbone signals at 3.48 ppm as well as side chain signals corresponding to $-\text{CH}-$ proton of isopropyl groups within 2.85 ppm-2.60 ppm and $-\text{CH}_3$ protons of isopropyl moiety at 1.05 ppm. The small shoulder at 1.10 ppm is associated with the two methyl groups introduced by the initiator from α -position of PIPOX. The signal at 8.34 ppm is assigned to amide proton of CAP, whereas the signals at 8.16 ppm and 7.59 ppm were assigned to two different benzylic protons of CAP, respectively. The protons at 6.47 ppm, 5.06 ppm, 4.1 ppm and 3.2 ppm were correlated to $-\text{CH}$ proton neighbouring to chlorine atoms, benzylic proton neighbouring to secondary alcohol, $-\text{CH}$ proton neighbouring to amide unit and $-\text{CH}_2$ protons neighbouring to primary alcohol, respectively. Slight shift in the signals corresponding to PIPOX and CAP in PIPOX-CAP conjugate confirmed the formation of the conjugate. Due to overlapping of the secondary and primary alcohol protons of CAP appeared at ~ 3.0 -3.5 ppm and PIPOX backbone protons appeared at 3.48 as a broad signal, the ratio of the CAP attached PIPOX to unconjugated PIPOX could not be determined.

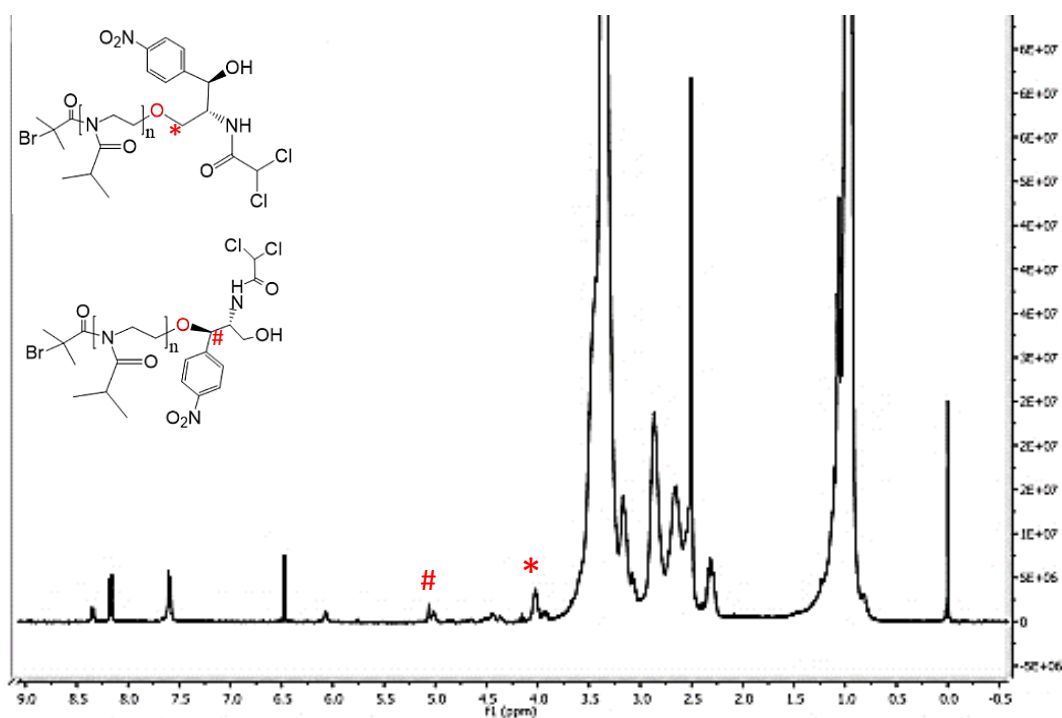


Figure 3.1. $^1\text{H-NMR}$ spectrum of PIPOX-CAP in CDCl_3 .

PIPOX-CAP conjugate was additionally analyzed using Raman spectroscopy. SERS spectra of PIPOX-CAP, CAP and PIPOX-OR are represented in Figure 3.2. SERS spectrum of PIPOX-CAP conjugate contains signals corresponding to both PIPOX and CAP, thus suggests the conjugation of CAP to PIPOX. Specifically, three characteristic SERS peaks of CAP appeared at 1609 cm^{-1} , 1361 cm^{-1} and 1114 cm^{-1} correlated with aromatic ring stretching, $-\text{NO}_2$ symmetric stretching and $-\text{NH}$ in plane bending, respectively (see the peaks marked with pound sign in Figure 3.2). PIPOX SERS peaks appeared at 2867 cm^{-1} ($-\text{CH}$ stretching vibration), 2931 cm^{-1} (symmetric $-\text{CH}_2$ stretch), 2960 cm^{-1} (asymmetric $-\text{CH}_2$ stretching), 1426 cm^{-1} ($-\text{CH}_3$ bending) and 1118 cm^{-1} ($-\text{CH}_2$ twisting vibrations) and were marked with stars in Figure 3.2.

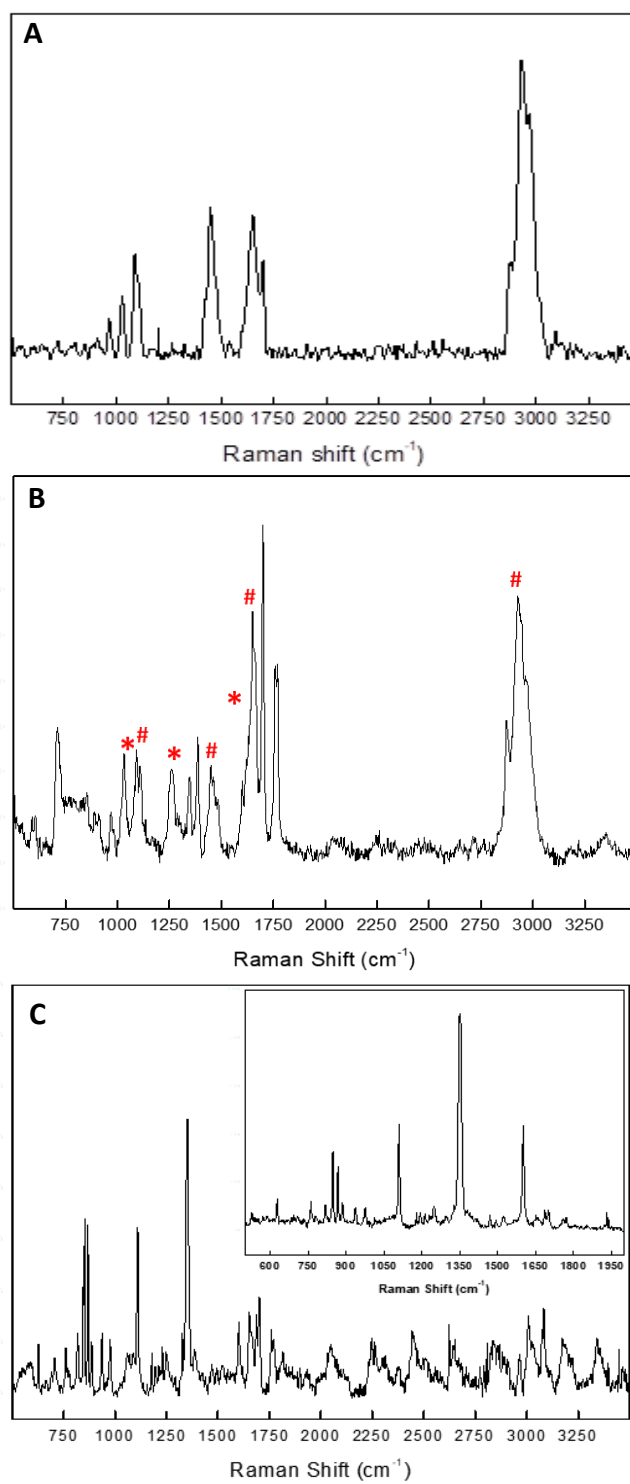


Figure 3.2. SERS spectra of (A) PIPOX-OR, (B) PIPOX-CAP and (C) CAP.

Of note, prior to preparation of PIPOX self-aggregates, the antibacterial activity of PIPOX-CAP conjugate was examined using agar plating method. No significant activity against *E.coli* was observed. This may be explained by drastically lowered antimicrobial activity of CAP *via* conjugation. CAP is a broad spectrum bacteriostatic drug acting as an inhibitor for protein synthesis through binding the large ribosome subunit (50S) at the peptidyl transferase centre A site, preventing binding of the next charged tRNA [293–295]. Therefore, the reduced activity of PIPOX-CAP conjugates could be due to either reduced affinity to ribosome subunit or diminished diffusion capability into the bacterial cell due to PIPOX chains. Tiller and coworkers also reported the diminished antibacterial activity of Ciprofloxacin (CIP) against *S. aureus*, *Streptococcus mutans*, *E. coli*, *Pseudomonas aeruginosa*, and *Kleisella pneumonia* after direct conjugation of CIP to PMEOX, PEOX, and PEG. They explained the reduced activity of the PMEOX-CIP conjugates by the diminished affinity of conjugate to the enzyme since CIP kills the bacteria *via* hindering the intracellular enzyme gyrase or depressing diffusion capability of the drug into the bacterial cell [76].

3.4.2. pH-induced self-aggregation of PIPOX-OR and PIPOX-CAP

PIPOX-OR and PIPOX-CAP aggregates were prepared by dissolving both polymers at acidic pH (pH = 2.5) and gradually increasing the solution pH to neutral conditions (pH 7.5) at 25 °C using 0.1 M NaOH solution. Figures 3.3A shows the evolution of hydrodynamic diameter as a function of increasing pH for PIPOX-OR and PIPOX-CAP. For PIPOX-OR, self-association of the chains started above pH 5.0 when the amide groups of PIPOX deprotonated (pK_a of PIPOX ~ 5.2) and the hydrophobic association among PIPOX chains enhanced. On the other hand, self-aggregation of PIPOX-CAP began at slightly lower pH (~ pH 4.5). Zeta potential changes for PIPOX-OR and PIPOX-CAP in 0.2 mg/mL *via* increasing pH were also confirmed the formation of PIPOX-CAP self-aggregates at ~ pH 4.5. The isoelectric point of PIPOX-

CAP was determined as ~ pH 3.5 that was slightly lower than that of PIPOX-OR (Figure 3.4). The reason for this could be the enhanced interactions between the CAP units attached to the PIPOX chain end leading to enhanced association of PIPOX chains at lower pH values. Importantly, the standard deviations calculated over 10 different size measurements were smaller for PIPOX-CAP, indicating formation of aggregates with more uniform size. This is also seen in size distribution curves of PIPOX-OR and PIPOX-CAP in 10 mM phosphate buffer at pH 7.5 and 25 °C (Figure 3.3B). This can be explained by the more hydrophobic end-group of PIPOX-CAP, enhancing the self-association of PIPOX chains and providing formation of more uniform aggregates. It must be born in mind that the effect of end-group on self-aggregation of PIPOX and the aggregate size was discussed in Chapter 2 of this dissertation [285]. The effect of chain end units on the self-assembly of hydrophilic polymers has also been reported by several other research groups as well [296].

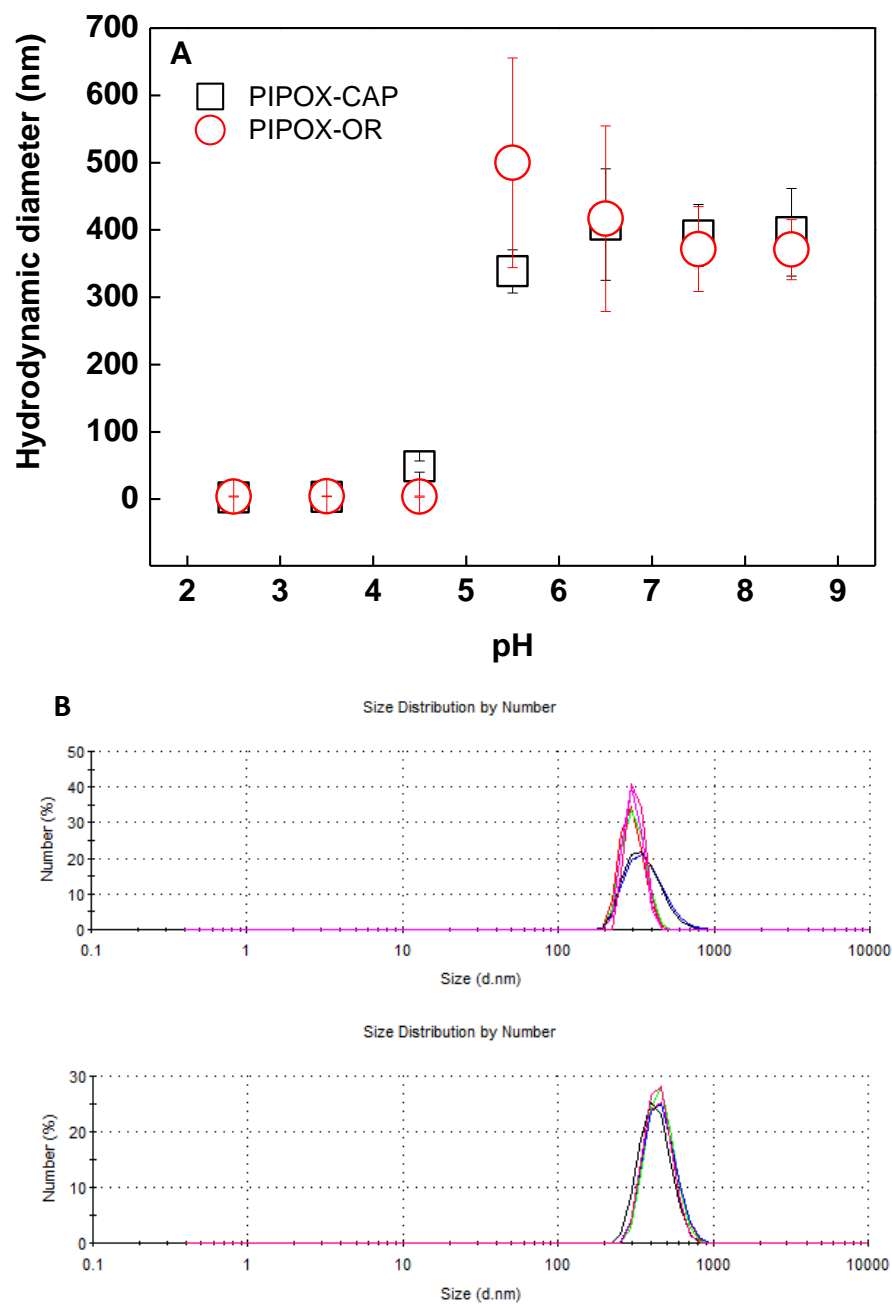


Figure 3.3. (A) Evolution of hydrodynamic diameter of PIPOX-OR and PIPOX-CAP in 10mM phosphate buffer with increasing pH at 25 °C. (B) Size distribution curves of PIPOX-OR and PIPOX-CAP by number at pH 7.5. Size distribution curves obtained from several individual measurements of the same sample are represented with different colors.

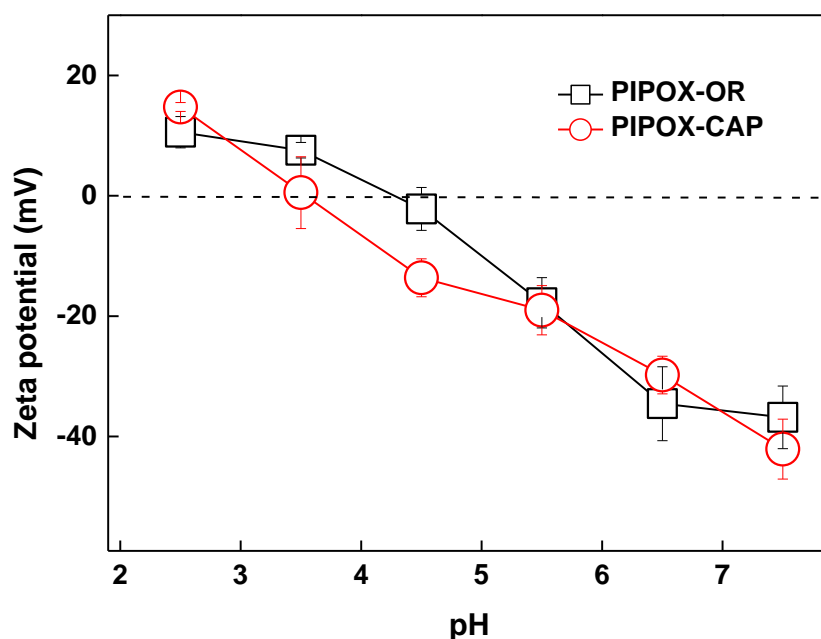


Figure 3.4. Zeta potential changes for PIPOX-OR and PIPOX-CAP in 0.2 mg/mL via increasing pH.

pH-triggered disassembly of PIPOX aggregates at 37 °C

PIPOX-OR and PIPOX-CAP aggregates were formed at pH 7.5 and 25 °C in 10 mM phosphate buffer at 0.2 mg/mL polymer concentration. The temperature of the aggregate solutions was then increased to 37 °C at pH 7.5. The dissolution of the aggregates was followed by gradually decreasing the solution pH to acidic conditions and measuring the hydrodynamic diameter of PIPOX using dynamic light scattering (DLS) technique.

Figure 3.5A and Figure 3.5B show the change in hydrodynamic diameter of PIPOX-OR and PIPOX-CAP as a function of decreasing pH at 37 °C, respectively. The evolution of hydrodynamic size with increasing pH at 25 °C is plotted for comparison for each graph. For both PIPOX samples, the hydrodynamic diameter decreased gradually as the pH was lowered due to protonation of the amide nitrogens on PIPOX

and dissolution of the aggregates. Hysteresis was recorded for both PIPOX-OR and PIPOX-CAP during the disintegration. For example, the hydrodynamic diameter of PIPOX-OR was 3.8 nm at pH 4.5 and 25 °C. However, aggregates as large as ~ 206.7 nm were detected at pH 4.5 at 37 °C. Hysteresis was more remarkable for PIPOX-CAP aggregates. No disintegration was observed at pH 4.5 for PIPOX-CAP aggregates. The hysteresis can be correlated with the intra- and inter-molecular hydrophobic association between the PIPOX chains, suppressing the protonation of the amide nitrogens and partial removal of PIPOX chains from the aggregates. The reason for greater hysteresis in case of PIPOX-CAP aggregates is the stronger association among PIPOX-CAP chains arising from more hydrophobic CAP end units. Figure 3.6 shows the hydrodynamic size distribution curves of PIPOX-OR and PIPOX-CAP with decreasing pH at 37 °C.

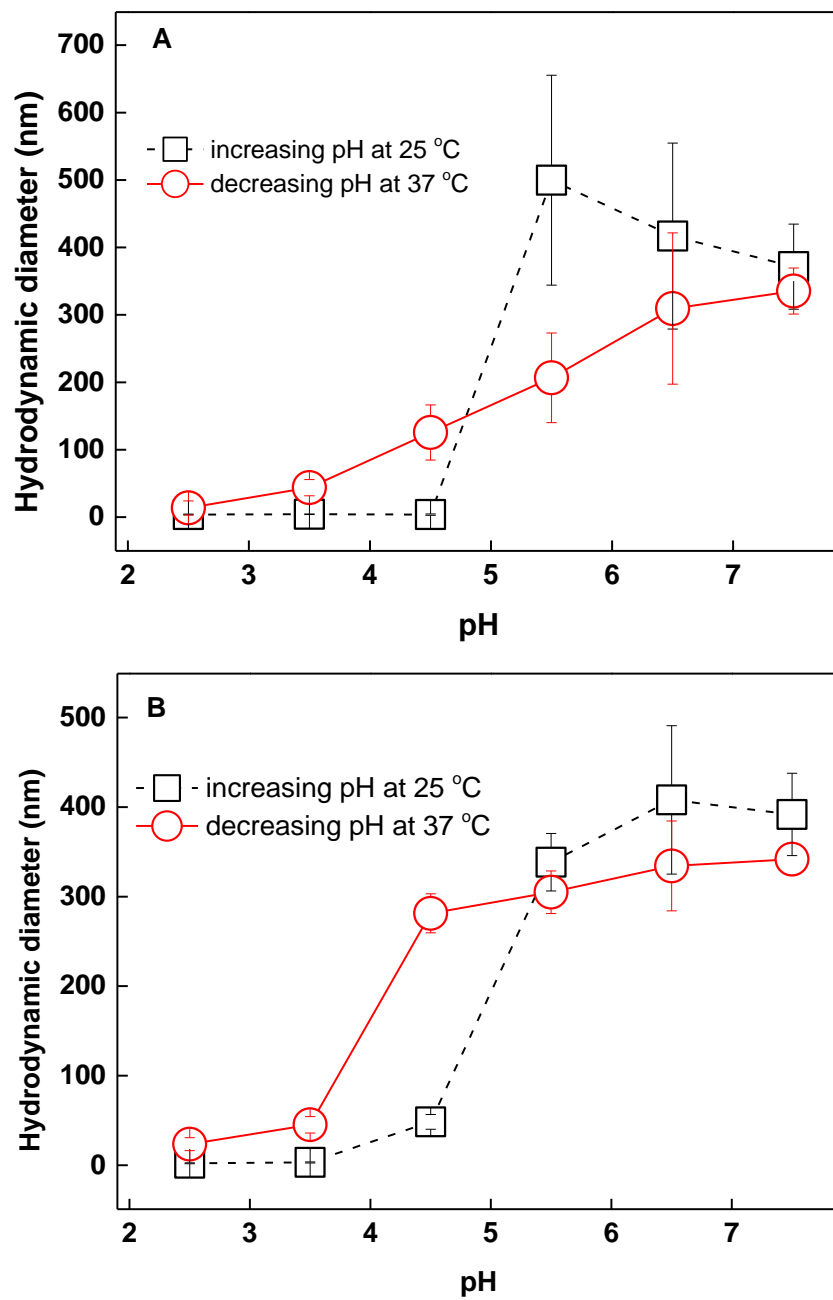


Figure 3.5. The evolution of hydrodynamic diameter of PIPOX-OR (A) and PIPOX-CAP (B) as a function of decreasing pH at 37 °C. Evolution of hydrodynamic diameter with increasing pH at 25 °C is plotted for comparison.

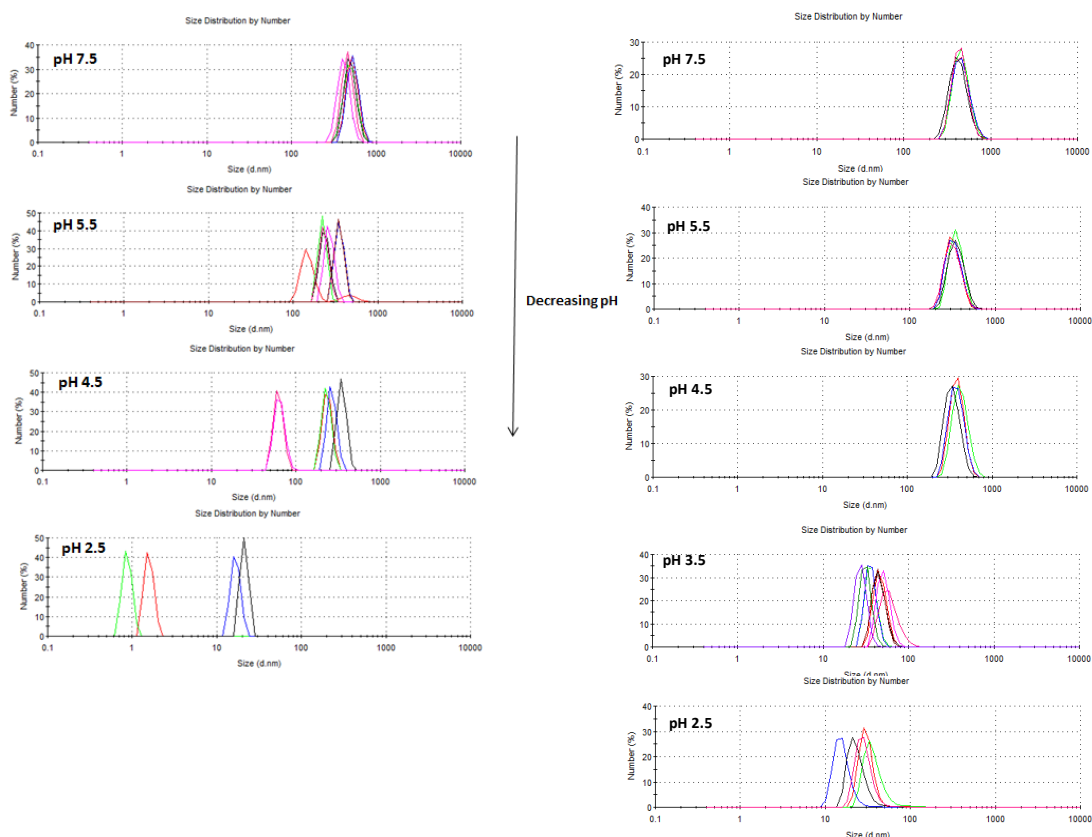
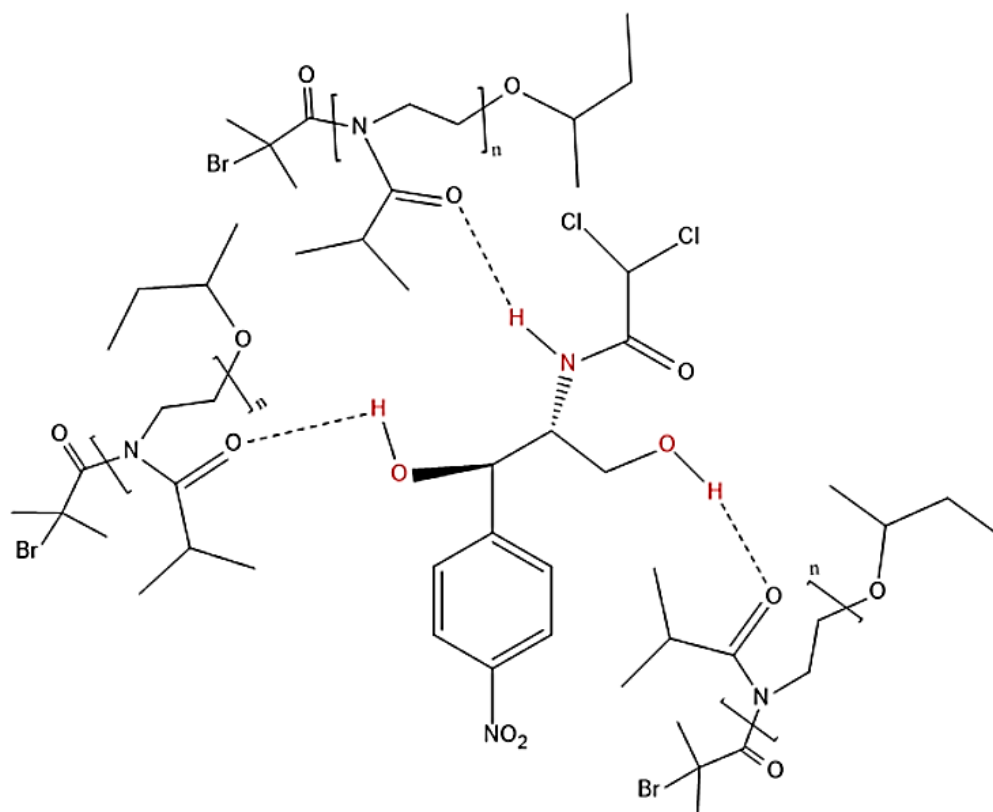


Figure 3.6. The hydrodynamic size distribution curves of PIPOX-OR (left) and PIPOX-CAP (right) with decreasing pH at 37 °C.

3.4.3. CAP loading into PIPOX-OR and PIPOX-CAP aggregates

PIPOX-OR and PIPOX-CAP were dissolved separately in 0.1 mg/mL CAP solution prepared in phosphate buffer at pH 2.5. Self-assembly of PIPOX was induced in the presence of CAP molecules by gradually increasing the pH of the solutions to pH 7.5. The solutions were stirred overnight at room temperature for encapsulation of CAP into PIPOX aggregates. Free CAP molecules were removed by multiple centrifugation. CAP and PIPOX were expected to associate through hydrogen bonding interactions between hydroxyl groups of CAP and amide units of PIPOX and hydrophobic association among isopropyl side chains of PIPOX with nitro-benzyl

sites of CAP. Scheme 3.2 displays the schematic representation of interactions between PIPOX and CAP.



Scheme 3.2 Schematic illustration of the molecular interactions of PIPOX and CAP.

Figure 3.7A and 3.7B contrast the hydrodynamic size of PIPOX-CAP (A) and PIPOX-OR (B) in 0.1 mg/mL CAP solution and 10 mM phosphate buffer at pH 7.4, respectively. The average sizes of the aggregates were smaller than the aggregate sizes obtained in 10 mM phosphate buffer for PIPOX-OR. For example, self-assembly of PIPOX-OR in 10 mM phosphate buffer and in 0.1 mg/mL CAP solution at pH 7.4 resulted in formation of 345 nm and 100 nm aggregates, respectively. Similarly, PIPOX-CAP formed aggregates with average sizes of 425 and 260 nm in 10 mM

phosphate buffer and in 0.1 mg/mL CAP solution at pH 7.4, respectively. SEM images were in good agreement with DLS results, displaying larger aggregates for PIPOX-OR or PIPOX-CAP in 10 mM phosphate buffer than that in 0.1 mg/mL CAP solution (Figure 3.8). The difference in size between DLS and SEM results was due to the fact that DLS measured the hydrodynamic diameter, the diameter of the particles together with the water layer attached to them, whereas SEM provided information about the projected area diameter of the aggregates. The lower aggregate sizes recorded in CAP solution suggested that the presence of CAP molecules partly inhibited self-assembly of PIPOX-OR or PIPOX-CAP in CAP solution possibly due to CAP molecules which prevented the self-association of PIPOX. The reason for the larger size of PIPOX-CAP than that of PIPOX-OR could be the enhanced association of free CAP molecules with CAP end-groups of PIPOX, inducing the self-assembly through the end-groups. Increment in diameter of drug loaded micelles formed from polymer drug conjugates compared to pristine analogues has been reported [77,297–299]. Specifically, Yang et al. reported that micelles formed from mPEG-PLA-curcumin conjugate were significantly larger than mPEG-PLA micelles. They suggested that the presence of curcumin in the hydrophobic moiety alters the driving force of self-assembly and the conjugate architecture might cause a crowding impact (meaning that higher number of functional groups interacting with each other in case of conjugate) triggering the formation of bigger micelles [299].

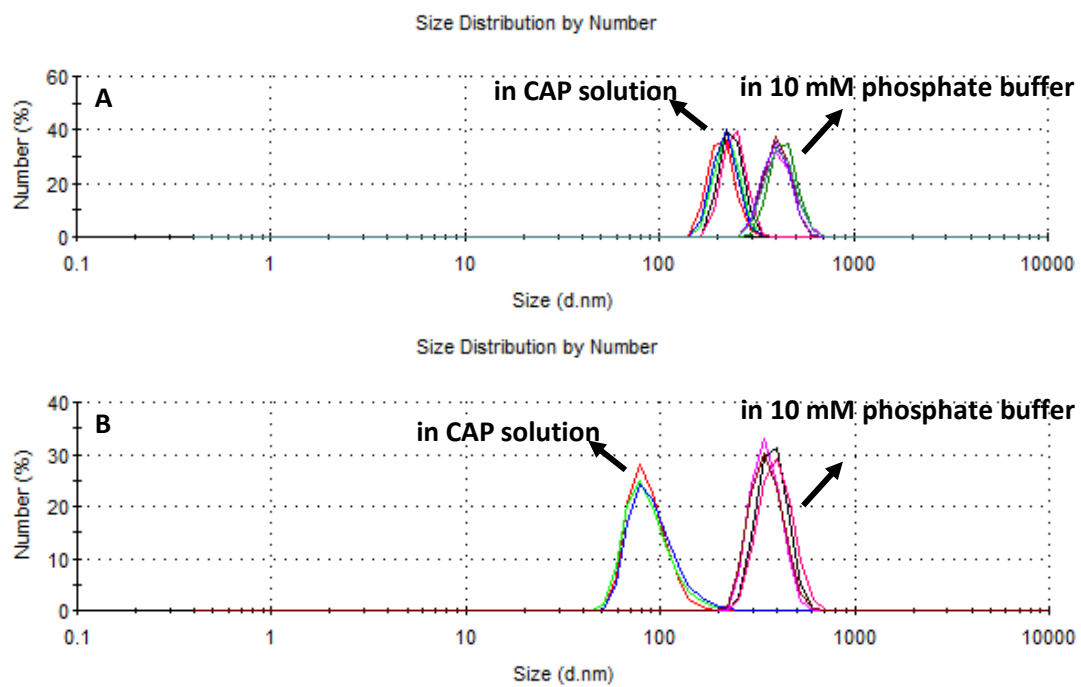


Figure 3.7. Comparison of the hydrodynamic size of PIPOX-CAP in 0.1 mg/mL CAP solution and in 10 mM phosphate buffer at pH 7.4 (A). Hydrodynamic size distributions of PIPOX-OR in 0.1 mg/mL CAP solution and in 10 mM phosphate buffer at pH 7.4 (B) are shown for comparison.

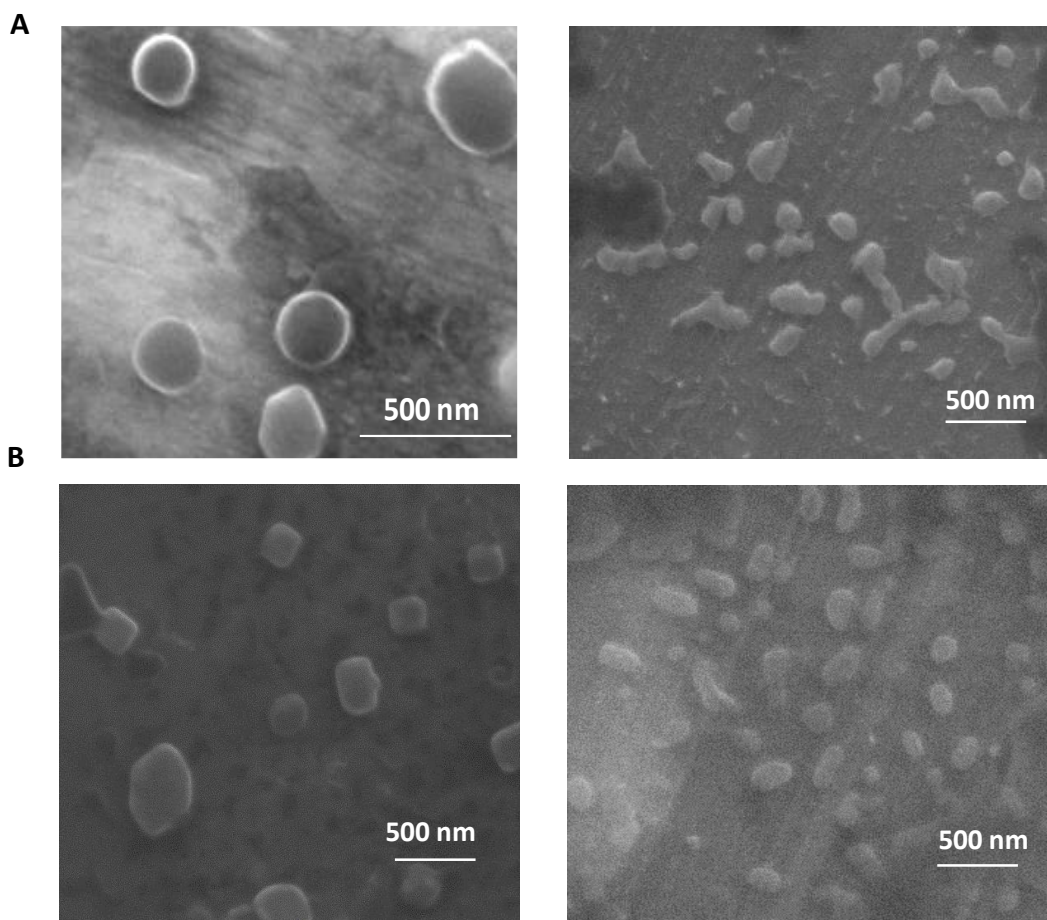


Figure 3.8. SEM images of (A) PIPOX-OR aggregates in 10 mM phosphate buffer (left), in 0.1 mg/mL CAP solution (right), and (B) PIPOX-CAP aggregates in 10 mM phosphate buffer (left), in 0.1 mg/mL CAP solution (right) at pH 7.5.

The larger aggregate size for PIPOX-CAP also resulted in loading greater amount of CAP into PIPOX-CAP aggregates than that loaded into PIPOX-OR aggregates under identical conditions. The amount of CAP loaded into PIPOX aggregates was calculated by measuring the absorbance of CAP in PIPOX solutions before and after removal of the free CAP molecules followed by quantification using calibration curves of CAP prepared at pH 7.5 and 25 °C. The difference in CAP amount before and after removal of the free CAP molecules was attributed to the CAP loaded into aggregates. The amount of CAP loaded into PIPOX-OR and PIPOX-CAP aggregates were calculated as 23.2 μg and 61.1 μg , respectively. Figure 3.9 contrasts the loading

efficacy into PIPOX-OR and PIPOX-CAP aggregates. We suggest that PIPOX-CAP conjugate may provide more hydrophobic CAP core for aggregates compared to the pristine PIPOX aggregates. This leads to enhanced interaction with free CAP molecules with inner core of aggregates resulted in higher loading amount of CAP. In addition, conjugation of CAP at chain end might increase the affinity between the encapsulated drug and micellar core. Of note, Li and coworkers also reported the enhancement of loading content of DOX into PEOX-*hyd*-DOX conjugate *via* increasing chemical compatibility between micelle core and loaded drug [77].

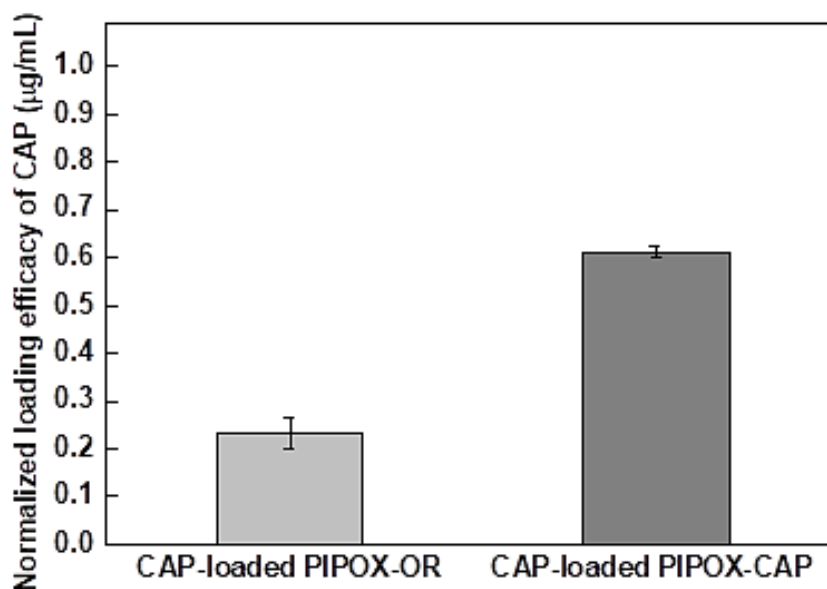


Figure 3.9. Normalized CAP-loading efficacies of PIPOX-OR and PIPOX-CAP self-aggregates. Normalized values were calculated by dividing the absorbance of CAP-loaded PIPOX-OR and CAP-loaded PIPOX-CAP to the absorbance of CAP at 220 nm.

3.4.4. CAP release from PIPOX-OR and PIPOX-CAP aggregates

CAP loaded PIPOX-OR and PIPOX-CAP aggregate solutions were separately put into dialysis membranes and dialysed against PBS at either pH 7.5 or pH 5.0 at 25 °C or 37 °C. The pH of the aggregate solution in the membrane was adjusted prior to dialysis. CAP release from PIPOX aggregates was monitored by following the intensity of the peak at 275 nm using UV-Visible Spectroscopy. The amount of CAP released from the aggregates was quantified using calibration curves. Of note, the absorbance of CAP is affected by the pH. Therefore, calibration curves were prepared separately for every release condition. Figures 3.10A and 3.10B show the amount of CAP released at pH 7.5/37 °C and pH 5.0/37 °C as a function of time from PIPOX-OR and PIPOX-CAP aggregates, respectively. For both of the samples, release at pH 7.5/25 °C and pH 5.0/25 °C are plotted for comparison.

Both aggregates were formed at pH 7.5 and 25 °C. Therefore, CAP release from both aggregates at pH 7.5/25 °C occurred through self-diffusion mechanism. To examine the temperature-responsive release from aggregate surface, CAP release was followed at pH 7.5/37 °C and the data was contrasted with that at pH 7.5/25 °C. CAP release at pH 7.5/37 °C was slightly higher than that at pH 7.5/25 °C for PIPOX-OR aggregates. The difference was greater for PIPOX-CAP aggregates possibly due to greater amount of CAP encapsulation which also resulted in greater amount of release within the same time interval. To examine the pH-responsive release from aggregate surface, CAP release was followed at pH 5.0/25 °C and the data was contrasted with that obtained at pH 7.5/25 °C. At pH 5.0/25 °C, PIPOX-OR aggregates showed pH-responsive release due to protonation of the PIPOX amide units and dissolution of the aggregates. Importantly, PIPOX-CAP aggregates did not show pH-responsive release at pH 5/25 °C. This can be explained by the greater hysteresis that PIPOX-CAP exhibited during disintegration of the aggregates at 25 °C (Figure 3.11). It must be born in mind that hydrodynamic diameter remained almost constant with decreasing pH at 25 °C until pH 3.5 for PIPOX-CAP aggregates. This was the reason for not observing any pH response for PIPOX-CAP aggregates at pH 5.0/25 °C. Both PIPOX-OR and PIPOX-

CAP aggregates demonstrated the greatest amount of CAP release at pH 5.0/37 °C due to release through both pH and temperature triggers. Of note, the cloud point of PIPOX used in this study was found as 37 °C in 10 mM phosphate buffer (Figure 2.19B). The transition of PIPOX chains from extended to globular conformation possibly formed voids at the aggregate surface, enhancing CAP release at 37 °C. Importantly, the amount of CAP released from PIPOX-CAP aggregates at pH 5.0/37 °C was almost three times higher than that released from PIPOX-OR aggregates due to greater loading capacity of PIPOX-CAP aggregates. The total amount of CAP released from PIPOX-OR and PIPOX-CAP aggregates under various conditions are represented in Figure 10C. A comparison of the relative % release amounts is represented in Figure 10D.

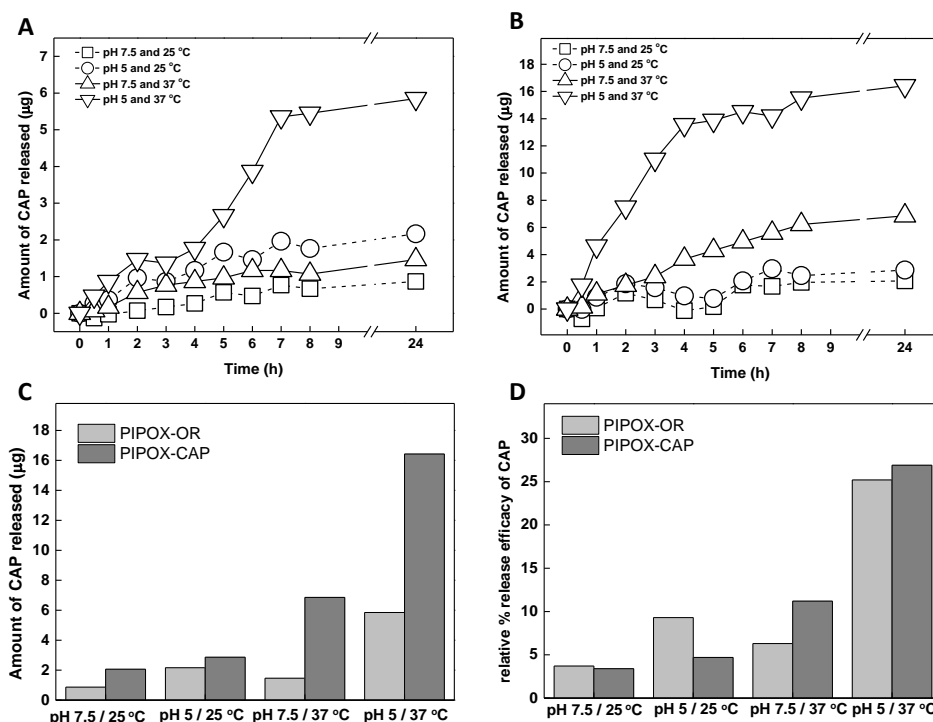


Figure 3.10. A) CAP release profile from PIPOX-OR aggregates at pH 7.5/25 °C; pH 7.5/37 °C; pH 5.0/25 °C and pH 5.0/37 °C. (B) CAP release profile from PIPOX-CAP aggregates at pH 7.5/25 °C; pH 7.5/37 °C; pH 5.0/25 °C and pH 5.0/37 °C. (C) Comparison of the total CAP amount released from PIPOX-OR and PIPOX-CAP aggregates at pH 7.5/25 °C; pH 7.5/37 °C; pH 5.0/25 °C and pH 5.0/37 °C after 24 hours. (D) Comparison of relative % release from PIPOX-OR and PIPOX-CAP aggregates at pH 7.5/25 °C; pH 7.5/37 °C; pH 5.0/25 °C and pH 5.0/37 °C. Relative % release were calculated.

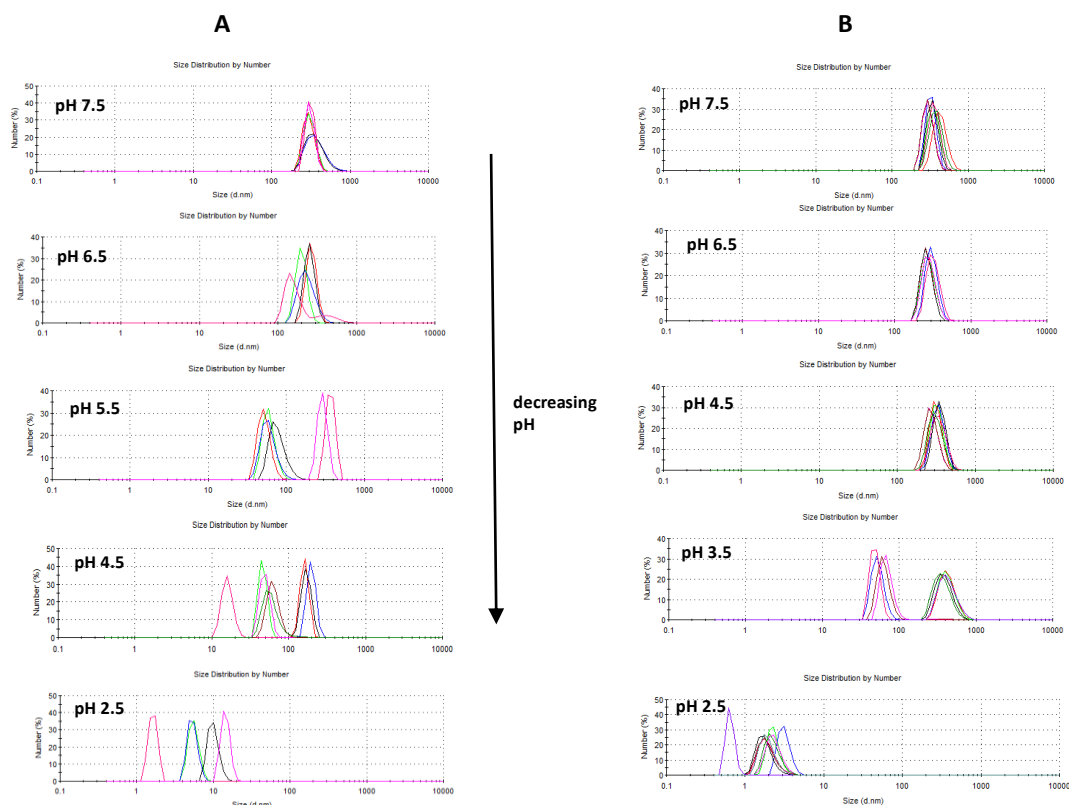


Figure 3.11. The hydrodynamic size distribution curves of PIPOX-OR (A) and PIPOX-CAP (B) with decreasing pH at 25 °C.

3.5. Conclusion

PIPOX-CAP conjugate was synthesized with permanent conjugation of CAP to the ω -end of PIPOX as an alternative to previously synthesized analogue PIPOX-OR. Self-aggregation of PIPOX-CAP was contrasted with that of PIPOX-OR. Similar size aggregates were formed from both polymers in phosphate buffer solution while critical aggregation pH was slightly different. On the other hand, the diameter of PIPOX-OR self-aggregates formed in CAP solution was significantly lower compared to that of PIPOX-CAP counterpart. The loading and release of a model antibiotic CAP into/from PIPOX self-aggregates were examined at neutral and acidic pH at a physiologically related temperature. PIPOX-CAP self-aggregates with larger size revealed higher loading capacity for CAP that could be correlated with enhanced interactions between

the free CAP molecules and CAP moiety attached to the PIPOX end. Release of CAP from both aggregates were monitored and the maximum amount of drug released was found at pH 5.0 and 37 °C due to the pH- and temperature- triggered release of drug. This study presents the critical effect of PIPOX end-group on loading and release properties of PIPOX self-aggregates.

CHAPTER 4

EFFECT OF SIDE CHAIN VARIATION ON SURFACE AND BIOLOGICAL PROPERTIES OF POLY(2-ALKYL-2-OXAZOLINE) MULTILAYERS*

4.1. Chapter Summary

Multilayers of Poly(2-alkyl-2-oxazoline)s (PAOX)s with varying side chains were constructed through LbL self-assembly using TA. Surface morphology, stability, wettability and stimuli-responsive drug release properties of the films were correlated with antiadhesive and antibacterial properties of the surfaces. Thickness, roughness, wettability and stability of multilayers were affected by the chemical nature of PAOX side chain, phase behaviour of PAOX and the binding strength between the layers. PAOX-multilayers showed remarkably different release trends for Ciprofloxacin (CIP) especially at acidic pH and 37 °C. Release trends were in good agreement with the antibacterial activity of the films against *S.aureus*. PAOX-multilayers showed antibacterial activity against *E.coli* despite the differences in the CIP amount released from surface. Multilayers with greater wettability exhibited greater resistance against adsorption onto the model protein Bovine Serum Albumin (BSA) and was more effective to reduce the adherence of *E.Coli*. None of the PAOX-films exhibited antiadhesiveness against *S.aureus*.

*The content of this chapter was previously submitted as a revised manuscript to Elsevier Ltd. (Cagli, E.; Ugur, E.; Ulsan, S.; Banerjee, S.; Erel-Goktepe, I. *European Polymer Journal*).

4.2. Introduction

PAOXs are an important class of bioinspired polymers. Their structural similarity to polypeptides has imparted significant biological properties to PAOXs, such as biocompatibility, nontoxicity and anti-fouling [1–3]. PAOXs cannot be detected easily by the immune system (stealth behaviour) [4,5]. Therefore, they constitute an alternative to PEG, which is the most commonly used polymer in biomedical applications. In addition, the chemical stability of PAOXs was reported to be greater than PEG due to lower polarization of the N-vicinal C–H bond than the O- vicinal C–H bond in the PEG structure [300]. Temperature-responsive properties of PAOXs have been extensively investigated [2,6–17]. Among PAOXs, LCST-type phase behaviour of PIPOX in aqueous solution at a temperature (35–39°C for PIPOX with varying M_n and concentrations [2]) within the physiological range makes it specifically applicable in biomedical area.

Layer-by-layer (LbL) self-assembly of polymers is a powerful technique to functionalize and modify surfaces to impart desired characteristics. H-bonded multilayers of neutral polymers and polyacids are of interest to prepare multilayer films with pH-responsive properties at mild pH conditions [205,301]. In addition, toxicity of neutral polymers was reported to be lower than the polycations, making hydrogen-bonded multilayers attractive for biomedical applications [302].

LbL self-assembly of PAOXs was first demonstrated by Erel et al. [208], and further investigated by others, providing detailed information about the effect of deposition conditions on the multilayer growth [303,304] as well as thermodynamics of LbL assembly of various PAOXs [210]. Stabilization of silver nanoparticles by PEOX and LbL deposition of such PEOX stabilized silver nanoparticles and TA were reported [211]. Recently, reorganization of free-floating PEOX/TA multilayers into fibers at acidic conditions has been reported [305]. Preparation of hollow LbL capsules of PAOXs, the effect of temperature on morphological changes of the capsule shell and loading/release of fluorescent dye molecules into/from hollow capsules have been

investigated [213]. PAOX based 2D and 3D LbL films have also been investigated for biological applications. Intracellular degradability, healing, low-fouling and redox responsive properties of PAOX multilayers have been reported [214,306–308]. We have previously reported Doxorubicin (DOX) release from multilayers of PIPOX and water-soluble complexes of TA and DOX in response to change in pH and temperature of the environment [178].

Different from these studies, herein, we report the fabrication of LbL films of PEOX/TA and PIPOX/TA and compare them with respect to i) film properties, i.e. growth, morphology, wettability, stability; ii) CIP release and antibacterial behavior at physiologically related pH and temperature conditions; and iii) protein and bacterial antiadhesive properties. The differences in surface properties of the films are correlated with the differences observed in biological properties of the films. To the best of our knowledge, for the first time, a detailed analysis of stimuli-responsive release properties of PAOX multilayers at various pH and temperatures is presented and the remarkable differences are explained through phase behaviour of polymers and structure-property relationship in LbL films. In addition, this study presents strategies to make PAOX multilayers stable at physiologically related pH and temperature conditions without any additional steps such as hydrolysis and crosslinking as earlier demonstrated for PAOX LbL films [214]. Considering the potential of PAOXs for use in biomedical applications, this study is important in the sense that it generates fundamental knowledge on chemical structure-property relationship in PAOX multilayers and the effect of surface properties on antiadhesive and antibacterial properties of the films.

4.3. Experimental

4.3.1. Materials

Branched poly(ethylenimine) (BPEI; Mw 25 000), 2-ethyl-2-oxazoline (>99%), sodium hydroxide, hydrochloric acid, ethanolamine (>99%), cadmium acetate

dihydrate (98%), α -bromoisobutyl bromide (98%), acetonitrile (>99.9%), phosphate buffer saline, Luria Bertani (LB) broth and 2-butanol (>99%) were purchased from Sigma-Aldrich Chemical Co. Monobasic sodium phosphate buffer ($\text{NaH}_2\text{PO}_4 \cdot 2\text{H}_2\text{O}$), isobutyronitrile (>98%), Mueller-Hinton (MH) broth, and TA were purchased from Merck Chemicals. All chemicals were used as received. Deionized H_2O was purified by passage through a Milli-Q system (Millipore).

4.3.2. NMR and GPC measurements

^1H -NMR measurements were carried out at room temperature using a Bruker Spectrospin Avance DPX-400 Ultrashield instrument operating at 400 MHz. ^1H -NMR samples were prepared via dissolving 5 mg sample into 0.5 mL solvent. Sample was scanned for 50 seconds during measurement. GPC measurements were carried out with an Agilent instrument (model 1100) consisting of refractive index detectors and three Macherey–Nagel columns which were packed with a highly crosslinked macroporous, spherical polystyrene-divinyl-benzene polymer matrix (columns 300×7.7 mm, particles $5 \mu\text{m}$). As eluent, 0.01 mol/L LiBr/dimethylformamide was used at a flow rate of 0.7 mL/min at 50°C . The calibration was performed using poly(methyl methacrylate) standards (Polymer Laboratories).

4.3.3. Synthesis of 2-IPOX, PEOX and PIPOX

2-IPOX and poly(2-isopropyl-2-oxazoline) with 2-butoxy end capping (PIPOX) were synthesized as described Chapter 2, Section 2.3.2. GPC chromatogram for PIPOX and PEOX was given in Appendix B, Figure B1 and Figure B5, respectively. GPC traces of PIPOX: $M_n = 6210$ g/mol, PDI 1.25 (Appendix B: Figure B.1). GPC traces of PEOX: $M_n = 5738$ g/mol, PDI 1.16 (Appendix B: Figure B.4).

4.3.4. Deposition of multilayers

Silicon wafers, quartz or glass substrates were immersed in concentrated sulfuric acid for 85 minutes and rinsed with deionized water. After drying under nitrogen flow, substrates were immersed into 0.25 M NaOH solution for 10 minutes. The substrates were then rinsed with DI water and dried under nitrogen flow. BPEI, TA, PEOX and PIPOX solutions were prepared using 10 mM phosphate buffer solution. Prior to multilayer deposition, one bilayer of BPEI (0.5 mg/mL) and TA (0.2 mg/mL) was deposited onto each substrate at pH 5.5 as a precursor film. Multilayers were deposited by immersing the BPEI/TA coated substrates alternately into solutions of PIPOX (0.2 mg/mL) or PEOX (0.2 mg/mL) and TA (0.2 mg/mL) at pH 2.5 for 15 minutes each with two intermediate rinsing steps in between. Rinsing solutions were 10 mM phosphate buffer at pH 2.5. TA solution was refreshed every 1 hour during film fabrication to avoid degradation of TA. Thickness measurements were conducted using a spectroscopic ellipsometer of Optosense, USA (OPT-S6000). AFM imaging was performed using an NT-MDT Solver P47 AFM in tapping mode using Si cantilevers.

4.3.5. CIP loading and release into/from multilayers

CIP was dissolved in 10 mM phosphate buffer at pH 2.5 to form a 0.1 mg/mL solution. pH of CIP solution was then increased to 7.4 prior to loading into multilayers. One glass substrate (1 cm x 1cm) coated with 49-layer PIPOX/TA or PEOX/TA was immersed into 20 mL of 0.1 mg/mL CIP solution at pH 7.4 for 12 hours. Of note, CIP was not soluble in 10 mM phosphate buffer at pH 7.4 at a concentration of 0.1 mg/mL. Therefore, CIP was first dissolved at pH 2.5 and then the solution pH was increased to 7.4.

To calculate the amount of CIP loaded into PEOX/TA and PIPOX/TA multilayers, CIP solution was excited at 280 nm and the fluorescence intensity of CIP at 415 nm was recorded before and after the multilayers were immersed in the CIP solution. The

excitation and emission slits were 5.0 nm and 5.0 nm, respectively. Of note, the concentration of the CIP solution was too high for fluorescence measurements. Therefore, the CIP solution was diluted by adding 10 mM phosphate buffer at pH 7.4 and 25 °C into 14 μ L of CIP loading solution to form a final volume of 2 mL prior to fluorescence measurements. The dilution factor was taken into account for calculating the CIP amount in the solution before and after CIP loading into multilayers. The amount of CIP in the solution before and after immersion of the multilayers was quantified using calibration curves. The difference in CIP amount was attributed to the amount of CIP loaded into multilayers.

For release experiments, each 1 cm x 1 cm glass slide coated with 49-layers of PEOX/TA or PIPOX/TA was immersed into 20 mL PBS under various conditions, i.e. pH 7.4/25 °C; pH 7.4/37 °C; pH 6.0/25 °C; pH 6.0/37 °C. CIP release as a function of time was followed using Hitachi F-2500 fluorescence spectrophotometer by measuring the fluorescence intensity of the peak at 415 nm and 440 nm at pH 7.4 and pH 6.0, respectively. The amount of CIP release was quantified using calibration curves prepared at release conditions.

4.3.6. Stability of multilayers

Stability of CIP loaded and unloaded multilayers were examined by immersing 13-layer PEOX/TA and PIPOX/TA films into PBS (pH 7.4 and pH 6.0) at 25 °C or 37 °C and following the evolution of film thickness or the intensity of the peak at 215 nm in the UV-Visible spectra of multilayers as a function of time. UV-visible spectroscopy measurements were carried out using a 100 Bio-Cary Varian UV-visible spectrophotometer. Films were dried prior to measurements.

4.3.7. Static contact angle measurements

The static water contact angles were measured using Attension Theta Lite optical tensiometer. 3 DI water droplets (2 μL each) were deposited onto each coated substrate. 10 independent measurements were recorded with 16 millisecond frame intervals at 25 °C for each droplet. In contact angle experiments, odd layers are polymers and even layers are TA.

4.3.8. Bacterial growth conditions

Biological tests were conducted by one of our group member, Sinem Ulasan. Luria Bertani (LB) broth and Mueller Hinton (MH) broth were prepared in deionized water, filter sterilized using 0.45 μm filters and autoclaved prior to use. MH agar at pH 6.0 and pH 7.4 were used for Kirby-Bauer tests while LB broth and LB agar were used for pre-culture preparation and agar plating, respectively. For Kirby-Bauer test, bacteria were grown at either 25 °C or 37 °C. All bacterial experiments were performed using *S. aureus* ATCC 29213 and *E. coli* ATCC 8739.

4.3.9. Minimum Inhibitory Concentration (MIC) analysis

Minimum inhibitory concentrations for *E.coli* and *S.aureus* were determined using a serial dilution method. Both bacterial strains were retrieved from glycerol stocks, inoculated in LB broth individually and incubated for 4 hours at 37 °C and 160 rpm. These pre-cultures were then added to 5 mL of fresh LB broth at 1:100 (v/v) dilution and both bacteria were grown at 37 °C and 160 rpm until their OD₆₀₀ reached ~ 1.0 (which corresponds to ~ 10⁹ CFU/mL of bacteria). A stock solution of CIP was prepared in 1 mM phosphate buffer at pH 4.0, which was then diluted to different concentrations in LB medium. For *E.coli*, LB with 20 different CIP concentrations ranging between 0.005 $\mu\text{g/mL}$ and 0.750 $\mu\text{g/mL}$ were prepared. For *S.aureus*, 20 different CIP concentrations ranging between 0.2 $\mu\text{g/mL}$ and 2.0 $\mu\text{g/mL}$ were

prepared. The bacteria cultures at OD₆₀₀ ~1.0 were then added at a dilution of 1:100 (v/v) to 5 mL of LB containing different concentrations of CIP. As control, bacterial cultures without CIP were also included for both types bacteria. All bacterial cultures were then incubated overnight at 37 °C and 160 rpm. After overnight growth, their optical densities at 600 nm were measured and the lowest CIP concentration that inhibited bacterial growth for each strain was assigned as the MIC.

4.3.10. Kirby-Bauer Test[‡]

25 µL of overnight cultures of *E. coli* ATCC 8739 and *S. aureus* ATCC 29213 grown in LB broth (OD₆₀₀ ~1.5) were separately added onto glass substrates coated with 3- and 7- layers of PEOX/TA or PIPOX/TA films. After 1 hour of incubation at 37 °C with shaking at 54 rpm, the substrates were washed twice with PBS, immersed in 5 mL of fresh PBS, vortexed for 1 minute and sonicated for 5 minutes to get adherent bacteria into the solution. The PBS containing the de-attached bacteria was diluted 1:100 with PBS and 80 µL of this solution was spread plated on LB agar plates. Colonies were counted after overnight growth at 37 °C.

4.3.11. Agar-Plating Method[‡]

25 µL of overnight cultures of *E. coli* ATCC 8739 and *S. aureus* ATCC 29213 grown in LB broth (OD₆₀₀ ~1.5) were separately added onto glass substrates coated with 3- and 7- layers of PEOX/TA or PIPOX/TA films. After 1 hour of incubation at 37 °C with shaking at 54 rpm, the substrates were washed twice with PBS, immersed in 5 mL of fresh PBS, vortexed for 1 minute and sonicated for 5 minutes to get adherent bacteria into the solution. The PBS containing the de-attached bacteria was diluted 1:100 with PBS and 80 µL of this solution was spread plated on LB agar plates. Colonies were counted after overnight growth at 37 °C.

[‡] Kirby Bauer test and agar plating experiments were performed by Sinem Uluşan.

4.3.12. Statistical analysis

All the results were normalized to control (assumed as 100) and standard deviation of the means was used. The parametric t-test was applied to all experimental groups and the significance of the results was determined by using a two-tailed p value, where p value ≤ 0.05 was accepted as significant at 95% confidence interval.

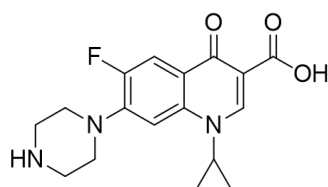
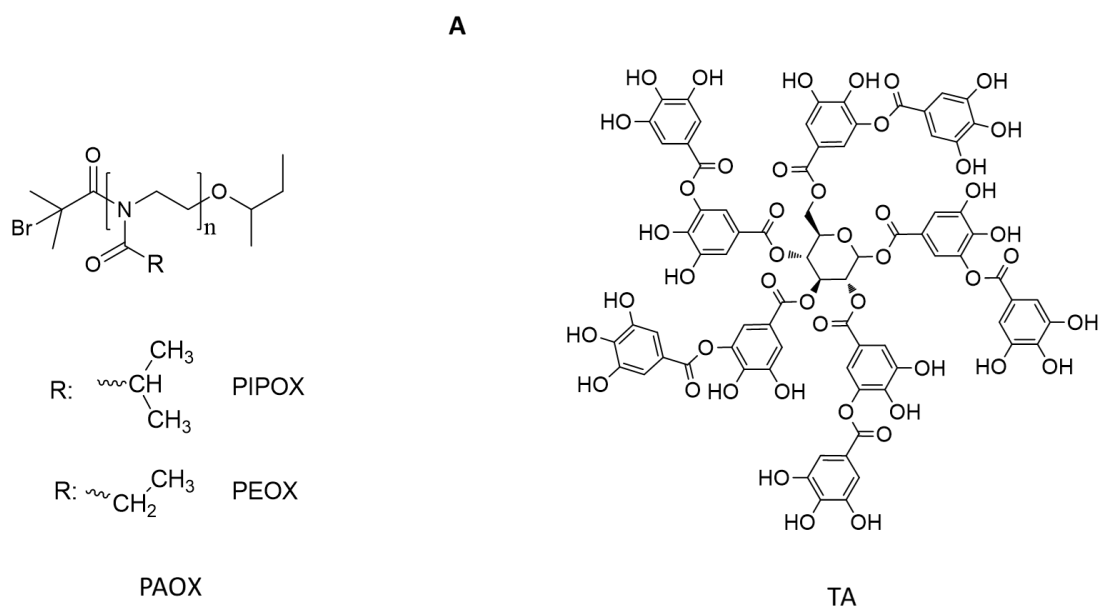
4.4. Results and Discussion

4.4.1. Preparation of Multilayers

PEOX/TA and PIPOX/TA multilayers were constructed at pH 2.5 using LbL technique. We have recently reported two pK_a values for TA, i.e. $pK_{a,1} = 6.5$ and $pK_{a,2} = 8$ [178]. At pH 2.5, phenolic hydroxyl groups of TA were in the protonated form. Multilayers were assembled at the surface through H-bonding interactions among carbonyl groups of PEOX or PIPOX and phenolic hydroxyl groups of TA. Figure 4.1A shows the chemical structures of PAOXs, TA and CIP. Figure 4.1B shows LbL growth of PEOX/TA and PIPOX/TA multilayers. Both films showed linear growth profiles with ~ 2.4 nm and ~ 3.0 nm increment per bilayer for PEOX/TA and PIPOX/TA films, respectively. The slightly higher thickness increment for PIPOX/TA films can be correlated with the differences in hydrophobicity and chain conformation of the two polymers. PIPOX was expected to adopt a less expanded coil conformation than PEOX due to the presence of isopropyl side chains bringing greater hydrophobicity to PIPOX. Thus, in contrast to PIPOX which possibly adsorbed in more globular form at the surface, PEOX adsorbed in the form of extended chains resulting in thinner films. The association of PIPOX and TA was also expected to be greater than that among PEOX and TA due to greater hydrophobicity of PIPOX. The contribution of hydrophobic interactions among the interacting polymer pairs to LbL growth and multilayer stabilization has been reported earlier [309]. Hoogenboom and De Geest also observed a similar phenomenon and explained the higher thickness of LbL films with increasing PAOX hydrophobicity by the chain conformation as well as increasing

hydrophobic interactions among the multilayers [210]. Of note, LbL deposition of PAOX with polyacids have been reported previously by us and other research groups [178,208,211,306,307].

It is worth mentioning that we could successfully deposit PIPOX and TA multilayers at pH 2.5 without using 1 bilayer of BPEI and TA (both deposited at pH 5.5) as the precursor layers. However, we could not obtain a robust film growth in case of PEOX and TA films. The more hydrophobic PIPOX possibly provided better adhesion onto the surface than PEOX. For comparison of PEOX/TA and PIPOX/TA multilayers, we preferred preparation of multilayers under identical conditions. Therefore, 1 bilayer of BPEI and TA was used as the precursor layers for both types of the films.



CIP

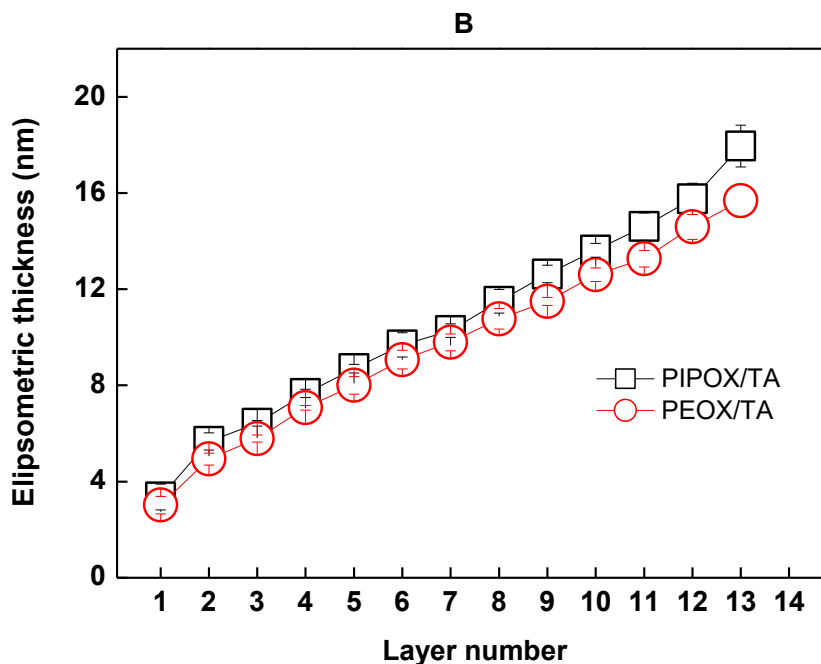


Figure 4.1. (A) Chemical structures of PAOXs, TA and CIP. (B) LbL growth of PIPOX/TA (square) and PEOX/TA(circle) films at pH 2.5 and 25 °C. Multilayers were deposited onto BPEI/TA precursor layers with a thickness of 4.7 nm. Thickness values do not include the precursor thickness.

AFM imaging was performed to contrast the morphology of PEOX/TA and PIPOX/TA multilayers. Figure 4.2A shows the AFM images and surface roughness values of 13-layer films of PEOX/TA and PIPOX/TA. Self-association of polyphenols has been reported earlier [310]. In addition, deposition of TA in the aggregated state in LbL assembly has been suggested before due to thickness values which were greater than the molecular dimensions of TA [311,312]. In the light of these findings, the origin of the surface roughness is attributed to self-association of TA through intermolecular hydrogen bonding interactions among hydroxyl groups at acidic conditions leading to deposition of TA in the aggregated form. The roughness increased from ~ 13.5 nm to ~ 23.0 nm and ~ 11.3 nm to ~ 14.5 nm as the layer number increased from 7 to 13 for PEOX/TA and PIPOX/TA films, respectively (see Figure 4.3A for AFM images of 7-layer PEOX/TA and PIPOX/TA films). The reason for

increasing roughness with increasing layer number might be the incomplete and irregularly packed TA layers (see Figure 4.3B for AFM image of 1-layer of TA). A TA-layer had aggregates which formed the higher parts of the layer as well as holes which formed the lower parts of the surface. Considering the adsorption kinetics, when a substrate coated with TA as the topmost layer was exposed to either PEOX or PIPOX solution, the probability of adsorption onto TA aggregates would be higher than deposition onto the holes. The situation was expected to be similar when a substrate coated with PEOX or PIPOX as the topmost layer was exposed to TA solution. This was possibly the reason for increasing surface roughness with increasing layer number. Note that the difference in roughness values between 13-layer PEOX/TA and PIPOX/TA films was larger than that of 7-layer films. AFM images of 7-layer films (Figure 4.3A) showed that PEOX/TA film was inhomogeneous and had large and fused aggregates which might have contributed to more significant roughness increase with increasing layer number. In addition, the difference in roughness between PEOX/TA and PIPOX/TA multilayers might have resulted from the difference in binding strength among the layers. The hydrophobic association among PIPOX and TA layers was expected to be greater than that among PEOX and TA resulting in greater number of binding points between the layers and more intense films with relatively smooth surfaces. The correlation between the surface roughness and conformational state of multilayers was reported by Rubner [302] and Sukhishvili [313] for electrostatic and hydrogen-bonded multilayers, respectively.

PEOX/TA and PIPOX/TA films were also compared with respect to wettability. The evolution of contact angles was followed as a function of layer number. As shown in Figure 4.2B, the contact angles varied between 40°- 47° and 60°-64° for PEOX/TA with PEOX topmost layer and PIPOX/TA with PIPOX topmost layer, respectively. For both films, lower contact angle values were recorded when TA was the topmost layer compared to those ending with either PEOX or PIPOX. This was possibly due to phenolic hydroxyl groups of TA providing greater wettability [314]. However, PEOX/TA films had lower contact angle (varied between 37°-42°) than PIPOX/TA

films (varied between 45°-49°) even when both films had TA as the outmost layer. The wettability of multilayer films is correlated with the outmost layer [315]. Despite the same topmost layer, the higher contact angle of PIPOX/TA multilayers was possibly arising from the interpenetration of the layers and the contribution of more hydrophobic PIPOX to the topmost part of PIPOX/TA films.

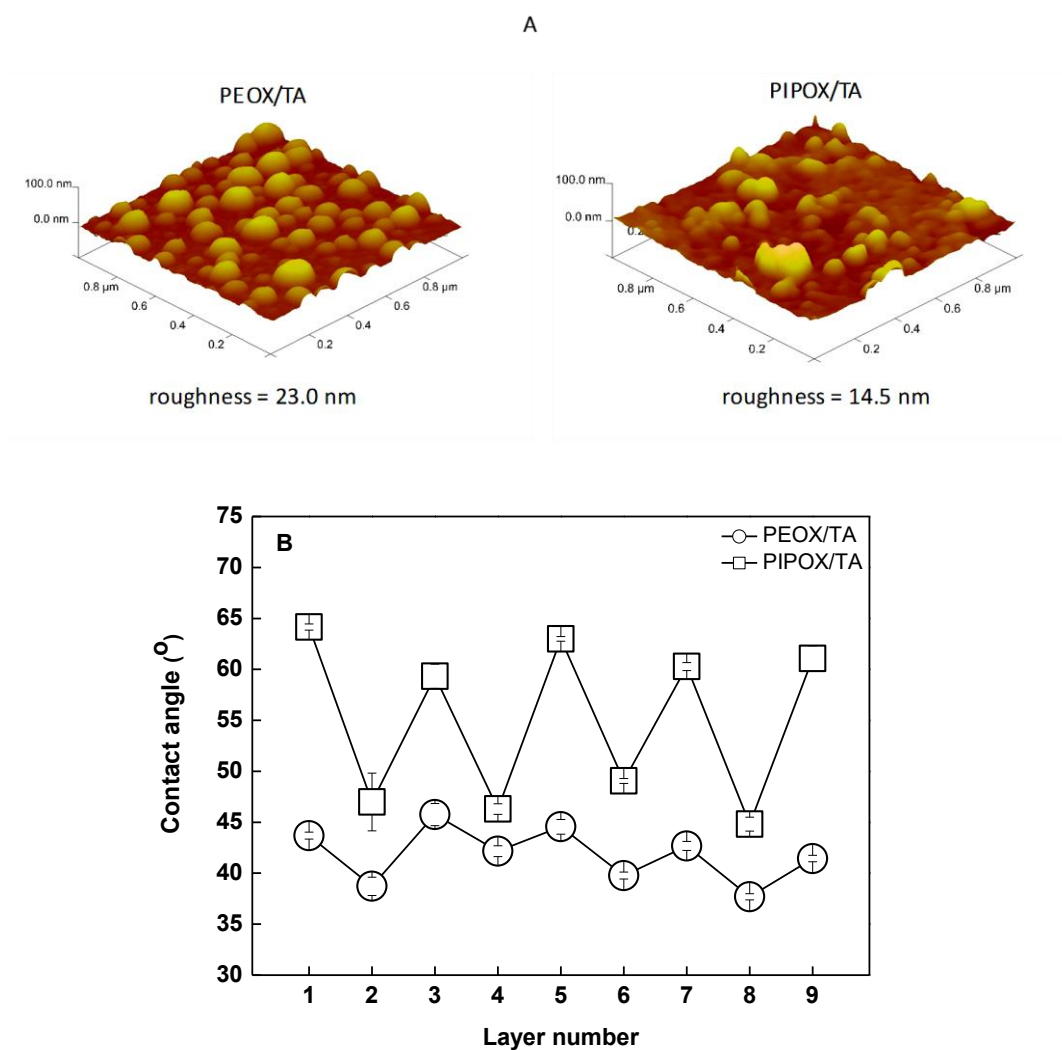


Figure 4.2. A) AFM topography images of 13 layers of PEOX/TA and PIPOX/TA. Roughness values were recorded from images with 2x2 μm^2 scan size. (B) Evolution of static contact angle of PEOX/TA (\circ) and PIPOX/TA (\square) films as a function of layer number. Multilayers were deposited onto BPEI/TA precursor layers. Odd layer numbers correspond to PEOX or PIPOX topmost layer.

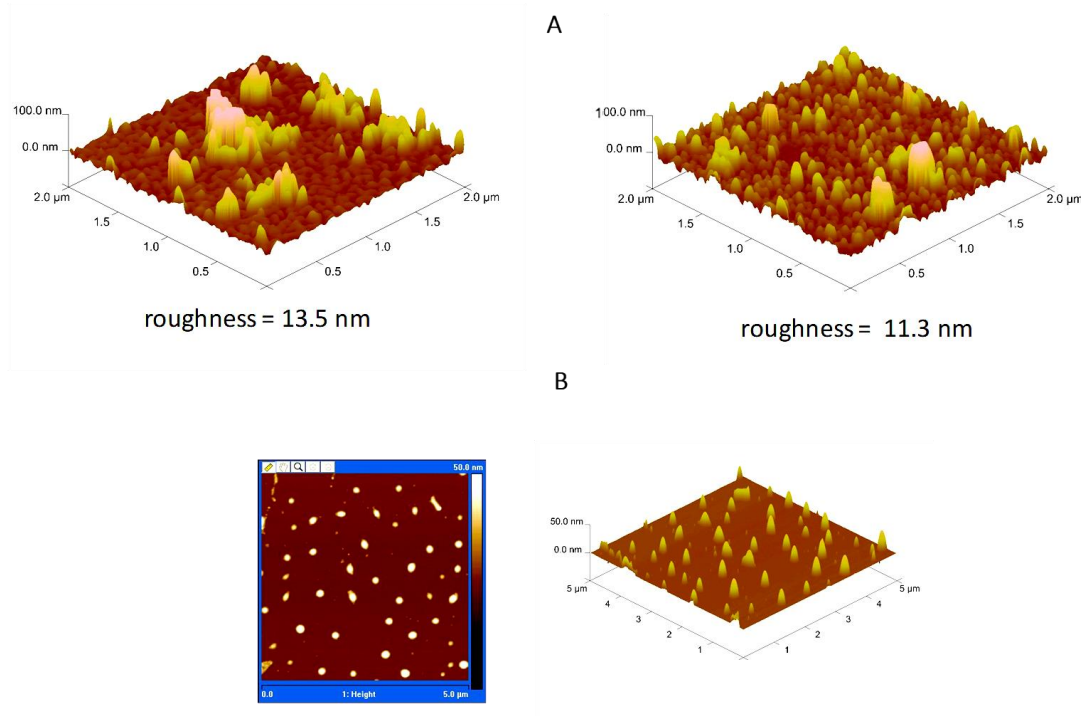


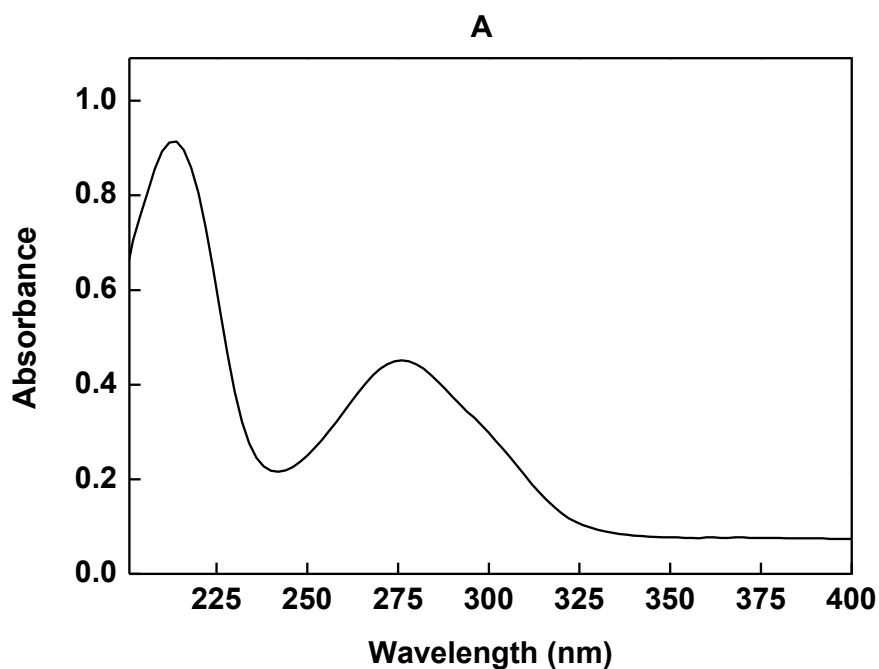
Figure 4.3. AFM topography images of (A) 7-layer PEOX/TA and PIPOX/TA films with $2 \times 2 \mu\text{m}^2$ scan size. Roughness values were recorded from images with $2 \times 2 \mu\text{m}^2$ scan size. (B) AFM topography images of 1-layer of TA with $5 \times 5 \mu\text{m}^2$ scan size.

CIP loading into multilayers

CIP loaded PEOX/TA and PIPOX/TA multilayers were prepared by immersing the multilayers into CIP solution at pH 7.4 for 12 hours. Increasing pH from 2.5 to 7.4 allowed ionization of some of the free phenolic hydroxyl groups of TA within the multilayers. The driving force for CIP loading was mainly electrostatic interactions between free phenolate groups of TA and protonated piperazinyl amino groups of CIP ($pK_{a,1} = 6.1$ associated with the carboxylic acid groups and $pK_{a,2} = 8.7$ associated with the secondary amino groups [316]). Additionally, hydrogen bonding interactions among CIP and TA possibly contributed to CIP loading into multilayers. As mentioned earlier, TA has a $pK_{a,1}$ of 6.5 and $pK_{a,2}$ of 8.0 [178]. At pH 7.4, it has both phenolic hydroxyl and phenolate groups which remained free after LbL construction.

Those phenolic hydroxyl groups could have formed hydrogen bonds with carbonyl groups of CIP.

UV-Visible Spectra of PEOX/TA and PIPOX/TA multilayers exhibited two peaks at 215 nm and 275 nm. TA shows 2 peaks at 220 nm and 275 nm in 10 mM phosphate buffer at pH 2.5 (Figure 4.4A). Therefore, we mainly correlated these peaks with TA. Cipro loading into multilayers was performed at pH 7.4. Cipro absorbs strongly at 275 nm and relatively weak at 328 nm and 339 nm in 10 mM phosphate buffer at pH 7.4 (Figure 4.4B). The peak at 275 nm in the absorption spectra of multilayers slightly broadened with a slight increase in intensity upon CIP loading (Figure 4.5). We did not observe any peaks specific to CIP in the absorption spectra of PAOX multilayers possibly due to overlapping of CIP and TA peaks and relatively low amount of CIP within the multilayers compared to TA.



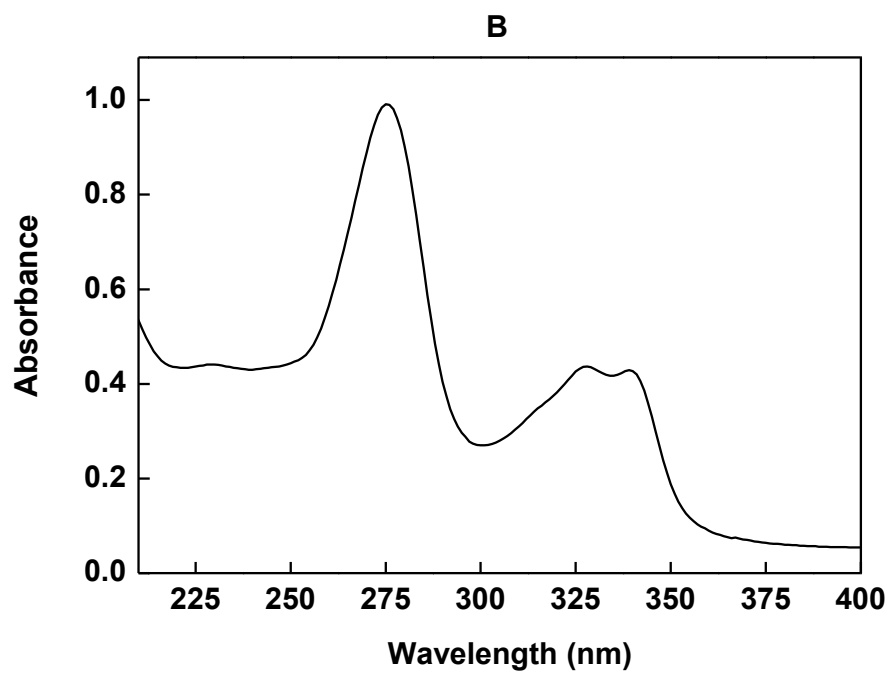


Figure 4.4. UV-Visible spectra of (A) TA in 10 mM phosphate buffer at pH 2.5 and (B) CIP in 10 mM phosphate buffer at pH 7.4. Concentrations of TA and CIP were both 0.001 mg/mL.

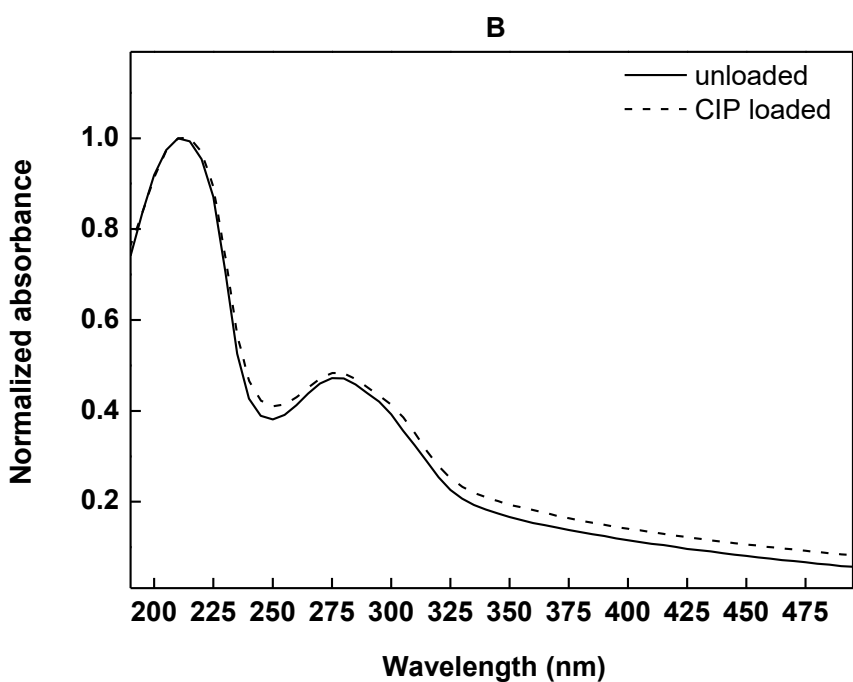
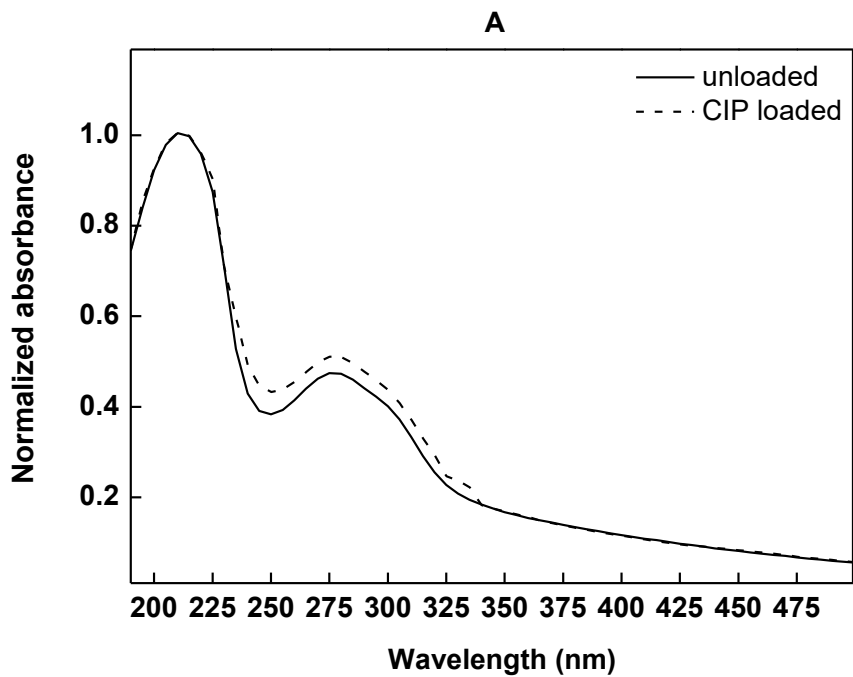


Figure 4.5. UV-Visible spectra of 49-layer PEOX/TA (Panel A) and PIPOX/TA (Panel B) films coated on both sides of quartz substrates before (solid-line) and after CIP loading (dash-line).

The comparison of surface morphology of the multilayers before and after CIP loading suggested smoothing of the surfaces upon CIP loading with a decrease in surface roughness from ~ 14.5 nm to ~ 7.7 nm for PEOX/TA and from ~ 23.0 nm to ~ 16.7 nm for PIPOX/TA multilayers. Figure 4.6 contrasts AFM images of 13-layer PEOX/TA and PIPOX/TA films before and after CIP loading. As discussed earlier, deposition of TA in the aggregated state was the origin of formation of rough multilayer surfaces. When multilayer coated substrates were exposed to CIP solution, relatively small CIP molecules (compared to PEOX, PIPOX or TA) possibly adsorbed onto both higher and lower parts (holes) of the film. This possibly resulted in partial filling of the holes by CIP molecules and a decrease in surface roughness.

The amount of CIP loaded into PEOX/TA and PIPOX/TA multilayers was approximated using fluorescence spectroscopy technique. Fluorescence intensity of CIP was recorded before and after multilayers were immersed into 0.1 mg/mL CIP solution prepared in 10 mM phosphate buffer. The amount of CIP was quantified using calibration curves. The difference in CIP amount between the initial (before loading) and final (after loading) cases was attributed to the amount of CIP loaded into multilayers. The amount of CIP loaded into 49-layer PEOX/TA and PIPOX/TA films (each deposited onto 1 cm x 1 cm glass substrate) was 539 μg and 461 μg , respectively. Loading efficiency was calculated as 30% and 26% for PEOX/TA and PIPOX/TA multilayers, respectively.

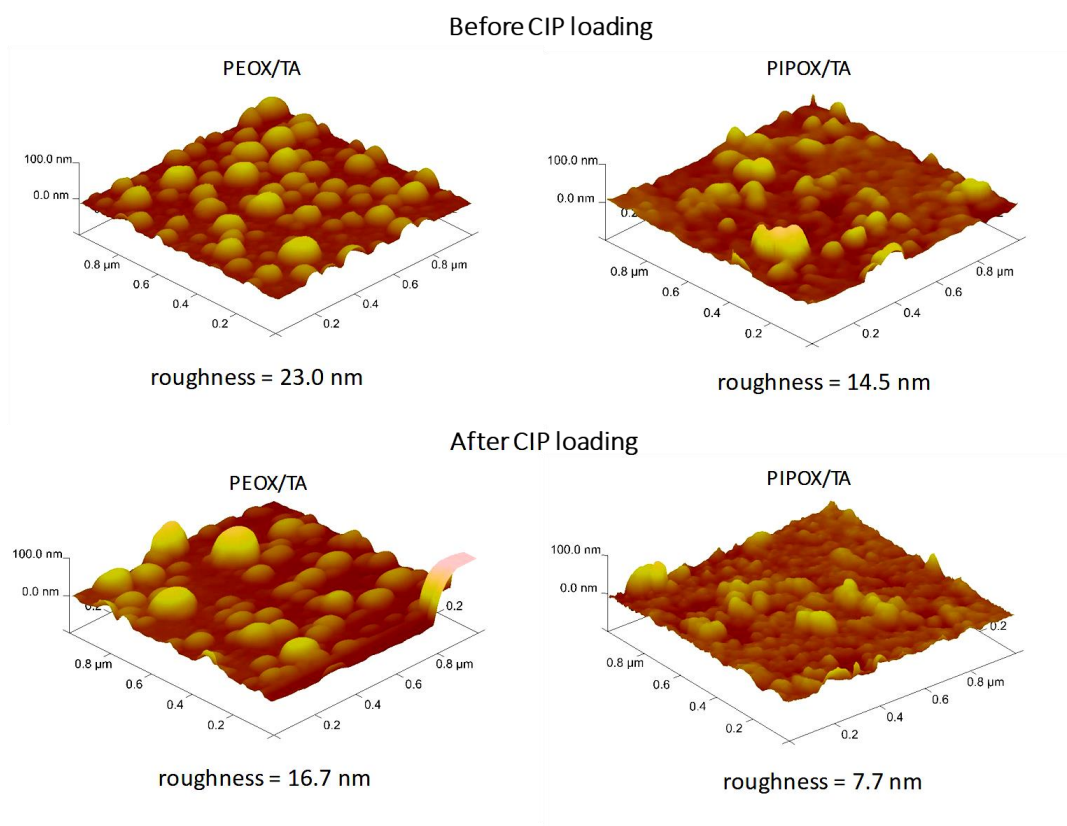


Figure 4.6. AFM topography ($1\mu\text{m} \times 1\mu\text{m}$) images of 13-layer PEOX/TA and PIPOX/TA films before and after CIP loading. Roughness values were recorded from images with $2 \times 2\mu\text{m}^2$ scan size.

4.4.2. Stability and wettability testing after immersion into PBS

Stability of both unloaded and CIP loaded multilayers were examined in PBS at pH 7.4 at $25\text{ }^\circ\text{C}$ and $37\text{ }^\circ\text{C}$ by following the evolution of film thickness as a function of time using ellipsometry (Figure 4.7). We found that unloaded PEOX/TA multilayers gradually eroded with time at both temperatures. The film almost completely removed from the surface after 24 hours at $37\text{ }^\circ\text{C}$. The amount of material remained at the surface at $25\text{ }^\circ\text{C}$ was $\sim 20\%$ greater than that at $37\text{ }^\circ\text{C}$ after 24 hours. The disintegration of PEOX/TA films can be explained by disruption of hydrogen bonding interactions among the layers due to ionization of TA with increasing pH from 2.5 to 7.5. In

addition to pH increase, the relatively high salt content of PBS (0.002 M NaH_2PO_4 , 0.008 M Na_2HPO_4 , 0.0027 M KCl and 0.137 M NaCl) compared to 10 mM phosphate buffer might have induced further ionization of TA. It must be born in mind that LbL deposition was performed using polymer and rinsing solutions prepared in 10 mM phosphate buffer. Of note, enhanced ionization of polyacids in the presence of salt ions has been reported earlier [309]. We speculate that the increase in the number of phenolate groups might have led to electrostatic repulsion among the ionized TA molecules. In addition, the salt ions penetrating into the multilayers to compensate the excess negative charge might have resulted in an increase in osmotic pressure which caused diffusion of water into the multilayers followed by swelling and disintegration of the layers. A comparison of the data obtained at 25 °C and 37 °C showed that increasing temperature from 25 °C to 37 °C resulted in ~ 20% further loss from the surface, indicating the effect of increasing temperature on the disruption of hydrogen bonding interactions among the layers. In contrast to PEOX/TA multilayers, PIPOX/TA films were stable up to 24 hours without any loss from the surface. The greater stability of PIPOX/TA films can be attributed to stronger hydrophobic association among the polymer layers due to greater hydrophobicity of PIPOX. Effect of hydrophobicity on stability of hydrogen-bonded multilayers has been reported earlier [313].

CIP loaded PEOX/TA multilayers demonstrated a remarkably different stability profile in PBS at pH 7.4 at 25 °C and 37 °C. At both temperatures, PEOX/TA films remained stable within the duration of stability testing in the presence of CIP molecules. This was possibly due to screening of negative charges sourcing from phenolate groups of TA by positively charged piperazinyl amino groups of CIP molecules. In this way, destabilization of PEOX/TA films arising from excess negative charge within the multilayers might have been prevented, resulting in more stable films. Similar to unloaded PIPOX/TA multilayers, CIP integrated PIPOX/TA films were also quite stable under similar conditions. He et al. increased the stability of PEOX/PAA multilayers by partially hydrolyzing PEOX to introduce secondary

amine groups which enabled heat-induced crosslinking among the layers and stabilization of multilayers [214]. This study differs from that of He et al. in the sense that stable PAOX multilayers in PBS at 37 °C could be obtained without hydrolysis of PAOX or crosslinking of multilayers. We also monitored the stability of multilayers at 25 °C and 37 °C using UV-Visible Spectroscopy by following the intensity of the peak at 215 nm as a function of time (Figure 4.8). As discussed earlier, the peak at 215 nm was mainly correlated with TA. The evolution of the intensity of the peak at 215 nm was indirectly correlated with the stability of multilayers.

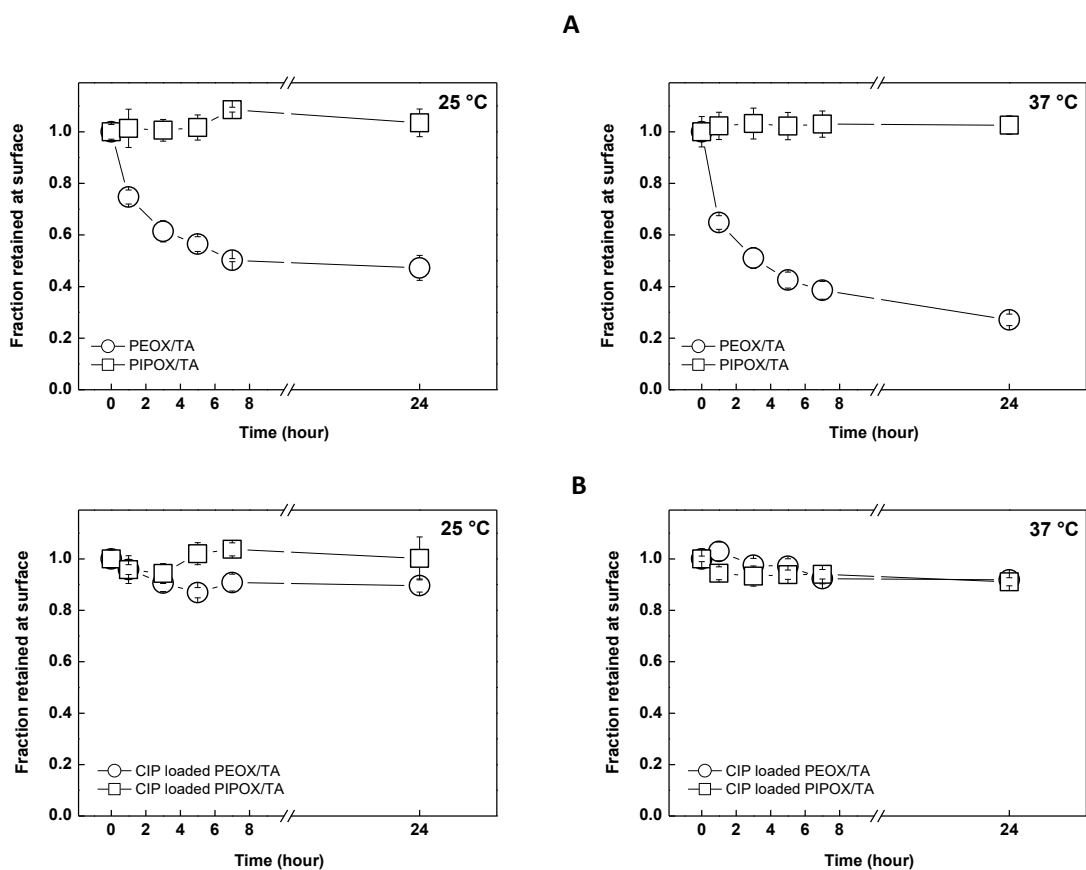


Figure 4.7. Fraction retained at the surface of 13-layer unloaded (A) and CIP loaded (B) PEOX/TA (circles) and PIPOX/TA (squares) films as a function of time after immersed into PBS at pH 7.4/25 °C or pH 7.4/37 °C. Fractions were calculated by normalizing the thickness values to the initial thickness of the films.

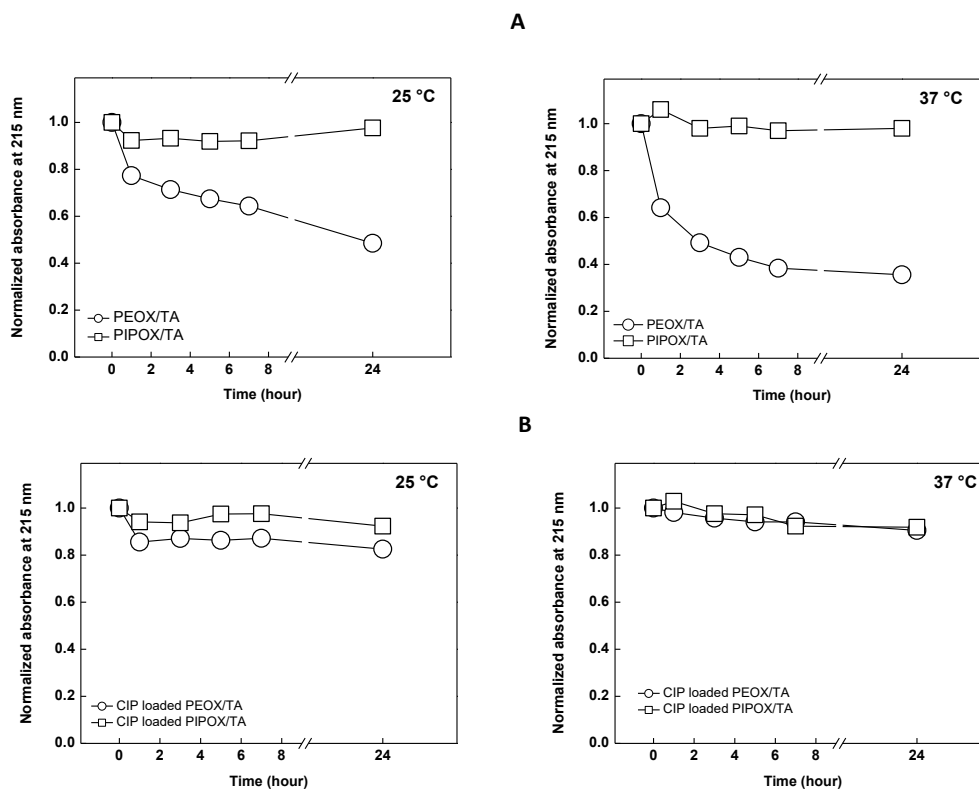


Figure 4.8. Normalized absorbance values at 215 nm for unloaded (A) and CIP-loaded (B) 49-layer PEOX/TA and PIPOX/TA films (coated on both sides of quartz substrates) as a function of time after immersion into PBS at pH 7.4/25 °C or pH 7.4/37 °C. Normalized absorbance values were calculated by normalizing the absorbance of the films at 215 nm to the initial absorbance at 215 nm.

The comparison of wettability of PEOX/TA and PIPOX/TA films before and after immersion into PBS at pH 7.4 and 37 °C is presented in Figure 4.9. The contact angle of PEOX/TA multilayers remained almost same after immersion into PBS at pH 7.4 and 37 °C. An increase of 6° was recorded for the contact angle of PIPOX/TA films after immersion into PBS at pH 7.4 and 37 °C due to LCST-type phase behaviour of PIPOX and increased hydrophobicity at 37 °C.

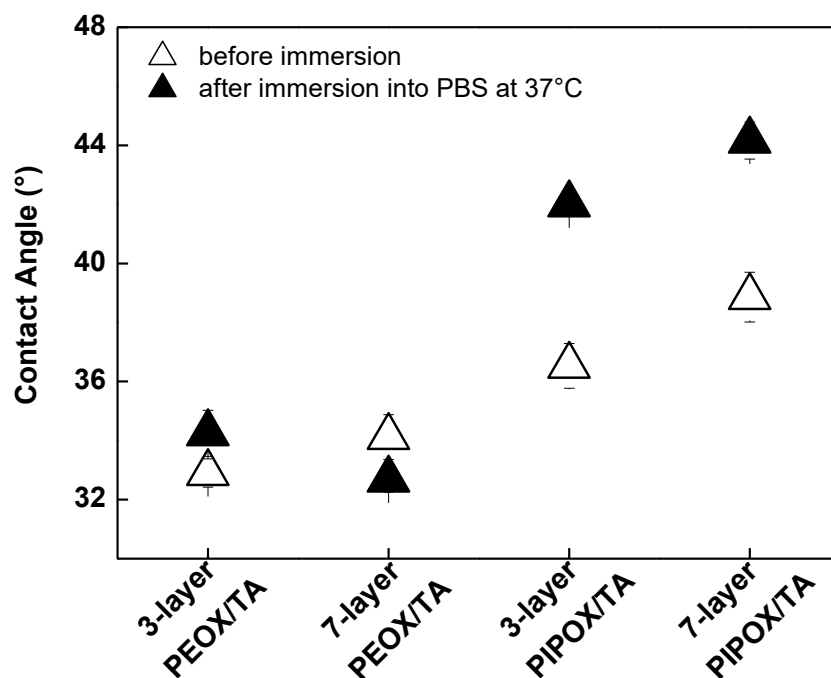


Figure 4.9. Static contact angle measurements of 3- and 7- layer PEOX/TA and PIPOX/TA films before and after immersion into PBS at pH 7.4/37 °C.

4.4.3. CIP release from multilayers

CIP is a model antibiotic commonly used to treat bacterial infections. CIP release from multilayers was performed in PBS at pH 7.4 as well as at pH 6.0 to mimic the slightly acidic environment at an infectious site in the body [317]. At each pH, release was performed at both 25 °C and 37 °C to understand the effect of temperature on CIP release from multilayers. Importantly, both films were stable at all conditions under examination (see Figure 4.10 for stability of PEOX/TA and PIPOX/TA at pH 6.0/25 °C and pH 6.0/37 °C).

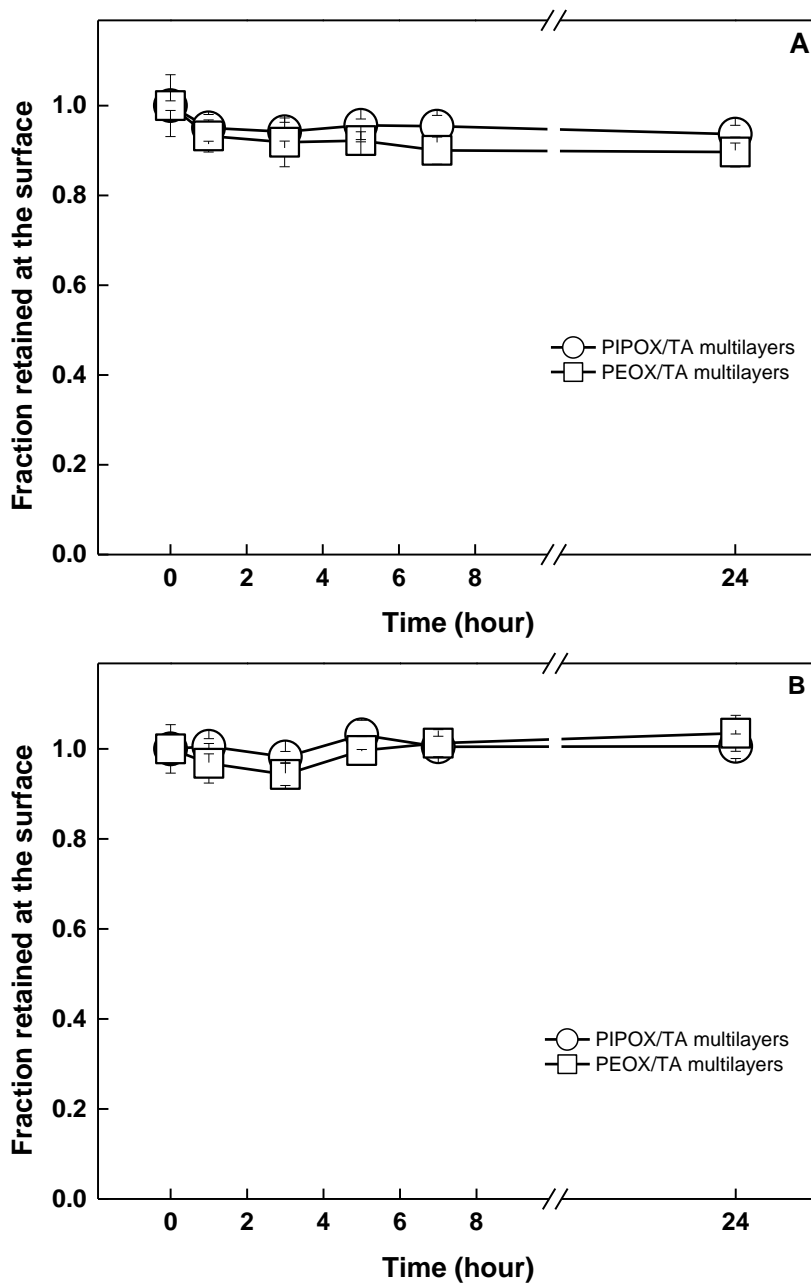


Figure 4.10. Fraction retained at the surface of CIP loaded 13-layer PEOX/TA and PIPOX/TA films as a function of time after immersed into PBS at pH 6.0/25 °C (A) and pH 6.0/37 °C (B). Fractions were calculated by normalizing the thickness values to the initial thickness of the films.

Figure 4.11A compares the total amount of CIP released from PEOX/TA and PIPOX/TA films (see Figure 4.12 for CIP release as a function of time from multilayer surfaces at various conditions). The amount of CIP released from multilayers was calculated by quantifying the fluorescence intensity data using calibration curves prepared at release conditions. % release was calculated through dividing the amount of CIP released under particular condition by the amount of CIP loaded into the multilayers (Figure 4.11B). A burst release took place at early stages, followed by slow and continuous release for both films under all conditions. To understand the pH effect on CIP release, release at pH 7.4/25 °C and pH 6.0/25 °C was contrasted. The release at pH 7.4/25 °C was correlated with: i) self-diffusion of CIP molecules from the surface and ii) salt-induced rearrangement within the multilayers in PBS. It must be born in mind that multilayer construction was performed using polymer and rinsing solutions prepared in 10 mM phosphate buffer solutions. CIP loading solution was also prepared in 10 mM phosphate buffer solution. However, release experiments were conducted in PBS. PBS is a mixture of 0.002 M NaH₂PO₄, 0.008 M Na₂HPO₄, 0.0027 M KCl and 0.137 M NaCl, thus contains higher amount of salt ions than 0.01 M phosphate buffer solution. Accordingly, the amount of salt ions penetrating from the solution into multilayers is suggested to be greater in PBS solution than that in 10 mM phosphate buffer. It is possible that the salt ions penetrating into multilayers could have partially disrupted electrostatic association among TA and CIP due to competitive interactions among TA/Cipro and TA/salt ions. This could be one of the reasons for the release of CIP at pH 7.4 and 25 °C. Additionally, ionization of TA might have been enhanced in the presence of high concentration of salt ions which might have partially disrupted the association among TA and PAOXs (PEOX or PIPOX). This salt-induced rearrangement within the multilayers possibly formed relatively loosely bound multilayers with lower number of binding points among the layers compared to the films in 10 mM phosphate buffer and facilitated self-diffusion of CIP from multilayers. At pH 6.0/25 °C, both films released greater amount of CIP than that at pH 7.4/25 °C due to protonation of phenolate groups of TA and loss of electrostatic interactions among CIP and TA. Importantly, the amount of CIP released

from PEOX/TA multilayers was significantly greater than that from PIPOX/TA multilayers. The difference might be due to different amounts of CIP loaded into multilayers and relatively weak association of PEOX and TA layers, facilitating release of CIP from multilayers.

At pH 7.4 and 37 °C, PEOX/TA multilayers released slightly greater amount of CIP than that at pH 7.4 and 25 °C. This can be correlated with the disruption of hydrogen bonding or electrostatic association among TA layers and CIP with increasing temperature. The difference between the amount of CIP released at pH 7.4/25 °C and pH 7.4/37 °C was greater for PIPOX/TA films. This can be explained by conformational transition of PIPOX from extended to globular form at 37 °C leading to formation of voids within the multilayers which possibly facilitated the release of CIP. Enhanced release of functional molecules from multilayers composed of polymers with LCST-type phase behaviour has been reported previously by us and others [185,318].

At pH 6.0/37 °C, PEOX/TA and PIPOX/TA multilayers showed an opposite trend. CIP release from PEOX/TA was suppressed, whereas PIPOX/TA multilayers released significantly higher amount of CIP due to causative effect of dual trigger, i.e. pH and temperature. The suppression of CIP release from PEOX/TA might be due to the synergistic effect of the decrease in hydration of PEOX at 37 °C, enhancing hydrophobic association among PEOX and TA as well as increased hydrogen bonding interactions among the film layers at pH 6.0 resulting in entrapment of CIP molecules within the multilayers. Stabilization of polymer complexes with increasing temperature was reported before and explained by the enhanced hydrophobic interactions among the polymer pairs [319]. Scheme 4.1 shows the schematic representation of CIP release from PIPOX/TA and PEOX/TA multilayers at pH 6.0/37 °C. AFM imaging of multilayers after CIP release (Figure 4.13) at pH 7.4 and 37 °C showed increase in roughness (from 16.7 to 21.2 for 13-layer PEOX/TA and from 7.7 to 11.1 nm for 13-layer PIPOX/TA). The increase in roughness can be attributed to the defects that CIP could cause during release [320] as well as morphological changes

occurring within the multilayers at 37 °C.

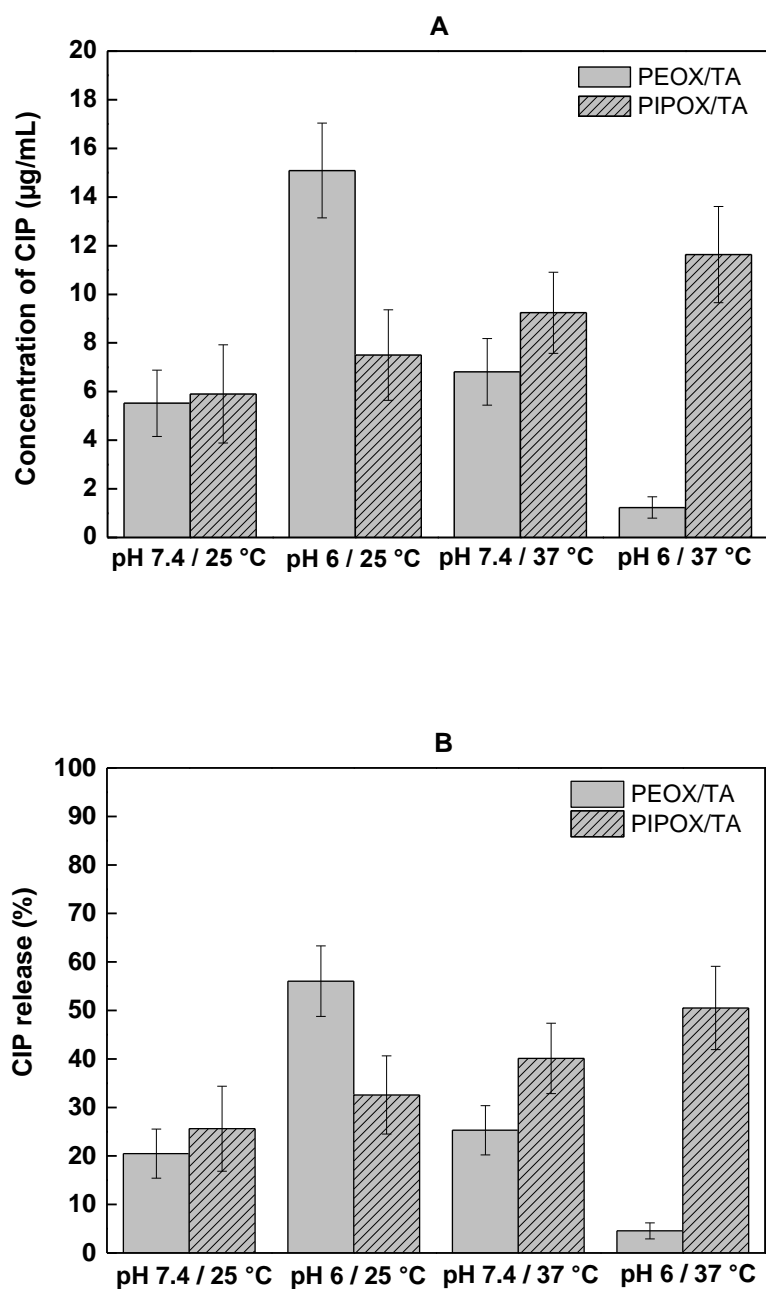


Figure 4.11. (A) Amount of CIP released from 49-layer PIPOX/TA and PEOX/TA films (deposited onto 1 cm x 1 cm glass substrates) at pH 7.4/25 °C, pH 7.4/37 °C, pH 6.0/25 °C and pH 6.0/37 °C after 24 hours. (B) % release of CIP from 49-layer PIPOX/TA and PEOX/TA films at pH 7.4/25 °C, pH 7.4/37 °C, pH 6.0/25 °C and pH 6.0/37 °C after 24 hours.

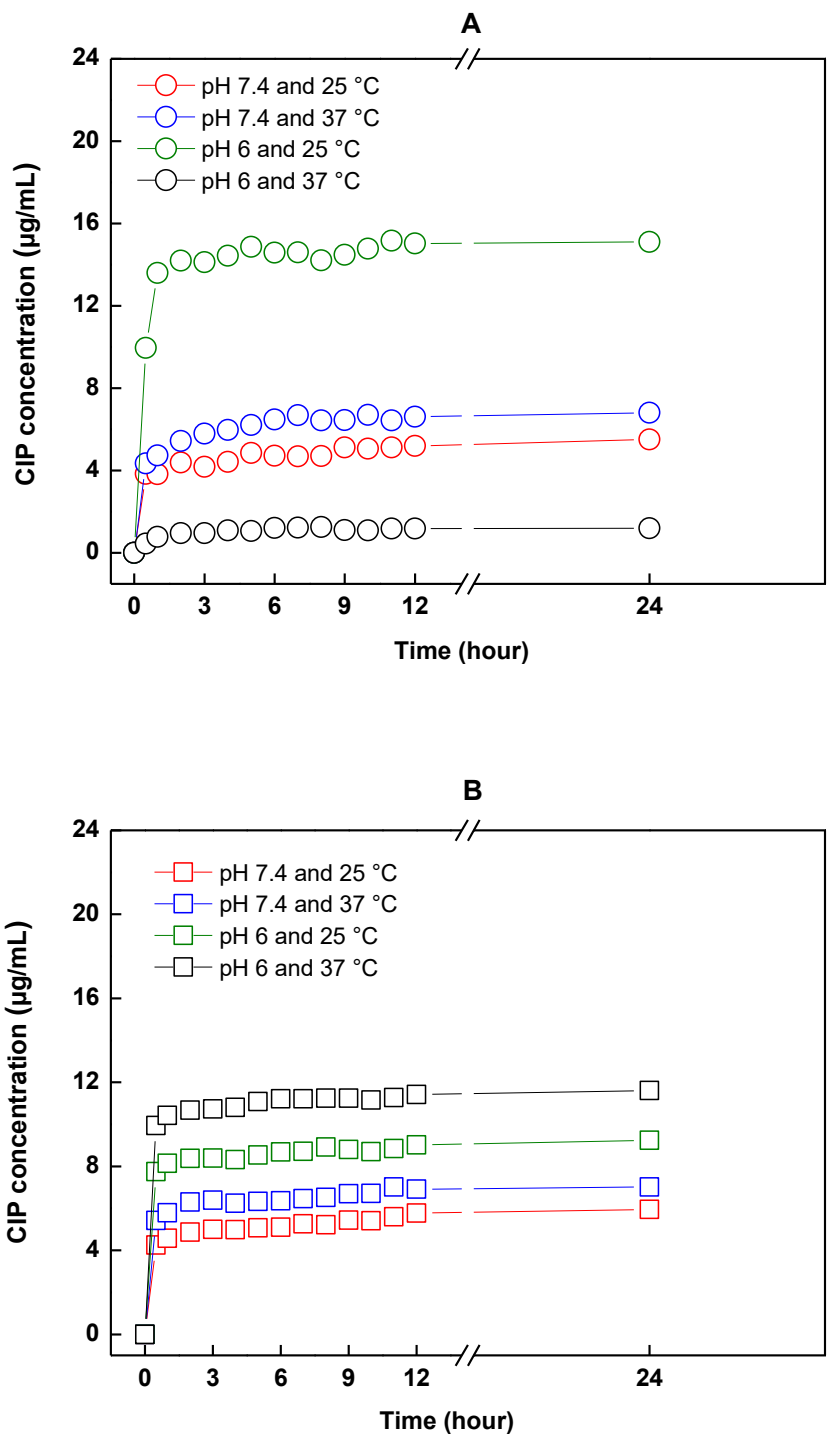
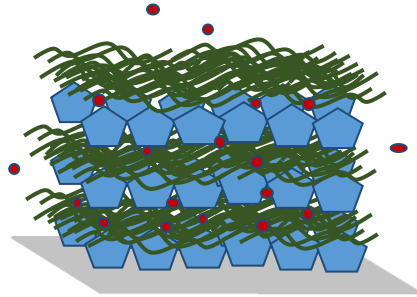
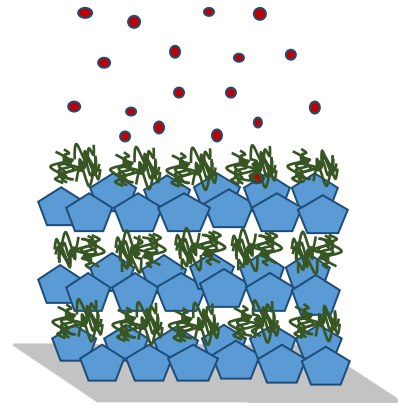


Figure 4.12. Concentration of CIP released from 49-layer (A) PEOX/TA and (B) PIPOX/TA films (deposited onto 1 cm x 1 cm glass substrates) at pH 7.4/37 °C; pH 6.0/37 °C; pH 7.4/25 °C and pH 6.0/25 °C as a function of time.

pH 6 and 37 °C



PEOX/TA multilayers



PIPOX/TA multilayers



TA

PEOX



PIPOX



CIP

Scheme 4.1. Schematic representation of CIP release from PEOX/TA and PIPOX/TA multilayers at pH 6.0 and 37 °C.

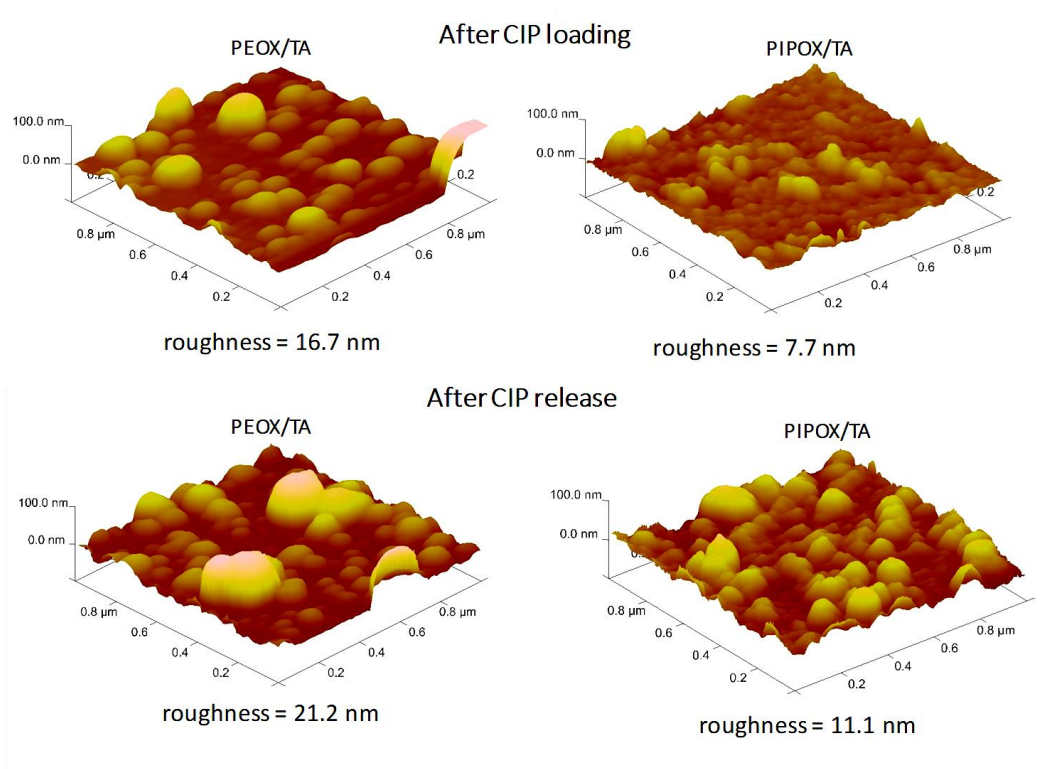


Figure 4.13. AFM height ($1\mu\text{m} \times 1\mu\text{m}$) images of 13-layer PIPOX/TA and PEOX/TA films before and after CIP release at pH 6.0 and 37°C . Roughness values were recorded from images with $2 \times 2\ \mu\text{m}^2$ scan size.

4.4.4. Antibacterial properties of multi-layer films of PIPOX/TA and PEOX/TA against *E. coli* and *S. aureus*

Antibacterial activities of CIP-loaded PIPOX/TA and PEOX/TA multilayers were assessed against model Gram-negative (*E. coli*) and Gram-positive (*S. aureus*) bacteria using a Kirby-Bauer test (Figure 4.14). CIP-loaded PEOX/TA and PIPOX/TA films showed a clear zone of inhibition of bacterial growth on MH agar at both pH (pH 7.4 and pH 6.0) and temperature (25°C and 37°C) conditions. Contrary to the distinctly different CIP amounts released under various conditions (Section 4.4.3), inhibition zones obtained using PEOX /TA and PIPOX/TA multilayers did not differ significantly (2.9-3.5 cm). Nevertheless, the highest inhibition zone was observed for PEOX/TA at pH 6.0 and 25°C which is in good agreement with the highest amount

of CIP release from PEOX/TA at this condition. MIC value for CIP was measured as 0.05 $\mu\text{g/mL}$ and 1.0 $\mu\text{g/mL}$ against *E. coli* and *S. aureus*, respectively. Of note, plasma concentration of CIP was reported as 2.3 mg/L and maximum plasma concentration was reached in 1.3 hour in first day following intake [321]. In case of *E. coli*, comparable zone sizes observed under different conditions was possibly due to the low MIC with CIP for this bacterial species. Since the amount of CIP released from both multilayers were much higher than the MIC for *E. coli*, it ensured that the bacteria were susceptible to death at all experimental conditions used. In case of *S. aureus*, similar zone sizes were recorded for both films at all conditions except PEOX/TA at pH 6.0/37 $^{\circ}\text{C}$, which exhibited no clear zone. This is in good agreement with the reduced release of CIP from PEOX/TA multilayers at pH 6.0 and 37 $^{\circ}\text{C}$, which was insufficient to inhibit bacterial growth.

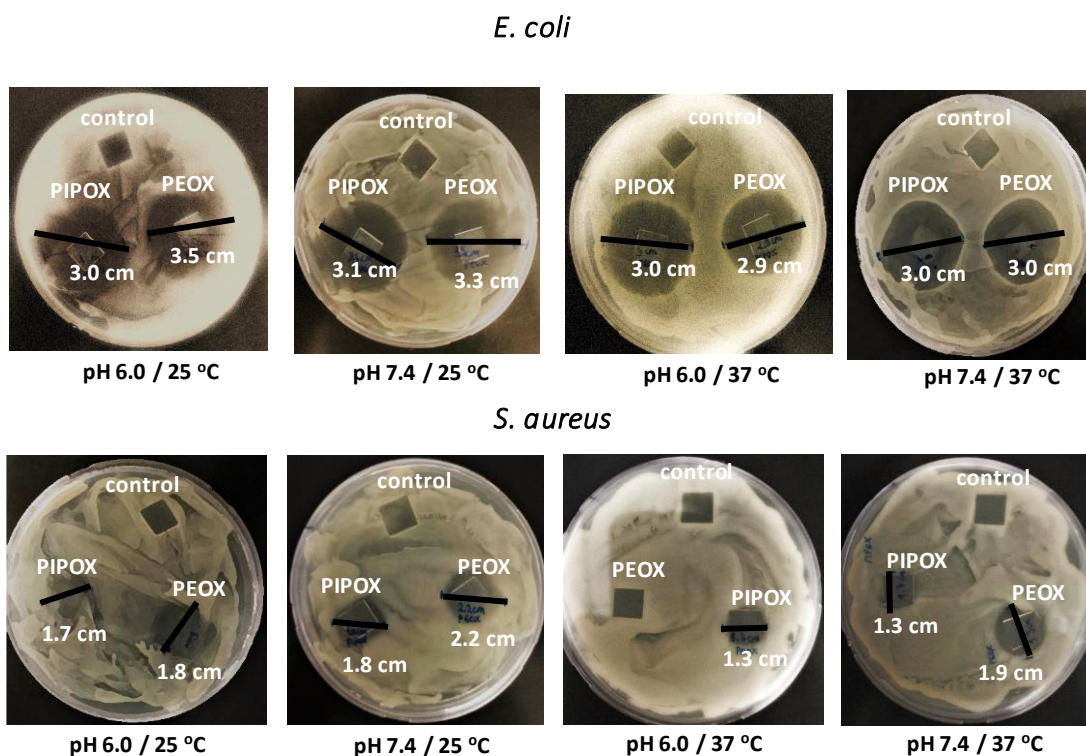


Figure 4.14. Kirby-Bauer test from CIP-loaded PIPOX/TA and PEOX/TA multilayers (coated onto glass substrates) against *E. coli* and *S. aureus* at pH 6.0/25 $^{\circ}\text{C}$; pH 7.4/25 $^{\circ}\text{C}$; pH 6.0/37 $^{\circ}\text{C}$ and pH 7.4/37 $^{\circ}\text{C}$. Uncoated sterile glass substrates were used as control substrates.

4.4.5. Bacterial anti-adhesive properties of multi-layers of PIPOX/TA and PEOX/TA against *E.coli* and *S. aureus*

Bacterial adhesion onto PEOX/TA and PIPOX/TA films (without any CIP) was determined with lag-phase cultures of *E.coli* ATCC 8739 and *S.aureus* ATCC 29213 using an agar plating method (Figure 4.15). Adhered bacteria from the substrates were taken into solution in PBS with sonication; all the bacteria in solution were then spread plated on LB agar plates and incubated at 37 °C for 16 hours. Colonies formed were counted and recorded. Identical sonication conditions and durations were used for all samples. All films had either PEOX or PIPOX as the outmost layer. In case of *E. coli*, the lowest colony number was observed for 3-layer PEOX/TA films with a 70% decrease compared to control. The anti-adhesive property was retained even in 7-layer films. However, the colony number overall was 18% higher than that for 3-layer films. The decrease in anti-adhesiveness observed with increasing layer numbers can be attributed to the increased surface roughness, which possibly provided greater surface area for bacterial adhesion. Figure 4.16 contrasts AFM images and surface roughness of 3- and 7-layer PEOX/TA films, which were treated in PBS at pH 7.4 and 37 °C for 1 hour. On the other hand, 3-layer PIPOX/TA films displayed low-fouling ability with only 30% decrease in colony number compared to the control (blank glass slide). Increasing layer numbers resulted in a complete loss of anti-adhesive property for PIPOX/TA multilayers. 7-layer PIPOX/TA multilayers displayed adhesion to *E.coli* that was even greater than the control. The driving force for the antifouling behaviour of neutral hydrophilic polymers is explained by the formation of a hydration layer on the surface, preventing the adhesion of bacteria [322]. Therefore, the difference in anti-adhesive properties of PEOX/TA and PIPOX/TA multilayers could be correlated with greater hydrophobicity of PIPOX at 37 °C. This is also in good agreement with the decrease in wettability of PIPOX/TA multilayers observed upon exposure to PBS at pH 7.4 and 37 °C (Section 4.4.2).

Contrary to the antiadhesive property against *E.coli*, neither of the films exhibited any anti-adhesive behaviour against *S.aureus*. *S. aureus* has been reported to have a

hydrophobic surface [323]. This would indicate that the hydrophobic interactions between the bacterial surface and the PAOX layer in the aqueous environment might have led to enhanced adhesion observed, especially in case of PIPOX with even greater hydrophobic properties. On the other hand, the surface charge of *E. coli* was reported to be slightly more negative compared to *S.aureus* in PBS at pH 7.0 [324]. Although PAOX is neutral at pH 7.4, multilayers are interpenetrated and the contribution of the underlying TA to the outmost layer cannot be ignored. This would mean that *E.coli*, with a greater surface negative charge, would be repelled more strongly compared to *S.aureus* by the phenolate groups of TA. Further studies specifically examining the surface characteristics of the polymers and the bacteria would be necessary to address the differences in bacterial adhesion between gram positive and negative bacteria on multilayers.

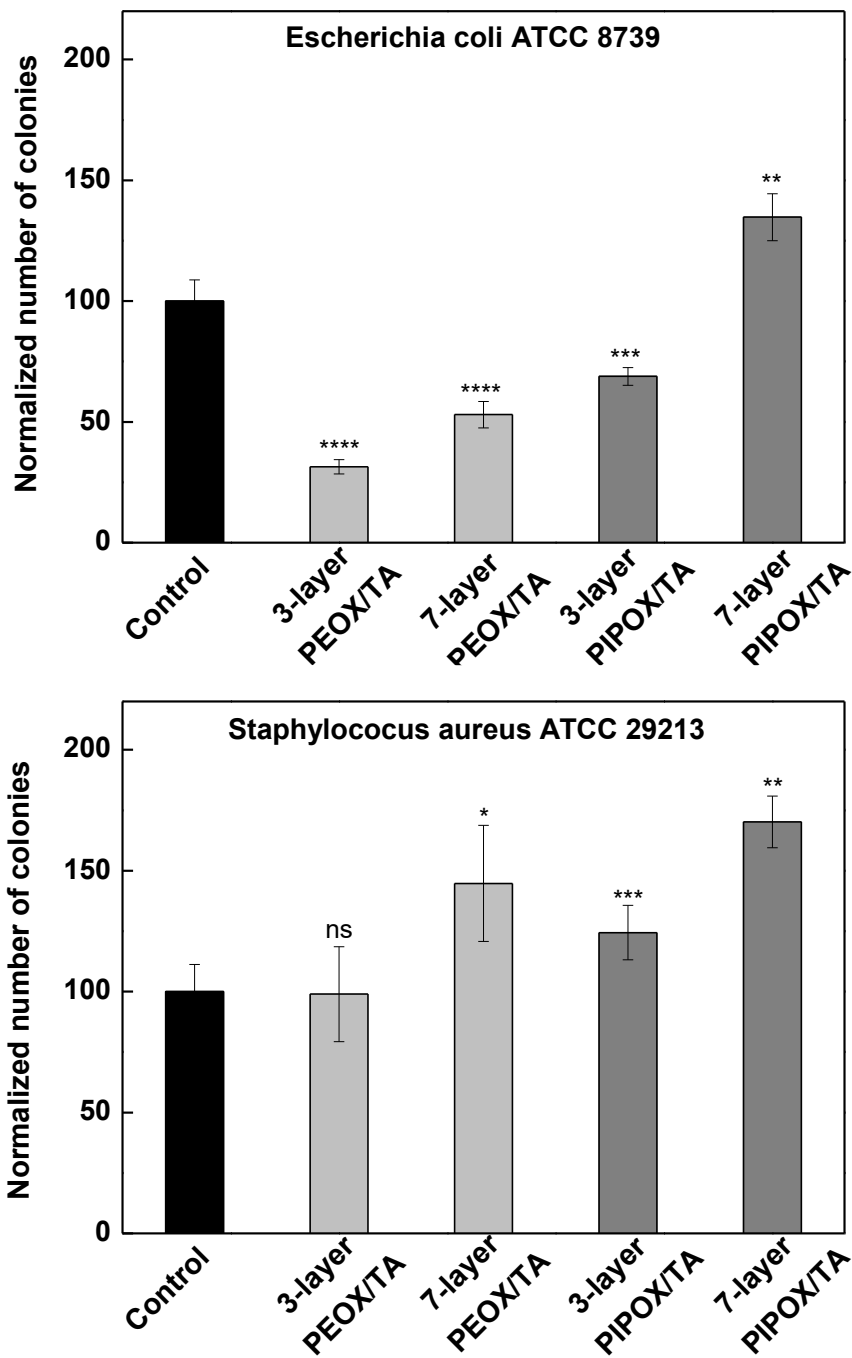


Figure 4.15. Number of colonies on 3- and 7-layer PIPOX/TA and PEOX/TA films (coated onto glass substrates) after 1 hour incubation at pH 7.4 with *E. coli* and *S. aureus*. Uncoated sterile glass substrates were used as control substrates. (* $P < 0.05$, ** $P < 0.005$, *** $P < 0.0005$, **** $P < 0.0001$ and ns= not significant).

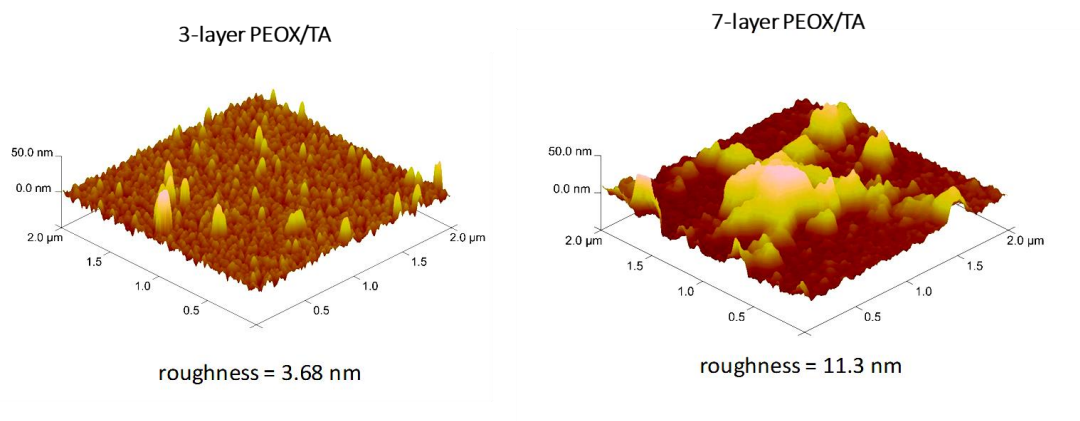


Figure 4.16. AFM height ($1\ \mu\text{m} \times 1\ \mu\text{m}$) images and surface roughness of 3- and 13-layer PEOX/TA films. Roughness values were recorded from images with $2 \times 2\ \mu\text{m}^2$ scan size.

4.4.6. Protein adhesion onto PIPOX/TA and PEOX/TA multilayers

BSA was used as a model protein to assess the anti-adhesive behaviour of PEOX/TA and PIPOX/TA multilayers against protein adsorption. Multilayers were immersed into 25 mg/mL BSA solution at pH 7.4 and $37\ ^\circ\text{C}$ for 1 hour. Ellipsometric thickness measurements of PEOX/TA and PIPOX/TA multilayers were measured before and after immersion into BSA solution (Figure 4.17). The increase in film thickness was correlated with BSA adsorption onto multilayers. As observed with the adhesiveness of *E. coli*, PIPOX/TA films were more adhesive towards BSA than PEOX/TA multilayers possibly due to greater hydrophobicity of PIPOX, promoting greater BSA adsorption. A correlation between protein and bacterial anti-adhesiveness of polymer modified surfaces has been suggested [325,326]. However, it was also reported that a surface revealing antifouling property against proteins did not display anti-adhesiveness against bacteria [327].

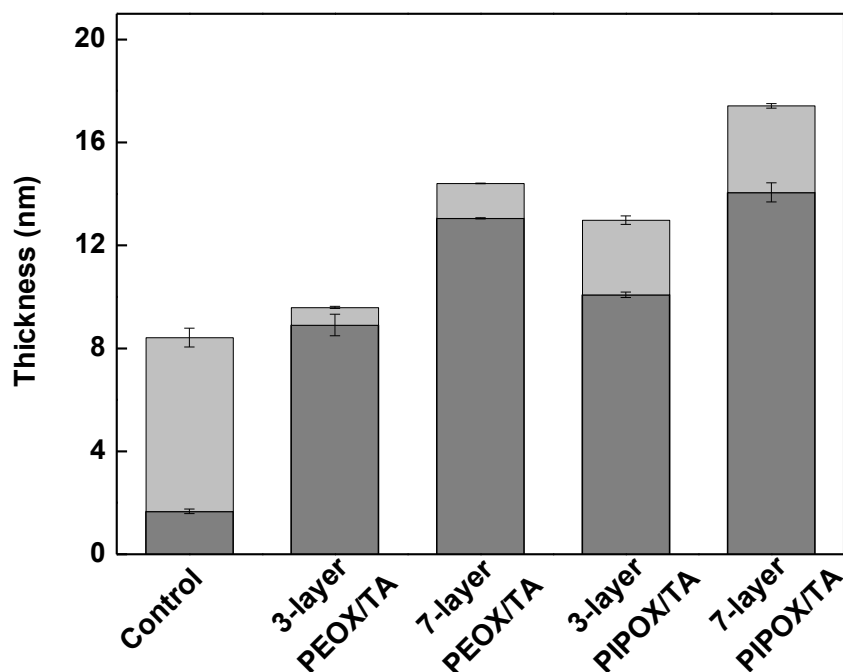


Figure 4.17. Evolution of film thickness upon BSA deposition at pH 7.4 and 37 °C. Dark and light grey parts correspond to the initial thickness and increment in film thickness upon BSA adsorption, respectively. Uncoated silicon wafer was used as control.

4.5. Conclusion

Multilayers of TA and PAOX with varying side chains were prepared at acidic conditions using LbL self-assembly technique. Thickness, surface morphology, wettability, stability, stimuli-responsive release and biological properties of PAOX multilayers were contrasted. The chemical nature of the side chains, conformation and phase behaviour of PAOXs, strength of association between the layers were all found to be critically dependent on both surface and biological properties. At 25 °C, all PAOX multilayers showed pH-responsive release of CIP at varying amounts at neutral and moderately acidic pH. At 37 °C, PAOX multilayers released remarkably different amounts of CIP at moderately acidic pH. The difference in the amount of CIP released from multilayers was correlated with the difference in the phase behaviour of PAOXs

at 37 °C. Results obtained from release experiments were in good agreement with the antibacterial activity of the surfaces against *S.aureus*. Although the amount of CIP released from different PAOX multilayers were different, all films showed antibacterial activity against *E.coli*. PAOX multilayers with greater wettability were more effective to reduce both *E.coli* and BSA adsorption at the surface. Increasing layer number resulted in a decrease or even a loss of antiadhesive behaviour of PAOX multilayers. Interestingly, PAOX multilayers did not exhibit anti-adhesive behaviour against *S. aureus*.

Different from other studies on PAOX LbL films [178,210,211,303–305], this study contrasts the surface properties of two different PAOX multilayers and uses this information as a basis to scrutinize the differences in biological properties of the films. The remarkable differences in surface and biological properties are explained through phase behaviour of polymers and structure-property relationship in LbL films. In addition, different from earlier work which required hydrolysis and crosslinking reactions to increase the stability of PAOX multilayers [214], this study presents a simple strategy to enhance multilayer stability for potential biomedical applications.

In the light of our findings, we suggest that multilayers of PAOX with isopropyl side chains are more promising for drug release and antibacterial applications due to dual stimuli-responsive behaviour and the greater amount of drug release from surfaces. On the other hand, multilayers of PAOX with ethyl substituent are more promising for protein and bacterial antiadhesive applications.

CHAPTER 5

SYNTHESIS AND CHARACTERIZATION OF PIPOX-DOXYCYCLINE CONJUGATE

5.1. Chapter Summary

Polymeric prodrugs are of great interest in biomedical field due to various advantages over small drug counterparts such as lower toxicity and side effects of drug and increasing solubility. Coupling drugs to polymers through hydrazone bond formation provides targeted release of drug molecules in response to pH changes at an infectious site of the body or at tumor tissues. This feature of hydrazone linkage based polymeric prodrugs is significant to minimize the side-effects of drugs to normal tissues. PAOXs have been widely studied polymer in biomedicine due to being non-toxic, non-immunogenic, biocompatible and hydrophilic. In this study, the poly(2-isopropyl-2-oxazoline)-*hyd*-doxycycline (PIPOX-*hyd*-DOXY) conjugate was synthesized through a three step mechanism. Several ester precursors of PIPOX were synthesized. Then, one of the precursor was used to follow up the conversion of ester functionalities to hydrazide moiety in presence of hydrazine hydrate. PIPOX-*hyd*-DOXY conjugate was obtained *via* reaction of hydrazide functionality of PIPOX with ketone group of DOXY leading to hydrazone bond formation between PIPOX and DOXY. Considering the advantages of hydrazone bond cleavage in slightly acidic media, PIPOX-*hyd*-DOXY may be a promising material for antibacterial applications in case of pH drops at an infectious site.

5.2. Introduction

Polymeric materials have been gained significant role in biomedical era to be used as elements for synthesis of macromolecule-drug conjugates and regulators for

controlled drug delivery applications [328,329]. Polymer-drug conjugates, so called polymeric prodrugs, are widely studied class of drug delivery systems. Different derivatives of polymer-conjugates have been investigated and used in various applications (i.e treatment of infections and cancer). Contrasted with small molecule counterparts, they demonstrate various advantages including; i) protecting drugs from deactivation in systemic circulation in living body, ii) enhancement of its pharmacokinetics, iii) decreasing the antigenic actions of drug leading to diminished immunological reaction of body, iv) providing passive and active targeting of pharmaceuticals, v) probability to construct advance carriers for delivery of bioactives, vi) increasing the solubility so does the bioavailability of drugs and vii) diminishing the systemic toxicity of drug [330].

Polymer-drug conjugates can be established either *via* direct conjugation of drugs to polymer without presence of any cleavable linkage between the polymer and drug [75,76,102,121,331–333] or *via* hydrolytically cleavable linkage between the bioactive and polymer [120,128–130]. The linkage to be used in conjugates should be stable in normal biological conditions, but cleavable under disease-specific circumstances such as acidic pH which is characteristics of infectious side of body or tumour tissues. By this way, release of therapeutics can be promoted when and where needed [139,142]. Hydrolytically labile bond can be imine [334], acetal [335], oxime [336] and orthoester [337]. Different from those, hydrazone bonds are of great interest due to their selective sensitivity to pH and their formation throughout facile combination with carbonyl functionality of cargo molecule and hydrazide moiety of polymer [338]. Hydrazone linkage is cleaved at acidic media (pH 5.0-6.0) leading to faster release of cargo in comparison with that released at physiological conditions (pH 7.4). Nevertheless, the fabrication of hydrazone linkage between the polymer and drug to form polymer prodrugs is not synthetically easy route that mostly require multi-step reactions. Coessens et al. demonstrated conjugation of Streptomycin onto either polyglutamine or dextran using hydrazone linkage. Simply, 4-nitrophenyl chloroformate functionalized polyglutamine or dextran was coupled with glycine N-

Boc-hydrazide followed by conjugation of streptomycin *via* hydrazone bond formation between drug and pre-functionalized polymers. Polyglutamine and dextran prodrugs were tested for hemolytic activity and found as non-hemolytic. Stability of polymer-streptomycin conjugates against hydrolytic degradation were tested at physiological and lysosomal pH. The cleavage of hydrazone linkage provided higher release rate of drug at lysosomal pH [140]. Later, Hruby et al. modified poly(ethylene oxide)-*b*-poly(allyl glycidyl ether) (PEO-PAGE) by reacting the double bonds at PAGE chain end with methyl sulfanylacetate to form ester moiety. Conversion of ester functionality to hydrazide in the presence of hydrazine hydrate yielded PEO-PAGE which was then coupled with DOX (PEO-PAGE-DOX) through hydrazone bond formation between polymer and DOX. DOX release from self-assembled PEO-PAGE-DOX micelles was examined at endosomal pH (pH 5.0) and at physiological pH (pH 7.4) at body temperatures. It was found that the amount of DOX released was 50% higher after 6 hours at pH 5.0 than that released at neutral conditions [142]. Neralla et al. fabricated spherical micelles from amphiphilic block copolymer consisting of PEG block forming corona and norbornene block coupled with DOX through hydrazone bond forming core. They contrasted DOX release behavior of micelles at acidic and neutral conditions. Different from others, they synthesized norbornene homopolymer from DOX-conjugated norbornene monomers which were prepared *via* combination of doxorubicin hydrochloride and norborne hydrazide in methanol in the presence of trifluoroacetic acid. Then, DOX-coupled norbornene homopolymer was used as macroinitiator for the addition of PEG block resulting in COPY-DOX block copolymer) [139]. Soon after, Wang et al. reported two different types of Curcumin conjugated acid-sensitive poly(ethylene glycol)-*co*-poly(lactic acid) (PEG-PLA). The copolymer was consisted of either one or two amphiphilic copolymer chains attached to curcumin. For each conjugate, PLA chain end was coupled with curcumin through hydrazone bond formation. The copolymer-Curcumin conjugates were either in linear form or phospholipid-like structure. When the drug loading dose, release rate, cellular uptake and cytotoxicity were contrasted for micelles assembled from linear and phospholipid-like conjugates, linear conjugate micelles

demonstrated higher loading capacity, faster release, enhanced cellular uptake and lower cytotoxicity [143]. Same group further examined the cytotoxicity of PEG-PLA-Curcumin conjugates against Hela cell line. They found that the polymeric residue produced after hydrolysis cleavage of hydrazone bond and residue of free curcumin demonstrated similar cytotoxicity [144].

Polymers employed in polymer-drug conjugates have to possess some common characteristics such as being highly soluble in aqueous media, nontoxic, biocompatible and non-immunogenic [339]. Among others, PEG and PAOXs are biocompatible, soluble, nontoxic and non-immunogenic polymers and attract growing attention of the researchers for use in biomedical applications. PAOXs are good alternatives to PEG due to their enhanced stability against oxidative degradation [283]. Especially, PEOX and PIPOX are of specific interest due to their temperature responsive behaviors in aqueous environment. Different from all studies reported on polymer-drug conjugates with hydrazone linkage, Li et al. reported the synthesis of PEOX-*hyd*-DOX conjugate *via* coupling DOX to PEOX with acid labile hydrazone linker and examined its self-assembly into micelles to physically entrap DOX into micelles. They demonstrated the enhanced antitumor effect with lowered toxicity of DOX when DOX-loaded PEOX-*hyd*-DOX conjugate micelles were employed *in vivo* [340].

In this study, we report the design, synthesis and characterization of PIPOX-*hyd*-Doxycycline conjugates (PIPOX-*hyd*-DOXY) to be employed in pH- and temperature triggered release of DOXY *via* cleavage of DOXY under slightly acidic conditions at a physiologically related temperature. DOXY is broad spectrum tetracycline-derivative antibiotic to be used for treatment of infections of skin, eye, malaria, Lyme's disease and gingivitis [341,342]. First, different ester precursors were synthesized *via* using methyl thioglycolate, N-(*tert*-butoxycarbonyl)-L-cysteine methyl ester and methyl 2-aminobenzoate as nucleophiles in termination step of CROP of 2-IPOX. Choosing from one of the precursor, N-(*tert*-butoxycarbonyl)-L-cysteine methyl ester functionalized PIPOX, ester moiety at the chain end was

converted to hydrazide which then was used to form hydrazone linkage between PIPOX and DOXY under ambient conditions. The precursors and final conjugate was characterized by $^1\text{H-NMR}$ and GPC. Further characterizations, micellar self-assembly of PIPOX-*hyd*-DOXY, pH- and temperature-induced release of DOXY from PIPOX-*hyd*-DOXY micelles and antibacterial activity of PIPOX-*hyd*-DOXY micelles will be further examined. Moreover, DOXY loading and release profiles and antibacterial activities of several conjugates synthesized from methyl thioglycolate end-capped PIPOX and methyl 2-aminobenzoate end-capped PIPOX ester precursors will be contrasted. This study is the first demonstrating DOXY conjugation to PIPOX *via* acid-labile hydrazone linkage.

5.3. Experimental

5.3.1. Materials

All reactions and polymerizations were carried out under inert atmosphere. All chemicals were used as received unless otherwise specified. Ethanolamine (>99%), cadmium acetate dihydrate (98%), α -bromo isobutyrylbromide (98%), acetonitrile (>99.9%), calcium hydride (95%), methanol (99.8%) and dimethyl sulfoxide (>99.9%) were purchased from Sigma-Aldrich. Isobutyronitrile (>98%) and hydrazinium hydroxide (~100%) were purchased from Merck chemicals. Doxycycline hydrochloride ($\geq 95\%$) was purchased from Fischer Bioreagents. The deionized water (DI) was purified by passage through a Milli-Q system (Millipore). SpectroPor7 regenerated cellulose dialysis membrane (molecular weight cutoff: 3.5 kDa) was used for purification of polymers.

5.3.2. Measurements

$^1\text{H-NMR}$ measurements were monitored in deuterated solvents (DMSO-d_6) using a Bruker spectropin Avance DPX-400 Ultra shield instrument at 400 MHz. The

residual protons of the not fully deuterated solvents used as an internal standard. $^1\text{H-NMR}$ data were reported as chemical shifts (δ , ppm) relative to tetramethylsilane (δ 0.00) with multiplicity (s=singlet, br=broad singlet, d=doublet, t=triplet, m=multiplet), coupling constant (Hz) and integration. Gel permeating chromatography (GPC) measurements were performed by Agilent instrument (Model 1100) consisting of refractive index (RI) detectors and three Macherey-Nagel columns packed with a highly cross-linked macroporous, spherical polystyrene-divinylbenzene polymer matrix (Columns 300×7.7 mm, particles $5 \mu\text{m}$). 0.01 M LiBr/DMF was used as an eluent at a flow rate of 0.7 mL/min at 50°C . The calibration was carried out using poly(methyl methacrylate) standards (Polymer Laboratories).

5.3.3. Synthesis and Characterization of Polymers

Synthesis and characterization of 2-IPOX

2-IPOX was synthesized *via* following the prescribed procedure [233] with slight modifications. Briefly, ethanolamine (0.052 mol, 3.5 mL) and isobutyronitrile (0.043 mol, 3.9 mL) were reacted into a schlenk flask containing cadmium acetate dihydrate (1.08 mmol, 0.29 g) under inert atmosphere with continuous magnetic stirring. The reaction was refluxed at 130°C for 48 hours. The crude product was distilled at 45°C under vacuum and stored in argon purged flask. $^1\text{H-NMR}$ (CDCl_3 , 400 MHz): δ (ppm) = 4.20 (t, $J= 9.0$ Hz, 2 H), 3.80 (t, $J= 9.3$ Hz, 2 H), 2.56 (m, $J= 7.3$ Hz, 1 H), 1.15 (d, $J= 6.9$ Hz, 3 H) (Appendix A: Figure A.1).

Synthesis and characterization of poly(2-isopropyl-2-oxazoline) (PIPOX)-N-(tert-Butoxycarbonyl)-L-cysteine methyl ester precursor

As reported by us before [285], acetonitrile (10.0 mL) and 2-isopropyl-2-oxazoline (2-IPOX, 41.0 mmol, 4.9 mL) were mixed in an argon purged condenser capped schlenk reactor and magnetically stirred. α -bromoisobutyl bromide (0.4 mmol, 0.01 equivalent) was added and the reaction flask was proceeded in a preheated oil bath at

80°C. Reaction mixture was cooled to room temperature after 24 hours and quenched with *N*-(*tert*-butoxycarbonyl)-L-cysteine methyl ester (0.03 equivalent). The termination was proceeded for 2 days more at 80°C. Reaction mixture was concentrated under reduced pressure at room temperature. The obtained product was dissolved in DI water and dialyzed against DI water for 2 days. Finally, the solution was freeze-dried. ¹H-NMR (DMSO-d₆, 400 MHz) δ 3.49 (br, 4H), 2.82- 2.61 (br, 1H), 1.10 (s, 6H), 0.9 (br, 6H) (Figure 5.2A). GPC traces of PIPOX: Mn = 11272 g/mol, PDI 1.35 (Figure 5.2D).

Synthesis and characterization of PIPOX-hydrazide precursor

PIPOX-*N*-(*tert*-butoxycarbonyl)-L-cysteine methyl ester precursor (0.6 g) was dissolved in methanol (0.84 mL) under inert atmosphere and hydrazine hydrate (0.084 mL) was added dropwise under constant stirring. The resultant mixture was stirred at room temperature for 24 hours. The solution was diluted to 5.0 mL with DI water and dialyzed against DI water for 24 hours and lyophilized at room temperature. Formation of PIPOX-hydrazide precursor was confirmed by thin layer chromatography (TLC) with R_f= 0.58 in ethanol.

Synthesis and characterization of PIPOX-hyd-Doxycycline conjugate (PIPOX-hyd-DOXY)

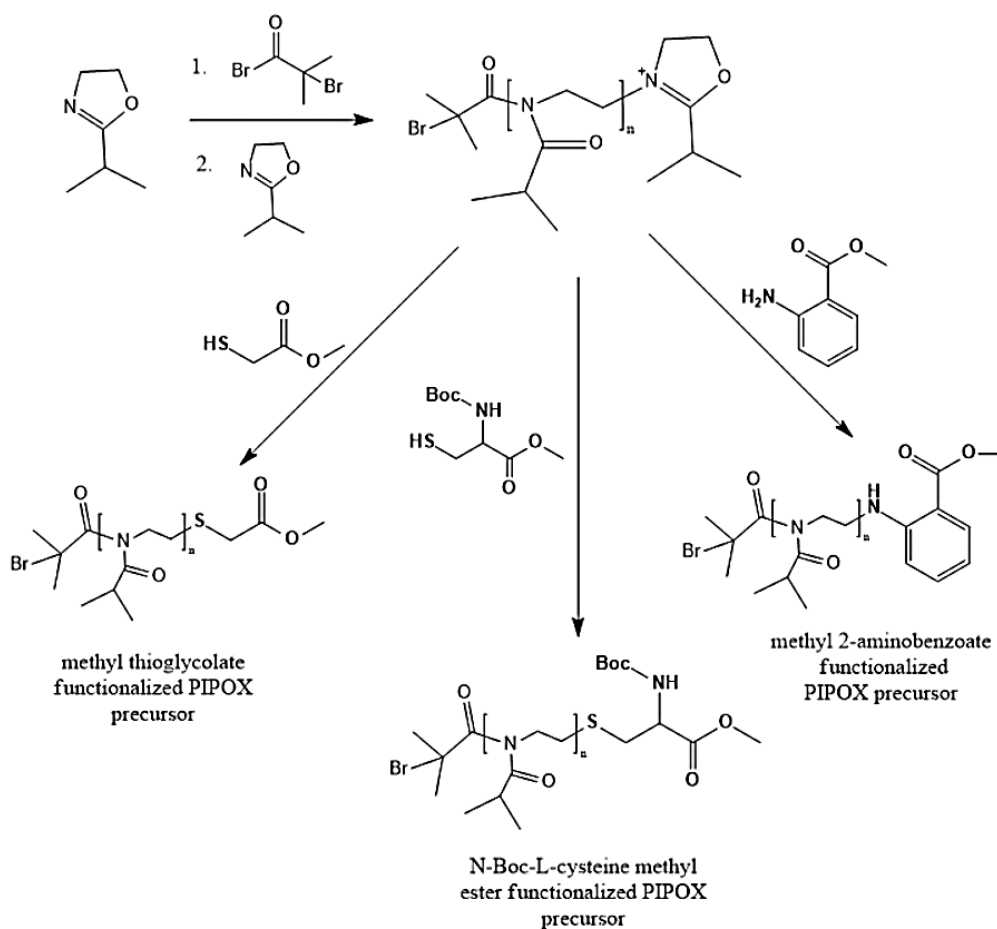
PIPOX-*hyd*-DOXY conjugate was achieved *via* construction of hydrazone bond between the ketone moiety of DOXY and hydrazide end of the PIPOX-hydrazide precursor *via* following the procedure prescribed before with slight modification [340]. Briefly, PIPOX-hydrazide (0.130 g) was dissolved in anhydrous DMSO (0.354 mL) under inert atmosphere. Then, acetic acid (0.010 mL) and doxycycline hydrochloride (5.5 mg) were added into reaction mixture under constant stirring. The final mixture was stirred in the dark at room temperature for 24 hours. At the end of the reaction, yellowish powder PIPOX-*hyd*-DOXY conjugate was obtained *via* precipitation with anhydrous ether followed by the filtering with Sephadex G25 column with DI water (pH 7.8, adjusted with 0.2 M sodium hydroxide aqueous

solution) as eluent. Finally, the solution was lyophilized. All steps were performed in the dark environment. Conjugate formation was confirmed by ¹H-NMR (Figure 5.2B) and TLC (Figure 5.2C). ¹H-NMR (DMSO-d₆, 400 MHz) δ 7.25 (d, 1H), 6.76 (m, 1H), 6.65 (d, 1H), 3.60 (br, 4H), 2.9 (br, 6H), 2.8- 2.65 (br, 1H), 2.67 (s, 1H), 2.56 (s, 1H), 1.5 (s, 3H), 1.2 (s, 6H) (Figure 2B). Formation of PIPOX-*hyd*-DOXY conjugate was confirmed by thin layer chromatography (TLC) with R_f= 0.84 in ethanol.

5.4. Results and Discussion

In this study, novel and water soluble PIPOX-*hyd*-DOXY conjugates were attempted to be synthesized aiming that pH-triggered release of DOXY will be achieved under slightly acidic conditions mimicking the infectious side of the body *via* cleavage of hydrazone bond.

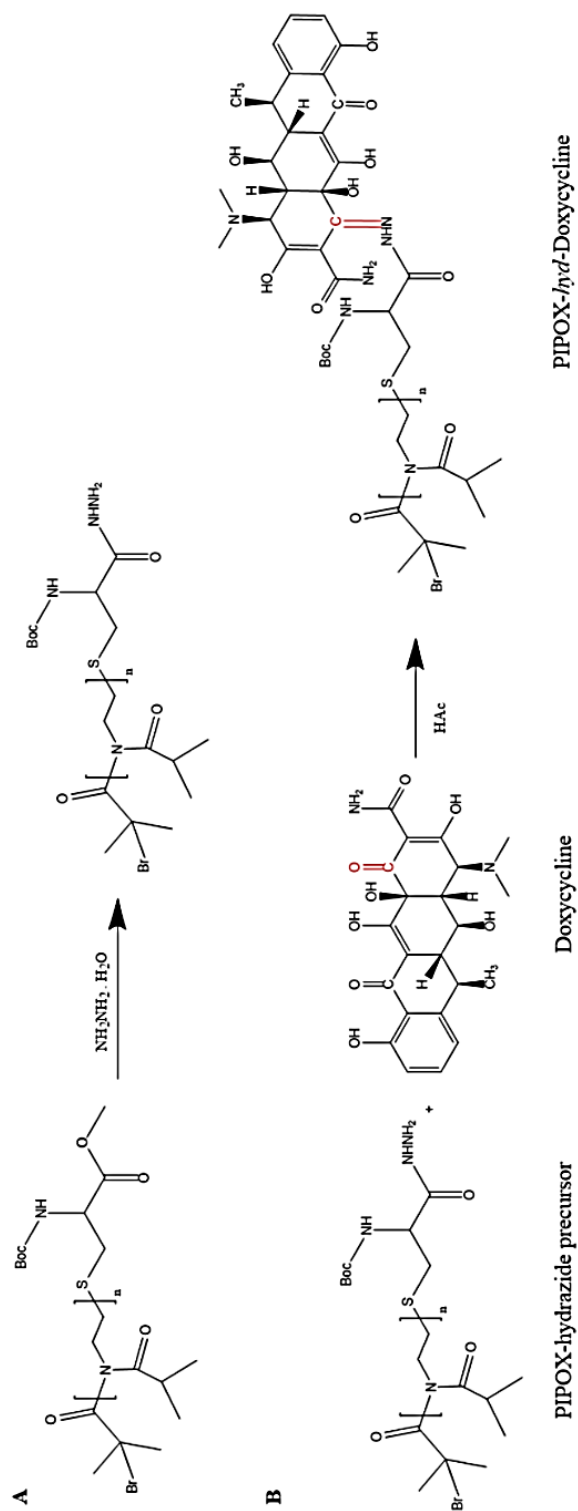
Several PIPOX-ester precursors were synthesized using methyl thioglycolate, N-(*tert*-butoxycarbonyl)-L-cysteine methyl ester and methyl 2-aminobenzoate as nucleophiles in termination step of CROP of 2-IPOX (Scheme 5.1). The significant points to be concerned while selecting the esters were: 1) they had to bear nucleophilic side in one end at which they can attack the active side of the propagating PIPOX chain, 2) they had to bear ester group at other side of the molecule which could further react with hydrazine to generate PIPOX-hydrazide precursors. In addition, differences in hydrophilicities of the ester groups attached to the ω-chain end is critical for the self-assembly of the PIPOX conjugate. This is because the alkyl or aryl group coming from ester contribute to the formation of the micellar cores together with drug, thus the variation of hydrophilicity of the ester group will affect the core-size of the micellar structure which is critical for the amount of drug loaded into micellar core.



Scheme 5.1 Synthesis routes of ester functionalized PIPOX precursor via termination of CROP of 2-IPOX.

Among all ester precursors, first PIPOX-N-(*tert*-butoxycarbonyl)-L-cysteine methyl ester precursor was chosen to synthesize PIPOX-*hyd*-DOXY conjugate. The successful synthesis of PIPOX-N-(*tert*-butoxycarbonyl)-L-cysteine methyl ester precursor was confirmed by $^1\text{H-NMR}$ Spectroscopy (Figure 5.1A). The sharp peaks appeared at 3.49 ppm, 2.82-2.61 ppm, 1.1 ppm and 0.9 ppm correspond to main chain ethylene protons, side chain $-\text{CH}$ proton, two $-\text{CH}_3$ protons of isopropyl side chain and two $-\text{CH}_3$ protons of α -bromo isobutryl moiety of PIPOX, respectively. Attachment of N-(*tert*-butoxycarbonyl)-L-cysteine methyl ester to ω -end of PIPOX was confirmed by the presence of the peaks at 4.3 ppm, 3.7 ppm, 2.5 ppm and 1.3 ppm

correlated with –CH proton neighboring to carbonyl group, –CH₂ protons neighboring to thiol moiety, –CH₃ protons neighboring to oxygen of ester moiety and protons of three CH₃ group of –Boc moiety of N-(*tert*-butoxycarbonyl)-L-cysteine methyl ester group, respectively. The number-average molecular weight of PIPOX-N-(*tert*-butoxycarbonyl)-L-cysteine methyl ester was determined as 11272 g/mol with polydispersity index (PDI) of 1.35 by GPC (Figure 5.1D). GPC results suggested narrow molecular weight distribution for the ester precursor. Afterward, PIPOX-N-(*tert*-butoxycarbonyl)-L-cysteine methyl ester precursor was reacted with hydrazine hydrate to form PIPOX-hydrazide precursor (Scheme 5.2A). Then, it was immediately reacted with DOXY to conjugate DOXY to PIPOX through formation of acid-labile hydrazone linker (Scheme 5.2B). The formation of PIPOX-*hyd*-DOXY conjugate was firstly followed by thin layer chromatography. To confirm the formation of PIPOX-*hyd*-DOXY conjugate from PIPOX-hydrazide precursor, retardation factors (R_f) for PIPOX-*hyd*-DOXY conjugate, PIPOX-hydrazide precursor, DOXY and hydrazine hydrate were contrasted as shown in Figure 5.1C. Different R_f values for PIPOX-*hyd*-DOXY conjugate supported the conversion of PIPOX-hydrazide into PIPOX-*hyd*-DOXY conjugate. As shown in Figure 5.1B, the conjugation of DOXY to PIPOX was further approved by ¹H-NMR spectrum. The characteristic peaks of PIPOX at 3.60 ppm, 2.8-2.65 ppm, 1.2 ppm indicated the existence of PIPOX in conjugate structure but slight shift of the protons to the lower field further proved the functionalization of end-capping. In addition, the specific peaks of DOXY arose at 7.25 ppm, 6.76 ppm and 6.65 ppm corresponding to aromatic protons, 2.9 ppm corresponding to protons of two –CH₃ in amine moiety, 2.67 and 2.56 ppm corresponding to protons of two different –CH inside the cyclohexane moieties and 1.5 ppm corresponding to –CH₃ group attached to cyclohexane unit. Of note, characteristic ¹H-NMR peaks of DOXY were reported elsewhere before [343,344]. The conjugation of poly(2-ethyl-2-oxazoline) (PEOX) with anticancer drug, doxorubicin through hydrazone bond formation was earlier reported by Li *et al.* [340].



Scheme 5.2 . Synthesis route for (A) hydrazide functionalized PIPOX precursor from N-Boc-L cysteine methyl ester functionalized PIPOX and hydrazine hydrate (B) PIPOX-hyd-DOXY conjugate from PIPOX-hydrazide precursor through formation of hydrazone linker.

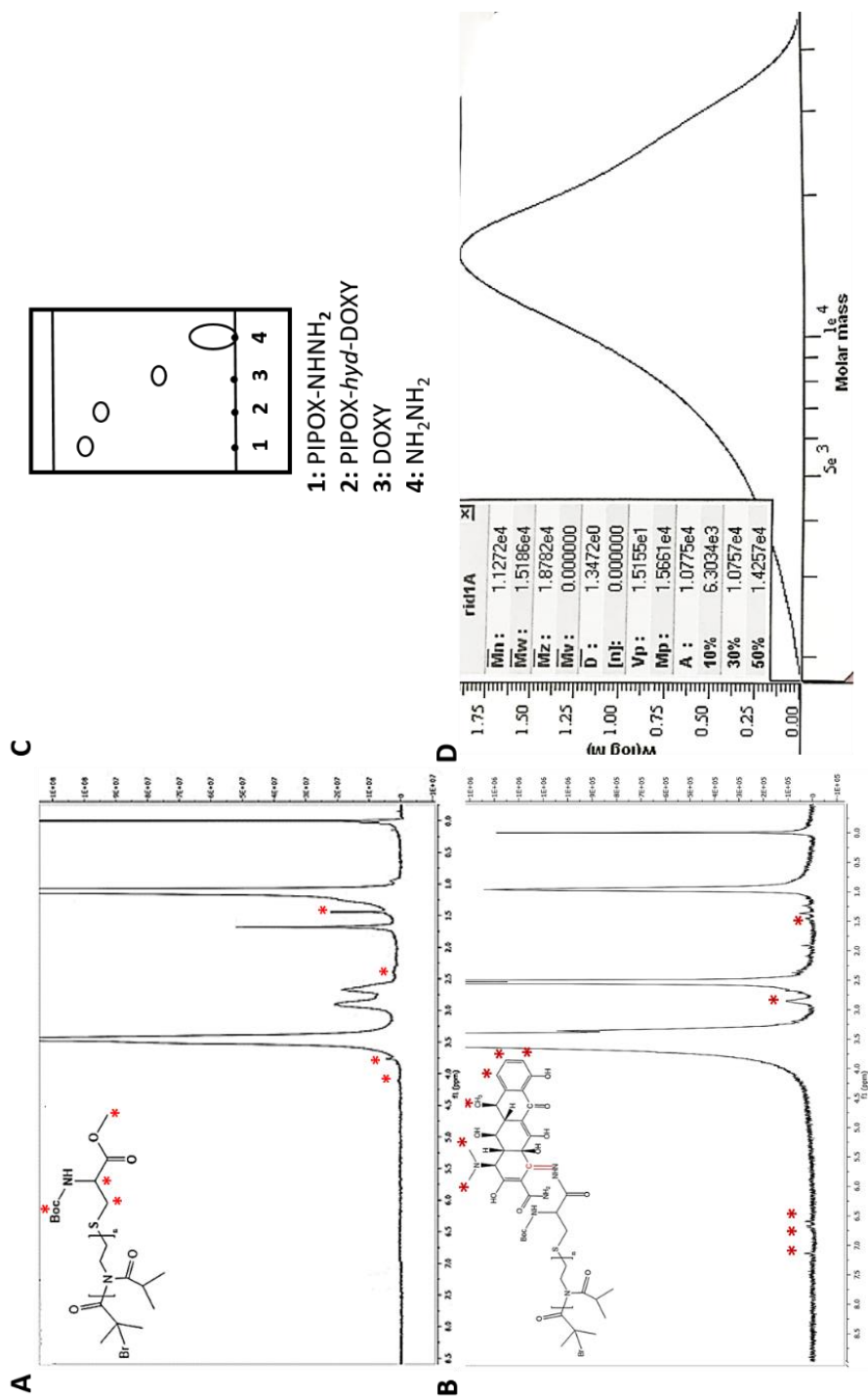


Figure 5. 1. ¹H-NMR spectra of (A) N-Boc-L cysteine methyl ester functionalized PIPOX, (B) PIPOX-hyd-DOXY. (C) Thin layer chromatograms of (1) PIPOX-NHNH₂, (2) PIPOX-hyd-DOXY, (3) DOXY and (4) NH₂NH₂; DOXY and PIPOX-hyd-DOXY, demonstrating fluorescence under 366 nm UV-lamp. (D) GPC chromatogram of N-Boc-L cysteine methyl ester functionalized PIPOX. ¹H-NMR samples were dissolved in deuterated DMSO.

5.5. Conclusion

In this study, PIPOX-*hyd*-doxycycline (PIPOX-*hyd*-DOXY) conjugates with acid-labile hydrazone bond between PIPOX and DOXY were synthesized. Firstly, ester precursors of PIPOX conjugates were synthesized using methyl thioglycolate, methyl 2-aminobenzoate and N-(*tert*-butoxycarbonyl)-L-cysteine methyl ester as terminating agents in CROP of 2-IPOX. Secondly, ω -end capping of N-(*tert*-butoxycarbonyl)-L-cysteine methyl ester precursor of PIPOX was converted to hydrazide. Then, hydrazide functionalized PIPOX precursor was used to synthesize PIPOX-*hyd*-doxycycline conjugate *via* formation of hydrazone linkage between the PIPOX and DOXY. This study can be the pioneer work for synthesis of several derivatives of PAOX conjugates in presence of hydrazone linkage to be used in various applications in biomedical field.

CHAPTER 6

CONCLUSION AND OUTLOOK

This PhD thesis examined the synthesis, aqueous solution behavior and layer-by-layer self-assembly of PAOXs.

In Chapter 2, the effect of pH on aqueous solution behaviour of PIPOX has been examined. For the first time, pH-dependent self-aggregation of PIPOX was recorded at a temperature significantly lower than LCST of PIPOX. Spherical PIPOX aggregates were detected above pH 5.0 at 25 °C in aqueous solution. End group functionality, polymer and salt concentration were all found to be critical on self-aggregation of PIPOX and the size of aggregates formed. Moreover, it was found that increasing salt concentration of PIPOX solution led to formation of larger aggregates at acidic conditions but smaller aggregates at higher pH values when compared to the size of PIPOX aggregates in solutions with low salt concentration. The large aggregates at high salt concentrations under acidic conditions were formed *via* salt-trigger where the salt anions acted as bridges between the positively charged amide units, inducing the aggregation of PIPOX chains. In contrast, above pH 5.0, where PIPOX got deprotonated and formation of aggregates was induced *via* pH-trigger, increasing salt concentration destroyed the hydrogen bonding among water molecules as well as the hydrogen bonding network constructed by water molecules and PIPOX, resulting in formation of smaller aggregates. We have also found that cloud point temperature of PIPOX solutions was affected by the formation of PIPOX aggregates in solution. The cloud point temperature for PIPOX at acidic pH was slightly lower than that observed for PIPOX solution at pH 7.5 due to greater hydrophilicity of the PIPOX chains at acidic pH. This study presents significant results on aqueous solution behaviour of PIPOX and presents a new triggering mechanism to prepare PIPOX self-aggregates.

In Chapter 3, pH-dependent aqueous solution behavior of 2-butoxy end-capped PIPOX (PIPOX-OR) and Chloramphenicol end-capped PIPOX (PIPOX-CAP) was contrasted. The effect of end-group on aggregate size, loading capacity and release properties was examined. Both PIPOX self-aggregates were similar in size in phosphate buffer. For CAP loading into PIPOX aggregates, self-assembly was induced in CAP solution. In CAP solution, hydrodynamic diameter of PIPOX-CAP self-aggregates were almost 2.5 times higher than that of PIPOX-OR due to enhanced hydrophobic association among PIPOX-CAP chains owing to more hydrophobic CAP end units. Aggregations of PIPOX-OR and PIPOX-CAP were both found to be reversible at 25 °C as well as 37 °C with some hysteresis due to intra- and inter-molecular hydrophobic association between the PIPOX chains, suppressing the protonation of the amide nitrogens and only partial removal of PIPOX chains from the aggregates. In good agreement with the size data, PIPOX-CAP aggregates had higher loading capacity for CAP molecules. PIPOX-OR and PIPOX-CAP showed different stimuli-responsive behaviour. Despite the high loading capacity, PIPOX-CAP aggregates did not show pH-response at 25 °C, while PIPOX-OR aggregates released CAP at moderately acidic conditions. This can be explained by suppression of dissolution of PIPOX-CAP aggregates due to stronger hydrophobic association among PIPOX-CAP chains than that among PIPOX-OR chains. The greatest amount of CAP was released at moderately acidic pH and 37 °C from both types of PIPOX aggregates indicating dual responsive behavior.

In Chapter 4, LbL self-assembled films of PAOXs with different side chains and TA were fabricated at strong acidic conditions. The effect of side chain variation on thickness, surface morphology, stability, wettability, protein and bacterial anti-adhesive and antibacterial properties of multilayers was explored. It was found that the chemical nature of side chain was critical on phase behaviour of PAOXs as well as the strength of association between the layers which affected both the surface and biological properties of the multilayers. PIPOX and TA provided more stable multilayers in PBS solution at 37 °C, whereas PEOX and TA multilayers gradually

disintegrated under the same conditions. This was due to greater hydrophobicity of PIPOX than that of PEOX providing greater stability to multilayer films. PEOX/TA multilayers displayed good wettability, providing anti-adhesiveness against BSA and *E.Coli*. Similar behaviour was not observed for PIPOX/TA multilayers due to LCST-type phase behaviour of PIPOX leading to more hydrophobic surfaces. However, transition of PIPOX from extended to globular conformation at 37 °C provided dual responsiveness to PIPOX/TA multilayers. These multilayers could release CIP from the surface in response to both pH and temperature and the amount of CIP released from PIPOX/TA was greater than that from PEOX/TA multilayers at moderately acidic pH at a physiologically related temperature. This feature provided good antibacterial properties specifically to PIPOX/TA multilayers. Importantly, the difference in CIP release profiles from PEOX/TA and PIPOX/TA multilayers was remarkable and was in good agreement with the antibacterial activity of the films against *S.Aureus*. Increasing layer number led to decrease or even a loss of antiadhesive behaviour of PAOX-multilayers.

In Chapter 5, PIPOX-*hyd*-doxycycline (PIPOX-*hyd*-DOXY) conjugates with acid-labile hydrazone bond between PIPOX and DOXY were synthesized *via* three step mechanism. In first step, ester precursors of PIPOX conjugates were synthesized using methyl thioglycolate, methyl 2-aminobenzoate and N-(*tert*-butoxycarbonyl)-L-cysteine methyl ester as a terminating agent in CROP of PIPOX. In second step, N-(*tert*-butoxycarbonyl)-L-cysteine methyl ester derivative of PIPOX was used to convert ester moiety at the chain end to hydrazide group using hydrazine hydrate. In final step, hydrazide functionalized PIPOX precursor was converted to PIPOX-*hyd*-doxycycline conjugate under ambient conditions *via* formation of hydrazone bond between the PIPOX and DOXY. Ester precursor, intermediate hydrazide functionalized PIPOX and final PIPOX-*hyd*-DOXY conjugate were characterized by ¹H-NMR and GPC.

Overall, this dissertation generated fundamental knowledge on synthesis of PAOX derivatives, aqueous solution behaviour of PAOXs and structure-property relationship

in PAOX multilayers. Considering the potential of PAOXs for use in biomedical applications, these results may form a basis for further development of PAOX based materials. For example, pH-dependent self-aggregation behaviour of PAOXs has been first demonstrated in this doctoral studies. There are still many parameters, e.g salt concentration, nature of chemical salt, to be further explored to understand the solution behaviour of PAOXs. Dual responsive PIPOX aggregates for stimuli responsive release of a wide spectrum antibiotic, CAP has been first explored in this doctoral thesis studies. Such aggregates can be further explored for *in vitro* studies to understand the potential of PIPOX aggregates for biomedical applications. PAOX multilayers are promising for surface modification of biomaterials for both anti-adhesive and anti-bacterial applications. PAOX multilayers of varying compositions can be further explored for different biological applications. Furthermore, various PIPOX-*hyd*-DOXY conjugates derived from several different ester precursors can be synthesized by following a similar synthetic route reported for PIPOX-*hyd*-DOXY derived from N-(*tert*-butoxycarbonyl)-L-cysteine methyl ester precursor of PIPOX. Self-assembly of PIPOX-*hyd*-DOXY conjugate into micellar aggregates and release of DOXY at moderately acidic pH conditions may have potential use in antibacterial applications. Since each conjugate will have different groups with various solubility attached by ester compound will form core of micelles, a comparison of the drug loading and release profiles into/from micelles will generate fundamental knowledge for the potential use of PIPOX-*hyd*-DOXY for drug delivery applications.

REFERENCES

- [1] A.A. Cavallaro, M.N. MacGregor-Ramiasa, K. Vasilev, Antibiofouling Properties of Plasma-Deposited Oxazoline-Based Thin Films, *ACS Appl. Mater. Interfaces*. 8 (2016) 6354–6362. doi:10.1021/acsami.6b00330.
- [2] C. Weber, R. Hoogenboom, U.S. Schubert, Temperature responsive biocompatible polymers based on poly(ethylene oxide) and poly(2-oxazoline)s, *Prog. Polym. Sci.* 37 (2012) 686–714. doi:10.1016/j.progpolymsci.2011.10.002.
- [3] R. Konradi, C. Acikgoz, M. Textor, Polyoxazolines for nonfouling surface coatings - A direct comparison to the gold standard PEG, *Macromol. Rapid Commun.* 33 (2012) 1663–1676. doi:10.1002/marc.201200422.
- [4] T.X. Viegas, M.D. Bentley, J.M. Harris, Z. Fang, K. Yoon, B. Dizman, R. Weimer, A. Mero, G. Pasut, F.M. Veronese, Polyoxazoline: Chemistry, properties, and applications in drug delivery, *Bioconjug. Chem.* 22 (2011) 976–986. doi:10.1021/bc200049d.
- [5] V.R. De La Rosa, Poly(2-oxazoline)s as materials for biomedical applications, *J. Mater. Sci. Mater. Med.* 25 (2014) 1211–1225. doi:10.1007/s10856-013-5034-y.
- [6] D. Schmaljohann, Thermo- and pH-responsive polymers in drug delivery, *Adv. Drug Deliv. Rev.* 58 (2006) 1655–1670. doi:10.1016/j.addr.2006.09.020.
- [7] C. Diab, Y. Akiyama, K. Kataoka, F.M. Winnik, Microcalorimetric Study of the Temperature-Induced Phase Separation in Aqueous Solutions of Poly(2-isopropyl-2-oxazolines), *Macromolecules*. 37 (2004) 2556–2562. doi:10.1021/ma0358733.
- [8] D. Christova, R. Velichkova, W. Loos, E.J. Goethals, F. Du Prez, New thermo-responsive polymer materials based on poly(2-ethyl-2-oxazoline) segments, *Polymer*. 44 (2003) 2255–2261. doi:10.1016/S0032-3861(03)00139-3.
- [9] M. Meyer, M. Antonietti, H. Schlaad, Unexpected thermal characteristics of aqueous solutions of poly(2-isopropyl-2-oxazoline), *Soft Matter*. 3 (2007) 430. doi:10.1039/b616678d.
- [10] Y. Katsumoto, A. Tsuchiizu, X. Qiu, F.M. Winnik, Dissecting the mechanism of the heat-induced phase separation and crystallization of poly(2-isopropyl-2-

- oxazoline) in water through vibrational spectroscopy and molecular orbital calculations, *Macromolecules*. 45 (2012) 3531–3541. doi:10.1021/ma300252e.
- [11] E. Haladjova, N. Toncheva-Moncheva, M.D. Apostolova, B. Trzebicka, A. Dworak, P. Petrov, I. Dimitrov, S. Rangelov, C.B. Tsvetanov, Polymeric nanoparticle engineering: From temperature-responsive polymer mesoglobules to gene delivery systems, *Biomacromolecules*. 15 (2014) 4377–4395. doi:10.1021/bm501194g.
- [12] A.I. Amirova, O. V. Golub, T.U. Kirila, A.B. Razina, A. V. Tenkovtsev, A.P. Filippov, The effect of arm number and solution concentration on phase separation of thermosensitive poly(2-isopropyl-2-oxazoline) stars in aqueous solutions, *Colloid Polym. Sci.* 294 (2016) 947–956. doi:10.1007/s00396-016-3853-3.
- [13] H. Schlaad, C. Diehl, A. Gress, M. Meyer, A. Levent Demirel, Y. Nur, A. Bertin, Poly(2-oxazoline)s as smart bioinspired polymers, *Macromol. Rapid Commun.* 31 (2010) 511–525. doi:10.1002/marc.200900683.
- [14] R. Hoogenboom, Poly(2-oxazoline)s: A polymer class with numerous potential applications, *Angew. Chemie - Int. Ed.* 48 (2009) 7978–7994. doi:10.1002/anie.200901607.
- [15] R. Hoogenboom, H. Schlaad, Thermoresponsive poly(2-oxazoline)s, polypeptoids, and polypeptides, *Polym. Chem.* 8 (2017) 24–40. doi:10.1039/C6PY01320A.
- [16] H. Uyama, S. Kobayashi, A Novel Thermo-Sensitive Polymer. Poly(2-isopropyl-2-oxazoline)., *Chem. Lett.* (1992) 1643–1646. doi:10.1246/cl.1992.1643.
- [17] J.S. Park, Y. Akiyama, F.M. Winnik, K. Kataoka, Versatile synthesis of end-functionalized thermosensitive poly(2-isopropyl-2-oxazolines), *Macromolecules*. 37 (2004) 6786–6792. doi:10.1021/ma049677n.
- [18] R. Hoogenboom, 50 Years of Poly(2-Oxazoline)S, *Eur. Polym. J.* 88 (2017) 448–450. doi:10.1016/j.eurpolymj.2017.01.014.
- [19] H. Schlaad, R. Hoogenboom, Poly(2-oxazoline)s and related pseudo-polypeptides, *Macromol. Rapid Commun.* 33 (2012) 1599. doi:10.1002/marc.201200571.
- [20] R. Luxenhofer, Y. Han, A. Schulz, J. Tong, Z. He, A. V. Kabanov, R. Jordan,

- Poly(2-oxazoline)s as polymer therapeutics, *Macromol. Rapid Commun.* 33 (2012) 1613–1631. doi:10.1002/marc.201200354.
- [21] O. Sedlacek, B.D. Monnery, S.K. Filippov, R. Hoogenboom, M. Hruby, Poly(2-oxazoline)s - Are they more advantageous for biomedical applications than other polymers, *Macromol. Rapid Commun.* 33 (2012) 1648–1662. doi:10.1002/marc.201200453.
- [22] A. Dworak, B. Trzebicka, A. Kowalczyk, C. Tsvetanov, S. Rangelov, Polyoxazolines-mechanism of synthesis and solution properties, *Polimery/Polymers.* 59 (2014) 88–94. doi:10.14314/polimery.2014.088.
- [23] M. Bauer, C. Lautenschlaeger, K. Kempe, L. Tauhardt, U.S. Schubert, D. Fischer, Poly(2-ethyl-2-oxazoline) as Alternative for the Stealth Polymer Poly(ethylene glycol): Comparison of in vitro Cytotoxicity and Hemocompatibility, *Macromol. Biosci.* 12 (2012) 986–998. doi:10.1002/mabi.201200017.
- [24] R. Obeid, Poly (2 - Oxazoline): The Structurally Diverse Biocompatibilizing Polymer, (2017).
- [25] B. Verbraeken, B.D. Monnery, K. Lava, R. Hoogenboom, The chemistry of poly(2-oxazoline)s, *Eur. Polym. J.* 88 (2017) 451–469. doi:10.1016/j.eurpolymj.2016.11.016.
- [26] O. Hinsberg, Ueber Piasenole, *Eur. J. Inorg. Chem.* 117 (1889) 862–866. doi:10.1161/01.STR.32.1.139.
- [27] M. Hatano, T. Asai, K. Ishihara, Design of Chiral Macrocyclic Complexes Based on trans-Chelation of $n : n$ Metal–Bidentate P , N - or N , N -Ligands, *Chem. Lett.* 35 (2006) 172–173. doi:10.1246/cl.2006.172.
- [28] J.A. Seijas, M.P. Vázquez-Tato, M.M. Martínez, M.G. Pizzolatti, Oxazoline as a useful tool in organic synthesis: Preparation of 4-aryl-1,2,3,4-tetrahydroisoquinoline alkaloid skeleton, *Tetrahedron Lett.* 46 (2005) 5827–5830. doi:10.1016/j.tetlet.2005.06.139.
- [29] Y.J. Lee, J. Lee, M.J. Kim, T.S. Kim, H.G. Park, S.S. Jew, Highly enantioselective synthesis of (R)- α -alkylserines via phase-transfer catalytic alkylation of o-biphenyl-2-oxazoline-4-carboxylic acid tert-butyl ester using cinchona-derived catalysts, *Org. Lett.* 7 (2005) 1557–1560. doi:10.1021/ol050228x.

- [30] M. Ishihara, H. Togo, An efficient preparation of 2-imidazolines and imidazoles from aldehydes with molecular iodine and (diacetoxyiodo)benzene, *Synlett.* (2006) 227–230. doi:10.1055/s-2005-923604.
- [31] I. Mohammadpoor-Baltork, A.R. Khosropour, S.F. Hojati, A novel and chemoselective synthesis of 2-aryloxazolines and bis-oxazolines catalyzed by Bi(III) salts, *Synlett.* (2005) 2747–2750. doi:10.1055/s-2005-918951.
- [32] S. Thorimbert, Palladium (0) Catalyzed Amination with N, O-bis-ter-Boc, *Tetrahedron Lett.* 34 (1993) 1159–1162. doi:10.1055/s-2006-951507.
- [33] H. Nishiyama, H. Sakaguchi, T. Nakamura, M. Horihata, M. Kondo, K. Itoh, Chiral and C₂-Symmetrical Bis(oxazolinylpyridine)rhodium(III) Complexes: Effective Catalysts for Asymmetric Hydrosilylation of Ketones, *Organometallics.* 8 (1989) 846–848. doi:10.1021/om00105a047.
- [34] H. Nishiyama, S.B. Park, K. Itoh, Stereoselectivity in hydrosilylative reduction of substituted cyclohexanone derivatives with chiral rhodium-bis(oxazolinyl)pyridine catalyst, *Tetrahedron: Asymmetry.* 3 (1992) 1029–1034. doi:10.1016/S0957-4166(00)86036-X.
- [35] A. Gissibi, M.G. Finn, O. Reiser, Cu(II)-aza(bisoxazoline)-catalyzed asymmetric benzoylations, *Org. Lett.* 7 (2005) 2325–2328. doi:10.1021/ol0505252.
- [36] F. Wiesbrock, R. Hoogenboom, M.A.M. Leenen, M.A.R. Meier, U.S. Schubert, Investigation of the living cationic ring-opening polymerization of 2-methyl-, 2-ethyl-, 2-nonyl-, and 2-phenyl-2-oxazoline in a single-mode microwave reactor, *Macromolecules.* 38 (2005) 5025–5034. doi:10.1021/ma0474170.
- [37] R. Hoogenboom, Poly(2-oxazoline)s: Alive and kicking, *Macromol. Chem. Phys.* 208 (2007) 18–25. doi:10.1002/macp.200600558.
- [38] K.P. Luef, R. Hoogenboom, U.S. Schubert, F. Wiesbrock, Microwave-assisted cationic ring-opening polymerization of 2-oxazolines, *Adv. Polym. Sci.* 274 (2016) 183–208. doi:10.1007/12_2015_340.
- [39] S. Kobayashi, Polymerization of Oxazolines, *Polym. Sci. A Compr. Ref.* 10 Vol. Set. 4 (2012) 397–426. doi:10.1016/B978-0-444-53349-4.00110-2.
- [40] S.N. T. Kagiya T. Maeda, K. Fukui, Ring Opening Polymerization Of 2-Substituted 2-Oxazolines, *Polym. Lett.* 4 (1966) 441–445. doi:10.1002/pol.1966.110040701.

- [41] A. Levy, M. Litt, Polymerization of cyclic imino ethers. II. Oxazines, *J. Polym. Sci. Part B Polym. Lett.* 5 (1967) 881–886. doi:10.1002/pol.1967.110050928.
- [42] C. Taubmann, R. Luxenhofer, S. Cesana, R. Jordan, First aldehyde-functionalized poly(2-oxazoline)s for chemoselective ligation, *Macromol. Biosci.* 5 (2005) 603–612. doi:10.1002/mabi.200500059.
- [43] H. Witte, W. Seeliger, Cyclische Imidsäureester aus Nitrilen und Aminoalkoholen, *Justus Liebigs Ann. Chem.* 1974 (1974) 996–1009. doi:10.1002/jlac.197419740615.
- [44] K. Kempe, M. Lobert, R. Hoogenboom, U.S. Schubert, Screening the synthesis of 2-substituted-2-oxazolines, *J. Comb. Chem.* 11 (2009) 274–280. doi:10.1021/cc800174d.
- [45] M. Meyer, H. Schlaad, Poly(2-isopropyl-2-oxazoline)-poly(L-glutamate) block copolymers through ammonium-mediated NCA polymerization, *Macromolecules.* 39 (2006) 3967–3970. doi:10.1021/ma060523c.
- [46] W. Seeliger, E. Aufderhaar, W. Diepers, R. Feinauer, R. Nehring, W. Thier, H. Hellmann, Recent Syntheses and Reactions of Cyclic Imidic Esters, *Angew. Chemie Int. Ed. English.* 5 (1966) 875–888. doi:10.1002/anie.196608751.
- [47] D.A. Tomalia, D.P. Sheetz, Homopolymerization of 2-alkyl- and 2-aryl-2-oxazolines, *J. Polym. Sci. Part A-1 Polym. Chem.* 4 (1966) 2253–2265. doi:10.1002/pol.1966.150040919.
- [48] D. Edington, E. Poeter, An invertible stratigraphic forward model that simulates sediment accumulation in fluvial environments, *Acta Univ. Carolinae, Geol.* 46 (2002) 387–390. doi:10.1016/0032-3861(80)90327-4.
- [49] R. Hoogenboom, M.W.M. Fijten, U.S. Schubert, Parallel Kinetic Investigation of 2-Oxazoline Polymerizations with Different Initiators as Basis for Designed Copolymer Synthesis, *J. Polym. Sci. Part A Polym. Chem.* 42 (2004) 1830–1840. doi:10.1002/pola.20024.
- [50] G. Volet, A.-C.L. Deschamps, C. Amiel, Association of hydrophobically α,ω -end-capped poly(2-methyl-2-oxazoline) in water, *J. Polym. Sci. Part A Polym. Chem.* 48 (2010) 2477–2485. doi:10.1002/pola.24019.
- [51] M. Glassner, D.R. D’Hooge, J. Young Park, P.H.M. Van Steenberge, B.D. Monnery, M.F.F. Reyniers, R. Hoogenboom, Systematic investigation of alkyl sulfonate initiators for the cationic ring-opening polymerization of 2-oxazolines

- revealing optimal combinations of monomers and initiators, *Eur. Polym. J.* 65 (2015) 298–304. doi:10.1016/j.eurpolymj.2015.01.019.
- [52] R.M. Paulus, C.R. Becer, R. Hoogenboom, U.S. Schubert, Acetyl halide initiator screening for the cationic ring-opening polymerization of 2-ethyl-2-oxazoline, *Macromol. Chem. Phys.* 209 (2008) 794–800. doi:10.1002/macp.200700506.
- [53] M. Einzmann, W.H. Binder, Novel functional initiators for oxazoline polymerization, *J. Polym. Sci. Part A Polym. Chem.* 39 (2001) 2821–2831. doi:10.1002/pola.1262.
- [54] B. Guillermin, S. Monge, V. Lapinte, J.J. Robin, How to modulate the chemical structure of polyoxazolines by appropriate functionalization, *Macromol. Rapid Commun.* 33 (2012) 1600–1612. doi:10.1002/marc.201200266.
- [55] S. Kobayashi, E. Masuda, S. ichiro Shoda, Y. Shimano, Synthesis of Acryl- and Methacryl-Type Macromonomers and Telechelics by Utilizing Living Polymerization of 2-Oxazolines, *Macromolecules.* 22 (1989) 2878–2884. doi:10.1021/ma00197a002.
- [56] O. Nuyken, G. Maier, A. Groß, H. Fischer, Systematic investigations on the reactivity of oxazolinium salts, *Macromol. Chem. Phys.* 197 (1996) 83–95. doi:10.1007/978-3-642-25243-3_31.
- [57] R. Luxenhofer, Robert and Han, Yingchao and Schulz, Anita and Tong, Jing and He, Zhijian and Kabanov, Alexander V and Jordan, Poly(2-oxazoline)s as Polymer Therapeutics, *Macromol. Rapid Commun.* 33 (2012) 1613–1631. doi:10.1002/marc.201200354.Poly(2-oxazoline)s.
- [58] R.M. Paulus, T. Erdmenger, C.R. Becer, R. Hoogenboom, U.S. Schubert, Scale-up of microwave-assisted polymerizations in continuous-flow mode: Cationic ring-opening polymerization of 2-ethyl-2-oxazoline, *Macromol. Rapid Commun.* 28 (2007) 484–491. doi:10.1002/marc.200600756.
- [59] M. Meyer, H. Schlaad, R. V March, V. Re, M. Recci, V. March, Poly (2-isopropyl-2-oxazoline) - Poly (L -glutamate) Block Copolymers through Ammonium-Mediated NCA Polymerization, *Macromolecules.* 39 (2006) 3967–3970. doi:10.1021/ma060523c.
- [60] J. Park, Y. Akiyama, F. Winnik, K. Kataoka, Versatile synthesis of end-functionalized thermosensitive poly (2-isopropyl-2-oxazolines),

- Macromolecules. (2004) 6786–6792. doi:10.1021/ma049677n.
- [61] B.D. Monnery, S. Shaunak, M. Thanou, J.H.G. Steinke, Improved synthesis of linear poly(ethylenimine) via low-temperature polymerization of 2-isopropyl-2-oxazoline in chlorobenzene, *Macromolecules*. 48 (2015) 3197–3206. doi:10.1021/acs.macromol.5b00437.
- [62] M. Glassner, M. Vergaelen, R. Hoogenboom, Poly(2-oxazoline)s: A comprehensive overview of polymer structures and their physical properties, *Polym. Int.* 67 (2018) 32–45. doi:10.1002/pi.5457.
- [63] B. Hoogenboom, Richard; Monnery, Method for the preparation of uniform, high molar mass cyclic amino ether polymers, WO 2016/008817 A1, 2016. doi:WO 2016/008817 A1.
- [64] R. Jordan, N. West, A. Ulman, Y.M. Chou, O. Nuyken, Nanocomposites by surface-initiated living cationic polymerization of 2-oxazolines on functionalized gold nanoparticles, *Macromolecules*. 34 (2001) 1606–1611. doi:10.1177/1090198103259163.
- [65] Y. Chujo, E. Ihara, H. Ihara, T. Saegusa, A Novel Silane Coupling Agent. 1. Synthesis of Trimethoxysilyl-Terminated Poly(N-acetylenimine), *Macromolecules*. 22 (1989) 2040–2043. doi:10.1021/ma00195a003.
- [66] M. Schmitz, M. Kuhlmann, O. Reimann, C.P.R. Hackenberger, J. Groll, Side-Chain Cysteine-Functionalized Poly(2-oxazoline)s for Multiple Peptide Conjugation by Native Chemical Ligation, *Biomacromolecules*. 16 (2015) 1088–1094. doi:10.1021/bm501697t.
- [67] R. Luxenhofer, R. Jordan, Click chemistry with poly(2-oxazoline)s, *Macromolecules*. 39 (2006) 3509–3516. doi:10.1021/ma052515m.
- [68] J.C. Rueda, H. Komber, J.C. Cedrón, B. Voit, G. Shevtsova, Synthesis of new hydrogels by copolymerization of poly(2-methyl-2-oxazoline) bis(macromonomers) and N-vinylpyrrolidone, *Macromol. Chem. Phys.* 204 (2003) 947–953. doi:10.1002/macp.200390062.
- [69] A. Cirpan, S. Alkan, L. Toppare, G. David, Y. Yagci, Synthesis and electroactivity of pyrrole end-functionalized poly(2-methyl-2-oxazoline), *Eur. Polym. J.* 37 (2001) 2225–2229. doi:10.1016/S0014-3057(01)00103-3.
- [70] S. Huber, N. Hutter, R. Jordan, Effect of end group polarity upon the lower critical solution temperature of poly(2-isopropyl-2-oxazoline), *Colloid Polym.*

- Sci. 286 (2008) 1653–1661. doi:10.1007/s00396-008-1942-7.
- [71] M.J. Isaacman, E.M. Corigliano, L.S. Theogarajan, Stealth Polymeric Vesicles via Metal-Free Click Coupling., *Biomacromolecules*. 14 (2013) 2996–3000. doi:10.1021/bm400940h.
- [72] G. Volet, T.X. Lav, J. Babinot, C. Amiel, Click-chemistry: An alternative way to functionalize poly(2-methyl-2-oxazoline), *Macromol. Chem. Phys.* 212 (2011) 118–124. doi:10.1002/macp.201000556.
- [73] Y. Shimano, K. Sato, S. Kobayashi, Synthesis of novel macromonomers and telechelics of poly(2-alkyl-2-oxazoline)s, *J. Polym. Sci. Part A Polym. Chem.* 33 (1995) 2715–2723. doi:10.1002/pola.1995.080331605.
- [74] V.R. De La Rosa, Z. Zhang, B.G. De Geest, R. Hoogenboom, Colorimetric IgG probes based on poly(2-alkyl-2-oxazoline)-coated gold nanoparticles, *Adv. Funct. Mater.* 25 (2015) 2511–2519. doi:10.1002/adfm.201404560.
- [75] M. Schmidt, L.K. Bast, F. Lanfer, L. Richter, E. Hennes, R. Seymen, C. Krumm, J.C. Tiller, Poly(2-oxazoline)-Antibiotic Conjugates with Penicillins, *Bioconjug. Chem.* 28 (2017) 2440–2451. doi:10.1021/acs.bioconjchem.7b00424.
- [76] M. Schmidt, S. Harmuth, E.R. Barth, E. Wurm, R. Fobbe, A. Sickmann, C. Krumm, J.C. Tiller, Conjugation of ciprofloxacin with poly(2-oxazoline)s and polyethylene glycol via end groups, *Bioconjug. Chem.* 26 (2015) 1950–1962. doi:10.1021/acs.bioconjchem.5b00393.
- [77] J. Li, Y. Zhou, C. Li, D. Wang, Y. Gao, C. Zhang, L. Zhao, Y. Li, Y. Liu, X. Li, Poly(2-ethyl-2-oxazoline)-doxorubicin conjugate-based dual endosomal pH-sensitive micelles with enhanced antitumor efficacy, *Bioconjug. Chem.* 26 (2015) 110–119. doi:10.1021/bc5004718.
- [78] A. Chen, H. Peng, I. Blakey, A.K. Whittaker, Biocidal Polymers: A Mechanistic Overview, *Polym. Rev.* 57 (2017) 276–310. doi:10.1080/15583724.2016.1223131.
- [79] C.J. Waschinski, S. Barnert, A. Theobald, R. Schubert, F. Kleinschmidt, A. Hoffmann, K. Saalwächter, J.C. Tiller, Insights in the antibacterial action of poly(methyloxazoline)s with a biocidal end group and varying satellite groups, *Biomacromolecules*. 9 (2008) 1764–1771. doi:10.1021/bm7013944.
- [80] Y. Xue, H. Xiao, Y. Zhang, Antimicrobial polymeric materials with quaternary

- ammonium and phosphonium salts, *Int. J. Mol. Sci.* 16 (2015) 3626–3655. doi:10.3390/ijms16023626.
- [81] A.M. Kelly, V. Kaltenhauser, I. Mühlbacher, K. Rametsteiner, H. Kren, C. Slugovc, F. Stelzer, F. Wiesbrock, Poly(2-oxazoline)-derived Contact Biocides: Contributions to the Understanding of Antimicrobial Activity, *Macromol. Biosci.* 13 (2013) 116–125. doi:10.1002/mabi.201200240.
- [82] C.J. Waschinski, V. Herdes, F. Schueler, J.C. Tiller, Influence of satellite groups on telechelic antimicrobial functions of polyoxazolines, *Macromol. Biosci.* 5 (2005) 149–156. doi:10.1002/mabi.200400169.
- [83] E.-R. Kenawy, S.D. Worley, R. Broughton, The Chemistry and Applications of Antimicrobial Polymers: A State-of-the-Art Review, *Biomacromolecules.* 8 (2007) 1359. doi:10.1021/BM061150Q.
- [84] H. Wang, C. V. Synatschke, A. Raup, V. Jérôme, R. Freitag, S. Agarwal, Oligomeric dual functional antibacterial polycaprolactone, *Polym. Chem.* 5 (2014) 2453. doi:10.1039/c3py01467c.
- [85] M.R.E. Santos, A.C. Fonseca, P. V. Mendonça, R. Branco, A.C. Serra, P. V. Morais, J.F.J. Coelho, Recent developments in antimicrobial polymers: A review, *Materials (Basel).* 9 (2016). doi:10.3390/MA9070599.
- [86] A.M. Bieser, Y. Thomann, J.C. Tiller, Contact-Active Antimicrobial and Potentially Self-Polishing Coatings Based on Cellulose, *Macromol. Biosci.* 11 (2011) 111–121. doi:10.1002/mabi.201000306.
- [87] A. Punia, P.R. Debata, P. Banerjee, N.-L. Yang, Structure–property relationships of antibacterial amphiphilic polymers derived from 2-aminoethyl acrylate, *RSC Adv.* 5 (2015) 95300–95306. doi:10.1039/C5RA17875D.
- [88] A. Alamri, M.H. El-Newehy, S.S. Al-Deyab, Biocidal polymers: synthesis and antimicrobial properties of benzaldehyde derivatives immobilized onto amine-terminated polyacrylonitrile, *Chem. Cent. J.* 6 (2012) 480. doi:10.1186/1752-153X-6-111.
- [89] C.P. Fik, C. Krumm, C. Muennig, T.I. Baur, U. Salz, T. Bock, J.C. Tiller, Impact of functional satellite groups on the antimicrobial activity and hemocompatibility of telechelic poly(2-methyloxazoline)s, *Biomacromolecules.* 13 (2012) 165–172. doi:10.1021/bm201403e.
- [90] B. Pidhatika, J. Möller, E.M. Benetti, R. Konradi, E. Rakhmatullina, A.

- Mühlebach, R. Zimmermann, C. Werner, V. Vogel, M. Textor, The role of the interplay between polymer architecture and bacterial surface properties on the microbial adhesion to polyoxazoline-based ultrathin films, *Biomaterials*. 31 (2010) 9462–9472. doi:10.1016/j.biomaterials.2010.08.033.
- [91] C.J. Waschinski, J.C. Tiller, Poly (oxazoline) s with Telechelic Antimicrobial Functions Poly (oxazoline) s with Telechelic Antimicrobial Functions, *Society*. 6 (2005) 235–243. doi:10.1021/bm049553i.
- [92] C.J. Waschinski, V. Herdes, F. Schueler, J.C. Tiller, Influence of Satellite Groups on Telechelic Antimicrobial Functions of Polyoxazolines, *Adv. Mater.* (2005) 149–156. doi:10.1002/mabi.200400169.
- [93] C.J. Waschinski, S. Barnert, A. Theobald, R. Schubert, F. Kleinschmidt, A. Hoffmann, K. Saalwa, J.C. Tiller, Insights in the Antibacterial Action of Poly (methyloxazoline) s with a Biocidal End Group and Varying Satellite Groups, *Biomacromolecules*. (2008) 1764–1771.
- [94] C.P. Fik, C. Krumm, C. Muennig, T.I. Baur, U. Salz, T. Bock, J.C. Tiller, Impact of Functional Satellite Groups on the Antimicrobial Activity and Hemocompatibility of Telechelic Poly(2-methyloxazoline)s, *Biomacromolecules*. (2012). doi:10.1021/bm201403e.
- [95] R. Haag, F. Kratz, Polymer therapeutics: Concepts and applications, *Angew. Chemie - Int. Ed.* 45 (2006) 1198–1215. doi:10.1002/anie.200502113.
- [96] B. Říhová, M. Jelínková, J. Strohalm, V. Šubr, D. Plocová, O. Hovorka, M. Novák, D. Plundrová, Y. Germano, K. Ulbrich, Polymeric drugs based on conjugates of synthetic and natural macromolecules. II. Anti-cancer activity of antibody or (Fab')₂-targeted conjugates and combined therapy with immunomodulators, *J. Control. Release*. 64 (2000) 241–261. doi:10.1016/S0168-3659(99)00140-6.
- [97] Y.J. Zhao, W. Wei, Z.G. Su, G.H. Ma, Poly (ethylene glycol) prodrug for anthracyclines via N-Mannich base linker: Design, synthesis and biological evaluation, *Int. J. Pharm.* 379 (2009) 90–99. doi:10.1016/j.ijpharm.2009.06.013.
- [98] G. Pintér, P. Horváth, S. Bujdosó, F. Sztaricskai, S. Kéki, M. Zsuga, S. Kardos, F. Rozgonyi, P. Herczegh, Synthesis and antimicrobial activity of ciprofloxacin and norfloxacin permanently bonded to polyethylene glycol by a thiourea linker, *J. Antibiot. (Tokyo)*. 62 (2009) 113–116. doi:10.1038/ja.2008.26.

- [99] M.C. Lawson, R. Shoemaker, K.B. Hoth, C.N. Bowman, K.S. Anseth, Polymerizable vancomycin derivatives for bactericidal biomaterial surface modification: Structure-function evaluation, *Biomacromolecules*. 10 (2009) 2221–2234. doi:10.1021/bm900410a.
- [100] J. Du, H.M.H.N. Bandara, P. Du, H. Huang, K. Hoang, D. Nguyen, S.V. Mogarala, H.D.C. Smyth, Improved biofilm antimicrobial activity of polyethylene glycol conjugated tobramycin compared to tobramycin in *Pseudomonas aeruginosa* biofilms, *Mol. Pharm.* 12 (2015) 1544–1553. doi:10.1021/mp500846u.
- [101] E.L. Ferguson, E. Azzopardi, J.L. Roberts, T.R. Walsh, D.W. Thomas, Dextrin-colistin conjugates as a model bioresponsive treatment for multidrug resistant bacterial infections, *Mol. Pharm.* 11 (2014) 4437–4447. doi:10.1021/mp500584u.
- [102] V. Buchta, L. Kubicova, S. Petr, M. Holc, Synthesis and characterisation of a new amphotericin B–methoxypoly (ethylene glycol) conjugate, *Bioorganic Med.* 11 (2001) 2833–2835. <http://www.sciencedirect.com/science/article/pii/S0960894X01005327>.
- [103] M. Sedláč, M. Antonietti, H. Cölfen, Synthesis of a new class of double-hydrophilic block copolymers with calcium binding capacity as builders and for biomimetic structure control of minerals, *Macromol. Chem. Phys.* 199 (1998) 247–254. doi:10.1002/(SICI)1521-3935(19980201)199: 2-9.
- [104] D.E. Herold, David A.; Keil, Katherine; Bruns, Oxidation of Polyethylene glycols by alcohol dehydrogenase, *Biochem. Pharmacol.* 38 (1989) 73–76. doi:10.1016/0006-2952(89)90151-2.
- [105] C. Elvira, A. Gallardo, J. San Roman, A. Cifuentes, Covalent polymer-drug conjugates, *Molecules*. 10 (2005) 114–125. doi:10.3390/10010114.
- [106] A. Abuchowski, J.R. McCoy, N.C. Palczuk, Effect of Covalent Attachment of Polyethylene Glycol on Immunogenicity and Circulating Life of Bovine Liver Catalase, *J. Biol. Chem.* 252 (1976) 3582–3586.
- [107] S. Zalipsky, Chemistry of polyethylene glycol conjugates with biologically active molecules, *Adv. Drug Deliv. Rev.* 16 (1995) 157–182. doi:10.1016/0169-409X(95)00023-Z.
- [108] S.D. Yoo, H. Jun, B.S. Shin, H.S. Lee, M.O. Park, P.P. DeLuca, K.C. Lee,

- Pharmacokinetic disposition of polyethylene glycol-modified salmon calcitonins in rats., *Sect. Title Pharmacol.* 48 (2000) 1921–1924. doi:10.1248/cpb.48.1921.
- [109] R.B. Greenwald, A. Pendri, D. Bolikal, Highly Water Soluble Taxol Derivatives: 7-Polyethylene Glycol Carbamates and Carbonates, *J. Org. Chem.* 60 (1995) 331–336. doi:10.1021/jo00107a010.
- [110] R.B. Greenwald, Y.H. Choe, J. McGuire, C.D. Conover, Effective drug delivery by PEGylated drug conjugates, *Adv. Drug Deliv. Rev.* 55 (2003) 217–250. doi:10.1016/S0169-409X(02)00180-1.
- [111] V. Rapozzi, S. Cogoi, P. Spessotto, A. Risso, G.M. Bonora, F. Quadrifoglio, L.E. Xodo, Antigenic effect in K562 cells of a PEG-conjugated triplex-forming oligonucleotide targeted to the bcr/abl oncogene, *Biochemistry.* 41 (2002) 502–510. doi:10.1021/bi011314h.
- [112] E. Hurwitz, N. Klapper, M. Wilchek, Inhibition of tumor growth by poly (ethylene glycol) derivatives of anti-ErbB2 antibodies, (2000) 226–234.
- [113] R.W. Moreadith, T.X. Viegas, M.D. Bentley, J.M. Harris, Z. Fang, K. Yoon, B. Dizman, R. Weimer, B.P. Rae, X. Li, C. Rader, D. Standaert, W. Olanow, Clinical development of a poly(2-oxazoline) (POZ) polymer therapeutic for the treatment of Parkinson’s disease – Proof of concept of POZ as a versatile polymer platform for drug development in multiple therapeutic indications, *Eur. Polym. J.* 88 (2017) 524–552. doi:10.1016/j.eurpolymj.2016.09.052.
- [114] W.H. Velander, R.D. Madurawe, A. Subramanian, G. Kumar, G. Sinai-Zingde, J.S. Riffle, C.L. Orthner, Polyoxazoline-Peptide adducts that retain antibody avidity, *Biotechnol. Bioeng.* 39 (1992) 1024–1030. doi:10.1002/bit.260391006.
- [115] M.C. Woodle, C.M. Engbers, S. Zalipsky, New Amphipatic Polymer—Lipid Conjugates Forming Long-Circulating Reticuloendothelial System-Evading Liposomes, *Bioconjug. Chem.* 5 (1994) 493–496. doi:10.1021/bc00030a001.
- [116] A. Mero, G. Pasut, L.D. Via, M.W.M. Fijten, U.S. Schubert, R. Hoogenboom, F.M. Veronese, Synthesis and characterization of poly(2-ethyl 2-oxazoline)-conjugates with proteins and drugs: Suitable alternatives to PEG-conjugates?, *J. Control. Release.* 125 (2008) 87–95. doi:10.1016/j.jconrel.2007.10.010.
- [117] D. Angewandte, M. Chemie, Polymeric prodrugs, 245 (1997) 1–8.

- [118] H. Patel, D.A. Raval, D. Madamwar, S.R. Patel, Polymeric prodrug: Synthesis, release study and antimicrobial property of poly(styrene-co-maleic anhydride)-bound acriflavine, *Angew. Makromol. Chemie.* 263 (1998) 25–30. doi:10.1002/(SICI)1522-9505(19981215)263:1<25::AID-APMC25>3.0.CO;2-9.
- [119] M. Sedlák, M. Pravda, F. Staud, L. Kubicová, K. Týčová, K. Ventura, Synthesis of pH-sensitive amphotericin B-poly(ethylene glycol) conjugates and study of their controlled release in vitro, *Bioorganic Med. Chem.* 15 (2007) 4069–4076. doi:10.1016/j.bmc.2007.03.083.
- [120] S. Lv, Z. Tang, D. Zhang, W. Song, M. Li, J. Lin, H. Liu, X. Chen, Well-defined polymer-drug conjugate engineered with redox and pH-sensitive release mechanism for efficient delivery of paclitaxel, *J. Control. Release.* 194 (2014) 220–227. doi:10.1016/j.jconrel.2014.09.009.
- [121] R.B. Greenwald, H. Zhao, J. Xia, A. Martinez, Poly(ethylene glycol) Transport Forms of Vancomycin: A Long-Lived Continuous Release Delivery System, *J. Med. Chem.* 46 (2003) 5021–5030. doi:10.1021/jm030202g.
- [122] F.M.H. De Groot, L.W.A. Van Berkom, H.W. Scheeren, Synthesis and biological evaluation of 2'-carbamate-linked and 2'-carbonate-linked prodrugs of paclitaxel selective activation by the tumor-associated protease plasmin, *J. Med. Chem.* 43 (2000) 3093–3102. doi:10.1021/jm0009078.
- [123] O. Schiavon, G. Pasut, S. Moro, P. Orsolini, A. Guiotto, F.M. Veronese, PEG-Ara-C conjugates for controlled release, *Eur. J. Med. Chem.* 39 (2004) 123–133. doi:10.1016/j.ejmech.2003.10.005.
- [124] M. Miyamoto, K. Naka, M. Shiozaki, Y. Chujo, T. Saegusa, Preparation and Enzymatic Activity of Poly[(N-acylimino)ethylene]-Modified Catalase, *Macromolecules.* 23 (1990) 3201–3205. doi:10.1021/ma00215a001.
- [125] A. Nathan, S. Zalipsky, S.I. Ertel, S.N. Agathos, M.L. Yarmush, J. Kohn, Copolymers of Lysine and Polyethylene Glycol: A New Family of Functionalized Drug Carriers, *Bioconjug. Chem.* 4 (1993) 54–62. doi:10.1021/bc00019a008.
- [126] C.D. Conover, H. Zhao, C.B. Longley, K.L. Shum, R.B. Greenwald, Utility of poly(ethylene glycol) conjugation to create prodrugs of amphotericin B, *Bioconjug. Chem.* 14 (2003) 661–666. doi:10.1021/bc0256594.

- [127] S. Gac-Breton, J. Coudane, M. Boustta, M. Vert, Norfloxacin-poly (L-lysine citramide imide) conjugates and structure-dependence of the drug release, *J. Drug Target.* 12 (2004) 297–307. doi:10.1080/10611860410001724477.
- [128] M. Sobczak, K. Nurzynska, W. Kolodziejski, Seeking polymeric prodrugs of norfloxacin. part 2. synthesis and structural analysis of polyurethane conjugates, *Molecules.* 15 (2010) 842–856. doi:10.3390/molecules15020842.
- [129] M. Sobczak, G. Nałęcz-Jawecki, W.L. Kołodziejski, P. Goś, K. Żółtowska, Synthesis and study of controlled release of ofloxacin from polyester conjugates, *Int. J. Pharm.* 402 (2010) 37–43. doi:10.1016/j.ijpharm.2010.09.026.
- [130] M. Sobczak, Synthesis and characterization of polyester conjugates of ciprofloxacin, *Eur. J. Med. Chem.* 45 (2010) 3844–3849. doi:10.1016/j.ejmech.2010.05.037.
- [131] H.S. Yoo, J.E. Oh, K.H. Lee, T.G. Park, Biodegradable nanoparticles containing doxorubicin-PLGA conjugate for sustained release, *Pharm. Res.* 16 (1999) 1114–1118. doi:10.1023/A:1018908421434.
- [132] M. V C. Ustariz-Peyret, J. Coudane, Labile conjugation of a hydrophilic drug to PLA oligomers to modify a drug delivery system: cephadrin in a PLAGA matrix, *J. Microencapsul.* 17 (2008) 615–624. doi:10.1080/026520400417667.
- [133] H. Wang, L. Tang, C. Tu, Z. Song, Q. Yin, L. Yin, Z. Zhang, J. Cheng, Redox-responsive, core-cross-linked micelles capable of on-demand, concurrent drug release and structure disassembly, *Biomacromolecules.* 14 (2013) 3706–3712. doi:10.1021/bm401086d.
- [134] X.Q. Li, H.Y. Wen, H.Q. Dong, W.M. Xue, G.M. Pauletti, X.J. Cai, W.J. Xia, D. Shi, Y.Y. Li, Self-assembling nanomicelles of a novel camptothecin prodrug engineered with a redox-responsive release mechanism, *Chem. Commun.* 47 (2011) 8647–8649. doi:10.1039/c1cc12495a.
- [135] E.R. Gillies, J.M.J. Fréchet, pH-responsive copolymer assemblies for controlled release of doxorubicin, *Bioconjug. Chem.* 16 (2005) 361–368. doi:10.1021/bc049851c.
- [136] E.R. Gillies, J.M.J. Fréchet, A new approach towards acid sensitive copolymer micelles for drug delivery, *Chem. Commun.* 3 (2003) 1640–1641. doi:10.1039/b304251k.

- [137] Y. Jin, L. Song, Y. Su, L. Zhu, Y. Pang, F. Qiu, G. Tong, D. Yan, B. Zhu, X. Zhu, Oxime linkage: A robust tool for the design of pH-sensitive polymeric drug carriers, *Biomacromolecules*. 12 (2011) 3460–3468. doi:10.1021/bm200956u.
- [138] X. Hu, R. Wang, J. Yue, S. Liu, Z. Xie, X. Jing, Targeting and anti-tumor effect of folic acid-labeled polymer-Doxorubicin conjugates with pH-sensitive hydrazone linker, *J. Mater. Chem.* 22 (2012) 13303–13310. doi:10.1039/c2jm31130e.
- [139] V. Vijayakameswara Rao Neralla, S.R. Mane, A. Kishore, J. Das Sarma, R. Shunmugam, Norbornene derived doxorubicin copolymers as drug carriers with pH responsive hydrazone linker, *Biomacromolecules*. 13 (2012) 221–230. doi:10.1021/bm201478k.
- [140] V. Coessens, E. Schacht, D. Domurado, Synthesis of polyglutamine and dextran conjugates of streptomycin with an acid-sensitive drug-carrier linkage, *J. Control. Release*. 38 (1996) 141–150. doi:10.1016/0168-3659(95)00111-5.
- [141] Y. Bae, N. Nishiyama, S. Fukushima, H. Koyama, M. Yasuhiro, K. Kataoka, Preparation and biological characterization of polymeric micelle drug carriers with intracellular pH-triggered drug release property: Tumor permeability, controlled subcellular drug distribution, and enhanced in vivo antitumor efficacy, *Bioconj. Chem.* 16 (2005) 122–130. doi:10.1021/bc0498166.
- [142] M. Hrubý, Č. Koňák, K. Ulbrich, Polymeric micellar pH-sensitive drug delivery system for doxorubicin, *J. Control. Release*. 103 (2005) 137–148. doi:10.1016/j.jconrel.2004.11.017.
- [143] Z. Wang, C. Chen, Q. Zhang, M. Gao, J. Zhang, D. Kong, Y. Zhao, Tuning the architecture of polymeric conjugate to mediate intracellular delivery of pleiotropic curcumin, *Eur. J. Pharm. Biopharm.* 90 (2015) 53–62. doi:10.1016/j.ejpb.2014.11.002.
- [144] Y. Zhang, M. Gao, C. Chen, Z. Wang, Y. Zhao, Residue cytotoxicity of a hydrazone-linked polymer-drug conjugate: Implication for acid-responsive micellar drug delivery, *RSC Adv.* 5 (2015) 34800–34802. doi:10.1039/c5ra02097b.
- [145] R. Luxenhofer, S. Huber, J. Hytry, J. Tong, A. V. Kabanov, R. Jordan, Chiral and water-soluble poly(2-oxazoline)s, *J. Polym. Sci. Part A Polym. Chem.* 51 (2013) 732–738. doi:10.1002/pola.26437.

- [146] S. Kobayashi, T. Igarashi, Y. Moriuchi, T. Saegusa, Block Copolymers from Cyclic Imino Ethers: A New Class of Nonionic Polymer Surfactant, *Macromolecules*. 19 (1986) 535–541. doi:10.1021/ma00157a006.
- [147] M. Litt, F. Rahl, L.G. Roldan, Polymerization of cyclic imino ethers. VI. X-ray study of some polyaziridines, *J. Polym. Sci. Part A-2 Polym. Phys.* 7 (1969) 463–473. doi:10.1002/pol.1969.160070302.
- [148] C.H. Wang, G.H. Hsiue, New amphiphilic poly(2-ethyl-2-oxazoline)/ poly(L-lactide) triblock copolymers, *Biomacromolecules*. 4 (2003) 1487–1490. doi:10.1021/bm034190s.
- [149] Y. Zhao, Y. Zhou, D. Wang, Y. Gao, J. Li, S. Ma, L. Zhao, C. Zhang, Y. Liu, X. Li, PH-responsive polymeric micelles based on poly(2-ethyl-2-oxazoline)-poly(d,l-lactide) for tumor-targeting and controlled delivery of doxorubicin and P-glycoprotein inhibitor, *Acta Biomater.* 17 (2015) 182–192. doi:10.1016/j.actbio.2015.01.010.
- [150] M. Meyer, M. Antonietti, H. Schlaad, Unexpected thermal characteristics of aqueous solutions of poly(2-isopropyl-2-oxazoline), *Soft Matter*. 3 (2007) 430–431. doi:10.1039/b616678d.
- [151] Y. Katsumoto, A. Tsuchiizu, X. Qiu, F.M. Winnik, Dissecting the mechanism of the heat-induced phase separation and crystallization of poly(2-isopropyl-2-oxazoline) in water through vibrational spectroscopy and molecular orbital calculations, *Macromolecules*. 45 (2012) 3531–3541. doi:10.1021/ma300252e.
- [152] N. Oleszko, A. Utrata-Wesołek, W. Wałach, M. Libera, A. Hercog, U. Szeluga, M. Domański, B. Trzebicka, A. Dworak, Crystallization of poly(2-isopropyl-2-oxazoline) in organic solutions, *Macromolecules*. 48 (2015) 1852–1859. doi:10.1021/ma502586x.
- [153] T. Furuncuoğlu Özaltın, V. Aviyente, C. Atılğan, L. Demirel, Multiscale modeling of poly(2-isopropyl-2-oxazoline) chains in aqueous solution, *Eur. Polym. J.* 88 (2017) 594–604. doi:10.1016/j.eurpolymj.2016.10.013.
- [154] C.H. Wang, G.H. Hsiue, Synthesis and characterization of temperature- and pH-sensitive hydrogels based on poly(2-ethyl-2-oxazoline) and poly(D,L-lactide), *J. Polym. Sci. Part A Polym. Chem.* 40 (2002) 1112–1121. doi:10.1002/pola.10201.
- [155] E. Cagli, E. Yildirim, S.-W. Yang, I. Erel-Goktepe, An experimental and

- computational approach to pH-dependent self-aggregation of poly(2-isopropyl-2-oxazoline), *J. Polym. Sci. Part B Polym. Phys.* (2018) 1–12. doi:10.1002/polb.24773.
- [156] M.A. Meyers, P.-Y. Chen, A.Y.-M. Lin, Y. Seki, Biological materials: Structure and mechanical properties, *Prog. Mater. Sci.* 53 (2008) 1–206. doi:10.1016/j.pmatsci.2007.05.002.
- [157] J.A.A.W. Elemans, A.E. Rowan, R.J.M. Nolte, Mastering molecular matter. Supramolecular architectures by hierarchical self-assembly, *J. Mater. Chem.* 13 (2003) 2661–2670. doi:10.1039/b304972h.
- [158] S. Forster, T. Plantenberg, From self-organizing polymers to nanohybrid and biomaterials.pdf, *Angew. Chem. Int. Ed.* 41 (2002) 688–714.
- [159] V. Abetz, P. Simon, Phase Behaviour and Morphologies of Block Copolymers, *Block Copolym. I.* 189 (2005) 125–212. doi:10.1007/12_004.
- [160] A.L. Demirel, M. Meyer, H. Schlaad, Formation of polyamide nanofibers by directional crystallization in aqueous solution, *Angew. Chemie - Int. Ed.* 46 (2007) 8622–8624. doi:10.1002/anie.200703486.
- [161] R.H. Jin, Colloidal crystalline polymer generated in situ from growing star poly(oxazolines), *J. Mater. Chem.* 13 (2003) 672–675. doi:10.1039/b211674j.
- [162] V. Percec, M.N. Holerca, S.N. Magonov, D.J.P. Yeardley, G. Ungar, H. Duan, S.D. Hudson, Poly(oxazolines)s with tapered minidendritic side groups. The simplest cylindrical models to investigate the formation of two-dimensional and three-dimensional order by direct visualization, *Biomacromolecules.* 2 (2001) 706–728. doi:10.1021/bm015550j.
- [163] M. Seitz, T. Plesnivý, K. Schimossek, M. Edelmann, H. Ringsdorf, H. Fischer, H. Uyama, S. Kobayashi, Formation of hexagonal columnar mesophases by linear and branched oligo- and polyamides, *Macromolecules.* 29 (1996) 6560–6574. doi:10.1021/ma960270v.
- [164] D.J.P. Yeardley, G. Ungar, V. Percec, M.N. Holerca, G. Johansson, Spherical supramolecular minidendrimers self-organized in an “inverse micellar”-like thermotropic body-centered cubic liquid crystalline phase, *J. Am. Chem. Soc.* 122 (2000) 1684–1689. doi:10.1021/ja993915q.
- [165] H. Schlaad, C. Diehl, A. Gress, M. Meyer, A.L. Demirel, Y. Nur, A. Bertin, Poly(2-oxazoline)s as Smart Bioinspired Polymers, *Macromol. Rapid*

- Commun. 31 (2010) 511–525. doi:10.1002/marc.200900683.
- [166] G. Volet, V. Chanthavong, V. Wintgens, C. Amiel, Synthesis of monoalkyl end-capped poly(2-methyl-2-oxazoline) and its micelle formation in aqueous solution, *Macromolecules*. 38 (2005) 5190–5197. doi:10.1021/ma050407u.
- [167] R. Obeid, E. Maltseva, A.F. Thu, F. Tanaka, Temperature Response of Self-Assembled Micelles of Telechelic Hydrophobically Modified Poly (2-alkyl-2-oxazoline) s in Water, *Macromolecules*. 42 (2009) 2204–2214.
- [168] H. Möhwald, Surfactant layers at water surfaces, *Reports Prog. Phys.* 56 (1993) 653–685. doi:10.1088/0034-4885/56/5/002.
- [169] T.R. Baekmark, T. Wiesenthal, P. Kuhn, T.M. Bayerl, O. Nuyken, R. Merkel, New insights into the phase behaviour of lipopolymer monolayers at the air/water interface. IRRAS study of a polyoxazoline lipopolymer, *Langmuir*. 13 (1997) 5521–5523. doi:10.1021/la970610l.
- [170] H. Ahrens, T.R. Bækmark, R. Merkel, J. Schmitt, K. Graf, R. Raiteri, C.A. Helm, Hydrophilic/hydrophobic nanostripes in lipopolymer monolayers, *ChemPhysChem*. 1 (2000) 101–106. doi:10.1002/1439-7641(20000915)1:2<101::AID-CPHC101>3.0.CO;2-O.
- [171] C.A. Naumann, C.F. Brooks, G.G. Fuller, T. Lehmann, J. Rühle, W. Knoll, P. Kuhn, O. Nuyken, C.W. Frank, Two-dimensional physical networks of lipopolymers at the air/water interface: Correlation of molecular structure and surface rheological behavior, *Langmuir*. 17 (2001) 2801–2806. doi:10.1021/la000778y.
- [172] M.B. Foreman, J.P. Coffman, M.J. Murcia, S. Cesana, R. Jordan, G.S. Smith, C.A. Naumann, Gelation of amphiphilic lipopolymers at the air-water interface: 2D analogue to 3D gelation of colloidal systems with grafted polymer chains?, *Langmuir*. 19 (2003) 326–332. doi:10.1021/la0261390.
- [173] K. Lüdtke, R. Jordan, P. Hommes, O. Nuyken, C.A. Naumann, Lipopolymers from new 2-substituted-2-oxazolines for artificial cell membrane constructs, *Macromol. Biosci*. 5 (2005) 384–393. doi:10.1002/mabi.200500004.
- [174] Y. Li, X. Wang, J. Sun, Layer-by-layer assembly for rapid fabrication of thick polymeric films, *Chem. Soc. Rev.* 41 (2012) 5998–6009. doi:10.1039/c2cs35107b.
- [175] J. Borges, J.F. Mano, Molecular interactions driving the layer-by-layer

- assembly of multilayers, *Chem. Rev.* 114 (2014) 8883–8942. doi:10.1021/cr400531v.
- [176] R.K. Iler, Multilayers of Colloidal Particles, *J. COLLOID INTERFAcE Sci.* 21 (1966) 569–594. doi:10.1016/0095-8522(66)90018-3.
- [177] G. Decher, J.-D. Hong, K.H.A. Lau, J. Turkevich, H. Huebner, Buildup of ultrathin multiplayer films by a self-assembly process. II. Consecutive absorption of anionic and cationic bipolar amphiphiles and polyelectrolytes on charged surfaces, *Makromol. Chem.* 327 (1991) 321–327. doi:doi.org/10.1002/masy.19910460145.
- [178] M. Haktaniyan, S. Atilla, E. Cagli, I. Erel-Goktepe, pH- and temperature-induced release of doxorubicin from multilayers of poly(2-isopropyl-2-oxazoline) and tannic acid, *Polym. Int.* 66 (2017) 1851–1863. doi:10.1002/pi.5458.
- [179] E. Kharlampieva, S.A. Sukhishvili, Hydrogen-bonded layer-by-layer polymer films, *Polym. Rev.* 46 (2006) 377–395. doi:10.1080/15583720600945386.
- [180] I. Erel, Z. Zhu, A. Zhuk, S.A. Sukhishvili, Hydrogen-bonded layer-by-layer films of block copolymer micelles with pH-responsive cores, *J. Colloid Interface Sci.* 355 (2011) 61–69. doi:10.1016/j.jcis.2010.11.083.
- [181] B. Onat, V. Bütün, S. Banerjee, I. Erel-Goktepe, Bacterial anti-adhesive and pH-induced antibacterial agent releasing ultra-thin films of zwitterionic copolymer micelles, *Acta Biomater.* 40 (2016) 293–309. doi:10.1016/j.actbio.2016.04.033.
- [182] C. Ustoglu, E. Cagli, I. Erel-Goktepe, Layer-by-layer films of block copolymer micelles with cores exhibiting upper critical solution temperature behaviour, *Eur. Polym. J.* 96 (2017) 278–294. doi:10.1016/j.eurpolymj.2017.09.013.
- [183] D. Gundogdu, V. Bütün, I. Erel-Göktepe, Preparation of Layer-by-Layer Films with Remarkably Different pH-Stability and Release Properties Using Dual Responsive Block Copolymer Micelles, *Macromol. Chem. Phys.* 219 (2018) 1–12. doi:10.1002/macp.201800128.
- [184] S. Uluhan, V. Bütün, S. Banerjee, I. Erel-Goktepe, Biologically Functional Ultrathin Films Made of Zwitterionic Block Copolymer Micelles, *Langmuir.* (2018). doi:10.1021/acs.langmuir.8b01735.
- [185] I. Erel, H.E. Karahan, C. Tuncer, V. Bütün, A.L. Demirel, Hydrogen-bonded

- multilayers of micelles of a dually responsive dicationic block copolymer, *Soft Matter*. 8 (2012) 827–836. doi:10.1039/c1sm06248d.
- [186] Y. Sun, X. Zhang, C. Sun, Z. Wang, J. Shen, D. Wang, T. Li, Supramolecular assembly of alternating porphyrin and phthalocyanine layers based on electrostatic interactions, *Chem. Commun.* (1996) 2379. doi:10.1039/cc9960002379.
- [187] Y. Lvov, K. Ariga, T. Kunitake, Layer-by-Layer Assembly of Alternate Protein/Polyion Ultrathin Films, *Chem. Lett.* 23 (1994) 2323–2326. doi:10.1246/cl.1994.2323.
- [188] J. Sun, Y. Sun, Z. Wang, C. Sun, Y. Wang, X. Zhang, J. Shen, Ionic self-assembly of glucose oxidase with polycation bearing Os complex, *Macromol. Chem. Phys.* 202 (2001) 111–116. doi:10.1002/1521-3935(20010101)202:1<111::AID-MACP111>3.0.CO;2-D.
- [189] W. Kong, X. Zhang, M.L. Gao, H. Zhou, W. Li, J.C. Shen, A new kind of immobilized enzyme multilayer based on cationic and anionic interaction, *Macromol. Rapid Commun.* 15 (1994) 405–409. doi:10.1002/marc.1994.030151010.
- [190] D.G. Shchukin, A.A. Patel, G.B. Sukhorukov, Y.M. Lvov, Nanoassembly of Biodegradable Microcapsules for DNA Encasing, *J. Am. Chem. Soc.* 126 (2004) 3374–3375. doi:10.1021/ja036952x.
- [191] Y. Lvov, G. Decher, G. Sukhorukov, Assembly of Thin Films by Means of Successive Deposition of Alternate Layers of DNA and Poly(allylamine), *Macromolecules*. 26 (1993) 5396–5399. doi:10.1021/ma00072a016.
- [192] Y. Lvov, H. Haas, G. Decher, H. Möhwald, A. Mikhailov, B. Mtchedlishvily, E. Morgunova, B. Vainshtein, Successive Deposition of Alternate Layers of Polyelectrolytes and a Charged Virus, *Langmuir*. 10 (1994) 4232–4236. doi:10.1021/la00023a052.
- [193] G. Decher, J.B. Schlenoff, eds., *Multilayer Thin Films: Sequential Assembly of Nanocomposite Materials*, Second, Wiley-VCH Verlag GmbH & Co. KGaA, Weinheim, Germany, 2012. doi:10.1002/9783527646746.
- [194] P. Gentile, I. Carmagnola, T. Nardo, V. Chiono, Layer-by-layer assembly for biomedical applications in the last decade, *Nanotechnology*. 26 (2015). doi:10.1088/0957-4484/26/42/422001.

- [195] J.J. Richardson, M. Björnmalm, F. Caruso, Technology-driven layer-by-layer assembly of nanofilms, *Science* (80-.). 348 (2015). doi:10.1126/science.aaa2491.
- [196] F.X. Xiao, M. Pagliaro, Y.J. Xu, B. Liu, Layer-by-layer assembly of versatile nanoarchitectures with diverse dimensionality: A new perspective for rational construction of multilayer assemblies, *Chem. Soc. Rev.* 45 (2016) 3088–3121. doi:10.1039/c5cs00781j.
- [197] M. Raposo, R.S. Pontes, L.H.C. Mattoso, O.N. Oliveira, Kinetics of Adsorption of Poly(*o*-methoxyaniline) Self-Assembled Films, *Macromolecules.* 30 (1997) 6095–6101. doi:10.1021/ma970228f.
- [198] D. Kovacevic, S. Van der Burgh, A. De Keizer, M.A. Cohen Stuart, Kinetics of formation and dissolution of weak polyelectrolyte multilayers: Role of salt and free polyions, *Langmuir.* 18 (2002) 5607–5612. doi:10.1021/la025639q.
- [199] P.J. Yoo, N.S. Zacharia, J. Doh, K.T. Nam, A.M. Belcher, P.T. Hammond, Controlling surface mobility in interdiffusing polyelectrolyte multilayers, *ACS Nano.* 2 (2008) 561–571. doi:10.1021/nn700404y.
- [200] P.J. Yoo, K.T. Nam, J. Qi, S.-K. Lee, J. Park, A.M. Belcher, P.T. Hammond, Spontaneous assembly of viruses on multilayered polymer surfaces, *Nat. Mater.* 5 (2006) 234–240. doi:10.1038/nmat1596.
- [201] A.M. Díez-Pascual, P.S. Shuttleworth, Layer-by-layer assembly of biopolyelectrolytes onto thermo/pH-responsive micro/nano-gels, *Materials (Basel).* 7 (2014) 7472–7512. doi:10.3390/ma7117472.
- [202] L. Wang, Z. Wang, X. Zhang, J. Shen, L. Chi, H. Fuchs, A new approach for the fabrication of an alternating multilayer film of poly(4-vinylpyridine) and poly(acrylic acid) based on hydrogen bonding, *Macromol. Rapid Commun.* 18 (1997) 509–514. doi:10.1002/marc.1997.030180609.
- [203] W.B. Stockton, M.F. Rubner, Molecular-level processing of conjugated polymers. 4. Layer-by-layer manipulation of polyaniline via hydrogen-bonding interactions, *Macromolecules.* 30 (1997) 2717–2725. doi:10.1021/ma9700486.
- [204] S.A. Sukhishvili, S. Granick, Layered, erasable, ultrathin polymer films [7], *J. Am. Chem. Soc.* 122 (2000) 9550–9551. doi:10.1021/ja002410t.
- [205] S.A. Sukhishvili, S. Granick, Layered, erasable polymer multilayers formed by hydrogen-bonded sequential self-assembly, *Macromolecules.* 35 (2002) 301–

310. doi:10.1021/ma011346c.
- [206] E.B. Adatoz, S. Hendessi, C.W. Ow-Yang, A.L. Demirel, Restructuring of poly(2-ethyl-2-oxazoline)/tannic acid multilayers into fibers, *Soft Matter*. 14 (2018) 3849–3857. doi:10.1039/c8sm00381e.
- [207] K. Ariga, J.P. Hill, Q. Ji, Biomaterials and biofunctionality in layered macromolecular assemblies, *Macromol. Biosci.* 8 (2008) 981–990. doi:10.1002/mabi.200800102.
- [208] I. Erel, H. Schlaad, A.L. Demirel, Effect of structural isomerism and polymer end group on the pH-stability of hydrogen-bonded multilayers, *J. Colloid Interface Sci.* 361 (2011) 477–482. doi:10.1016/j.jcis.2011.05.033.
- [209] A.B. Da Fonseca Antunes, M. Dierendonck, G. Vancoillie, J.P. Remon, R. Hoogenboom, B.G. De Geest, Hydrogen bonded polymeric multilayer films assembled below and above the cloud point temperature, *Chem. Commun.* 49 (2013) 9663–9665. doi:10.1039/c3cc45068f.
- [210] A. Sundaramurthy, M. Vergaelen, S. Maji, R. Auzély-Velty, Z. Zhang, B.G. De Geest, R. Hoogenboom, Hydrogen Bonded Multilayer Films Based on Poly(2-oxazoline)s and Tannic Acid, *Adv. Healthc. Mater.* 3 (2014) 2040–2047. doi:10.1002/adhm.201400377.
- [211] S. Hendessi, P. Tatar Guner, A. Miko, A.L. Demirel, Hydrogen bonded multilayers of poly(2-ethyl-2-oxazoline) stabilized silver nanoparticles and tannic acid, *Eur. Polym. J.* 88 (2017) 666–678. doi:10.1016/j.eurpolymj.2016.10.039.
- [212] Y. Li, T. Pan, J. Liu, J. Sun, Healable Antifouling Films Composed of Partially Hydrolyzed Poly(2-ethyl-2-oxazoline) and Poly(acrylic acid), *ACS*. 9 (2017) 14429–14436. doi:10.1021/acsami.7b02872.
- [213] G. Paramasivam, M. Vergaelen, M.R. Ganesh, R. Hoogenboom, A. Sundaramurthy, Hydrogen bonded capsules by layer-by-layer assembly of tannic acid and poly(2-N-propyl-2-oxazoline) for encapsulation and release of macromolecules, *J. Mater. Chem. B*. 5 (2017) 8967–8974. doi:10.1039/c7tb02284k.
- [214] T. He, D. Jańczewski, S. Guo, S.M. Man, S. Jiang, W.S. Tan, Stable pH responsive layer-by-layer assemblies of partially hydrolysed poly(2-ethyl-2-oxazoline) and poly(acrylic acid) for effective prevention of protein, cell and

- bacteria surface attachment, *Colloids Surfaces B Biointerfaces*. 161 (2018) 269–278. doi:10.1016/j.colsurfb.2017.10.031.
- [215] N. Toncheva, C. Tsvetanov, S. Rangelov, B. Trzebicka, A. Dworak, Hydroxyl end-functionalized poly(2-isopropyl oxazoline)s used as nano-sized colloidal templates for preparation of hollow polymeric nanocapsules, *Polym. (United Kingdom)*. 54 (2013) 5166–5173. doi:10.1016/j.polymer.2013.07.042.
- [216] C. Legros, M.C. De Pauw-Gillet, K.C. Tam, S. Lecommandoux, D. Taton, PH and redox responsive hydrogels and nanogels made from poly(2-ethyl-2-oxazoline), *Polym. Chem.* 4 (2013) 4801–4808. doi:10.1039/c3py00685a.
- [217] M. Sedlák, Č. Koňák, A new approach to polymer self-assembly into stable nanoparticles: Poly(ethylacrylic acid) homopolymers, *Macromolecules*. 42 (2009) 7430–7438. doi:10.1021/ma9015032.
- [218] R. Nagarajan, K. Ganesh, Block copolymer self-assembly in selective solvents: Spherical micelles with segregated cores, *J. Chem. Phys.* 90 (1989) 5843–5856. doi:10.1063/1.456390.
- [219] M. Karayianni, S. Pispas, *Fluorescence Studies of Polymer Containing Systems*, Springer International Publishing Switzerland, Basel, 2016. doi:10.1007/978-3-319-26788-3.
- [220] Z. Sui, J.A. Jaber, J.B. Schlenoff, Polyelectrolyte complexes with pH-tunable solubility, *Macromolecules*. 39 (2006) 8145–8152. doi:10.1021/ma061098q.
- [221] K.W. Mattison, P.L. Dubin, I.J. Brittain, Complex Formation between Bovine Serum Albumin and Strong Polyelectrolytes: Effect of Polymer Charge Density, *J. Phys. Chem. B*. 102 (1998) 3830–3836. doi:10.1021/jp980486u.
- [222] G.D. Poe, W.L. Jarrett, C.W. Scales, C.L. McCormick, Enhanced Coil Expansion and Intrapolymer Complex Formation of Linear Poly(methacrylic acid) Containing Poly(ethylene glycol) Grafts, *Macromolecules*. 37 (2004) 2603–2612. doi:10.1021/ma035261i.
- [223] A.F. Thunemann, Polyelectrolyte-surfactant complexes (synthesis, structure and materials aspects), *Progr. Polymer Sci.* 27 (2002) 1473–1572.
- [224] E.E. Makhaeva, H. Tenhu, A.R. Khokhlov, Conformational changes of poly(vinylcaprolactam) macromolecules and their complexes with ionic surfactants in aqueous solution, *Macromolecules*. 31 (1998) 6112–6118. doi:10.1021/ma980158s.

- [225] J. Du, H. Willcock, J.P. Patterson, I. Portman, R.K. O'Reilly, Self-assembly of hydrophilic homopolymers: A matter of RAFT end groups, *Small*. 7 (2011) 2070–2080. doi:10.1002/sml.201100382.
- [226] X. Yu, S. Zhong, X. Li, Y. Tu, S. Yang, R.M. Van Horn, C. Ni, D.J. Pochan, R.P. Quirk, C. Wesdemiotis, W. Bin Zhang, S.Z.D. Cheng, A giant surfactant of polystyrene-(carboxylic acid-functionalized polyhedral oligomeric silsesquioxane) amphiphile with highly stretched polystyrene tails in micellar assemblies, *J. Am. Chem. Soc.* 132 (2010) 16741–16744. doi:10.1021/ja1078305.
- [227] Z. Hordyjewicz-Baran, L. You, B. Smarsly, R. Sigel, H. Schlaad, Bioinspired polymer vesicles based on hydrophilically modified polybutadienes, *Macromolecules*. 40 (2007) 3901–3903. doi:10.1021/ma070347n.
- [228] S. Arumugam, D.R. Vutukuri, S. Thayumanavan, V. Ramamurthy, Amphiphilic homopolymer as a reaction medium in water: Product selectivity within polymeric nanopockets, *J. Am. Chem. Soc.* 127 (2005) 13200–13206. doi:10.1021/ja051107v.
- [229] B. Hammouda, D.L. Ho, S. Kline, Insight into Clustering in Poly (ethylene oxide) Solutions, *Macromolecules*. (2004) 6932–6937. doi:10.1021/ma049623d.
- [230] B. Hammouda, Clustering in polar media, *J. Chem. Phys.* 133 (2010) 1–5. doi:10.1063/1.3484235.
- [231] M. Duval, Monitoring of cluster formation and elimination in PEO solutions, *Macromolecules*. 33 (2000) 7862–7867. doi:10.1021/ma000423l.
- [232] K. Devanand, J.C. Selser, Polyethylene oxide does not necessarily aggregate in water, *Nature*. 343 (1990) 739–741. doi:10.1038/343739a0.
- [233] S. Huber, R. Jordan, Modulation of the lower critical solution temperature of 2-Alkyl-2-oxazoline copolymers, *Colloid Polym. Sci.* 286 (2008) 395–402. doi:10.1007/s00396-007-1781-y.
- [234] T. van Mourik, M. Buhl, M.-P. Gaigeot, Density functional theory across chemistry, physics and biology, *Philos. Trans. R. Soc. A Math. Phys. Eng. Sci.* 372 (2014) 20120488–20120488. doi:10.1098/rsta.2012.0488.
- [235] Y. Zhao, D.G. Truhlar, The M06 suite of density functionals for main group thermochemistry, thermochemical kinetics, noncovalent interactions, excited

- states, and transition elements: Two new functionals and systematic testing of four M06-class functionals and 12 other function, *Theor. Chem. Acc.* 120 (2008) 215–241. doi:10.1007/s00214-007-0310-x.
- [236] M.J. Frisch, G.W. Trucks, H.B. Schlegel, G.E. Scuseria, M.A. Robb, J.R. Cheeseman, G. Scalmani, V. Barone, B. Mennucci, G.A. Petersson, H. Nakatsuji, M. Caricato, X. Li, H.P. Hratchian, A.F. Izmaylov, J. Bloino, G. Zheng, J.L. Sonnenberg, M. Hada, M. Ehara, K. Toyota, R. Fukuda, J. Hasegawa, M. Ishida, T. Nakajima, Y. Honda, O. Kitao, H. Nakai, T. Vreven, J.A. Montgomery Jr., J.E. Peralta, F. Ogliaro, M. Bearpark, J.J. Heyd, E. Brothers, K.N. Kudin, V.N. Staroverov, R. Kobayashi, J. Normand, K. Raghavachari, A. Rendell, J.C. Burant, S.S. Iyengar, J. Tomasi, M. Cossi, N. Rega, J.M. Millam, M. Klene, J.E. Knox, J.B. Cross, V. Bakken, C. Adamo, J. Jaramillo, R. Gomperts, R.E. Stratmann, O. Yazyev, A.J. Austin, R. Cammi, C. Pomelli, J.W. Ochterski, R.L. Martin, K. Morokuma, V.G. Zakrzewski, G.A. Voth, P. Salvador, J.J. Dannenberg, S. Dapprich, A.D. Daniels, Ö. Farkas, J.B. Foresman, J. V. Ortiz, J. Cioslowski, D.J. Fox, Gaussian 09, Revision D.01, Gaussian Inc. (2009) Wallingford CT. doi:10.1159/000348293.
- [237] A.D. Becke, Density-functional thermochemistry. III. The role of exact exchange, *J. Chem. Phys.* 98 (1993) 5648–5652. doi:10.1063/1.464913.
- [238] P.J. Stephens, F.J. Devlin, C.F. Chabalowski, M.J. Frisch, Ab Initio calculation of vibrational absorption and circular dichroism spectra using density functional force fields, *J. Phys. Chem.* 98 (1994) 11623–11627. doi:10.1021/j100096a001.
- [239] B. Delley, *Modern Density Functional Theory: A Tool for Chemistry*, 2nd ed., Elsevier Science, Amsterdam, 1995.
- [240] B. Delley, Analytic energy derivatives in the numerical local-density-functional approach, *J. Chem. Phys.* 94 (1991) 7245–7250. doi:10.1063/1.460208.
- [241] S. Grimme, Semiempirical GGA-Type Density Functional Constructed with a Long-Range Dispersion Correction, *J. Comput. Chem.* 27 (2006) 1787–1799. doi:10.1002/jcc.
- [242] B. Delley, The conductor-like screening model for polymers and surfaces, *Mol. Simul.* 32 (2006) 117–123. doi:10.1080/08927020600589684.
- [243] B. Mennucci, E. Cancès, J. Tomasi, Evaluation of Solvent Effects in Isotropic and Anisotropic Dielectrics and in Ionic Solutions with a Unified Integral

- Equation Method: Theoretical Bases, Computational Implementation, and Numerical Applications, *J. Phys. Chem. B.* 101 (1997) 10506–10517. doi:10.1021/jp971959k.
- [244] D. Frenkel, B. Smit, *Understanding Molecular Simulation From Algorithms to Application*, Second, Academic Press. A Division of Harcourt, Inc., 2002. doi:10.1063/1.4822570.
- [245] P. Kollman, Free Energy Calculations: Applications to Chemical and Biochemical Phenomena, *Chem. Rev.* 93 (1993) 2395–2417. doi:10.1021/cr00023a004.
- [246] T. Steinbrecher, I. Joung, D.A. Case, Soft-core potentials in thermodynamic integration: Comparing one- and two-step transformations, *J. Comput. Chem.* 32 (2011) 3253–3263. doi:10.1002/jcc.21909.
- [247] T. Steinbrecher, D.L. Mobley, D.A. Case, Nonlinear scaling schemes for Lennard-Jones interactions in free energy calculations, *J. Chem. Phys.* 127 (2007). doi:10.1063/1.2799191.
- [248] H. Sun, COMPASS: An ab Initio Force-Field Optimized for Condensed-Phase Applications Overview with Details on Alkane and Benzene Compounds, *J. Phys. Chem. B.* 102 (1998) 7338–7364. doi:10.1021/jp980939v.
- [249] D.J. Kim, C.H. Park, S.Y. Nam, Molecular dynamics simulations of modified PEEK polymeric membrane for fuel cell application, *Int. J. Hydrogen Energy.* 41 (2016) 7641–7648. doi:10.1016/j.ijhydene.2015.12.220.
- [250] M. Blanco, Molecular silverware. I. General solutions to excluded volume constrained problems, *J. Comput. Chem.* 12 (1991) 237–247. doi:10.1002/jcc.540120214.
- [251] C.F. Fan, B.D. Olafson, M. Blanco, S.L. Hsu, Application of Molecular Simulation To Derive Phase Diagrams of Binary Mixtures, *Macromolecules.* 25 (1992) 3667–3676. doi:10.1021/ma00040a010.
- [252] C. Pietsch, A. Vollrath, R. Hoogenboom, U.S. Schubert, A fluorescent thermometer based on a pyrene-labeled thermoresponsive polymer, *Sensors.* 10 (2010) 7979–7990. doi:10.3390/s100907979.
- [253] E.N. Savariar, S. V. Aathimanikandan, S. Thayumanavan, Supramolecular assemblies from amphiphilic homopolymers: Testing the scope, *J. Am. Chem. Soc.* 128 (2006) 16224–16230. doi:10.1021/ja065213o.

- [254] R. Obeid, E. Maltseva, A.F. Thünemann, F. Tanaka, F.M. Winnik, Temperature response of self-assembled micelles of telechelic hydrophobically modified poly(2-alkyl-2-oxazoline)s in water, *Macromolecules*. 42 (2009) 2204–2214. doi:10.1021/ma802592f.
- [255] A.M. Bivigou-Koumba, E. Görnitz, A. Laschewsky, P. Müller-Buschbaum, C.M. Papadakis, Thermoresponsive amphiphilic symmetrical triblock copolymers with a hydrophilic middle block made of poly(N-isopropylacrylamide): Synthesis, self-organization, and hydrogel formation, *Colloid Polym. Sci.* 288 (2010) 499–517. doi:10.1007/s00396-009-2179-9.
- [256] V. Castelletto, I.W. Hamley, Y. Ma, X. Bories-Azeau, S.P. Armes, A.L. Lewis, Microstructure and physical properties of a pH-responsive gel based on a novel biocompatible ABA-type triblock copolymer, *Langmuir*. 20 (2004) 4306–4309. doi:10.1021/la049859a.
- [257] A. Desii, F. Chiellini, C. Duce, L. Ghezzi, S. Monti, M.R. Tiné, R. Solaro, Influence of structural features on the self-assembly of short ionic oligopeptides, *J. Polym. Sci. Part A Polym. Chem.* 48 (2010) 889–897. doi:10.1002/pola.23840.
- [258] S.Y. Fung, C. Keyes, J. Duhamel, P. Chen, Concentration Effect on the Aggregation of a Self-Assembling Oligopeptide, *Biophys. J.* 85 (2003) 537–548. doi:10.1016/S0006-3495(03)74498-1.
- [259] E. Kesselman, O. Ramon, R. Berkovici, Y. Paz, ATR-FTIR studies on the effect of strong salting-out salts on the phase separation scenario in aqueous solutions of poly(N-isopropylacrylamide) [PNIPA], *Polym. Adv. Technol.* 13 (2002) 982–991. doi:10.1002/pat.279.
- [260] D. DHARA, P.R. CHATTERJI, Phase Transition in Linear and Cross-Linked Poly(*N*-Isopropylacrylamide) in Water: Effect of Various Types of Additives, *J. Macromol. Sci. Part C Polym. Rev.* 40 (2000) 51–68. doi:10.1081/MC-100100578.
- [261] L.F. McDevit, WF, Activity Coefficients of Nonelectrolyte Solutes in Aqueous Salt Solutions, *J. Phys. Chem.* (1951) 119–169.
- [262] S. Saito, M. Konno, H. Inomata, Volume Phase Transition of *N*-Alkylacrylamide Gels, *Adv. Polym. Sci.* 109 (1993) 207–232. doi:10.1295/kobunshi.54.462.

- [263] P.H. Von Hippel, a Hamabata, Model studies on the effects of neutral salts on the conformational stability of biological macromolecules., *J. Mechanochem. Cell Motil.* 2 (1973) 127–138.
- [264] X.M. Liu, L.S. Wang, L. Wang, J. Huang, C. He, The effect of salt and pH on the phase-transition behaviors of temperature-sensitive copolymers based on N-isopropylacrylamide, *Biomaterials.* 25 (2004) 5659–5666. doi:10.1016/j.biomaterials.2004.01.019.
- [265] M.K. Yoo, Y.K. Sung, Y.M. Lee, C.S. Cho, Effect of polyelectrolyte on the lower critical solution temperature of poly(N-isopropyl acrylamide) in the poly(NIPAAm-co-acrylic acid) hydrogel, *Polymer (Guildf).* 41 (2000) 5713–5719. doi:10.1016/S0032-3861(99)00779-X.
- [266] F.A. Plamper, A. Schmalz, M. Ballauff, A.H.E. Müller, Tuning the thermoresponsiveness of weak polyelectrolytes by pH and light: Lower and upper critical-solution temperature of poly(N,N-dimethylaminoethyl methacrylate), *J. Am. Chem. Soc.* 129 (2007) 14538–14539. doi:10.1021/ja074720i.
- [267] C. Gao, B. Chen, H. Möhwald, Thermosensitive poly(allylamine)-g-poly(N-isopropylacrylamide) copolymers: Salt-tuned phase separation, particle formation and their applicability on curved surface, *Colloids Surfaces A Physicochem. Eng. Asp.* 272 (2006) 203–210. doi:10.1016/j.colsurfa.2005.07.023.
- [268] M. Casolaro, Thermodynamic Behavior of Polyelectrolytes with the Lower Critical Solution Temperature (LCST) Phenomenon, *Polym. Adv. Technol.* 7 (1996) 831338.
- [269] H. Maeda, G.Y. Bharate, J. Daruwalla, Polymeric drugs for efficient tumor-targeted drug delivery based on EPR-effect, *Eur. J. Pharm. Biopharm.* 71 (2009) 409–419. doi:10.1016/j.ejpb.2008.11.010.
- [270] B. Mandal, K.K. Halder, S.K. Dey, M. Bhoumik, M.C. Debnath, L.K. Ghosh, Development and physical characterization of chloramphenicol loaded biodegradable nanoparticles for prolonged release, *Pharmazie.* 64 (2009) 445–449. doi:10.1691/ph.2009.8274.
- [271] M. Sedláč, Homopolymer self-assembly into stable nanoparticles: Concerted action of hydrophobic association and hydrogen bonding in thermoresponsive poly(alkylacrylic acid)s, *J. Phys. Chem. B.* 116 (2012) 2356–2364.

doi:10.1021/jp208445p.

- [272] C. Allen, Y. Yu, D. Maysinger, A. Eisenberg, Polycaprolactone-b-poly(ethylene oxide) block copolymer micelles as a novel drug delivery vehicle for neurotrophic agents FK506 and L-685,818, *Bioconjug. Chem.* 9 (1998) 564–572. doi:10.1021/bc9702157.
- [273] B.S. Förster, M. Antonietti, Amphiphilic Block Copolymers in Structure-Controlled Nanomaterial Hybrids, *Adv. Mater.* 10 (1998) 195–217. doi:10.1002/(SICI)1521-4095(199802)10:3<195::AID-ADMA195>3.0.CO;2-V.
- [274] C. Ma, P. Pan, G. Shan, Y. Bao, M. Fujita, M. Maeda, Core-Shell structure, biodegradation, and drug release behavior of poly(lactic acid)/poly(ethylene glycol) block copolymer micelles tuned by macromolecular stereostructure, *Langmuir.* 31 (2015) 1527–1536. doi:10.1021/la503869d.
- [275] D. Maysinger, O. Berezovska, R. Savic, P. Lim Soo, A. Eisenberg, Block copolymers modify the internalization of micelle-incorporated probes into neural cells, *Biochim. Biophys. Acta - Mol. Cell Res.* 1539 (2001) 205–217. doi:10.1016/S0167-4889(01)00110-0.
- [276] P. Yusan, I. Tuncel, V. Bütün, A.L. Demirel, I. Erel-Goktepe, PH-responsive layer-by-layer films of zwitterionic block copolymer micelles, *Polym. Chem.* 5 (2014) 3777–3787. doi:10.1039/c4py00040d.
- [277] D. Michael, I. Benjamin, Structure, Dynamics, and Electronic Spectrum of N , N '-Diethyl- p -nitroaniline at Water Interfaces. A Molecular Dynamics Study, *J. Phys. Chem. B.* 102 (1998) 5145–5151. doi:10.1021/jp9811068.
- [278] C. Hippus, V. Bütün, I. Erel-Goktepe, Bacterial anti-adhesive properties of a monolayer of zwitterionic block copolymer micelles, *Mater. Sci. Eng. C.* 41 (2014) 354–362. doi:10.1016/j.msec.2014.04.023.
- [279] Y. Chen, Y. Pang, J. Wu, Y. Su, J. Liu, R. Wang, B. Zhu, Y. Yao, D. Yan, X. Zhu, Q. Chen, Controlling the particle size of interpolymer complexes through host-guest interaction for drug delivery, *Langmuir.* 26 (2010) 9011–9016. doi:10.1021/la9048133.
- [280] R. Mészáros, L. Thompson, M. Bos, I. Varga, T. Gilányi, Interaction of sodium dodecyl sulfate with polyethyleneimine: Surfactant-induced polymer solution colloid dispersion transition, *Langmuir.* 19 (2003) 609–615.

doi:10.1021/la026616e.

- [281] X. Cui, S. Mao, M. Liu, H. Yuan, Y. Du, Mechanism of Surfactant Micelle Formation Mechanism of Surfactant Micelle Formation, *Langmuir*. 24 (2008) 10771–10775. doi:10.1021/la801705y.
- [282] B. Hammouda, D.L. Ho, S. Kline, Insight into clustering in poly(ethylene oxide) solutions, *Macromolecules*. 37 (2004) 6932–6937. doi:10.1021/ma049623d.
- [283] J. Ulbricht, R. Jordan, R. Luxenhofer, On the biodegradability of polyethylene glycol, polypeptoids and poly(2-oxazoline)s, *Biomaterials*. 35 (2014) 4848–4861. doi:10.1016/j.biomaterials.2014.02.029.
- [284] R. Takahashi, T. Sato, K. Terao, X.P. Qiu, F.M. Winnik, Self-association of a thermosensitive poly(alkyl-2-oxazoline) block copolymer in aqueous solution, *Macromolecules*. 45 (2012) 6111–6119. doi:10.1021/ma300969w.
- [285] E. Cagli, E. Yildirim, S.-W. Yang, I. Erel-Goktepe, An experimental and computational approach to pH-dependent self-aggregation of poly(2-isopropyl-2-oxazoline), *J. Polym. Sci. Part B Polym. Phys.* 57 (2019) 210–221. doi:https://doi.org/10.1002/polb.24773.
- [286] G.Y. Lee, K. Park, S.Y. Kim, Y. Byun, MMPs-specific PEGylated peptide-DOX conjugate micelles that can contain free doxorubicin, *Eur. J. Pharm. Biopharm.* 67 (2007) 646–654. doi:10.1016/j.ejpb.2007.03.023.
- [287] H.S. Yoo, K.H. Lee, J.E. Oh, T.G. Park, In vitro and in vivo anti-tumor activities of nanoparticles based on doxorubicin-PLGA conjugates, *J. Control. Release*. 68 (2000) 419–431. doi:10.1016/S0168-3659(00)00280-7.
- [288] H.S. Yoo, T.G. Park, Biodegradable polymeric micelles composed of doxorubicin conjugated PLGA-PEG block copolymer, *J. Control. Release*. 70 (2001) 63–70. doi:10.1016/S0168-3659(00)00340-0.
- [289] C. Matsumoto, P. D, S. Mishima, Y. Shimomura, Methicillin-Resistant Staphylococcus aureus and Staphylococcus Ocular Surface Infection Efficacy of Chloramphenicol Eye Drops, 0 (2002) 86–89. doi:10.1097/01.1C0.000(K)2934.
- [290] C. Krumm, S. Harmuth, M. Hijazi, B. Neugebauer, A. Kampmann, H. Geltenpoth, A. Sickmann, Antimicrobial Poly (2-methyloxazoline) s with Bioswitchable Activity through Satellite Group Modifi- cation **, *Angew.*

Commun. (2014) 3830–3834. doi:10.1002/anie.201311150.

- [291] B.C.J. Waschinski, J. Zimmermann, U. Salz, R. Hutzler, G. Sadowski, J.C. Tiller, Design of Contact-Active Antimicrobial Acrylate-Based Materials Using Biocidal Macromers, *Adv. Mater.* (2008) 104–108. doi:10.1002/adma.200701095.
- [292] V. Gomes, V.D.B. Bonifácio, G. Moutinho-fragoso, Green Synthesis of 2-Oxazoline-Based Microbicidal Polymers, in: *II Iberoam. Conf. Supercrit. Fluid*, 2010: pp. 1–7.
- [293] R.J. Anderson, P.W. Groundwater, A. Todd, A.J. Worsley, *Antibacterial Agents: Chemistry, Mode of Action, Mechanisms of Resistance and Clinical Applications*, 2012.
- [294] M.C. Das, A. Biswas, M. Chowdhury, J. Saha, Screening Antimicrobial Susceptibility of Gentamicin, Vancomycin, Azithromycin, Chloramphenicol and Cefotaxime Against Selected Gram Positive and Gram Negative Bacteria, *2* (2014) 324–331.
- [295] V. Kiruthika, S. Maya, M.K. Suresh, V. Anil Kumar, R. Jayakumar, R. Biswas, Comparative efficacy of chloramphenicol loaded chondroitin sulfate and dextran sulfate nanoparticles to treat intracellular Salmonella infections, *Colloids Surfaces B Biointerfaces*. 127 (2015) 33–40. doi:10.1016/j.colsurfb.2015.01.012.
- [296] R. Obeid, J.Y. Park, R.C. Advincula, F.M. Winnik, Temperature-dependent interfacial properties of hydrophobically end-modified poly(2-isopropyl-2-oxazoline)s assemblies at the air/water interface and on solid substrates, *J. Colloid Interface Sci.* 340 (2009) 142–152. doi:10.1016/j.jcis.2009.06.060.
- [297] A.L.Z. Lee, S. Venkataraman, S.B.M. Sirat, S. Gao, J.L. Hedrick, Y.Y. Yang, The use of cholesterol-containing biodegradable block copolymers to exploit hydrophobic interactions for the delivery of anticancer drugs, *Biomaterials*. 33 (2012) 1921–1928. doi:10.1016/j.biomaterials.2011.11.032.
- [298] S.H. Kim, J.P.K. Tan, F. Nederberg, K. Fukushima, J. Colson, C. Yang, A. Nelson, Y.Y. Yang, J.L. Hedrick, Hydrogen bonding-enhanced micelle assemblies for drug delivery, *Biomaterials*. 31 (2010) 8063–8071. doi:10.1016/j.biomaterials.2010.07.018.
- [299] R. Yang, S. Zhang, D. Kong, X. Gao, Y. Zhao, Z. Wang, Biodegradable

- polymer-curcumin conjugate micelles enhance the loading and delivery of low-potency curcumin, *Pharm. Res.* 29 (2012) 3512–3525. doi:10.1007/s11095-012-0848-8.
- [300] B. Pidhatika, M. Rodenstein, Y. Chen, E. Rakhmatullina, A. Mühlebach, C. Acikgöz, M. Textor, R. Konradi, Comparative stability studies of Poly(2-methyl-2-oxazoline) and Poly(ethylene glycol) brush coatings, *Biointerphases.* 7 (2012). doi:10.1007/s13758-011-0001-y.
- [301] S.A. Sukhishvili, S. Granick, Layered, Erasable, Ultrathin Polymer Films, *J. Am. Chem. Soc.* 122 (2000) 9550–9551. doi:10.1021/ja002410t.
- [302] H. Jeong, J. Hwang, H. Lee, P.T. Hammond, J. Choi, J. Hong, In vitro blood cell viability profiling of polymers used in molecular assembly, *Sci. Rep.* 7 (2017) 1–13. doi:10.1038/s41598-017-10169-5.
- [303] A.B. da Fonseca Antunes, M. Dierendonck, G. Vancoillie, J.P. Remon, R. Hoogenboom, B.G. De Geest, Hydrogen bonded polymeric multilayer films assembled below and above the cloud point temperature, *Chem. Commun.* 49 (2013) 9663. doi:10.1039/c3cc45068f.
- [304] C. Su, J. Sun, X. Zhang, D. Shen, S. Yang, Hydrogen-bonded polymer complex thin film of poly(2-oxazoline) and poly(acrylic acid), *Polymers (Basel).* 9 (2017). doi:10.3390/polym9080363.
- [305] E.B. Adatoz, S. Hendessi, C.W. Ow-yang, Restructuring of poly(2-ethyl-2-oxazoline)/tannic acid multilayers into fibers, *Soft Matter.* 14 (2018) 3849–3857. doi:10.1039/C8SM00381E.
- [306] K. Kempe, S.L. Ng, K.F. Noi, M. Müllner, S.T. Gunawan, F. Caruso, Clickable poly(2-oxazoline) architectures for the fabrication of low-fouling polymer capsules, *ACS Macro Lett.* 2 (2013) 1069–1072. doi:10.1021/mz400522e.
- [307] K. Kempe, S.L. Ng, S.T. Gunawan, K.F. Noi, F. Caruso, Intracellularly degradable hydrogen-bonded polymer capsules, *Adv. Funct. Mater.* 24 (2014) 6187–6194. doi:10.1002/adfm.201401397.
- [308] Y. Li, T. Pan, B. Ma, J. Liu, J. Sun, Healable Antifouling Films Composed of Partially Hydrolyzed Poly(2-ethyl-2-oxazoline) and Poly(acrylic acid), *ACS Appl. Mater. Interfaces.* 9 (2017) 14429–14436. doi:10.1021/acsami.7b02872.
- [309] E. Kharlampieva, V. Koziorskaya, S.A. Sukhishvili, Layer-by-layer hydrogen-bonded polymer films: From fundamentals to applications, *Adv. Mater.* 21

- (2009) 3053–3065. doi:10.1002/adma.200803653.
- [310] N.J. Baxter, T.H. Lilley, E. Haslam, M.P. Williamson, Multiple interactions between polyphenols and a salivary proline-rich protein repeat result in complexation and precipitation, *Biochemistry*. 36 (1997) 5566–5577. doi:10.1021/bi9700328.
- [311] I. Erel-Unal, S.A. Sukhishvili, Hydrogen-bonded multilayers of a neutral polymer and a polyphenol, *Macromolecules*. 41 (2008) 3962–3970. doi:10.1021/ma800186q.
- [312] T. Shutava, M. Prouty, D. Kommireddy, Y. Lvov, pH responsive decomposable layer-by-layer nanofilms and capsules on the basis of tannic acid, *Macromolecules*. 38 (2005) 2850–2858. doi:10.1021/ma047629x.
- [313] E. Kharlampieva, S.A. Sukhishvili, Hydrogen - Bonded Layer - by - Layer Polymer Films Hydrogen-Bonded Layer-by-Layer Polymer Films, 1797 (2006). doi:10.1080/15583720600945386.
- [314] Y.N. Jin, H.C. Yang, H. Huang, Z.K. Xu, Underwater superoleophobic coatings fabricated from tannic acid-decorated carbon nanotubes, *RSC Adv*. 5 (2015) 16112–16115. doi:10.1039/c4ra16074f.
- [315] Z. Zhang, T. Chao, S. Chen, S. Jiang, Superlow fouling sulfobetaine and carboxybetaine polymers on glass slides, *Langmuir*. 22 (2006) 10072–10077. doi:10.1021/la062175d.
- [316] C. Gu, K.G. Karthikeyan, Sorption of the antimicrobial ciprofloxacin to aluminum and iron hydrous oxides, *Environ. Sci. Technol*. 39 (2005) 9166–9173. doi:10.1021/es051109f.
- [317] T. Ueno, H. Tsuchiya, M. Mizogami, K. Takakura, Local anesthetic failure associated with inflammation: verification of the acidosis mechanism and the hypothetic participation of inflammatory peroxynitrite, *J. Inflamm. Res*. 1 (2008) 41–48. doi:10.2147/JIR.S3982.
- [318] E. Kharlampieva, V. Kozlovskaya, J. Tyutina, S.A. Sukhishvili, Hydrogen-bonded multilayers of thermoresponsive polymers, *Macromolecules*. 38 (2005) 10523–10531. doi:10.1021/ma0516891.
- [319] V. V. Khutoryanskiy, Z.S. Nurkeeva, G.A. Mun, A. V. Dubolazov, Effect of temperature on aggregation/dissociation behavior of interpolymer complexes stabilized by hydrogen bonds, *J. Appl. Polym. Sci*. 93 (2004) 1946–1950.

doi:10.1002/app.20661.

- [320] R.A. McAloney, V. Dudnik, M.C. Goh, Kinetics of salt-induced annealing of a polyelectrolyte multilayer film morphology, *Langmuir*. 19 (2003) 3947–3952. doi:10.1021/la026882s.
- [321] E.J. Begg, R.A. Robson, D.A. Saunders, G.G. Graham, R.C. Buttimore, A.M. Neill, G.I. Town, The pharmacokinetics of oral fleroxacin and ciprofloxacin in plasma and sputum during acute and chronic dosing, *Br. J. Clin. Pharmacol.* 49 (2000) 32–38. doi:10.1046/j.1365-2125.2000.00105.x.
- [322] V.G. Correia, M. Coelho, T. Barroso, V.P. Raje, V.D.B. Bonifácio, T. Casimiro, M.G. Pinho, A. Aguiar-Ricardo, Anti-biofouling 3D porous systems: the blend effect of oxazoline-based oligomers on chitosan scaffolds, *Biofouling*. 29 (2013) 273–282. doi:10.1080/08927014.2013.766172.
- [323] L.A.B. Rawlinson, J.P. O’Gara, D.S. Jones, D.J. Brayden, Resistance of *Staphylococcus aureus* to the cationic antimicrobial agent poly(2-(dimethylamino ethyl)methacrylate) (pDMAEMA) is influenced by cell-surface charge and hydrophobicity, *J. Med. Microbiol.* 60 (2011) 968–976. doi:10.1099/jmm.0.025619-0.
- [324] B. Gottenbos, D.W. Grijsma, H.C. van der Mei, J. Feijen, H.J. Busscher, Antimicrobial effects of positively charged surfaces on adhering Gram-positive and Gram-negative bacteria, *J. Antimicrob. Chemother.* 48 (2001) 7–13. doi:10.1093/jac/48.1.7.
- [325] J.N.. Fong, F.. Yildiz, Biofilm matrix proteins, *Microbiol. Spectr.* 3 (2015) 1–27. doi:10.1128/microbiolspec.MB-0004-2014.Biofilm.
- [326] A. Ducret, G.G. Hardy, Y. V Brun, Negative Bacteria, *Microbiol. Spectr.* 3 (2015) 1–45. doi:10.1128/microbiolspec.MB-0018-2015.Adhesins.
- [327] E. Ostuni, R.G. Chapman, M.N. Liang, G. Meluleni, G. Pier, D.E. Ingber, G.M. Whitesides, Self-assembled monolayers that resist the adsorption of proteins and the adhesion of bacterial and mammalian cells, *Langmuir*. 17 (2001) 6336–6343. doi:10.1021/la010552a.
- [328] R. Zhang, M.M. Jones, H. Moussa, M. Keskar, N. Huo, Z. Zhang, M.B. Visser, C. Sabatini, M.T. Swihart, C. Cheng, Polymer–antibiotic conjugates as antibacterial additives in dental resins, *Biomater. Sci.* 7 (2019) 287–295. doi:10.1039/C8BM01228H.

- [329] R. Tong, J. Cheng, Anticancer polymeric nanomedicines, *Polym. Rev.* 47 (2007) 345–381. doi:10.1080/15583720701455079.
- [330] J. Khandare, T. Minko, Polymer-drug conjugates: Progress in polymeric prodrugs, *Prog. Polym. Sci.* 31 (2006) 359–397. doi:10.1016/j.progpolymsci.2005.09.004.
- [331] N. Aumsuwan, S. Heinhorst, M.W. Urban, Antibacterial surfaces on expanded polytetrafluoroethylene; penicillin attachment, *Biomacromolecules.* 8 (2007) 713–718. doi:10.1021/bm061050k.
- [332] M. Sobczak, E. Witkowska, E. Olędzka, W. Kolodziejcki, Synthesis and structural analysis of polyester prodrugs of norfloxacin, *Molecules.* 13 (2008) 96–106. doi:10.3390/molecules13010096.
- [333] R. Yang, G. Mondal, D. Wen, R.I. Mahato, Combination therapy of paclitaxel and cyclophosphamide polymer-drug conjugates to treat advanced prostate cancer, *Nanomedicine Nanotechnology, Biol. Med.* 13 (2017) 391–401. doi:10.1016/j.nano.2016.07.017.
- [334] E.R. Gillies, J.M.J. Fréchet, pH-Responsive Copolymer Assemblies for Controlled Release of Doxorubicin, *Bioconjug. Chem.* 16 (2005) 361–368. doi:10.1021/bc049851c.
- [335] E.R. Gillies, J.M.J. Fréchet, A new approach towards acid sensitive copolymer micelles for drug delivery, *Chem. Commun.* (2003) 1640–1641.
- [336] Y. Jin, L. Song, Y. Su, L. Zhu, Y. Pang, F. Qiu, G. Tong, D. Yan, B. Zhu, X. Zhu, Oxime Linkage: A Robust Tool for the Design of pH-Sensitive Polymeric Drug Carriers, *Biomacromolecules.* 12 (2011) 3460–3468. doi:10.1021/bm200956u.
- [337] E.R. Gillies, J.M.J. Fréchet, Development of acid-sensitive copolymer micelles for drug delivery, *Pure Appl. Chem.* 76 (2004) 1295–1307.
- [338] J.B. Matson, S.I. Stupp, ChemComm Drug release from hydrazone-containing peptide amphiphiles w, *Chem. Commun.* 47 (2011) 7962–7964. doi:10.1039/c1cc12570b.
- [339] R. Duncan, Polymer conjugates as anticancer nanomedicines, *Nat. Rev. Cancer.* 6 (2006) 688–701. doi:10.1038/nrc1958.
- [340] J. Li, Y. Zhou, C. Li, D. Wang, Y. Gao, C. Zhang, L. Zhao, Y. Li, Y. Liu, X.

- Li, Poly(2-ethyl-2-oxazoline)-doxorubicin conjugate-based dual endosomal pH-sensitive micelles with enhanced antitumor efficacy, *Bioconjug. Chem.* 26 (2015) 110–119. doi:10.1021/bc5004718.
- [341] R.S. Patel, D.Y. Cho, C. Tian, A. Chang, K.M. Estrellas, D. Lavin, S. Furtado, E. Mathiowitz, Doxycycline delivery from PLGA microspheres prepared by a modified solvent removal method, *J. Microencapsul.* 29 (2012) 344–352. doi:10.3109/02652048.2011.651499.
- [342] G.B. Piccoli, M. Hachemi, I. Molfino, J.P. Coindre, C. Boursot, Doxycycline treatment in dialysis related amyloidosis: Discrepancy between antalgic effect and inflammation, studied with FDG-positron emission tomography: A case report, *BMC Nephrol.* 18 (2017) 1–6. doi:10.1186/s12882-017-0698-z.
- [343] S.B. Cambridge, D. Geissler, S. Keller, B. Cürten, A caged doxycycline analogue for photoactivated gene expression., *Angew. Chemie.* 45 (2006) 2229–31. doi:10.1002/anie.200503339.
- [344] A.F. Casy, A. Yasin, The identification and stereochemical study of tetracycline antibiotics by ¹H nuclear magnetic resonance spectroscopy, *J. Pharm. Biomed. Anal.* 1 (1983) 281–292. doi:10.1016/0731-7085(83)80040-5.

APPENDICES

A. NMR SPECTRA

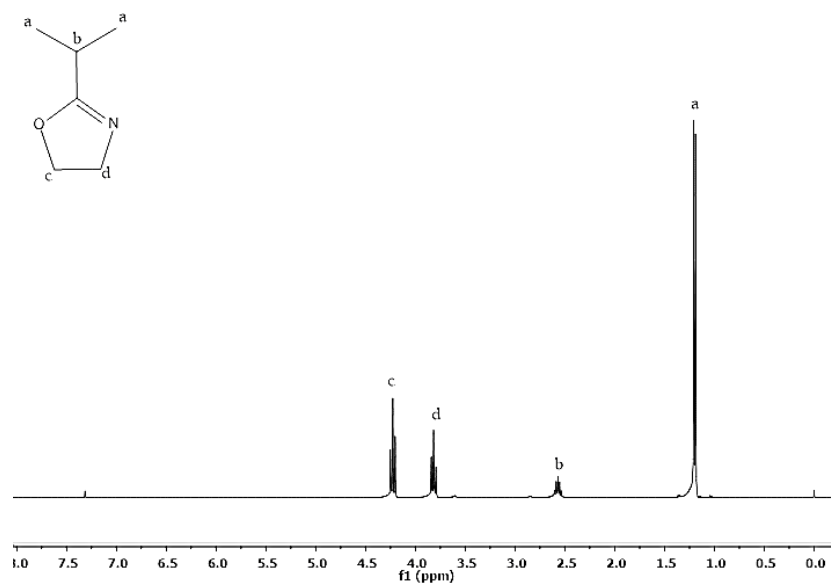


Figure A 1. ¹H-NMR of 2-isopropyl-2-oxazoline.

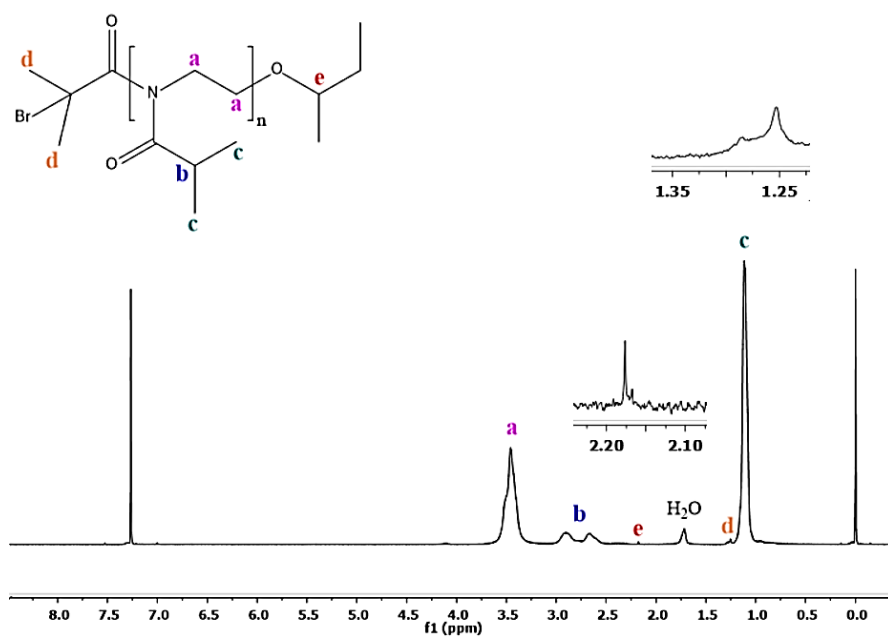


Figure A 2. $^1\text{H-NMR}$ of α -bromo- ω -2-butoxy-PIPOX.

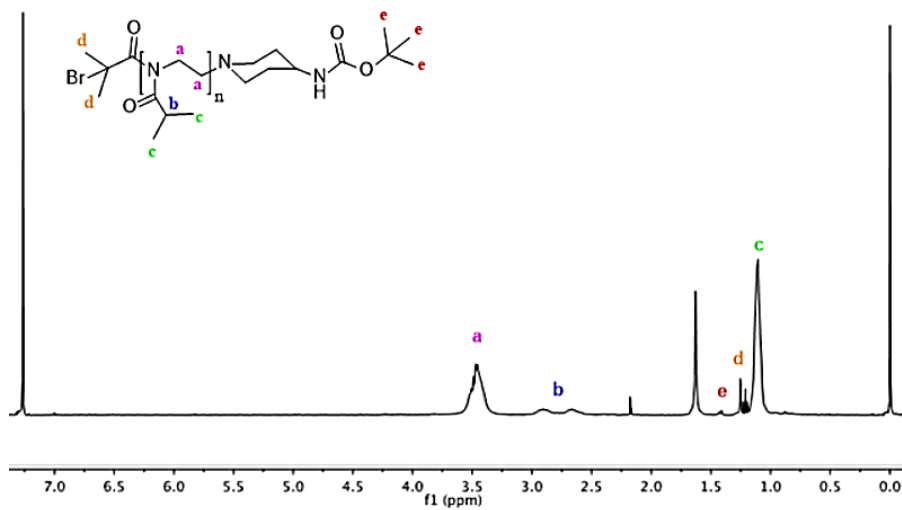


Figure A 3. $^1\text{H-NMR}$ of α -bromo- ω -N-boc-aminopiperidine-PIPOX.

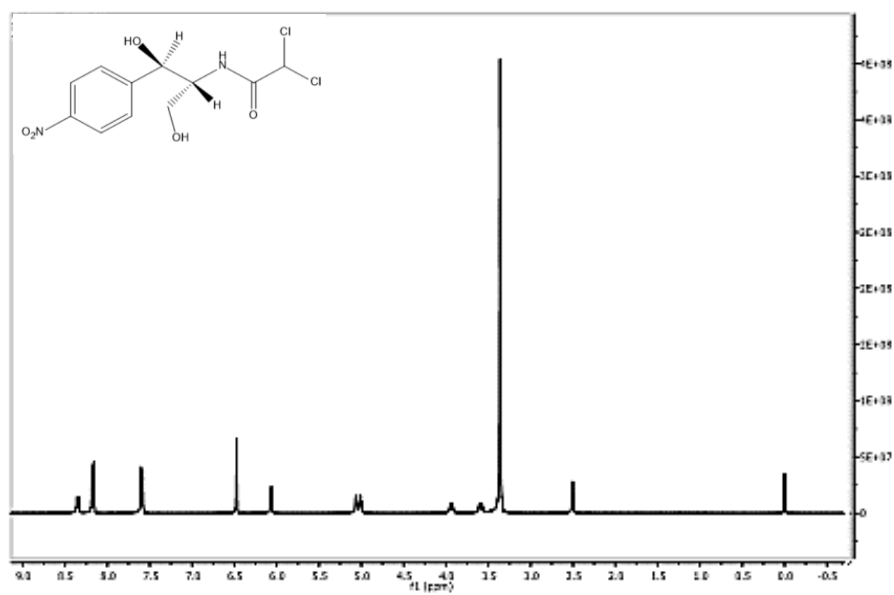


Figure A 4. ¹H-NMR spectra of Chloramphenicol (CAP)

B. GPC CHROMATOGRAMS

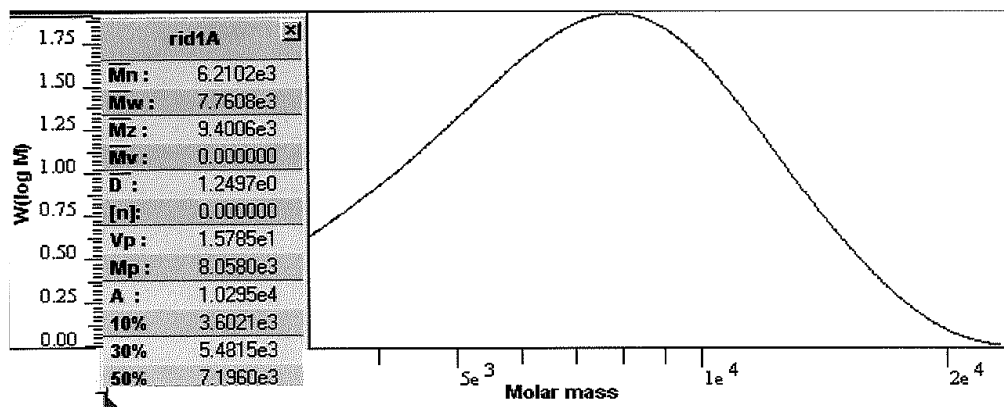


Figure B 1. GPC traces of α -bromo- ω -2-butoxy-PIPOX.

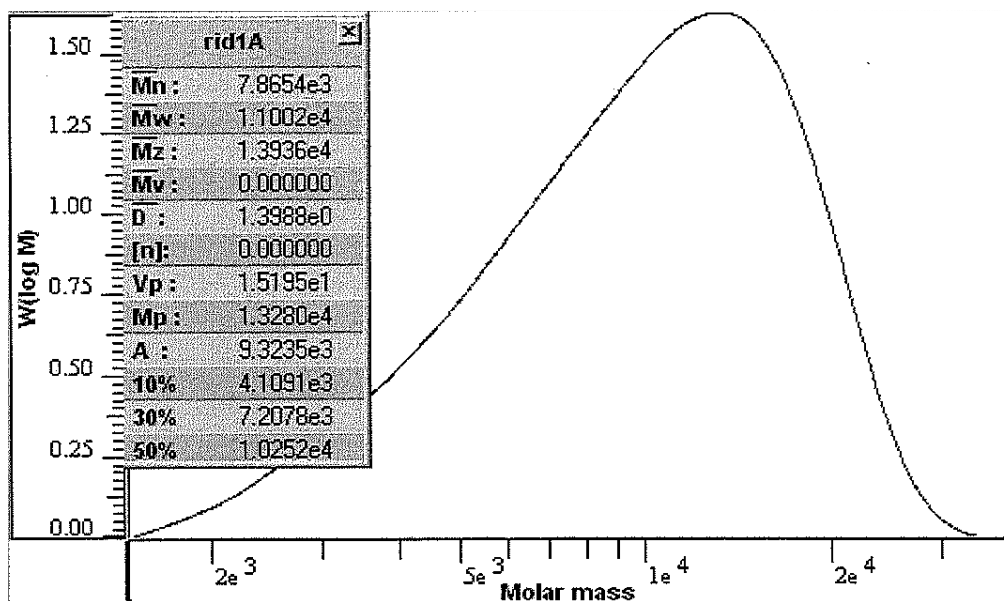


Figure B 2. GPC traces of α -bromo- ω -N-boc-aminopiperidine-PIPOX.

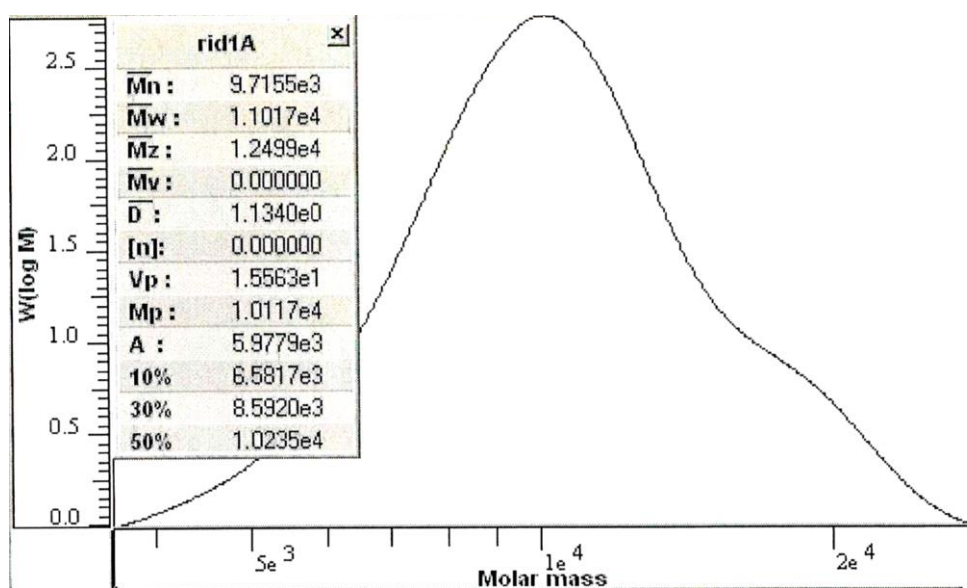


Figure B 3. GPC chromatogram of poly (2-isopropyl-2-oxazoline)-chloramphenicol (PIPOX-CAP) conjugate.

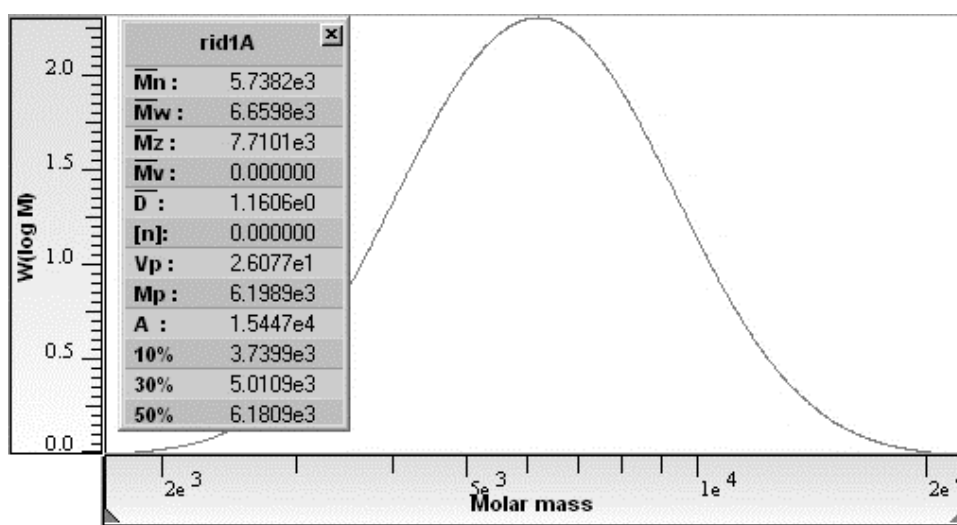


Figure B 4. GPC traces of poly(2-ethyl-2-oxazoline) (PEOX).

CURRICULUM VITAE

PERSONAL INFORMATION

Surname, Name : Çağlı, Eda
Nationality : Turkish (TC)
Date and Place of Birth : 7 Temmuz 1986, Niğde
Phone : +90 530 943 0943
E-mail : ecagli@metu.edu.tr, ecagli07@gmail.com

EDUCATION

Doctor of Philosophy (Ph.D.): (2013-2019)

Polymer Chemistry, Middle East Technical University, Ankara, Turkey
CGPA: 3.93/4.00 – **High Honor**

Master of Science (M.Sc.): (2011-2013)

Organic Chemistry, Middle East Technical University, Ankara, Turkey
CGPA: 3.76/4.00 – **High Honor**

Integrated Bachelor's and Non-Thesis Master of Science (B.Sc.): (2006-2011)

Chemistry Education, Middle East Technical University, Ankara, Turkey
CGPA: 3.13/4.00 – **Honor**

Prep School: (2005-2006)

High School: (2000-2004)

Mus Anatolian Teacher Training High School, Mus, Turkey
Mathematics and Science Branch
CGPA: 4.75/5.00

WORK EXPERIENCE

Research Assistant: (10.2011-02.2019)
Department of Chemistry, Middle East Technical University, Ankara, Turkey

LANGUAGES

English: Advanced

PUBLISHED ARTICLES

Akbar, M., **Cagli, E.**, Erel-Goktepe, I. (2019). Layer-by-layer Modified Superparamagnetic Iron Oxide Nanoparticles with Stimuli Responsive Drug Release Properties. *Macromolecular Chemistry and Physics*, 220 (4), doi: 10.1002/macp.201800422.

Cagli E., Erel-Goktepe, I. (2018). An Experimental and Computational Approach to pH-dependent Self-aggregation of Poly(2-isopropyl-2-oxazoline). *Journal of Polymer Science Part B: Polymer Physics*, 57(4), 210-221. doi: 10.1002/polb.24773.

Ustoglu, C., **Cagli E.**, Erel-Goktepe, I. (2017). Layer-by-layer films of block copolymer micelles with cores exhibiting upper critical solution temperature behavior, *European Polymer Journal*, 96, 278-294. doi: 10.1016/j.eurpolymj.2017.09.013.

Haktaniyan, M., Atilla, S., **Cagli E.**, Erel-Goktepe, I. (2017). pH- and temperature-induced release of doxorubicin from multilayers of poly(2-isopropyl-2-oxazoline) and tannic acid, *Polymer International*, 66 (12), 1851-1863. doi: 10.1002/pi.5458.

Dogan, O., **Cagli, E.** (2015). PFAM catalyzed enantioselective diethylzinc addition to imines. *Turkish Journal of Chemistry*, 39 (2), 1410-1439. doi: 10.3906/kim-1410-29.

MANUSCRIPTS IN PREPARATION

Cagli E., Ugur, E., Ulsan S., Banerjee, S., Erel-Goktepe, I. (revision submitted). Effect of Side Chain Variation on Surface and Biological Properties of Poly(2-alkyl-2-oxazoline) Multilayers

Cagli, E., Erel-Goktepe, I. (in preparation). Controlled release of Chloramphenicol (CAP) from nanoaggregates of poly(2-isopropyl-2-oxazoline)-CAP conjugate.

AWARDS AND HONORS

06.2014 Graduate Courses Performance Award
METU Graduate School of Natural and Applied Sciences

02.2011 High Honour Roll
Middle East Technical University

06.2010 High Honour Roll
Middle East Technical University

02.2010 High Honour Roll
Middle East Technical University

CONFERENCE PROCEEDINGS

ORAL PRESENTATIONS AND PAPERS

Cagli E., Ugur, E., Erel-Goktepe, I. (2018). Antibiotic Releasing Multilayers of Poly(2-isopropyl 2-oxazoline) and Tannic Acid. Talk presented at The 4th International Conference on Bioinspired and Biobased Chemistry & Materials, Nice, France.

Cagli E., Ugur, E., Ulsan S., Banerjee, S., Erel-Goktepe, I. (2018). Poly(2-alkyl 2-oxazoline) based multilayers as antibacterial coatings. Talk presented at VII. International Polymer Science and Technology Conference, Eskisehir, Turkey.

Cagli, E., Erel-Goktepe, I. (2017). Effect of pH, temperature and ionic strength on the self-aggregation of poly(2-isopropyl-2-oxazoline). Talk presented at 254th American Chemical Society National Meeting & Exposition, Washington DC, USA.

Cagli, E., Erel-Goktepe, I. (2016). Magnetothermally responsive polymer nanofilms of polyoxazoline block copolymer micelles. Talk presented at 6th EuCheMS Chemistry Congress, Seville, Spain.

POSTER PRESENTATIONS AND PAPERS

Cagli, E., Erel-Goktepe, I. (2017). The influence of environmental stimuli and polymer end groups on pH-induced self-aggregation behavior of poly(2-isopropyl-2-oxazoline) in aqueous media. Poster presented at 29th National Chemistry Congress, Ankara, Turkey.

Haktaniyan, M., Atilla, S., Cagli E., Erel-Goktepe, I. (2016) pH and temperature-triggered release of Doxorubicin from hydrogen-bonded multilayer thin films of poly(2-isopropyl-2-oxazoline). Poster presented at 6th EuCheMS Chemistry Congress, Seville, Spain.

Cagli, E., Erel-Goktepe, I. (2016). Controlled release of Paclitaxel from multilayers of block copolymer micelles with temperature- responsive coronae and pH-responsive cores. Poster presented at IUPAC World Polymer Congress (MACRO 2016), Istanbul, Turkey.

Haktaniyan, M., Atilla, S., Cagli E., Erel-Goktepe, I. (2016) Release of Doxorubicin from layer-by-layer films of poly(2-isopropyl-2-oxazoline). Poster presented at IUPAC World Polymer Congress (MACRO 2016), Istanbul, Turkey.

Ustoglu, C., Cagli E., Erel-Goktepe, I. (2016) Introducing upper critical solution temperature (UCST) to polymer multilayer films. Poster presented at IUPAC World Polymer Congress (MACRO 2016), Istanbul, Turkey.

Cagli, E., Dogan, O. (2012). Asymmetric diethylzinc addition to N-Sulphonylimine. Poster presented at 4th EuCheMS Chemistry Congress, Prague, Czech Republic.

Isci, M., Cagli, E., Dogan, O. (2012). New phosphine oxide aziridiny phosphonates as chiral Lewis bases for Abramov-type phosphonylation of aldehydes. Poster presented at 4th EuCheMS Chemistry Congress, Prague, Czech Republic.

Cagli, E., Dogan, O. (2012). PFAM catalyzed enantioselective diethylzinc addition to imines. Poster presented at 26th National Chemistry Congress, Mugla, Turkey.

REFERENCES

Name-Surname	Title	Position-Place	Phone	e-mail
Irem Erel-Göktepe	Assoc. Prof. Dr.	Faculty member Chemistry department/METU	+90 312 210 3233	erel@metu.edu.tr
Özdemir Doğan	Prof. Dr.	Faculty member Chemistry department/METU	+90 312 210 5134	dogano@metu.edu.tr